

DEVELOPMENT OF MICROFLUIDIC PLATFORMS FOR  
THERAPEUTIC PURPOSES

by

Elif Gençtürk

B.S. in Chemical Engineering, Boğaziçi University, 2013

M.Sc. in Chemical Engineering, Boğaziçi University, 2015

Submitted to the Institute for Graduate Studies in  
Science and Engineering in partial fulfillment of  
the requirements for the degree of  
Doctor of Philosophy

Graduate Program in Chemical Engineering

Boğaziçi University

2021



## ACKNOWLEDGEMENTS

In my thirteen years of education in Boğaziçi University, I have seen many sunrises and many sunsets; many good and bad times. The campuses, all of them except Kilyos, witnessed my laughter and as well as my tears. The tree-lined road where I left our building and went towards the dorms saw that I was in a hurry and that I was moving calmly. Putting on my headphones, going down the south campus to Bebek, walking to Beşiktaş from the seaside and countless dreams that I had on that road have now come to an end. I worked a lot, ate a lot, planned a lot, traveled a lot, talked a lot, loved a lot, cried a lot and been very happy. Even though the doctorate was a long and painful process, it was worth every second of it. I am happy that I have successfully completed my PhD and I thank myself. I'm glad I'm from Boğaziçi.

First of all, I would like to offer my deepest respect and love to my advisor Prof. Kutlu Ülgen. In our microfluidics adventure that we started together in graduate school, I shared many feelings with her both in my private life and in my school life. I will never forget that she always consoled me and supported me every time I went to her. I feel very lucky to have known her and I'm glad to have worked with her. I don't think I will leave her after my life in the Boğaziçi, and I always want to stay in touch with her. I would also like to thank my co-advisor, Prof. Şenol Mutlu, for accompanying us during my doctoral process, providing us with valuable ideas, opening the doors of his laboratories and helping us in all our academic work. I would like to express my respect and to Assoc. Prof. Nazar İleri Ercan and Prof. Alper Kiraz, who started to accompany us after my PhD qualifying exam and helped us in our progress. Finally, I would like to thank Assist. Prof. Pınar Pir and Assist. Prof. Muhammed Enes Oruç for devoting their precious time and knowledge to read and comment on my thesis.

I would like to thank my nuclear Gençtürk family, who have always supported me financially and morally since the day I started at Boğaziçi University, for always being there for me. I love my mother who cries with me in all my problems, my father who listens to us and worries about us, and my brother who always tries to find a solution. I feel very lucky

for having their prayers with me and it cannot be possible to finish this thesis without them. I am so glad that I have them. I sincerely hope that goodness and beauty await us in our future lives. In addition to my nuclear family, I offer my love to my mother's and father's side who never stop supporting me. I am grateful to them for not leaving us alone in our most difficult times and always being there for us. Thank you to all my cousins and nieces/nephews, especially Osman Tuna, who made my final year bearable.

We meet many people throughout our lives, and some of them become special to us. I would like to thank Elif Can and Meltem Baysal for adding lots of things to my life. I've laughed, cried, worked, watched, talked, walked with Elif Can since graduate school and all the paths led us to Meltem Baysal. Especially, in my last year, I realized how precious it is to eat, gossip, laugh and share something with you. It is excellent that I got to know you both and I love you. Also, thank you to all my high school and university friends for being in my life. Their friendships are one of the biggest assets that I have gained in my life.

I would like to thank dear Ekin Yurdakul and Müge Kasım for making the experiment nights that we spent long hours bearable. It was never easy to experiment all night in the dark, sitting in a chair and without sleep, and they both helped me without complaining about it. The songs we sang, the food we ate, the coffee we drank were all very precious and unique to me. It is magnificent to know both of you. In addition, I would like to especially thank Elif Esvap and Özlem Özbek. I will never forget the gossip we made over coffee. It was great working with you and being in the same lab. I also wish success to the entire KB 440 team in their work. I would also like to thank Chemical Engineering people, for being a part of this thesis and their support and companionship.

I acknowledge, this thesis has been financially supported by Boğaziçi Research Fund through the projects 13641D and 14261R.

## **ABSTRACT**

### **DEVELOPMENT OF MICROFLUIDIC PLATFORMS FOR THERAPEUTIC PURPOSES**

This thesis describes the present state of the development and applications of microfluidic systems used in cell biology and analyses of experiments conducted with in-house fabricated thermoplastic based microfluidic devices. COP based microreactors are produced by hot embossing and thermocompression bonding methods. Yeast and mammalian (THP-1) cells are employed in microfluidic experiments where RFP:Nop56 protein is used to track changes in cell cycle as well as protein synthesis within the yeast cells and GFP:ASC gene with a role in apoptosis is used to track the drug effects on THP-1 cells. HU, metformin, temsirolimus and HMF are administered to yeast cells and their response to these drugs are investigated. By computational systems biology approach, a genome-scale metabolic model specific to the yeast is reconstructed, and the inhibitory effect of HMF on growth and ethanol production is elaborated by estimating the internal flux distribution within the yeast metabolic network. To develop putative treatment strategies towards cancer, the COP based microreactor is integrated with Cr/Au interdigitated electrodes to test TTFields. In the high electrical field experiment, the yeast cells go through electroporation and in the low electrical field experiment, the cells have prolonged mitosis. Furthermore, human monocytic leukemia cell line THP-1 cells are tested in two-phase microfluidic devices, where cells are confined to droplets with several inhibitors/drugs. An increase in the fluorescence intensity of the ASC gene responsible for apoptosis is observed in cells under the influence of drugs. An important conclusion of this thesis is that these microfluidic platforms can be successfully used for studying the drug effects on tumors, observe cell to cell heterogeneity and may shed light on the putative treatment strategies towards cancer. These microreactors are still open for research and development, and solutions need to be found for each case separately.

## ÖZET

### MİKROAKIŞKAN PLATFORMLARIN TERAPÖTİK AMAÇLI GELİŞTİRİLMESİ

Bu tez, hücre biyolojisinde kullanılan mikroakışkan sistemlerin geliştirilmesinin ve uygulamalarının güncel durumuyla, laboratuvarımızda üretilen termoplastik tabanlı mikroakışkan cihazlarla yapılan deneylerin analizlerini açıklamaktadır. COP tabanlı mikrobiyoreaktörler, sıcak kabartma ve termo sıkıştırılmalı bağlama yöntemleriyle üretildi. Mikroakışkan biyoreaktör deneylerinde maya hücreleri RFP:Nop56 proteininin hücre döngüsündeki değişikliklerini ve protein sentezini izlemek için kullanılırken, memeli hücreleri (THP-1) apoptozda rolü olan GFP:ASC geninin takibi için kullanıldı. Maya hücrelerine HU, metformin, temsirolimus ve HMF kimyasalları uygulanarak hücrenin bu ilaçlara yanıtları araştırıldı. Hesaplamalı sistemler biyolojisi yaklaşımıyla, mayaya özgü genom ölçeğinde bir metabolik model yeniden yapılandırıldı ve HMF'nin büyüme ve etanol üretimi üzerindeki engelleyici etkisi, maya metabolik ağı içindeki iç akış dağılımı akı denge analizi ile hesaplanarak detaylandırıldı. Kanser karşı uygun tedavi stratejileri geliştirmek ve elektrik alan etkisini (TTFFields) incelemek için, COP tabanlı mikrobiyoreaktöre iç içe Cr/Au elektrotlar entegre edildi. Yüksek elektrik alan deneyinde, maya hücreleri elektroporasyondan geçerken, düşük elektrik alan deneyinde hücrelerin mitoz süresi uzadı. Ayrıca, insan monositik lösemi hücre hattı THP-1 hücreleri, damlacık tabanlı iki fazlı mikroakışkan aygıtlarda üç farklı inhibitör ilaç ile test edildi. İlaçların etkisi altındaki hücrelerde apoptozdan sorumlu ASC geninin floresan yoğunluğunda bir artış gözlemlendi. Bu tezin ortaya koyduğu en önemli sonuç, mikroakışkan platformların tümörler üzerindeki ilaç etkilerini incelemek ve hücreden hücreye heterojenliği gözlemlemek için başarıyla kullanılabileceği, dolayısıyla da kansere yönelik geliştirilecek tedavi stratejilerine ışık tutabileceğidir. Bu mikroakışkan biyoreaktörler halen araştırma ve geliştirmeye açıktır ve incelenen durumlarda sisteme özgü çözümler bulunması gerekmektedir.

## TABLE OF CONTENTS

ACKNOWLEDGEMENTS .....	iv
ABSTRACT .....	vi
ÖZET .....	vii
LIST OF FIGURES .....	xiii
LIST OF TABLES .....	xxii
LIST OF SYMBOLS .....	xxiii
LIST OF ACRONYMS/ABBREVIATIONS .....	xxiv
1. INTRODUCTION.....	1
2. ADVANCES IN MICROFLUIDIC DEVICES MADE FROM THERMOPLASTICS USED IN CELL BIOLOGY AND ANALYSES .....	6
2.1. Cultivation: Organism-on-a-Chip .....	11
2.1.1. Culturing of Bacterial Cells .....	12
2.1.2. Fungi Cultivation .....	14
2.1.3. Zebra Fish Cultivation .....	15
2.1.4. Fruit Fly (Drosophila) Cultivation .....	17
2.1.5. Mammalian Cell Cultivation .....	18
2.1.5.1. 3D Culturing .....	20
2.1.5.2. Electric Field-based Microfluidic Systems .....	22
2.1.6. Tissue Engineering (TE) .....	24
2.2. Separation/Isolation .....	30
2.2.1. DNA-RNA Extraction/Isolation .....	31
2.2.2. Separation/Isolation of Microorganisms .....	32
2.2.3. Separation of Blood Cells .....	34
2.2.4. Separation/Isolation of Tumor Cells .....	36
2.2.5. Separation/Isolation of Other Cells .....	40
2.3. Detection and Analysis .....	41
2.3.1. Electro-based Detection .....	41
2.3.2. Magnetic Field Based Detection .....	44
2.3.3. Chemical Detection .....	45

2.3.4. Biosensing/Biosensor Based Detection .....	47
2.3.5. PCR Based Detection Systems Based on Genetic Material .	51
2.3.6. Miscellaneous Detection Systems for Diseases .....	52
2.3.6.1. Fluorescence Based Detection for HIV Point of Care Testing Systems .....	52
2.3.6.2. Sensors for Detection and Analysis of Cancer .....	52
2.3.6.3. Morphology Based Detection and Analysis Systems for Diagnostic Purposes .....	55
2.4. Reaction: Microbial Fuel Cells .....	57
2.5. Conclusion/Future Directions .....	59
3. DESIGNING AND FABRICATION OF A THERMOPLASTIC MADE MICROBIOREACTOR FOR YEAST CULTURING .....	60
3.1. Materials .....	62
3.2. Design of the Microfluidic Device .....	62
3.3. Device Fabrication .....	63
3.3.1. Computational Fluid Dynamics (CFD) Simulations .....	63
3.3.2. Mold Preparation .....	64
3.3.2.1. Photolithography .....	64
3.3.2.2. Electrochemical wet etching .....	65
3.3.3. Drilling Inlet-Outlet Reservoirs and Planarization .....	65
3.3.4. Hot-embossing .....	66
3.3.5. Thermo-compression bonding .....	66
3.4. Medium Preparation and Microscopy .....	66
3.5. Microfluidic Device Operation .....	68
3.6. Results and Discussion .....	68
3.6.1. Effect of Hydroxyurea on Yeast Cells .....	70
3.6.2. Effect of Metformin on Yeast Cells .....	74
3.6.3. Effect of Temsirolimus on Yeast Cells .....	78
3.6.4. Effect of 5-hydroxymethylfurfural on Yeast Cells .....	79
3.7. Conclusion .....	85
4. DECIPHERING THE EFFECT OF 5- HYDROXYMETHYLFURFURAL (HMF) ON BIOMASS GENERATION AND ETHANOL PRODUCTION .....	88

4.1. Methods .....	90
4.1.1. Computational Tools and Model .....	90
4.1.2. Flux Balance Analysis .....	90
4.1.3. Flux Variability Analysis .....	90
4.1.4. Flexibility of the Network .....	91
4.1.5. Flux Coupling and Regulation .....	91
4.1.6. Flux Scanning Based on Enforced Objective Flux .....	93
4.1.7. Knocking Out Reactions and Genes .....	93
4.2. Results and Discussion .....	93
4.2.1. FBA, FVA and Flexibility of the Network .....	94
4.2.2. Classification of Reactions (in terms of coupling)	
Functioning towards Growth or Ethanol Production .....	95
4.2.3. Flexibility of Reactions (in terms of subsystems) .....	95
4.2.4. Flux Coupling and Regulation .....	108
4.2.5. Transcriptional vs Metabolic Regulation .....	112
4.2.6. FSEOF and Reaction/Gene Deletions .....	114
4.2.7. Gene Deletions .....	118
4.3. Achievements .....	119
<b>5. THERMOPLASTIC MICROFLUIDIC BIOREACTORS WITH INTEGRATED ELECTRODES TO STUDY TUMOR TREATING FIELDS ON YEAST CELLS .....</b>	<b>122</b>
5.1. Materials and Methods .....	125
5.1.1. Materials .....	125
5.1.2. Overview of the Microfluidic Device and Platform .....	126
5.1.3. Device Fabrication .....	127
5.1.4. Medium Preparation and System Operation .....	128
5.1.5. Impedance and Electrical Field Analysis .....	129
5.2. Results and Discussion .....	133
5.2.1. Impedance Analysis and Electrical Field Calculations .....	134
5.2.2. Electrical Field Effect on Yeast Cells .....	136
5.2.2.1. Cells Not Treated by Electrical-field .....	136
5.2.2.2. High Voltage Treated Cells: Electroporation .....	137

5.2.2.3. Low Voltage Treated Cells: Prolongation of Mitosis .....	140
5.2.3. Highlights (Pros and Cons) of Thermoplastic Materials for Batch Fabrication of Microdevices .....	141
5.3. Conclusion .....	142
6. MAMMALIAN CELL EXPERIMENTS USING TWO PHASE MICROFLUIDIC DEVICES .....	143
6.1. Materials and Methods .....	145
6.1.1. Materials .....	145
6.1.2. THP-1 Cell Culture Preparation .....	146
6.1.2.1. Sterilization .....	146
6.1.2.2. Preparation of RPMI Complete Medium .....	146
6.1.2.3. Preparation of Inoculum .....	146
6.1.2.4. Preparation of Frozen Stock Cultures .....	147
6.1.2.5. Preparation of Oil and Drug Phase .....	147
6.1.3. Experimental Setup of the Microfluidic Device Platform and Operation .....	149
6.2. Results and Discussion .....	150
6.2.1. Interaction of NLRP3 and ASC within the Cell and Their Roles .....	150
6.2.2. Confinement of THP-1 Cells within the Droplets without Drug (Control Experiment) .....	152
6.2.3. Temsirolimus Experiment .....	154
6.2.4. Rifabutin Experiment .....	156
6.2.5. BAY 11-7082 Experiment .....	158
6.3. Conclusion .....	160
7. CONCLUSIONS AND RECOMMENDATIONS .....	162
7.1. Conclusions .....	162
7.2. Recommendations .....	164
REFERENCES .....	166
APPENDIX A: PERMISSIONS FOR REUSED FIGURES .....	215
A.1. Permission for Figure 1.1 .....	215
A.2. Permission for Figure 2.1 .....	216

A.3. Permission for Figure 2.2 .....	217
A.4. Permission for Figure 2.3 .....	218
A.5. Permission for Figure 2.4 .....	221
A.6. Permission for Figure 2.5 .....	222
A.7. Permission for Figure 2.6 .....	223
A.8. Permission for Figure 2.7 .....	224
A.9. Permission for Figure 2.8 .....	225

## LIST OF FIGURES

Figure 1.1.	Microbioreactor types .....	3
Figure 2.1.	(a) Schematic view of the microfluidic system (b) Photograph of the PMMA chamber .....	12
Figure 2.2.	The 5 layers of the microfluidic device and assembled view of the temperature-controlled chip .....	15
Figure 2.3.	Microwell designed chip (top) and micropatterned chip (bottom)	28
Figure 2.4.	Chip test results for (a) A Rh+ (b) B Rh+ (c) AB Rh+ (d) (e) O Rh+ blood types respectively. (e) (f) Thalassemia samples with smaller RBCs and lower hematocrit. (d) Healthy blood sample (f) (i) Normal blood sample (age 23; male) (ii) Thalassemia blood sample (age 37; male) .....	35
Figure 2.5.	The schematic illustration of the two-stage microfluidic system	39
Figure 2.6.	(a) The layers of the microfluidic system. (b) Assembled chip microphotograph .....	46
Figure 2.7.	The design of the centrifugal LAMP microdevice .....	50
Figure 2.8.	(a) mini-MFC schematic illustration (b) Gold anodic layer on glass and PMMA anodic well layer (c) Image of the bonded PMMA anodic well layer on glass substrate (d) Metal straw sealed by silicon rubber to the anodic layer (e) Assembled mini-MFC.....	58

Figure 3.1.	(a) Schematic illustration of the device design (b) Simulation of trapping mechanism with parallel channel designs showing 16 equivalent stagnation points in C shaped regions (c) Particle tracing at different time points .....	63
Figure 3.2.	(a) Experimental setup (b) In-house fabricated microbioreactor placed on microscopy stage with external tubing connections (c) Fabricated microfluidic device .....	67
Figure 3.3.	Microfluidic device used for single cell tracking .....	68
Figure 3.4.	Schematic representation of cell cycle phases and checkpoints .....	69
Figure 3.5.	The brightfield (BF), fluorescence (Fluo) and merged microscopy images of yeast cells before, during and after hydroxyurea (HU) treatment .....	71
Figure 3.6.	(a) Time profile of the cell count. (b) Time profile of the cell perimeter (population). (c) Time profile of the fluorescence intensity (Vertical lines indicate the start and end of HU application) (d) Duration of G1 phases before and after HU treatment .....	72
	..	
Figure 3.7.	(a) Long spheroidal shape of yeast cell during YNB HU experiment (Chamber 2) (b) Time profile of single cell volume during YNB HU experiment (Chamber 1) (c) Time profiles of single mother and daughter cells integrated fluorescence density and perimeter before, during and after YNB HU experiment (Chamber 1) .....	73
Figure 3.8.	(a) Time profile of cell count (b) Time profile of cell perimeter (population) (c) Time profile of the fluorescence intensity	

	(Vertical lines indicate the start and end of metformin application)	
	(d) Duration of S/G2/M phases before and after metformin treatment .....	75
Figure 3.9.	(a) Time profiles of the single cells (b) Time profiles of single mother and daughter cells integrated fluorescence density and perimeter before, during and after metformin experiment .....	77
Figure 3.10.	(a) Time profile of cell count (population) (b) Time profile of cell perimeter/cell count (population) (c) Time profile of single cell perimeter (d) Time profile of fluorescence intensity/cell count (population) (Vertical lines show the interval of temsirolimus treatment) .....	80
Figure 3.11.	Conversion pathways of furfural and HMF .....	81
Figure 3.12.	(a) Time profile of cell count (b) Time profile of total cell perimeter (c) Time profile of single cell perimeters (Vertical lines on the graphs shows the HMF feeding period .....	82
Figure 3.13.	Time profile of fluorescence intensity at single cell level (inset shows the fluorescence intensity in the first 150 min) .....	83
Figure 3.14.	Time profile of perimeter and fluorescence intensity of individual mother and daughter cells .....	84
Figure 4.1.	(a) Ethanol production pathway under HMF effect (b) Stoichiometric matrix of the model .....	89
Figure 4.2.	(a) The number of reactions in which each of the metabolite involved in the network Frequency for different ranges of flux span at growth limited by oxygen uptake rate: (b) Objective: Biomass for control model (c) Objective: Ethanol for control	

	model (d) Objective: Biomass for HMF model (e) Objective: Ethanol for HMF model .....	92
Figure 4.3.	Reaction classifications (a) Objective: Biomass for control model (b) Objective: Ethanol for control model (c) Objective: Biomass for HMF model (d) Objective: Ethanol for HMF model .....	96
Figure 4.4.	Flexibility of network based on subsystems for 100% maximum objective. Control model (left) and HMF model (right) for biomass generation .....	98
Figure 4.5.	Flexibility of network based on subsystems for 90% maximum objective. Control model (left) and HMF model (right) for biomass generation .....	99
Figure 4.6.	Flexibility of network based on subsystems for 80% maximum objective. Control model (left) and HMF model (right) for biomass generation .....	100
Figure 4.7.	Flexibility of network based on subsystems for 70% maximum objective. Control model (left) and HMF model (right) for biomass generation .....	101
Figure 4.8.	Flexibility of network based on subsystems for 60% maximum objective. Control model (left) and HMF model (right) for biomass generation .....	102
Figure 4.9.	Flexibility of network based on subsystems for 50% maximum objective. Control model (left) and HMF model (right) for biomass generation .....	103

Figure 4.10.	Flexibility of network based on subsystems for 100% maximum objective. Control model (left) and HMF model (right) for biomass generation .....	104
Figure 4.11.	Flexibility of network based on subsystems for 90% maximum objective. Control model (left) and HMF model (right) for biomass generation .....	105
Figure 4.12.	Flexibility of network based on subsystems for 80% maximum objective. Control model (left) and HMF model (right) for biomass generation .....	105
Figure 4.13.	Flexibility of network based on subsystems for 70% maximum objective. Control model (left) and HMF model (right) for biomass generation .....	106
Figure 4.14.	Flexibility of network based on subsystems for 60% maximum objective. Control model (left) and HMF model (right) for biomass generation .....	106
Figure 4.15	Flexibility of network based on subsystems for 50% maximum objective. Control model (left) and HMF model (right) for biomass generation .....	107
Figure 4.16.	Flux coupling network of (a) control and (b) modified models. Nodes show the reactions and colors are based on subsystems ....	109
Figure 4.17.	Regulation types of the model and subsystems (a) Total results under the treatment of HMF (b) Mitochondrial transport (c) Oxidative phosphorylation (d) Sterol metabolism (e) Extracellular transport (f) Glycerolipid metabolism (g) Pentose phosphate pathway (h) Nucleotide salvage pathway (i) Purine and pyrimidine biosynthesis (j) Phospholipid biosynthesis (k) Glycine and serine	

	metabolism (l) Folate metabolism (m) Valine leucine and isoleucine metabolism .....	113
Figure 4.18.	FSEOF algorithm result: The identified reactions and their flux changes (a) control model (b) modified model .....	115
Figure 4.19.	Reaction deletion cases based on FSEOF and OptKnock for control model. Red lines depict the FSEOF single deletions, green lines show FSEOF multiple deletions, blue lines are for OptKnock deletions and black lines are used to describe the reduced growth rate cases with OptKnock .....	116
Figure 4.20.	Reaction deletion cases based on FSEOF and OptKnock for HMF model. Red lines depict the FSEOF single deletions, green lines show FSEOF multiple deletions, blue lines are for OptKnock deletions and black lines are used to describe the reduced growth rate cases with OptKnock .....	117
Figure 4.21.	Single (top) and double (bottom) deletion of genes for control model .....	119
Figure 4.22.	Single (top) and double (bottom) deletion of genes for modified model .....	120
Figure 5.1.	(a) Design of the microfluidic device with cell and nutrient inlets of 1, 2 and 3 (b) Fabricated device of COP (c) Electrode images within a chamber at 4X, 20X and 40X magnification (d) Experimental setup schematic .....	123
Figure 5.2.	Chip fabrication steps .....	130
Figure 5.3.	Electrical circuit model of the test setup used during cell experiments. CEDL is the electrical double layer capacitor formed	

between gold electrode and electrolyte.  $R_{sol}$  is the resistance of the bulk of the electrolyte solution. The voltage difference across this resistance forms the electric field the cells experience.  $R_s$  is the series resistance of the voltage source. It can also account for the series resistances of the ammeters used to measure the AC current flowing through the circuit.  $C_{sol}$  which models the capacitance of the bulk solution between electrodes is not shown for clarity purposes .....

131

Figure 5.4. Nyquist plots of DIW, Nop56, Rp15 and YPD media for 0.1  $\mu\text{L}/\text{min}$  flow rate. Real and imaginary impedance values is marked for the used frequencies of 150 and 200 kHz in the cell experiments .....

134

Figure 5.5. Cell count and cell perimeter-time profiles of (a) not-electrical-field treated cells as control group showing regular proliferation with increasing number and perimeter (b) 6.58 V/cm electrical-field treated cells showing absence of proliferation with no cell count increase, electroporation happens and cell perimeter increases only in the first 150 min, and (c) 1.33 V/cm electrical-field treated cells showing delayed proliferation with constant cell size and cell count in the first 150 min and 250 min, respectively .

138

Figure 5.6. Fluorescence intensity and single cell perimeter-time profiles of (a) not-electrical-field treated cells showing regular proliferation. Decline in the fluorescence intensity at the beginning is due to shock of a new confined microaerated environment. With adaptation to the environment, increase in the fluorescence intensity starts. Perimeter profiles show the increase in the perimeter of single cell with time, then suddenly drops to almost its half due to cell division and then both mother's and daughter's perimeters again monotonically increase (b) 6.58 V/cm electrical-field treated cells showing the absence of proliferation. The

	perimeters of single cells increase in the first 150 min, then stay constant without dividing. Continuous decline in the fluorescence intensity points to the cell death, and (c) 1.33 V/cm electrical-field treated cells showing dimensional changes of the individual cells with delayed budding time and delayed increase in the fluorescence intensity as evidence of maintained Nop56 protein functionality .....	139
Figure 5.7.	Time-lapse microphotographs of yeast cells experiments. Cells in the control group show regular increase in number and perimeter. Cells treated with 6.58 V/cm electrical-field show blurring borders with time as evidence of undergoing electroporation. Cells treated with 1.33 V/cm electrical-field stays almost the same at the beginning of the experiments then show delayed mitosis division	140
Figure 6.1.	Schematic of droplet generation in passive and active techniques .	143
Figure 6.2.	THP-1 cells (a) Brightfield microscopy images of THP-1 cells (b) Fluorescence microscopy images of THP-1 cells (c) THP-1 cells confined in a droplet .....	144
Figure 6.3.	(a) Experimental setup of the microfluidic device platform (b), (c) General view of the chip (d) Inlets of the device (e) Channels for droplet generation (f) Channels for droplet storage .....	148
Figure 6.4.	ASC (PYCARD) interaction map .....	150
Figure 6.5.	Control experiments results (a) Time profile of cell count (b) Time profile of normalized fluorescence intensity (a.u.) (c) Time profiles of single cells' normalized fluorescence intensity (a.u.) (d) Percentages of increase, constant and decrease states of single cells' fluorescence intensity .....	153

- Figure 6.6. THP-1 cells are under the treatment of temsirolimus (a) Time profile of cell count (b) Time profile of normalized fluorescence intensity (a.u.) (c) Time profiles of single cells' normalized fluorescence intensity (a.u.) (d) Percentages of increase, constant and decrease states of single cells' fluorescence intensity ..... 155
- Figure 6.7. THP-1 cells are under the treatment of rifabutin (a) Time profile of cell count (b) Time profile of normalized fluorescence intensity (a.u.) (c) Time profiles of single cells' normalized fluorescence intensity (a.u.) (d) Percentages of increase, constant and decrease states of single cells' fluorescence intensity ..... 157
- Figure 6.8. THP-1 cells are under the treatment of BAY 11-7082 (a) Time profile of cell count (b) Time profile of normalized fluorescence intensity (a.u.) (c) Time profiles of single cells' normalized fluorescence intensity (a.u.) (d) Percentages of increase, constant and decrease states of single cells' fluorescence intensity ..... 159

## LIST OF TABLES

Table 2.1.	Summary of properties for thermoplastics .....	7
------------	--	---

**LIST OF SYMBOLS**

$d$	Gap
$E$	Electric field
$f$	Frequency
$V$	Voltage
$Z$	Impedance magnitude
$\theta$	Phase angle
$\omega$	Angular frequency

## LIST OF ACRONYMS/ABBREVIATIONS

3D	Three dimensional
AAO	Anodic aluminium oxide
ABC	Acrylonitrile butadiene styrene
AFM	Atomic force microscopy
AIDS	Acquired immune deficiency syndrome
ASC	Apoptosis-associated speck-like protein containing a CARD
BCAA	Branched chain amino acids
BOPP	Biaxially oriented polypropylene
BM	Bulk mixing
BSA	Bovine serum albumin
CA	Cellulose acetate
CAD	Computer aided design
CCD	Charge-coupled device
CE	Capillary electrophoresis
CFD	Computational fluid dynamics
ChRWR	Channel rhodopsin wide receiver
CINCA	Chronic infantile neurological cutaneous and articular syndrome
CLR	C-type lectin receptors
CNC	Computer numerical control
COBRA	Constraint-based reconstruction and analysis toolbox
COP	Cyclo olefin polymer
CTC	Circulating tumor cells
CV	Cyclic voltammetry
DAMP	Danger associated molecular patterns
DC	Direct current
DEP	Dielectrophoresis
DIW	Deionized water
DMSO	Dimethyl sulfoxide
dNTP	Deoxyribonucleoside triphosphates

DO	Dissolved oxygen
DSA	Double sided adhesive
DXRL	Deep X-ray lithography
EC	Endothelial cell
EDL	Electrical double layer
EF	Electric fields
EGFR	Epidermal growth factor receptor
EIS	Electrochemical impedance spectroscopy
EOF	Electroosmotic flow
EPEC	Enteropathogenic E. Coli
ES	Embryonic stem cells
ESEM	Environmental scanning electron microscope
FBA	Flux balance analysis
FBS	Fetal bovine serum
FCA	Flux coupling analysis
FDA	Food and drug administration
FEA	Finite element model
FET	Fish embryo toxicity
FN	Fibronectin
FOPBR	Fiber optic particle plasmon resonance
FOV	Field of view
FP	Fabry-Perot
FPGA	Field Programmable Gate Array
FRIM	Fluorescence ratiometric imaging
FSEOF	Flux scanning based on enforced objective flux
FTIR	Fourier transform infrared spectroscopy
FVA	Flux variability analysis
GASI	Geometrically activated surface interaction
GFP	Green fluorescent protein
HDPE	Polyethylene-high density
HFRD	High flow rate device
HIV	Human immunodeficiency virus
HMF	5-hydroxymethyl furfural

HQ	Hydroquinone
HRP	Horseradish peroxidase
HU	Hydroxyurea
HUVEC	Human umbilical vein cell
HTMSU	Highthroughput microsampling unit
IKK	I $\kappa$ B kinase
IMES	Integrated microfluidic electrostatic sampler
IPA	Isopropyl alcohol
ITO	Indium tin oxide
LAMP	Loop mediated isothermal amplification
LDPE	Polyethylene-low density
LDR	Ligase detection reaction
LN	Liposome nanoparticles
LOC	Lab on a chip
LOD	Limits of detection
LP	Lipopolyplex
LRR	Leucine rich repeat
mAB	Monoclonal antibody
MCL	Mantle cell lymphoma
MF	Microfluidic focusing
MFC	Microbial fuel cell
MPs	Magnetic particles
MSC	Mesenchymal stem cells
MTB	Mycobacterium tuberculosis
MWS	Muckle-Wells syndrome
NASBA	Nucleic acid sequence-based amplification
NES	Nanoengineered surface
NLR	(NOD)-like receptors
NP	Nanoparticle
NPS	Nanoengineered polystyrene surfaces
Nylon	Polyamide
OD	Optical densiyy
ODN	Oligonucleotides

PAA	Poly(ethylene glycol)-grafted poly(acrylic acid)
PAMAM	Polyamidoamine
PAMP	Pathogen associated molecular patterns
PC	Polycarbonate
PCR	Polymerase chain reaction
PDA	Polydopamine
PDAC	Pancreatic ductal adenocarcinoma
PDMS	Polydimethylsiloxane
PEEK	Polyetheretherketone
PEG-DA	Poly(ethylene glycol) diacrylate
PEM	Proton exchange membrane
PET	Polyethylene terephthalate
PETG	Polyethylene terephthalate glycol
PHABO	Primary human alveolar bone osteoblasts
PI3K	Phosphoinositide 3-kinase
PIKK	Phosphatidylinositol 3-kinaserelated kinase
PKB	Akt/protein kinase B
PLA	Poly(lactic acid)
PMMA	Polymethyl methacrylate
PP	Polypropylene
PS	Polystyrene
PSA	Pressure-sensitive adhesive
PSMA	Prostate-specific membrane antigen
PSU	Polysulfone
PTFE	Polytetrafluoroethylene
PU	Polyurethane
PVA	Poly(vinyl alcohol)
PVC	Polyvinyl chloride
RAVEN	Reconstruction, Analysis and Visualization of Metabolic Networks
RBC	Red blood cell
RFP	Red fluorescent protein
RIF	Reflectometric interference spectroscopy

RLR	RIG-I-like receptor
RNR	Ribonucleotide reductase
RRM	Resazurin dye reduction
SAM	Self-assembled monolayer
SDA	Strand displacement amplification
SE	Staphylococcus epidermidis
SFC	Single-field chip
SFE	Semi-continuous flow electroporation
STPP	Sodium tripolyphosphate
SWV	Square wave voltammetry
T2D	Type 2 diabetes
TB	Tuberculosis
TE	Tissue engineering
TIR	Translocated intimin receptor
TLR	Toll-like receptor
TOR	Target of rapamycin
TPL	Two photon lithography
TTFields	Tumor treating fields
TWEAK	TNF-like weak inducer apoptosis
UTI	Urinary tract infections
VEGF	Vascular endothelial growth factor
WBC	White blood cells
XRD	X-ray diffraction
YNB	Yeast nitrogen base
$\mu$ FCM	Microfluidic flow cytometry
$\mu$ CP	Microcontact printing
$\mu$ FFE	Microfluidic free-flow electrophoresis
$\mu$ -MACS	Microfluidic magnetic activated cell sorting
$\mu$ OT	Micro-optical tweezers
$\mu$ RT-PCR	Micro-reverse transcription polymerase chain reaction

## 1. INTRODUCTION

In cell biological studies, the multi-well plates or microscopy slides are well known traditional methods for the *in vitro* cell culturing. Billions of cells fill a well plate or a bioreactor and the overall performance of the population is analyzed. However, some of the cells in a population can behave differently and process optimization is required for the analysis of the diversity within the population. By traditional methods, it was not possible to observe the changes at the single-cell level (Boitard *et al.*, 2012). From the beginning of the 1980s, microsystems have begun to be developed and these systems have revolutionized the possibilities of cell analyses, e.g. isolated single cells have been observed with the help of miniaturization of devices and systems. By using simple experimental systems, live-cell monitoring and several analyses can be done, where sample volume requirement is very small. Immobilization of cells at the pre-determined locations can be achieved and different types of analytical instrumentation can be used to perform analyses. Cell guiding, cell isolation or cell detection experiments can be conducted with high-throughput microfluidic devices (Hümmer *et al.*, 2016).

Microfluidic device design is the most important step of the studies related to this field. Designed device should meet all of the requirements and should be capable of performing the desired experiments. Computer aided design (CAD) tools such as L-Edit, AutoCAD or SolidWorks can be used to design the device and the simulation programs such as COMSOL Multiphysics can be employed to reveal the dynamics within the device. After designing the device, many fabrication methods can be applied to obtain the desired device that has to function properly. Wet and dry etching, 3D printing, photolithography, injection molding, hot embossing, oxygen plasma bonding or thermal bonding are the most widely used device fabrication techniques (Tsao and DeVoe, 2009). New generation microfluidic devices include electrodes, internal structures and other functionalities to enhance the performance of the device. In the case of electrical stimulation, systems, that include electrodes for directly applying currents to the cells, have been developed. For example; wound healing, regenerative medicine and stem cell differentiation into cardiac tissue have benefited from the electrical simulation studies (Pavesi *et al.*, 2016).

On the other hand, electrical fields of high strength applied to aqueous suspensions of living cells have significant effects on the cell membranes and even kill the organism. Blood cells, algal cell, bacteria or yeast cells can be used in electric field applied experiments (Hülshager *et al.*, 1983). Moreover, piezoelectric-driven microfluidic systems can be used for droplet sorting. Isolation of cell populations or chemicals can be arranged via sorting and this simplifies the process of making the desired analysis (Shemesh *et al.*, 2010).

In the experimental part of this thesis, fabrication and operation of microbioreactor are considered. Microbioreactors can basically be produced in two types: single phase (continuous) and two phase (droplet) (Figure 1.1). Single-phase microbioreactors contain miscible liquids whereas two-phase microbioreactors include two or more immiscible liquids. There is a continuous fluid flow within the single-phase devices and generally, fresh medium is sent through the cell trapped regions. Waste is collected from the outlet of the device. Cell response towards changing environment can be observed in these type of microbioreactors. However, in two-phase devices, droplets are generated and the cells are confined in those droplets. Detection and identification of pathogens, antibiotic susceptibility testing, microbial physiology studies and biotechnical applications can be performed via droplet microfluidics (Kaminski *et al.*, 2016). This system offers a high degree of automation and enables high throughput screens. Cells survive in droplets and environmental changes around or within a droplet can be monitored by monitoring the secreted products (Shembekar *et al.*, 2016).

In the computational part of this thesis, the Constraint-Based Reconstruction and Analysis Toolbox (COBRA) which is a MATLAB software is used to predict quantitatively the cellular/multicellular biochemical networks with constraint-based modelling. COBRA has found widespread application in biology, biomedicine and biotechnology. *Saccharomyces cerevisiae*, *Escherichia coli* or Homo sapiens models including several metabolites, reactions and genes can be uploaded the MATLAB software and quality controlled reconstruction, modeling, topological analysis, strain and experimental design and network visualization can be done (Heirendt *et al.*, 2019). Single phase microfluidic device experiments and COBRA analysis are made by employing *Saccharomyces cerevisiae*. The development of healthcare takes the advantage of the research on organisms that can give valuable genetic information about Homo sapiens.

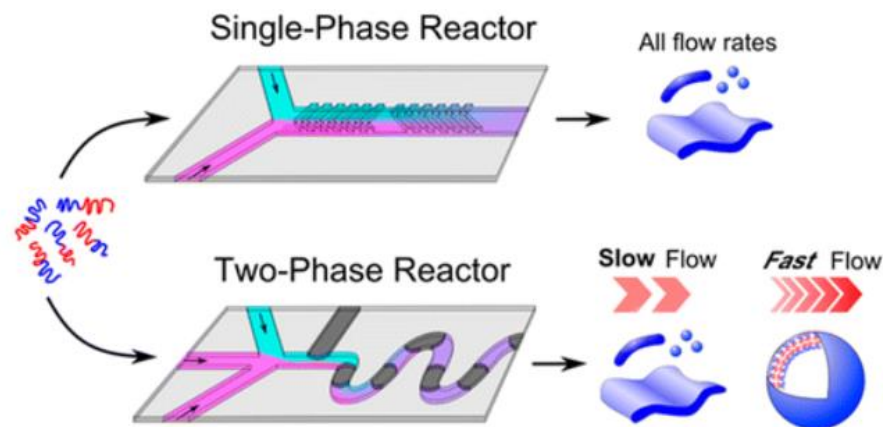


Figure 1.1. Microbioreactor types (Xu *et al.*, 2016).

Yeast cells are unicellular (single-cell) eukaryotic organisms and they can proliferate by budding, asexually. They have been used as a model organism of human due lots of matching genes. Moreover, the shortness of the duplication time of yeast cells make easier to work with these cells compared to human cells (90min and 24h for yeast and human cell, respectively). Since yeast and human cells have certain similarities, cellular response, chronological lifespan and aging process in yeast cells can be associated with those in human. Consequently, there can be an opportunity to determine the diseases at early stages and improve treatments. Moreover, yeast cell dimensions can change form species to species but generally they are 3 or 4 $\mu$ m in diameter being suitable for microfluidic studies (Legras *et al.*, 2007).

THP-1 mammalian cells were confined within the droplets in two phase microfluidic device experiments. Acute monocytic leukemia patient is used to produce the THP-1 which is a human monocytic cell line. This cell line expresses valuable results for investigating monocyte structure and functions in both health and disease (Bosshart and Heinzelmann, 2016). THP-1 cells have large, round and single-cell morphology. They produce IL-1 and expresses Fc and C3b receptors during the absence of immunoglobulins (Tsuchiya *et al.*, 1980), (Genin *et al.*, 2015). These cells are generally used as in vitro cancer models. Within the scope of this thesis study, the development of single and two-phase microfluidic platforms were conducted with the ultimate aim of identification of inhibitors/putative drugs against several diseases including cancer. Microfluidic device design was drawn via AutoCAD and its performance, i.e. the functionality and operability, was investigated via

COMSOL Multiphysics software. Microfluidic devices were fabricated via hot embossing and thermo-compression bonding methods by using cyclo olefin polymer (COP). The behavior of RFP tagged yeast cells (RFP:Nop56) against several inhibitors/drugs were observed in the devices. Moreover, electric field was integrated into the next generation microfluidic devices.

Here, again thermoplastics made microfluidic devices were fabricated via hot embossing and thermo-compression bonding techniques and Cr/Au electrodes in the interdigitated form were embedded in the designed devices. Nutrient type, budding time and electric field magnitude were the parameters in these experiments. Afterwards, two-phase microfluidic devices were employed for fast drug screening. THP-1 cells were confined within the droplets with several drugs. In these experiments, it was analyzed how the cell would respond to the drug in a limited nutrient environment. Finally, COBRA toolbox was used to analyze the network based results of yeast cells under drug treatment. Flux balance, flux variability analysis and flexibility of the network were obtained. Flux coupling, regulation and deletion strategies were determined and the propagating effects of the applied inhibitors/drugs within the cell was deciphered.

In the first part of the study, thermoplastic made microfluidic devices used in cell biology and analysis is presented. Thermoplastic materials have recently been used to fabricate microfluidic platforms to perform experiments on cellular studies or environmental monitoring, with low cost disposable devices. This part describes the present state of the development and applications of microfluidic systems used in cell biology and analyses since the year 2000. Cultivation, separation/isolation, detection and analysis, and reaction studies are extensively discussed, considering only microorganisms and mammalian cell related studies in the microfluidic platforms. The advantages/disadvantages, fabrication methods, dimensions, and the purpose of creating the desired system are explained in detail.

The second part includes the experiments conducted with single phase microfluidic devices. Cyclo Olefin Polymer (COP) based microbioreactors on a microfluidic chip were produced in house by hot-embossing and thermo-compression bonding methods. The chip allows two different experiments to be performed via red fluorescent protein (RFP) tagged nucleolar Nop56 yeast cells at the same time. The results of up to 20 h long experiments are

captured by taking brightfield and fluorescent microscopy images of the trapped cells every 9-15 min. The expression of Nop56 protein was densely observed under control and drug/inhibitor environments. Hydroxyurea (HU), metformin, temsirolimus and 5-hydroxymethylfurfural (HMF) were used in the experiments.

In the third part, computational study of the thesis is shown. COBRA toolbox of MATLAB software is used to make quantitative analysis of IMM904 model (*Saccharomyces cerevisiae*) with and without HMF constraint. The link between ethanol production and growth under HMF supplied/unsupplied nutrient conditions were discussed. The fourth part represents the tumor-treating fields (TTFields) study done with yeast cells in a single phase microfluidic devices. Tumor-treating fields (TTFields) are alternating electrical fields of intermediate frequency and low intensity that can slow or inhibit tumor growth by disrupting mitosis division of cancerous cells through cell cycle proteins. In this work, for the first time, an in-house fabricated cyclo-olefin polymer made microfluidic bioreactors are integrated with Cr/Au interdigitated electrodes to test TTFields on yeast cells with fluorescent protein:Nop56 gene. A small gap between electrodes (50  $\mu\text{m}$ ) allows small voltages (<150 mV) to be applied on the cells; hence, uninsulated gold electrodes are used in the non-faradaic region without causing any electrochemical reaction at the electrode-medium interface. Electrochemical modeling as well as impedance characterization and analysis of the electrodes are done using four different cell nutrient media. Finally, transition from single phase to two phase microfluidic devices and yeast cells to mammalian cells are explained. Many screening experiments are conducted in droplet based microfluidic devices. Confined mammalian cells were monitored in an unchanging environment with the time interval of 1 h. The motivation for using droplet based microfluidic system is the fast drug screening against several diseases including cancer. THP-1 cells with green fluorescent protein (GFP) tagged ASC genes were used in the experiments with temsirolimus, rifabutin and BAY 11-7082 drugs/inhibitors.

## 2. ADVANCES IN MICROFLUIDIC DEVICES MADE FROM THERMOPLASTICS USED IN CELL BIOLOGY AND ANALYSES

Miniaturization of devices and systems by means of microfabrication technologies has become very popular in scientific advances, and micro-nanofluidics field has thus emerged. Particularly, the electronics and chemical, biological and medical fields have benefited from the developing microscale technologies. Conventional laboratory handling, processing and analytical techniques are revolutionized by the help of microfluidics. In biochemical and biomedical fields polymer-based materials are primarily used since their surface can be easily modified (Yi *et al.*, 2008).

Being composed of linear and branched molecules, the thermoplastic materials, are durable against temperature and pressure changes and they do not perform any structural breakdown. The properties/characteristics of thermoplastics used to fabricate chips are summarized in Table 2.1. Thermoplastic-based materials have good physical and chemical characteristics such as low electrical conductivity and high chemical stability, and they are suitable for mass production at low cost. Thermoplastics can be softened and let to flow by applying heat and pressure. During cooling, the softened polymer hardens and it takes the shape of the container or mold without any chemical change (Kricka *et al.*, 2002), (Ebewele 2000).

Low-cost fabrication methods for high-throughput production can be successfully used in thermoplastics made microfluidic systems. It is very important to select the material type by taking the design of the device into consideration. The compatibility of the material with the chemicals, as well as with the applied temperature and pressure, microfabrication techniques and functional components involved in the miniaturized systems should be planned in detail before constructing the microfluidic system (Nunes *et al.*, 2010). According to Table 2.1, most of the thermoplastics are biocompatible except ABS and PPO. In order to follow the changes inside the microfluidic devices under microscope, transparency of the selected material is very important. Therefore PEEK and PP are not suitable to work with. Currently, most of the experiments are conducted with fluorescently tagged molecules or cells.

The auto-fluorescence characteristic of the polymer used to create the microfluidic device can be another problem during experiments. The fabricated microfluidic device should have low auto-fluorescence to obtain reliable results. Moreover, the surface properties like hydrophobicity and gas/liquid permeabilities affect the cell adhesion and proliferation.

Table 2.1. Summary of properties for thermoplastics (Shadpour *et al.*, 2006), (Tayrac *et al.*, 2007), (Rosenzweig *et al.*, 2015), (Chang *et al.*, 2012), (Crawford *et al.*, 2015).

Thermoplastics	Thermal expansion coefficient (m/(m K)) $10^{-6}$	Young's modulus (GPa)	T <sub>g</sub> (°C)	T <sub>m</sub> (°C)	Solubility parameter $\delta$ (MPa) <sup>1/2</sup>
Cyclo olefin (co) polymer (COC/COP)	60-70	1.7-3.2	70-180	190-320	17.7
Polymethyl methacrylate (PMMA)	70-77	2.4-3.4	105	250-260	20.1
Polyethylene terephthalate (PET)	59.4	2-2.7	70	255	20.5
Polyethylene-Low density (LDPE)	100-200	0.11-0.45	-125	105-115	17.6
Polyethylene-High density (HDPE)	120	0.8	-80	120-180	18.2
Polypropylene (PP)	72-90	1.5-2	-20	160	16.3
Polystyrene (PS)	70	3-3.5	95	240	18.7
Polycarbonate (PC)	65-70	2.6	145	260-270	19.4
Polyvinyl chloride (PVC)	54-110	2.4-4.1	80	100-260	19.4
Polyamide (Nylon)	110	2.5	47-60	190-350	28
Polysulfone (PSU)	55-60	2.48	185	180-190	18.7
Polylactic acid (PLA)	740	3.5	60-65	150-160	
Polytetrafluoroethylene (PTFE)	112-135	0.4	115	326	12.6
Polyetheretherketone (PEEK)	26	4-24	143	343	21.9
Acrylonitrile butadiene styrene (ABS)	72-108	1.4-3.1	105	Amorphous	18.8

Table 2.1. Summary of properties for thermoplastics (Shadpour *et al.*, 2006), (Tayrac *et al.*, 2007), (Rosenzweig *et al.*, 2015), (Chang *et al.*, 2012), (Crawford *et al.*, 2015). (cont.)

Thermoplastics	Water absorption (%)	O <sub>2</sub> permeability	Biocompatibility	Transparency	Water absorption (%)
Cyclo olefin (co) polymer (COC/COP)	0.01	NA	Biocompatible	Transparent	Low
Polymethyl methacrylate (PMMA)	0.1-0.4	0.1	Biocompatible	Transparent	Low
Polyethylene terephthalate (PET)	0.16	0.03	Biocompatible	Transparent	Medium
Polyethylene-Low density (LDPE)	0.005-0.015	2	Biocompatible	Both opaque and transparent	Medium
Polyethylene-High density (HDPE)	0.005-0.01	0.4	Biocompatible	Both opaque and transparent	Medium
Polypropylene (PP)	0.01-0.1	1.7	Biocompatible	Both opaque and transparent	Medium
Polystyrene (PS)	0.02-0.15	2	Biocompatible	Transparent	High
Polycarbonate (PC)	0.23	1	Biocompatible	Transparent	High
Polyvinyl chloride (PVC)	0.04-0.4	0.04	Biocompatible	Transparent	High
Polyamide (Nylon)	1.6-1.9	0.03	Biocompatible	Transparent	High
Polysulfone (PSU)	0.2-0.8	NA	Biocompatible	Translucent	High
Polylactic acid (PLA)	0.68	NA	Biocompatible (problematic)	Transparent	High
Polytetrafluoroethylene (PTFE)	0.005-0.01	3	Biocompatible	Translucent	High
Polyetheretherketone (PEEK)	0.1-0.5	0.1	Biocompatible	Opaque	NA
Acrylonitrile butadiene styrene (ABS)	0.05-1.8	0.5	Not suitable	Both opaque and transparent	High

As these discussions and literature (Table 2.1) suggest, only PMMA, COP/COC and PS is left as convenient thermoplastics for cell studies. Although other thermoplastics, like PC, PET and PTFE seem to be feasible, their physical properties are not suitable for cell imaging. In this review, PMMA, COP/COC or PS made microfluidic devices, which are fabricated mainly to work with living organisms and tissues will be focused. PMMA is the most extensively used one for cell biology applications. COP/COC and PS are promising substrates. When the publications since the year 2000 are examined, more than 70% of the

research belongs to PMMA, and there are only 12 publications (9%) on COP/COC made devices used in works related to cells (WOS). Nevertheless, as will be discussed below in the following sections, COP/COC is a rising substrate for the commercialization of the thermoplastics made microfluidic devices. PMMA has chemical inertness to many solutions and solvents, and it has low auto-fluorescence background. Unfortunately, it is affected by ethanol, IPA, acetone and other important solvents used in microfabrication and sterilization. High mechanical strength, hardness and rigidity are the advantageous characteristics of the PMMA substrate. This material exhibits excellent transparency. The polishing of PMMA is also easy (Goodman 1994). It has good thermal stability and insulation properties. In addition, PMMA displays low water absorption and excellent water resistance. On average 92% of light in the visible range can pass through a typical PMMA grade. PMMA materials can be found easily at low-cost. Most importantly, PMMA is a biocompatible polymer (Industries), except when their surfaces are treated with ozone or O<sub>2</sub> plasma.

The COP/COC is a fully saturated olefin polymer and it shows very little interaction with various proteins. The material's ring structure provides high stability. COP/COC polymer has smaller Young's modulus than PMMA, and its rigidity and strength are higher. This also makes the dimensional stability property of COP/COC polymer better (Piruska *et al.*, 2005). COP/COC polymer shows resistance against acids, bases, and almost all solvents including ethanol, IPA and acetone and it has the lowest water absorbency among all plastics. This polymer's stability does not change under moisture conditions, exhibiting a good structure for microfluidic device fabrication (Yi *et al.*, 2008). The high moisture barrier of COP/COC is beneficial; when working with cell cultures, the cells are consuming oxygen of water more, instead of its absorption onto the surface of the polymers. COP/COC material shows an inert low binding surface property. The optical transmission properties and the low auto-fluorescence background signal of COP/COC is good enough to visualize the fluorescently tagged materials or cells (Nunes *et al.*, 2010). PS is widely used in molecular and cell biology studies due to its biocompatibility. Petri dishes, test tubes, microplates, and other laboratory containers are all made of PS (Abdel-Wahab *et al.*, 2017). PS has high transparency and good material rigidity, has high resistivity against alcohols, polar solvents and alkaline (Becker & Gartner 2000). The surface of PS is suitable for long-term cell studies. Despite all these appealing characteristics, the thermo-compression bonding of PS pieces has rarely been utilized, and not enough attention has been put to push the research

further into device applications. However, compared to COP/COC and PMMA it has higher background auto-fluorescence. Photolithography, oxidation, e-beam evaporation, wet etching, sputtering, injection molding, micromilling, laser ablation, CNC machining, hot embossing, and CO<sub>2</sub> laser engraving are some of the methods applied to create the patterns of microfluidic devices. Double sided adhesive, UV/ozone assisted thermal bonding, solvent assisted thermal bonding, pressure sensitive adhesive tape, laminating adhesive or thermal fusion bonding were some of the common methods to seal these devices.

So far, microfluidic devices made from thermoplastics are simple systems lacking active components such as micropumps, microvalves and sensors. Interfacial interactions play important role for the performance of the microfluidic devices. Several surface modification techniques, such as plasma or UV treatment, can be applied to the polymers to control the surface properties (Workman *et al.*, 2008). Hydrophilic surface is required to have smooth and consistent flow of analyte within the microchannels to conduct and to monitor the experiments properly. Moreover, cell or tissue interactions with biocompatible materials can be managed by biological recognition. In order to increase this biological recognition, most often proteins are coated on the surface of the device (Qiu *et al.*, 2015). For example, PC12 cell adhesion, proliferation and differentiation into a microfluidic neural interface platform were enhanced via polypeptide surface treatment (Raasch *et al.*, 2015).

In another example, biotinylated-BSA was used to treat the surface of the microfluidic device to immobilize the mother yeast cells (Xie *et al.*, 2012). We have been fabricating microfluidic devices using thermoplastic substrates like PMMA, COP/COC and PS by hot embossing, chemical etching and thermal bonding methods. These 1nL microbioreactors are successfully used for yeast culturing. Fortunately, for yeast cell cultivation, COP/COC, PMMA and PS made microfluidic devices do not require any modifications on the surface (Puza *et al.*, 2017). Cell or tissue culturing, separation, detection, analysis or reaction-production studies can be conducted in microfluidic devices by using small sample volumes.

In addition, high-throughput drug screening, single cell or molecule analysis and manipulation, drug delivery and therapeutics, biosensing, and point-of-care diagnostics are some of the biological applications that can be accomplished via these devices (Yeo *et al.*, 2011), (Becker and Heim, 2000), (Mart *et al.*, 2010), (Mauk *et al.*, 2013). Although

microfluidic devices are capable of making high-throughput screening by using small amount of consumables, commercialization of these devices is not at the desired level. This might be the result of challenges encountered such as finding adequate funding for product development and manufacturing during the commercialization steps. However, a few companies have overcome these steps, and they have introduced their products into the market. Pico-Gen Picodroplet Formation Chips by Sphere Fluidics Ltd., Multiflux by Dolomite Microfluidics or Chips by Microfluidic ChipShop are the examples of commercialized products. Microfluidic products in the market can be increased if industrial partners and academic partners can come together and reach an agreement. Moreover, as the developments increase in both bioMEMS technologies and commercialization of microfluidic equipment, real-world problems can be solved by researchers effectively at high throughput and low cost. At the end, point-of-care diagnostics, rapid, quantitative and multiplexed immunoassays, biosensors or instruments for rapid detection of pathogens can be produced more and people's problems or diseases can be resolved in an easy and fast way (Volpatti and Yetisen, 2014), (Chin *et al.*, 2012). Here, thermoplastics made microfluidic devices, that have been used to study living-organisms or tissues are described. The part includes 4 main titles, which are related to Cultivation: Organism-on-a-chip, Separation/Isolation, Detection and Analysis and Reaction: Microbial Fuel Cells in thermoplastic made microfluidic devices.

### **2.1. Cultivation: Organism-on-a-Chip**

Cells, capable of dividing and increasing in size, continue to grow when the appropriate media and conditions are available. It is generally accepted that, a single cell is a building block for human life. Every cell includes a genetic material that holds the secret to inherited diseases. The scientists have improved the methods to study the behavior of single cells. The effects of the amount and type of the nutrients, temperature, humidity and gaseous atmosphere on cells can be investigated to provide optimum cultivation conditions. The cell's response in a culture is measured to reveal the relation between other kinds of cells, carcinogenic agents or eventual drugs. Nowadays, these experiments can be conducted in a precisely controlled micro-environments, where low volume of sample and energy were needed. High-throughput screening can also be conducted in these microfluidic devices (Coriell Institute for Medical Research, 2017), (Chaudry 2021).

### 2.1.1. Culturing of Bacterial Cells

Cell culturing experiments have been conducted with several living organisms. In 2005, Szita and his colleagues have fabricated PMMA and PDMS made microbio reactors to monitor bacteria cells, *Escherichia coli* (*E. coli*). A multiplexed microbio reactor system including magnetic motors for magnetic stirring and optics to observe the optical density (OD), were used to measure the parameters, dissolved oxygen (DO) and pH, during fermentation. The microbio reactors included a reactor chamber of 2mm in height and 10mm in diameter, three microchannels of  $500\mu\text{m} \times 500\mu\text{m}$  and PDMS membrane for oxygenation. The system can make four parallel microbial fermentations (Szita *et al.*, 2005).

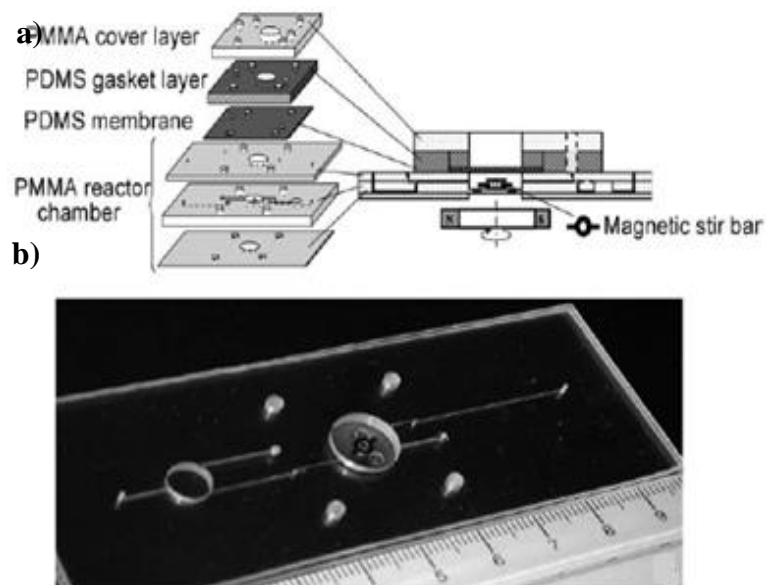


Figure 2.1. (a) Schematic view of the microfluidic system (b) Photograph of the PMMA chamber (Zhang *et al.*, 2006).

Another study with bacteria cells in polymer-based microbio reactor system is capable of measuring optical density (OD), pH and dissolved oxygen (DO) in real-time. Continuous cultivation of *Escherichia coli* (*E. coli*) was done in microbio reactor of 150 $\mu\text{L}$  volume with membrane aeration. The device consists of PMMA and PDMS layers with three connecting microchannels of 250 $\mu\text{m}$  height and 250 $\mu\text{m}$  width (Figure 2.1). The surface modification of PMMA and PDMS parts of the device was conducted via poly(ethylene glycol)-grafted poly(acrylic acid) (PAA) copolymer films to obtain bio-inert surfaces resistant to non-

specific protein adsorption and cell adhesion. This surface modification reinforced the cultivation time and prevented wall growth of the cells (Zhang *et al.*, 2006). In 2010, glass slides and polymer films were used to create the low-cost and detachable microfluidic chips by applying adhesive wax as bonding material. This biocompatible wax-based microfluidic chips were used to perform PCR tests and to culture GFP-tagged (Green fluorescence protein) *Escherichia coli* (*E. coli*) to see the effect of the antibiotic ciprofloxacin concentration on the *E. coli* migration. The fluorescence expression was found to decrease as the ciprofloxacin concentration increased in the reagent cell. Otherwise *E. coli* cells survived 15 days in the chip without any leakage (Gong *et al.*, 2010). In the same year, Skolimowski and his colleagues built a five layer microfluidic chip allowing the gas transition and examined the active oxygen depletion. Simulations were performed via COMSOL Multiphysics 3.5a to follow the relation between O<sub>2</sub> generation and measured oxygen concentration. *Pseudomonas aeruginosa* bacterium was used in the microchip to examine the growth patterns under different oxygen concentrations. GFP-tagged bacterium was allowed to grow in the flow chambers of the device.

The oxygen concentration affected the attachment of bacterium to the substrate (Skolimowski *et al.*, 2010). The drug resistance of several bacterial strains *Escherichia coli*, *Shigella flexneri*, *Shigella boydii*, *Shigella sonnei* and Uropathogenic *E. coli* were tested using Resazurin dye reduction method (RRM) as the colorimetric antibiogram in the PMMA microfluidic system and 96-well microtiter plates. PMMA device consisted of 40 microwells of 20 $\mu$ l volume, and there are microchannels of 215 $\mu$ m width and 157 $\mu$ m height in between the microwells for connection. Bacteria suspensions were inoculated into the wells both of the 96-well plates and microfluidic device. Visual and OD<sub>620</sub> results of the microfluidic system and 96-well microtiter plates were compared with the standard turbidity tests. The data obtained from both systems were compatible with each other, so the developed microfluidic device can be used in the determination of antibiogram of the drug-resistant bacteria (Elavarasan *et al.*, 2013).

Recently, the determination of *Escherichia coli* K12 concentration was done by using positively and negatively charged electrospun poly(vinyl alcohol) (PVA) nanofibers in PMMA made microchannels. Fiber distribution and fiber mat height on analyte retention were also examined. In order to have large surface area for analyte concentration and to

obstruct size-related retention of the *E. coli* cells, the 3D morphology of the mats was improved. The device had four parallel microchannels of 42 $\mu$ m height, 1mm width and 20mm length. Positively charged nanofibers showed better performance than the negatively charged ones. Then, the negatively charged nanofibers were customized with anti-*E.coli* antibodies, and consequently they became capable of specific capture of the bacterial cells (Matlock-colangelo *et al.*, 2016).

### 2.1.2. Fungi Cultivation

PMMA made microfluidic devices were also employed for fungi cultivation. As a new approach for the cultivation, monodispersed agar beads were produced by using a temperature-controlled microfluidic device with 5 layers. The dimensions of the agar beads were determined by the flow, which can be dispersed or continuous (Figure 2.2). These agar beads were used as the substrate for the *Cordyceps militaris* cells. This technology is seen as a promising one because several experiments can be performed, like encapsulating biomaterials, enzymes, drugs into agar beads, for biomedical applications (Lin *et al.*, 2011). In another study on fungal and bacterial cells, Bolic *et al.* developed a milliliter-scale bioreactor (0.5-2mL volume) consisting of gas connections, heater, temperature sensor, optical fibers, magnetic stirrer and optical sensors. pH, dissolved oxygen and optical density can be measured and the system is capable of aeration and mixing. The performance of the device was evaluated by considering mixing time, residence time distribution and oxygen transfer rates at several conditions.

The mixing time was determined as 0.4 s – 2 s, and the oxygen transfer rate was 1000 h<sup>-1</sup>. Bacterial and yeast cells (*Lactobacillus paracasei* and *Saccharomyces cerevisiae* cells) were successfully cultivated in the device (Bolic *et al.*, 2016). By using ultrasonic hot embossing and welding techniques, microfluidic devices made from PC were fabricated and the functionality of these devices was shown via yeast cultivation experiments. Cells survived at least 22h in the device and enhanced green fluorescent protein (eGFP) expression was observed with a supply of the inducer galactose. It is proven that, ultrasonic processing can be used for microfluidic device fabrication mostly in the future to conduct microbial analysis (Runge *et al.*, 2017).

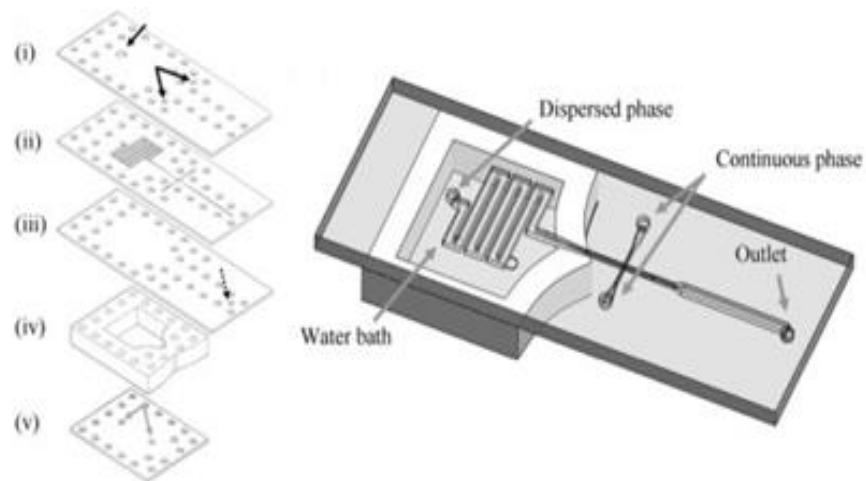


Figure 2.2. The 5 layers of the microfluidic device and assembled view of the temperature-controlled chip (Lin *et al.*, 2011).

### 2.1.3. Zebra Fish Cultivation

The zebrafish is the mostly used vertebrate model organism in scientific studies. Zebrafish (*Danio rerio*), which can be used for drug research and environmental toxicology studies, was investigated for its developmental analysis in 3D multilayer microfluidic system. By using this system, one embryo can be kept in one trap and each of these embryos can be encoded. In large scale, it is possible to make high-throughput docking and recovery of single embryos. The device included conical traps of 2mm in diameter at the top plane and 1.6mm in diameter at the bottom plane.

Heating manifold and a piezo-electric ultrasonic micropump were combined within the device. Wild type and GFP tagged Tg(fli1a:EGFP) zebrafish embryos were trapped, and kept for 3 days via active suction-based immobilization and then analyzed. 100% trapping of the cells was attained successfully, and these cells kept their positions during the 72h experiments. This system can also be adapted to the kinetic analysis of pharmacological agents prohibiting blood vessel growth (angiogenesis) in zebrafish (Akagi *et al.*, 2012, Akagi *et al.*, 2013a). In 2013, another PMMA made microfluidic device for zebrafish was developed, and the environmental Scanning Electron Microscope (ESEM) imaging was used to observe the zebrafish larvae. There were an engraved reservoir (6 mm x 6 mm x 0.5 mm), 36 circular microwells (0.75mm diameter and 0.5mm height) and 6 microchannels (10 mm

x 0.3 mm x 0.75 mm) in the chip. The reservoir with the multiple semispherical microwells, located in the device, was to keep the larvae and to drain the excess medium. In order to activate the device, a paper filter was used, and the trapping of the larvae was achieved by the suction of the cells due to water drainage. This microfluidic system was important for the ESEM imaging for prospective laser microsurgery and tissue regeneration. However, the experiments were not successful due to the damaged tissues under low vacuum environment, and more optimization was needed to make ESEM imaging without tissue damaging (Akagi *et al.*, 2013b).

In 2014, Akagi *et al.* developed another microfluidic system to trap and immobilize the transgenic zebrafish embryos with the help of low-pressure suction. The PMMA made microchip platform consisted of piezoelectric microdiaphragm pumps, embryo-trapping suction manifold, drug delivery manifold and tin oxide heating element. Gambit 2.3 and Finite-volume-based Fluent 6.3 softwares were used for computational fluid dynamics (CFD) simulations. Embryo loading and recovery were done in the main channel (1.7mm × 1.5mm × 55mm), single embryo trapping and immobilization were conducted in an array of 16 traps, and the drug delivery was done via a drug delivery channel (1mm × 0.5mm × 120mm). This system was capable of making rapid and automated manipulation of zebrafish cells for drug discovery (Akagi *et al.*, 2014). A year later, Akagi and his group improved their microfluidic system and this system was able to reveal the morphological features of the zebrafish larvae by employing ESEM imaging technology. Microwells were used to keep the yolk of the zebrafish larvae and microchannels were used to provide immobilization of the larvae (Akagi *et al.*, 2015).

In another study on zebrafish, continuous flow embryo sorter device capable of analyzing, sorting and dispensing of the zebrafish embryos was developed. In order to actuate the system, DC gearmotors with a D-shaped output shaft (3mm diameter) was integrated to the system. In the main body of the device, a rectangular channel (1.5mm width and 1.7mm height) for embryo loading, sorter wheel (20mm diameter) and suction manifold (0.5mm width and 1.8mm height) for keeping the embryos in position during the rotation were located, whereas in the 3D printed part, DC motor and stainless steel ball bearings (5mm diameter and 7mm thickness) were present. By this study, a new concept for rapid and automated zebrafish embryos sorting device was introduced (Fuad, and Wlodkowic 2013).

Electronic interface integrated Lab-on-a-chip biomicrofluidic device was used to make automatic immobilization, cultivation and treatment of zebrafish embryos. The design and optimization of the microfluidic device were done with Gambit 2.3 CFD simulation program. Main channel for embryo loading ( $1.7\text{mm} \times 1.5\text{mm} \times 55\text{mm}$  dimensions), 20 traps for embryo trapping and immobilization, and a plenum suction manifold of 0.7mm height for creating the drag force to immobilize the cells were located within the device. Field Programmable Gate Array (FPGA) hardware/software controlled the cell loading and immobilization, flow dynamics, temperature and image acquisition of zebrafish embryos (Wang *et al.*, 2013). Furthermore, Zhu et al. (2013) fabricated a minimized high-throughput Lab-on-a-Chip microfluidic device to perform fish embryo toxicity (FET) assay. The device had 96-well microtiter plate, main loading channel ( $68\text{mm} \times 1.8\text{mm} \times 1\text{mm}$ ) and 21 miniaturized embryo traps ( $1.5\text{mm} \times 1\text{mm}$ ). Gambit 2.3 and Finite-volume based Fluent 6.3 softwares were used to run CFD simulations. Rapid loading, separating, immobilizing of the zebrafish cells in the traps, providing continuous perfusion and live imaging were done with this 3D device. The off-chip interface carried peristaltic pumps, USB-imaging station and ITO heaters. In addition, anti-angiogenesis drug tests were performed in this device, and the image acquisition was done with an imaging cytometer (Zhu *et al.*, 2012). Fluorescence Ratiometric Imaging (FRIM) technology was employed to develop the zebrafish embryos in a microfluidic device. FRIM technology can make the kinetic quantification of the aqueous oxygen gradients, and the oxygen consumption of the cells can be measured. The device included a main loading channel of  $52\text{mm} \times 1.8\text{mm} \times 1\text{mm}$  dimensions for embryo loading and toxicant transportation, 18 embryo traps of  $1.5\text{mm} \times 1\text{mm}$  sizes for trapping and immobilization, a suction manifold with the interconnecting channels ( $0.3\text{mm} \times 1.6\text{mm} \times 0.5\text{mm}$ ) and a sensing manifold with Presens Sensor Foils. This microfluidic system can be used to reveal the metabolism and physiology of the cells in the future (Zhu *et al.*, 2015).

#### **2.1.4. Fruit Fly (*Drosophila*) Cultivation**

In 2016, a PMMA made microfluidic device for *Drosophila* was fabricated to study the actions of the flies in the system. In the device, the chambers with visual and auditory stimuli were used to manage the liquid food presentations. A behavior chamber ( $20\text{mm} \times 15\text{mm} \times 2\text{mm}$  dimensions) and a feeding alcove ( $400\mu\text{m}$  width) were placed in the chip for flies to feed from a microchannel ( $200\mu\text{m}$  width and  $50\mu\text{m}$  height). The behavior of the flies

and microfluidic food channel were video recorded. According to the repeated experiments, the flies learned to access the food in a more direct way (Navawongse *et al.*, 2016).

### 2.1.5. Mammalian Cell Cultivation

There are many microfluidic device studies in the literature using human cells. More than a decade ago, a co-culture system was implemented in a microfluidic environment to study the co-cultured cell behavior. The height and width of the trenches placed in the device was 20 $\mu$ m. Using human U937 and MG-63 cell lines, monitoring of real-time cytokines release and non-contact co-culturing processes were accomplished in this system (Wei *et al.*, 2006). For cell and tissue culturing experiments, PMMA, PS, PC and COC substrates were investigated as the biocompatible materials alternative to PDMS. In order to decrease the adsorption of hydrophobic compounds, UV-generated ozone or oxygen plasma surface treatments were done on the polymer substrates. The validity of the surface treatment was evaluated via contact angle of water on the surface. In order to reveal the biocompatibility, human hepatoma (HepG2) cells were used on the treated surfaces of the microfluidic chips (culture chambers of 4mm diameter  $\times$  200 $\mu$ m). After cultivation of the cells on well-plates, they were exposed to acridine orange and propidium iodide solutions for viability tests.

PDMS and PMMA showed a lower recovery of the hydrophobic compounds. After surface treatment, HepG2 cells were stuck to the PMMA substrate due to the unstable peroxides on the PMMA surface after the treatment. PC and COC chips showed good performance about gas permeability and COC is better than PC due to its lower auto-fluorescence. Overall, PC and COC chips were mostly suitable for incorporation of cells and tissues (van Midwoud *et al.*, 2012). Dissolved oxygen (DO) level is very important for the cells used in the tissue engineering applications. Shear-stress acting on the cells may give information about the DO level. Using HT1080 cells the transportation of the oxygen through the fabricated microbioreactor was first investigated, then low-shear stress at the cell level and oxygen tension of the materials and dimensions were regulated. There were two channels inside the microbioreactors, one of them is the culture channel of 4cm  $\times$  300 $\mu$ m  $\times$  300 $\mu$ m (L  $\times$  W  $\times$  H) dimensions placed in the bottom sheet, and the other one is the oxygen supply channel of 5cm  $\times$  300 $\mu$ m  $\times$  1mm (L  $\times$  W  $\times$  H) dimensions on the top plate. There was a silicone rubber sheet in between these channels and the device was sealed with the

biocompatible double sided adhesive tape. The number of cells and their viability (Fluorescent live/dead staining), cell density and the circularity of the cells were investigated (Abaci *et al.*, 2012). HEK-293T cells were cultivated in PDMS and PMMA microfluidic devices to reveal the optimum conditions for growth under several experimental conditions such as with or without the cell adhesion agent poly-D-lysine. Microchannel geometries, thicknesses and flow rates in the devices were also evaluated. The PMMA chip had three distinct microchannel structures (linear, zigzag and square waves) of 40 $\mu$ m height  $\times$  0.4mm width and 3.68 $\mu$ L volume. The other chip had 40 $\mu$ m height with serpentine structures of 100 $\mu$ m width. The length changed between 10 and 80mm and the volume was 17.8 $\mu$ L. poly-D-lysine increased the cell adhesion and viability under continuous or discontinuous flow. Cell adhesion was mostly seen in the corners of the microchannels and in large channels due to lower flow rate. This recent study provides an insight into the future works on microbio-reactor design (Penaherrera *et al.*, 2016). In 2009, the hard top-soft bottom microfluidic devices were fabricated by combining the advantages of elastomeric devices with the rigid plastic devices. The polyethylene terephthalate glycol (PETG), cyclic olefin copolymer (COC) or PS were used as hard tops and the channels were imprinted by hot embossing. The hard tops were bonded to elastomeric PDMS or polyurethane (PU). The device included an X region and the height of this area was 200 $\mu$ m while the height of other channels was 30 $\mu$ m.

HepG2 cells and C2C12 cells were cultured in the devices, and it was observed that the cell survival was  $\sim$ 100% (Mehta *et al.*, 2009). A microfluidic device made of polytetrafluoroethylene (PTFE) was fabricated to conduct the encapsulation of living, therapeutically-active cells within monodisperse alginate microspheres. HEK293, U-2 OS and PC12 cell lines (GFP tagged) were successfully encapsulated and loss of cell viability was minimum. High and medium guluronic acid concentrated alginate samples were more applicable to micro-reaction processes (Workman *et al.*, 2008). Due to limited functions of PDMS polymer, conventional plastics are used to rapidly prototype microfluidic systems. Thermal scribing, one-step fabrication method, was used to produce the PS made microfluidic devices. The applicability of the system was shown via induction of functional neutrophil extracellular traps (NETs). The experiments were helpful to understand the mechanism of neutrophil culture systems (Chandrasekaran *et al.*, 2017). Nanoparticle (NP) study is very popular in scientific research. NPs find place in potential applications of

biomedical, optical and electronic fields. NPs build a bridge between the bulk materials and atomic or molecular structures, and they provide high specific surface area, high reactivity and rapid diffusion (Nomura *et al.*, 2013). Koh *et al.* (2010) worked with NPs to examine the Bcl-2 down-regulation at the mRNA and protein levels with cellular uptake and apoptosis by using K562 human erythroleukemia cells and G3139 as the drug, and they produced a multi-inlet microfluidic hydrodynamic focusing (MF) system. The MF chip had a microchannel of 254 $\mu$ m width and 150 $\mu$ m height.

The lipopolyplex (LP) nanoparticles produced via MF method were smaller than those produced by bulk mixing (BM) method. In addition, Bcl-2 antisense uptake was higher in MF LP nanoparticles and these nanoparticles were more influential in down-regulation of Bcl-2 protein level than the BM LP nanoparticles (Koh *et al.*, 2010). In order to increase the transmission of exogenous oligonucleotides (ODN) *in vitro*, the semi-continuous flow electroporation (SFE) chip was used with the liposome nanoparticles (LNs) containing the target ligand. K562 cells and transferrin-targeted lipoplex encapsulating ODN G3139 nanoparticles were mixed and incubated to increase the nanoparticle binding. In the fabricated microchip, electric pulses were applied during the mixture flow through the channel. By using micromilling machine, aluminum piece was cut into two halves to construct the serpentine channel and these Al pieces were used as both electrodes and channel walls in SFE. Since electroporation application makes cell membranes permeable, ODN transmission efficiency was higher when the non-targeted LNs and SFE were combined rather than utilizing targeted LNs alone (Wang *et al.*, 2010).

2.1.5.1. 3D Culturing. Nowadays, cell cultures are created in 3D environment to imitate the *in vivo* conditions. 3D cultured cells are more reminiscent of the native tissue from which they originated. They can conceive more elaborate extracellular matrix and better intercellular communication (Ravi *et al.*, 2015), (Fey and Wrzesinski, 2013). 3D cultured cells are independent of the cell density in contrast to 2D cultured cells. 3-dimensional (3D) cell culture-based chemosensitivity assay was performed in the microfluidic cell culture chip, which contained 36 microbioreactors of 1.5mm diameter and 1mm height. Human colorectal adenocarcinoma cells were loaded to the microfluidic device to obtain information about the micro-scale perfusion of 3D cell culture and chemosensitivity assay. This platform

provides stable, well-defined and biologically more relevant culture environment to perform high-precision and high-throughput 3D cell-culture based assay (Wu *et al.*, 2011).

Huang *et al.* (2013) developed another high-throughput 3D microfluidic cell culture system including 30 microbioreactors. The system was capable of implementing durable thermal conditions for cell culturing and efficient sample loading, and contained multiple medium perfusion mechanisms with waste medium collector for bioassays. The microchannels of 2.3mm length, 0.5mm width and 1.5mm height were used to deliver the medium to the microbioreactors. The other medium microchannels (5.4mm length, 0.1mm width and 0.1mm height) were used to send the medium to the waste reservoirs (diameter: 3.6mm and height: 2.5mm). In the fabricated device, chemosensitivity assay, the DNA content detection (via fluorescence labeling) and viability experiments were conducted by using human oral cancer cell line (OEC-M1) (Huang *et al.*, 2013a). High-throughput 3D cell culture, drug administration and quantitative in situ assays were conducted in a micro-scaffold array system. The microfluidic device included sponge-like micro-scaffolds for absorption of cell or drug loading as well as for avoiding cell loss during medium exchange. The device had 96 microwell array with 2mm diameter on the top layer for culture and drug medium, and had smaller 96 microwell array with 1.5mm diameter on the bottom layer for 3D cell culture. RFP-labeled NIH3T3 fibroblasts, human fibrosarcoma cells (HT1080), human hepatocellular carcinoma cells (HepG2) and human non-small lung cancer cells (NCI-H460) were cultured in this device, and the cells were stained with fluorescence for imaging. In this system, cancer cells showed higher drug resistance than those on the planar high-density multiwall plates (2D). These 3D cultured cells were independent of the cell density in contrast to 2D cultured cells (Li *et al.*, 2014). Nery *et al.* developed flow-through sensor array to perform cell viability and cell toxicity tests in a microbioreactor system. Cell toxicity experiments were conducted with A549 cells treated with 1,4-dioxane and 5-fluorouracil. COMSOL Multiphysics program was used to run the simulations of the designed system. The device included several layers; PMMA layer consisting of a microchannel, PDMS layer and PCB sensor array. In order to enhance the functionality of the device, the rectangular obstacles of 0.35mm  $\times$  1.2mm dimensions were placed in the microchannel (0.8mm width and 0.35mm height). The comparison of the system with the standard methods indicated that this system can be successfully used to carry out cell culture monitoring and drug testing experiments after toxic treatment (Nery *et al.*, 2014).

2.1.5.2. Electric Field-based Microfluidic Systems. Electrophoresis, electroosmosis or electroporation are generally applied to manipulate the biological cells and record their responses (Cemazar *et al.*, 2013). An electrotaxis study was conducted in a microfluidic cell culture chip. Two types of chips were used: The single-field chip (SFC) consisted of only one microchannel of 3000 $\mu\text{m}$  width, 70 $\mu\text{m}$  height and 15mm length. The multi-field electrostatic chip (MFC) included a cell culture microchannel of 24mm length, having three segments of 5000 $\mu\text{m}$ , 1667 $\mu\text{m}$ , and 1000 $\mu\text{m}$  dimensions. In SFC, three distinct electric fields (EFs) were applied and the cellular response was recorded. Numerical simulation was done via CFD-ACE+ software and the results were compared with those of the measured ones. In the MFC chip, CL1-5 and CL1-0 lung cancer cell lines were used, and these two cancer cell lines gave distinct answers under different EFs (Huang *et al.*, 2009). Multilayer contactless dielectrophoresis (cDEP) system was developed, where sample and electrode channels were placed on different layers.

Several simulations were performed via COMSOL and the results were validated experimentally. The developed device had identical characteristics with the other cDEP devices and capable of increasing fluid throughput. The limiting elements in these devices were the breakdown voltage of the barrier material and the capability of producing high-voltage/high-frequency signals. Fluid electrode channels were placed perpendicularly on the top and bottom of the sample channel (in one end) which was made of 900 $\mu\text{m}$  thick PMMA. PC film layers were used to separate the fluid electrodes from the sample channel which had 850 $\mu\text{m}$  saw tooth structures. The ultimate aim was to immobilize the cells in the saw tooth structure with the application of the electric field. When the electric field was applied, individual cells (MDA-MB-231 human breast cells) began to create the pearl chains, and they travel through the saw tooth structure for trapping. The difference of this device from other devices was that the fluid electrodes and the sample channels were separated from each other by a thin film (Sano *et al.*, 2012). For cell trapping, a stable electrode with a salt bridge was combined with the microfluidic sensor chip. HEK293 cells were used in this system and the PMMA device of 8-10 $\mu\text{m}$  depth was fabricated. By using FIB milling, the micropores of 1.5-2 $\mu\text{m}$  in diameter were created at the middle of the cell trapping area to form the incubation-type planar patch clamp. The laser-induced channel currents of channel rhodopsin wide receiver (ChRWR) expressing HEK 293 sensor cell was measured. The results were compared with the pipette patch clamp design, and they were found to be

compatible with each other (Uno *et al.*, 2014). In another study, PMMA cell culture microchip and a multichannel lens-free CMOS (complementary metal-oxide semiconductor) / LED imaging system were combined to monitor the cell growth. LabVIEW program was used to manage the CMOS/LED imaging system.

The microchip includes a circular hole of 6 mm in radius for cell loading, a circular mixing chamber of 5mm in radius, a circular medium chamber of 3mm in radius and a rectangular cell culture chamber of 8mm × 6mm dimensions. HepG2 cancer cells were tested in this system, and cytotoxicity experiments were conducted by using cyclophosphamide solution at several concentrations. Cell proliferation in the device was monitored, and cell growth was successfully obtained under different environmental conditions (Chang *et al.*, 2015). In the same year, 1D scanning detector and a parallel array of flow channels were coupled to create the parallel microfluidic cytometer (PMC) for cell screening assays. A live-cell translocation assay using a NF- $\kappa$ B/GFP fusion protein in Chinese hamster ovary cells, CD3/CD28 receptor capping in Jurkat cells and nuclear translocation of NF- $\kappa$ B in Jurkat T-cells employing antibody label were successfully cultured in this system (Cheung *et al.*, 2015). Micro-optical tweezers ( $\mu$ OT) were combined with microfluidic device for trapping as well as for accomplishing the mechanical and chemical spectroscopic analyses of the cells. The microfluidic device was made of hybrid PMMA and glass, and  $\mu$ OT achieved the trapping and exciting the Raman and fluorescence response of the cells. Microprism reflectors were created by Two Photon Lithography (TPL) on the fibre facets to make optical trapping inside the microfluidic device. The channels in the device had 60 $\mu$ m height, 1mm width and 2cm long. Red blood cells (RBCs) and tumor cells were used in the system, and the device was capable of the trapping cells by setting the power output at each prism at 5mW. In addition, monitoring of the single cell response with different environmental stress can be conducted (Liberale *et al.*, 2013). There are several advantages of using microfluidic devices for culturing experiments. Most importantly, scientists can make high-throughput analysis by using a single device. These devices allow to conduct parallel experiments. Experimental conditions such as temperature, cultivation time, and oxygen or pH level settings can be arranged more precisely. In order to monitor the cell growth during cultivation, several imaging technologies, i.e. ESEM or FRIM, can be integrated to the microfluidic devices. Rapid loading, separating, immobilizing of cells and continuous perfusion through the device can be realized in an easy way. Cell manipulation and cell

response observations can be made instantly via these microfluidic devices. In vivo conditions can be created in the 3D culturing chips, and experiments can be done in a stable, well defined and biologically relevant culture environment to obtain high-precision and high-throughput.

### **2.1.6. Tissue Engineering (TE)**

Since the beginning of the 21<sup>st</sup> century bio-based materials have been used in many research fields. Healthcare facilities need continuous innovations and the engineering applications in new materials contributes to the development of such innovations. According to the statistics, 100,000 people are on the donor waiting list and 22 people on the average die every day due to insufficiency in organ or tissue. Over the past decade, tissue engineering has made subtle progress in finding solutions to these problems. The field of TE combines notion of materials science, engineering, medicine and biology to improve cells, tissues and organs performance (Bedian *et al.*, 2017), (Gershlak *et al.*, 2017), (Limongi *et al.*, 2017). First tissue engineering study involving PMMA in microfield was developed by Dalby and his colleagues. The reaction between primary human osteoprogenitor cell populations and nanotopographies of 10nm in size was examined. Colloidal lithography and polymer demixing on silicon was used to generate the topographies and then they were hot embossed on PMMA. Cell morphology, cell cytoskeleton, adhesion formation, cell growth and differentiation were studied using human bone marrow cells (Dalby *et al.*, 2006). The microfabrication and microcontact printing methods were combined to create a spherical organoid (spheroid) microarray culture system. Cylindrical cavities of 300 $\mu$ m diameter were placed in the chip and these cavities were characterized as either supporter or inhibitor of the cell adhesion. Collagen (Col) and polyethylene glycol were used to generate the adhesive and non-adhesive regions in the chip, respectively. Primary hepatocytes were produced as identical spheroids in the middle of the cavities, and hepatocytes were produced as the cuboidal shaped organoids, similar to the in vivo experiments (Fukuda *et al.*, 2006).

The chitosan microfibers coated with the collagen are necessary for cell cultivation, and can be produced in PMMA made microfluidic devices. One of these devices was fabricated with 45 $^{\circ}$  cross-junction microchannel (200 $\mu$ m width and the 1.5mm height) to pass the chitosan solution and sodium tripolyphosphate (STPP). Hydrodynamic focusing

was used to create the laminar flow. Schwann cells and fibroblast cells were cultured in these chitosan microfibers, which create satisfying environment for the cells. In tissue engineering applications, they can be used as the scaffold for cell cultures (Yeh *et al.*, 2010). In the study on prosthetic cornea matter, PMMA was treated by the help of polydopamine-based adhesive surface chemistry for the improvement of the biointegration of soft tissues. Polydopamine (PDA) treatment with cell adhesive peptide RGD (PDA-PEG-RGD) increased the corneal epithelial cell proliferation and keratocytes. Adhesion to the collagen gels was achieved by PDA but was not achieved by PDA-PEG-RGD and untreated PMMA.

When the subcutaneous implantation was applied, tissue reaction to polydopamine-coated surfaces was benevolent even after 45 days. Tissue integration of implants with soft tissues can be operated with polydopamine-based surface chemistries (Jeong *et al.*, 2011). Microengineering of vascular structures were also investigated in microfield studies by the combination of self-assembled monolayer (SAM)-based cell transfer and gelatin methacrylate hydrogel photopatterning methods. Two SAM desorption tools, which are photoinduced and electrochemically triggered, were displayed during the transfer of human umbilical vein cell (HUVEC) from oligopeptide SAM-coated surfaces to the hydrogel. In order to generate the microvascular structure, a perfusion culture chamber made of PMMA was used. This study can be seen as a good start for more complex, vascularized tissue constructs for regenerative medicine and tissue engineering applications with the combination of SAM-based cell transfer and hydrogel photocrosslinking (Sadr *et al.*, 2011). Microfluidic hydrogels with helical microchannels were produced and their perfusion features were evaluated both experimentally and numerically (COMSOL Multiphysics V4.2). Helical microchannels and straight microchannels were compared with each other by means of cell viability and post-encapsulation. The cooled agarose solution was injected into the PMMA chamber, fabricated via laser etcher. The chamber has 24mm × 12mm × 5mm inner dimension with 2.5mm hole. In order to have different sized helical microchannels several helical springs were employed. Rhodamine B solution and NIH 3T3 cell line were used to reveal the diffusion property and the cell viability under perfusion culture of microfluidic hydrogels, respectively. Helical microchannels were better than straight microchannels in perfusion ability and oxygen and nutrient delivery to cells (Huang *et al.*, 2013b). Two different kinds of nanoengineered polystyrene surfaces (NPS), including nanopillar (NPS-Pi) or nanopore (NPS-Po) were fabricated to study the topographical effects

of surfaces on MC3T3-E1 cells. When compared with the flat substrates, NPS has serious effects on cells in terms of cell morphology, attachment, proliferation and osteogenic differentiation. In addition, cell proliferation and osteogenesis differentiation were better in NPS-Po (Cha *et al.*, 2013). By using microinjection molding technique, osteoinductive micro-pillared PS surfaces were fabricated for bone replacement operations. Micro topography parameters, pillars diameter, aspect ratio and spacing, were evaluated according to MC3T3-E1 cell adhesion and proliferation criteria after 1, 3 and 7 days from seeding. It is observed that, micro-pillared surfaces were better than flat surfaces (Lucchetta *et al.*, 2015).

In 2013, another study on tissue engineering was done by Sivashankar et al. 3D microfluidic system capable of continuous perfusion was established to monitor the liver tissue cultures. The microfluidic device includes PMMA microbioreactors which were connected with each other, and poly(ethylene glycol) diacrylate (PEG-DA) microstructures with mesothelial cells were placed in these microbioreactors. The major roles of the mesothelial cells were to contribute to adhesive surface and help tissue repair. Hematoxylin and eosin (H&E) staining method was used to stain the tissue parts, and terminal deoxynucleotide transferase (dUTP) nick end labeling (TUNEL) assay was utilized to monitor the DNA fragments. The liver tissue conserved its viability after twelve days of culture (Sivashankar *et al.*, 2013). Primary human alveolar bone osteoblasts (PHABO) morphogenesis was investigated in both microchip-based 3D-static conditions and 3D-fluid flow-mediated biomechanical stimulation in perfusion bioreactors. The morphogenesis of the PHABO was evaluated by respective imaging, fluorescence based live/dead staining, SEM and time-lapse imaging techniques. Cubic microcavities of 300 $\mu\text{m}$  length was placed in the microstructured area of 10mm  $\times$  10mm in the PMMA made microfluidic device. In static cultures and fluid-flow mediated cultures PHABO showed different morphogenesis, and mechanobiological studies under hard tissue-specific environments stimulate the osteoblasts to bone phenotype (Altmann *et al.*, 2014). In 2013, mechanical microconnector system (mMS) was created to regulate the retracted spinal cord stumps. This system was made of PMMA to fill the spinal cord tissue gap after transection. Two discs consisted of 55 small (265 $\mu\text{m}$  inner diameter) and 15 large honeycombs (550 $\mu\text{m}$  inner diameter). The spinal cord stumps were sent through the honeycomb-structured holes by the negative pressure utilization at the outlet tubing system of the mMS and these stumps kept their location in the

mMS walls. Axonal regrowth was achieved after 2, 5 and 19 weeks with the mMS, and in-bleeding or cyst was not observed (Brazda *et al.*, 2013). In 2015, a new cell line was created by combining spheroids and tissues in microfluidic device without need of scaffolds or metabolic biosynthesis. Liposome fusion, bio-orthogonal chemistry, and cell surface engineering were used in the device by taking the advantage of click chemistry. The device has Y-shaped channel to mix the cell suspensions including C3H10T1/2 stem cells. The dimensions of the parabolic channels are 170 $\mu$ m width, 200 $\mu$ m height and 1.5cm length. By using this system, bio-orthogonal chemical groups with the help of click chemistry was created in a rapid, straightforward and flexible way (Brien *et al.*, 2015).

In another bone-related study, several parameter effects on the vascularization of bone-mimicking tissues were investigated. The design aims to create a link between the macroscale and microscale tissue engineering studies. Here, the effect of endothelial cell (EC) density, cell ratio among ECs, mesenchymal stem cells (MSCs) and osteo-differentiated MSCs, culture medium, hydrogel type and tissue geometry parameters were researched. The geometry and oxygen gradient of the hydrogels were optimized by using computational simulations (Rhinceros and COMSOL), and the analyses of microvascular network features were done. Mcells/ml ECs, 10:1:0 cell ratio, osteo-medium,  $2 \times 2 \times 5$ mm<sup>3</sup> cage and 2.5 mg/ml fibrin (60%) + collagen (40%) hydrogels were the best choices to produce bone-mimicking pre-vascularized matrices. Isolation of specific cellular populations and genetic analyses can be conducted in this system (Bersini *et al.*, 2016). Although PDMS is a preferred polymer for cell-based research, it has adverse effects on cells due to high gas permeability and surface hydrophobicity of the material. Therefore, the performance of a PS made microfluidic device was tested by using PS substrate of 1.2 mm thickness and compared to that of PDMS. In this process, COP (at the bottom) and cellulose acetate (CA) were used to flatten the surface and prevent adhesion between PS and COP, respectively. Human umbilical vein endothelial cells (HUVEC) culturing in one application and blood neutrophil under chemoattractant exposure observation in another application were conducted. The results showed that, PS made microfluidic devices can be used for long-term cell studies (Young *et al.*, 2011). A microfluidic platform with improved 3D gel capabilities, controlled surface properties and better high-volume functions was produced in COC via commercially-viable fabrication methods. Human microvascular endothelial cells (hMVECs) were used in the experiments and the results showed that COC has no negative

effect on cells like PDMS devices (Jeon *et al.*, 2011). Multi-organ-tissue-flow (MOTiF) biochip including a perfusable membrane was constructed in COC to be used in cell culture experiments. Nutrition medium supply, catabolic cell metabolites removal and shear stress application on endothelial cells (ECs) can be achieved. The results obtained on cell viability, EC marker protein expression and adhesion of ECs under low and high shear stress environment were compared with the two-dimensionally perfused flow chambers under stable environment. MOTiF biochip provided higher cellular density in monolayer with increased cell layer thickness (Raasch *et al.*, 2015). Body-on-a-chip device was also produced to imitate the drug distribution and metabolism processes in the body.

Pumpless 14 chamber (chambers were considered as distinct organs) microfluidic cell culture device was fabricated to conduct the separation between the barrier and nonbarrier cell cultures as well as to reveal the interactive responses between the cell lines. A549 (liver) and Caco2 (GI) represented the barrier lines and HepG2 C3A (liver), Meg01 (bone marrow) and HK2 (kidney) represented the nonbarrier lines. The device comprised of polycarbonate frame, 0.5mm thick two layers silicon gaskets for cell/organ chambers, 0.25mm thick two layers of PMMA gaskets for channels, porous PC membrane and 1.6mm thick silicone gaskets. Cell lines lived 7 days in the device. By using this system, the usefulness of building, managing and cultivating of multi-organ microphysiological system was proved (Miller and Shuler, 2016).

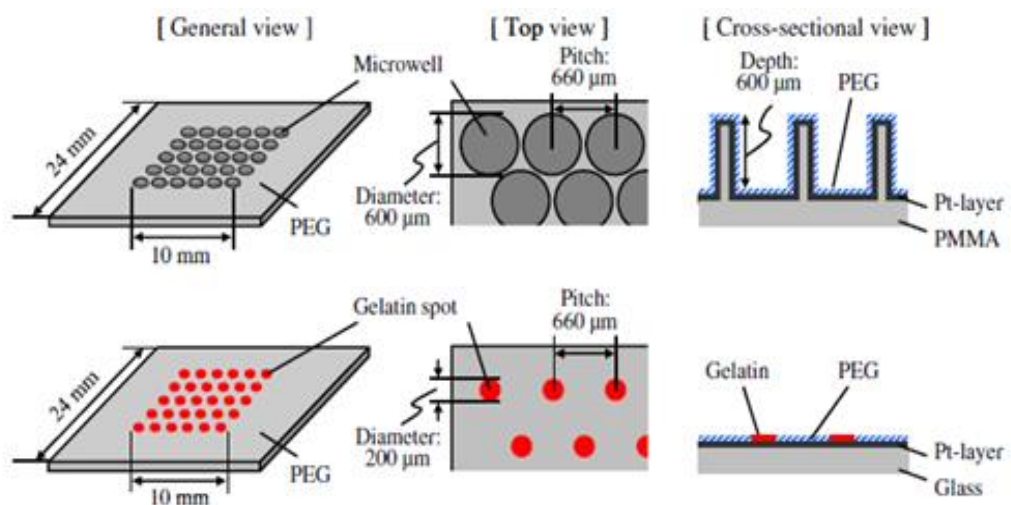


Figure 2.3. Microwell designed chip (top) and micropatterned chip (bottom) (Sakai *et al.*, 2011a).

Microwell chip and micropatterned chip were operated and compared by monitoring the proliferation and differentiation characteristics of the embryoid bodies (EB) obtained from the mouse embryonic stem (ES) cells (Figure 2.3). The microwell chip had 270 microwells (each 600 $\mu$ m in diameter and depth). In order to coat the surface with PEG, the chip was immersed into the 50% ethanol solution of 2.5mM PEG with a thiol group. For the micropatterned chip, 270 gelatin spots (200 $\mu$ m in diameter) were created on the glass substrate via microcontact printing. The remaining area was again coated with PEG to increase the nonadhesive property. High cell growth rate and expression of the endotherm as well as an increment in the mesoderm markers were seen in the EBs in the micropatterned chip. The proliferation and differentiation of the EBs may vary from design to design (Sakai *et al.*, 2011a). Another microdevice was developed to produce spheroids with almost the same size, and this device was capable of transferring these spheroids from floating situation to a micropatterned adherent culture. 270 microwells, which were PEG treated to obtain the nonadhesive surface, were located on the PMMA frame and PDMS sheet.

On the PMMA frame, the microwells (600 $\mu$ m diameter, depth and pitch sizes) were created via programmable micro-milling technology. On the bottom of the PMMA frame, PDMS of 400  $\mu$ m thickness was bonded. In this study, first mouse ES cells and then 3T3 cells, HepG2 cells, primary rat hepatocytes were sequentially produced as spheroids in each microwell chip. This technology can be auspicious in spheroid studies (Sakai and Nakazawa, 2011b). The polymer surfaces, which have changeable cell-attractive and cell-repellent characteristics, were used for local lift-off of the mammalian cells. In order to implement the cell adhesion, colloidal microgels were used to create micropatterned thermoresponsive polymer coatings. The microgels of 200 $\mu$ m were fabricated through automated nanodispensing or microcontact printing ( $\mu$ CP).

The microfluidic device was made of PMMA plate, double sided sticky pressure-sensitive adhesive (PSA) foil and a glass with microgel patterns at the bottom. The microchannel was created on the PSA foil of 86 $\mu$ m height, 500 $\mu$ m width and 1cm length. L929 mouse fibroblasts were cultivated and the cell detachment was accomplished via both of the coating strategies depending on the temperature shift. The lower limit of the surface coverage was determined by changing the average microgel distance and the cell detachment efficiency (Uhlig *et al.*, 2016). In another study on cell attachment and alignment using

physically microstripped-nanoengineered polystyrene surfaces (PMS-NPS), the PMS-NPS was produced via nano-injection molding, UV-photolithography and electroforming methods. Controlled MG-63 cell attachment and alignment were conducted by biophysical cue (without biochemical cue) and PMS-NPSs were found to be better than flat PS surfaces (Cha *et al.*, 2016). In order to study the cell-nanoengineered surface (NES) interactions PS nano Petri dishes were fabricated. During mass fabrication via nano-injection, Taguchi method was used to evaluate the fabrication parameters as well as to optimize and conduct efficient and reliable cell culture studies. MG-63 cell attachment and proliferation was examined in nano Petri dishes including nanopore arrays with and without the oxygen plasma treatment.

The nanopore array surface gave better performance than the flat surfaces for cell attachment and proliferation (Cha *et al.*, 2014). The advantages of the microfluidic platforms employed for tissue engineering studies can be summarized as the effective management of multi-organ microphysiological systems, biointegration of soft tissues, tissue integration of implants, microengineering of vascular structures, monitoring parameter effects on the vascularization of bone-mimicking tissues, isolation of specific cellular populations, imitating the drug distribution and metabolism processes in the body.

## **2.2. Separation/Isolation**

In biological and biomedical research as well as in clinical therapy, cell separation or cell sorting methods are mostly used to perform analyses. For example; in some cases, circulating tumor cells (CTCs), red blood cells (RBCs) and white blood cells (WBCs) are held together in blood samples and CTCs should be separated to work with. Cell separation with low risk of contamination is very important to further study of a targeted cell or an individual cell in an isolated area. Heterogeneous cell populations can only give lumped averaged data about the populations, but one can obtain an important result from an isolated subpopulation via cell sorting. There are many technologies for cell isolation such as flow cytometry, laser capture microdissection, limiting dilution, manual cell picking or microfluidic devices. In the following parts, studies on cell isolation in microfluidic devices will be discussed in detail (Tomlinson *et al.*, 2013, (Gross et al., 2015).

### 2.2.1. DNA-RNA Extraction/Isolation

In prokaryotic cell domain, bacteria cells occupy a large area, and *Escherichia coli* (*E. coli*) cells are the widely used pathogen among all, in many experiments. In 2004, Chung *et al.* employed immobilized beads in their microfluidic device to extract DNA from lysed cells. The device included channels of 2mm in width and 1mm in depth. The solution in the device flowed back and forth, and the DNA was successfully isolated in the device. The experiments conducted with serum had higher efficiency (Chung *et al.*, 2004). In 2007, optimal fuzzy sliding-mode control (OFSMC) bio-microfluidic device was fabricated with 8051 microprocessors. In this system, the collision of molecules was increased via back and forth process to enhance the biochemical reaction efficiency, and DNA extraction experiment was performed. Extraction beads were immobilized in the channels of OFSMC device, and *E. coli* cells were fed to the system.

The device was made of PMMA, and plasma generator was used before bonding. When the beads were immobilized, the extraction efficiency is higher than that of the free beads (Chung *et al.*, 2007). Geissler and his group employed *Bacillus atrophaeus* subsp. *globigii* spores for the nucleic acid separation. PMMA made microfluidic device was used to manage the bead-based mechanical cell lysis of the bacteria. The chip was composed of the mechanical slides of PMMA and a metal disk with microbeads in the lysis chamber. Cell destruction was handled via the collisions and frictional forces were created by the metal disk magnetic actuation. Gathered DNA molecules were counted via PCR method. The composition of the lysis matrix such as size or amount of the microbeads and the instrumental parameters, like duration and frequency of the agitation, affected the yield of the experiment (Geissler *et al.*, 2011). The isolation and amplification of eukaryotic mRNA from *Cryptosporidium parvum* (*C. parvum*) cells were performed in another type of microfluidic device. The surface of the microfluidic channels of the device was carboxylated via UV/ozone and coated with polyamidoamine (PAMAM) dendrimers to enhance the binding of the thymidine oligonucleotide (oligo(dT)25) for nucleic acid sequence-based amplification (NASBA) reaction. The device includes 6 microchannels of 35 $\mu$ L volume to perform mRNA isolation and amplification. mRNA was successfully separated from *C. parvum* oocysts (Reinholt *et al.*, 2014). Viruses are neither prokaryotic nor eukaryotic pathogens, and duplicate their DNA or RNA only inside the living cells of other organisms.

They cause infectious diseases and can affect all type of living forms (Koonin *et al.*, 2006). In order to detect the nanovirus (NoV) in oysters, cell concentration, lysis (RNA extraction), nucleic acid amplification and detection operations were assembled in one microfluidic device. The virus concentration and lysis events were conducted by charge switchable microbeads in shape changeable microchamber. The murine NoVs were adsorbed on the microbeads and their RNA was extracted via bead beating. Then, the extracted RNA was sent to the amplification chamber and finally murine NoVs in oyster were detected. The microfluidic device was produced from PMMA and PDMS. The PMMA chamber layer has 1mm height, 40mm length and 10mm width (Chung *et al.*, 2015).

### **2.2.2. Separation/Isolation of Microorganisms**

Cell separation has been conducted using several organisms and systems. The trapping and qualification of neutral particles such as polystyrene beads (representing non-living organisms) and living cells (*E. coli* as gram-negative bacteria and *Enterococcus faecalis* as gram-positive bacteria), were considered in a microfluidic study. Dielectrophoretic trapping ability of these different particles was tested in this platform. PMMA and glass wafer were used to create the microfluidic device. Bacteria and polystyrene beads were separated easily when the optimum frequency was set. The voltage amplitude affected the trapping event (Chow and Du, 2011).

Dielectric behavior of different bacterial species under different conditions can be used for separation and detection of pathogens. Not only *E. coli* but also other types of bacterial cells have been studied in microfluidic devices. In 2016, multiplex sorting and detection of *Salmonella typhimurium* (*S. typhimurium*) and *E. coli* 0157 from several cultures were done in a magnetophoresis-based microfluidic chip. Dynabeads anti-salmonella and Hyglos-Streptavidin magnetic beads of various sizes with conforming pathogen-specific biotinylated recombinant phages were used to arrest the cells. The PMMA device comprised of a separation chamber (3mm width, 10mm length and 100 $\mu$ m height) and a buffer inlet channel (1mm) divided into 3 similar channels of 0.4mm width and outlet channels of 0.4mm width. The depth of the device was 100 $\mu$ m. Biaxially oriented polypropylene (BOPP) tape was used to seal the device. 72% *S. typhimurium*-bound Dynabeads and 67% *E. coli* 0157-bound Hyglos beads were recovered from 10 $\mu$ L mixture in 1.2min. It was proved that, more than

one pathogen containing cultures can be sorted and isolated (Ngamsom *et al.*, 2016). An integrated microfluidic electrostatic sampler (IMES) was developed including a unipolar charging chamber, a half cylinder precipitation electrode and a collection chip, which had half-open microchannel for air transport. During the experiments, airborne molecules were sent through the charging chamber, then with the help of the electrostatic field, precipitation occurred in the half-open microchannel. Collection liquid was fed into the microchannel, which then transported the molecules to the collection reservoir. The dimensions of the collection chamber was 100mm × 30mm × 2mm and the width of the PMMA made microchannel was 2mm. In order to produce the half-open microchannel, the hydrophobic mesh was bonded via adhesive tape. *Bacillus subtilis* cells were used and the collection efficiency was around 16%. The particle loss on the hydrophobic mesh affected the collection efficiency of the system (Ma *et al.*, 2016).

Fungi, especially *Saccharomyces cerevisiae* (*S. cerevisiae*), are the model organisms of eukaryotic cells. Cell guiding experiments were done in the microfluidic device by applying dielectrophoresis (DEP) to the *S. cerevisiae* cells. It was monitored that, as the flowrate increased, guiding efficiency decreased in the device. Moreover, several medium conductivities and frequencies were tested, and the DEP behavior of cells was monitored. The microfluidic device included glass, polyethylene (PET) and ITO covered PMMA layers (being used as counter electrode) and a microchannel of 80µm height and 300µm width. By using this system, pre-treatment steps of PCR amplification of DNA can be conducted via dielectrophoresis guiding of the cells to gather and isolate them from a complex sample (Christensen *et al.*, 2007). In another study, a capillary-driven, self-propelled PCR was developed for the quantitative real-time detection of pathogenic microorganisms in less than 18 minutes. The new autonomous disposable plastic, COP, was used for the fabrication of the device, which consisted of two microchannels; one for PCR and the other for controlling the capillary flow of the solution (a driving microchannel). The microchannels had 150µm height and 150µm length and the walls of the microchannels were coated with non-ionic surfactant to create a hydrophilic surface. The system also had high and low temperature aluminum heater blocks. The chip was integrated with a fluorescence detection system to analyze the amplified product (human β-actin, *E.coli* DNA and *E.coli* O157) on the chip. This chip and detection system were successfully applied for highly sensitive reproducible quantitative DNA analysis (Tachibana *et al.*, 2015). In a study conducted with *C. parvum*

cells (parasite), the separation of cells from polystyrene beads (analogous to pathogens) was performed in spiral microchannels. External force or additional buffer was not used in the system, and the particle isolation was done by the application of high flowrates. The channel length, flowrate, particle size and particle concentration parameters were investigated to optimize the separation. The device was made of PMMA, and included a focusing channel with 6 loops of 30 $\mu\text{m}$  height and 170 $\mu\text{m}$  width. Inertial focusing was used for the first time and polystyrene beads of 4 to 7.5 $\mu\text{m}$ , similar size to pathogens, were successfully examined at channel Reynolds numbers of about 100 (Jimenez *et al.*, 2017).

### 2.2.3. Separation of Blood Cells

Adult human has an average of 5 liters of blood in the body. Delivering of oxygen and other nutrients to living cells and removing the waste products, fighting with the diseases and plug forming in a damaged blood vessel are the roles of the red blood cells, white blood cells and platelets in the blood, respectively (Dean 2005). In some analyses, it is necessary to separate these cell types from blood. Quantitative information can be obtained by using buffers with several conductivities and with the application of microfluidic system. Particle retention was accomplished by dielectrophoresis (DEP) employing polystyrene beads of 500nm, 2 $\mu\text{m}$  and 6 $\mu\text{m}$  in diameter and erythrocytes of around 6 $\mu\text{m}$  in diameter. Cross-over frequency, i.e. transition from negative to positive DEP frequency, was determined, and the separation of beads of several sizes were accomplished in the microfluidic device, which included platinum electrodes with interdigitated or intercastellated structures deposited on glass or nitride. A fluidic chamber of 10mm length, 4mm width and 30 $\mu\text{m}$  height was used. Significant quantitative data about the retention of beads and blood cells were gathered and active DEP forces were roughly calculated in this study (Auerswald and Knapp, 2003). Human arteriolar system, including circular channel cross-section, network asymmetry, bifurcation and side channels, was modeled in the microfluidic device, which had a channel diameter ranging from 200 $\mu\text{m}$  to 100 $\mu\text{m}$ .  $\mu\text{PIV}$  (micro-Particle Image Velocimetry) method was used to reveal the flow field within the device by using fluorescently labeled tracers. Red blood cells (RBCs) were separated from the blood sample and used in the device for the analysis of cell-depletion layer. Finally, the quantification of haematocrit distribution was made through the Neubauer haemocytometer with the RBS collected from the outlet of the device (Carugo *et al.*, 2013).

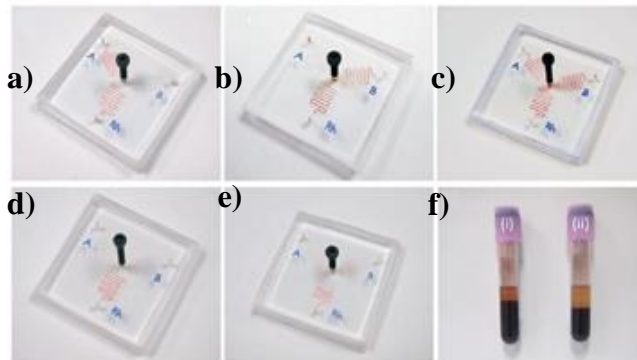


Figure 2.4. Chip test results for (a) A Rh<sup>+</sup> (b) B Rh<sup>+</sup> (c) AB Rh<sup>+</sup> (d) (e) O Rh<sup>+</sup> blood types respectively. (e) (f) Thalassemia samples with smaller RBCs and lower hematocrit. (d) Healthy blood sample (f) (i) Normal blood sample (age 23; male) (ii) Thalassemia blood sample (age 37; male) (Chen *et al.*, 2015).

In another study, white blood and red blood cells were separated from each other by using density difference feature of the cells in the microfluidic device. The device separation technique was based on magnetic-levitation of the cells in a magnetic field. In order to monitor the cells, a smartphone was used. The microcapillary channel of 1mm × 1mm cross section and 50mm height, N52 grade neodymium magnets and side mirrors were located in the magnetic levitation chip. FITC and DAPI stained blood cells were used in the device and the images taken via the smartphone were analyzed by the ImageJ program. In this system, white and red blood cells were isolated and quantified easily by using imaging with magnetic levitation (i-LEV) platform (Baday *et al.*, 2016).

Immunomagnetic-based cell separation was managed by designing a high throughput microfluidic device. The CD45-conjugated magnetic particles were used to tag the white blood cells (WBCs). WBCs were captured by the help of the magnetic field, which was created via magnets in the chip. The immunomagnetic-based system depends on the magnetic and fluid dynamic forces under laminar flow in the device. Before the experiments, a finite element model (FEA) via COMSOL Multiphysics was created to optimize the cell separation mechanism. The microfluidic system included a separation chamber of 10mm width, 40mm length and 500μm height. When the separation was completed, the captured WBCs were counted, and 99.9% WBCs were isolated from the blood (Gourikutty *et al.*, 2016).

The cell separation, cell lysis and DNA purification experiments by using rat blood samples were carried out in a microfluidic device, which included microfilter, micromixer, micropillar array, microweir, microchannel, microchamber and porous matrix. Continuous flow operation was conducted in the microfluidic device and crossflow filtration was used to isolate the blood cells. Cell lysis was done via guanidine buffer and genomic DNA was kept by porous matrix. Fluent software was employed for flow characterization. Two main parts located in the microfluidic platform were microfilter for cell isolation and microchannel for cell lysis and DNA purification. The device was made of PMMA, silicon and glass-PDMS layers including two tortuous microchannels (30 $\mu$ m height, 200 $\mu$ m width and 160mm length). 37ng DNA was isolated and separated from the 1 $\mu$ L blood, and it only took 50min to complete the experiment (Chen *et al.*, 2007). A cost effective calorimetric COP made diagnostic device was fabricated for ABO and Rh blood typing. The microfluidic device consisted of screw pump, serpentine reaction channels, chaotic micromixers and low aspect ratio filters (Figure 2.4). The maximum loading volume was determined as 6  $\mu$ L, and 1  $\mu$ L blood sample collected via finger prick method was loaded into the loading reservoir and 5  $\mu$ L of PBS buffer was introduced into all channels. The pressure difference occurring between the interactive (matched) and non-interactive (mismatched) blood types caused the PBS buffer solution to separate the non-aggregated RBCs out of the outlet reservoir in just 1 min. When the blood sample contained related antigen, then an agglutination reaction occurred and agglutinated RBCs blocked the filters near the outlet and the reaction channel turned red. The device was also used for testing the thalassemia (a type of anemia) blood samples with smaller RBCs (Chen *et al.*, 2015).

#### **2.2.4. Separation/Isolation of Tumor Cells**

In cancer, unhealthy cells divide continuously and they can spread throughout the body. Therefore, it is really important to identify and perform several analyses on cancer cells. Circulating tumor cells (CTCs) in whole blood were isolated by the help of monoclonal antibodies (mABs) in a highthroughput microsampling unit (HTMSU). CTCs were not labeled, but they were detected via conductivity sensor after capturing. The microfluidic device included 51 high-aspect ratio linear or sinusoidally constructed microchannels of 35 $\mu$ m width and 150 $\mu$ m length. The effectiveness of capturing CTCs from the whole blood was found to be >97%. Trypsin was used to release the captured CTCs from mABs, and the

enumeration was done by detection electrodes at 100% detection efficiency (Adams *et al.*, 2008). In 2011, high recovery rate was achieved in capturing the CTCs. Several simulations were performed parametrically to enable the capturing of rare target cells in the microfluidic device. High flow rate device (HFRD) was produced according to the results of simulations. In the first and second sections of the device, the widths were 130 $\mu$ m and 30 $\mu$ m, respectively. CTCs (MCF-7 cells) were gathered and spiked in 40% hematocrit solutions of human red blood cells. On the average, 80% recovery rate was attained in capturing the CTCs in the HFRD (Park *et al.*, 2011). In another study, separation and detection of the rare cells existing in the peripheral blood mononuclear cells were investigated in a disk shaped microfluidic device. Magnetic field was created to increase the trapping efficiency. The inlet reservoir, which can hold 300 $\mu$ L cell solution, was used for introducing the cell culture and trapping. The disk had 12cm diameter and 4 compartments placed on it was used to perform 4 experiments. Here, MCF7 cells attached to magnetic beads were employed to represent CTCs as the target and Jurkat clone E6-1 was employed to represent the leukocytes. Positive selection of rare cells from the abundant ones was obtained via the magnetic field. Cell separation, autoMACS (magnetic activated cell sorting) comparison and cell viability analyses were managed in this microfluidic system. 80% of rare cells (MCF7) was detected, and this result was 20% higher than those obtained by autoMACS. However, the viability of the cells was around  $90 \pm 20\%$ , which may result from the damage of the trapped cells (Chen *et al.*, 2012). Another high-throughput separation of CTCs from the blood was conducted in a microfluidic system integrating 3 modules. The first system was made of COC for CTC selection.

The CTC selection bed had 30 $\mu$ m width and 150 $\mu$ m height, and this module included anti-EpCAM antibodies for blood processing. The second system was impedance module and made of PMMA. This module included two perpendicular microchannels of 50 $\mu$ m  $\times$  75 $\mu$ m and 75 $\mu$ m  $\times$  75 $\mu$ m width  $\times$  height. The first microchannel was used to carry the cells through this module, and the second one was used to make single cell impedance measurements (CTC counting). The final module, also made of PMMA, was used for staining and imaging. There were two sets of microchannels; 8 $\mu$ m base and either 6 $\mu$ m or 50 $\mu$ m height. Blood samples with local resectable and metastatic pancreatic ductal adenocarcinoma (PDAC) were analysed via this modular device for phenotypic identification. EpCAM positive CTCs from PDAC patients were successfully detected, and

with this system CTC assay time was reduced to 1.5h instead of 8h of conventional methods (Kamande *et al.*, 2013). In 2014, Jackson *et al.* fabricated surface treated (UV-induced) microfluidic devices having different sized microfluidic channels to isolate and analyse CTCs. For colorimetric assay and imaging, the fluorescent dye-labeled oligonucleotides were immobilized on the surface of the channels. PMMA, COC and PC made channels were used but PC was eliminated due to its high auto-fluorescence characteristics, which interfered with the fluorescence imaging of CTCs. In order to select the CTCs from the blood sample, anti-EpCAM was coated on the surface of the devices. There was 50-curvilinear channels (30.6mm length, 150 $\mu$ m height and 30 $\mu$ m width) in the device to create the cell selection bed, which had 596mm<sup>2</sup> surface area.

COC made microfluidic devices achieved higher clinical CTC yield and better purity of the selected fractions than the PMMA made devices (Jackson *et al.*, 2014). Two-stage microfluidic device was developed for sorting and isolation of the CTCs. The first stage of the chip enabled the separation of the white blood cells (WBC) via microfluidic magnetic activated cell sorting ( $\mu$ -MACS), and the second stage accomplished the CTC isolation via geometrically activated surface interaction (GASI) chip. In order to create the device, PMMA and polyester films were used (Figure 2.5). The chamber of the device had 930 $\mu$ m height and 1mL volume. The cancer cell isolation ability of the system was ranging from 10.19% to 22.91%. The system was capable of identifying the heterogeneous CTCs according to their features (Hyun *et al.*, 2015). The tumor cell isolation was alternatively achieved via a negative selection method, which did not require any biomarker expression. CTC separation from the blood sample was proceeded in a PMMA made microfluidic chip without any tumor specific antigen.

In the microfluidic system, first white blood cells (WBCs) were separated via magnetophoresis, then red blood cells (RBCs) were isolated by a micro-slit membrane, and only tumor cells remained. The CTC separation chip contained two main modules, the first one included microfluidic chamber with magnetic array around it for WBC separation, and the second one included circular parylene-C membrane for RBC isolation. The dimensions of the chamber was 20mm  $\times$  40mm  $\times$  500 $\mu$ m (W $\times$ L $\times$ H). In the experiments, WBCs and RBCs were successfully separated from the whole blood and more than 80% CTC recovery was accomplished (Gourikutty *et al.*, 2016).

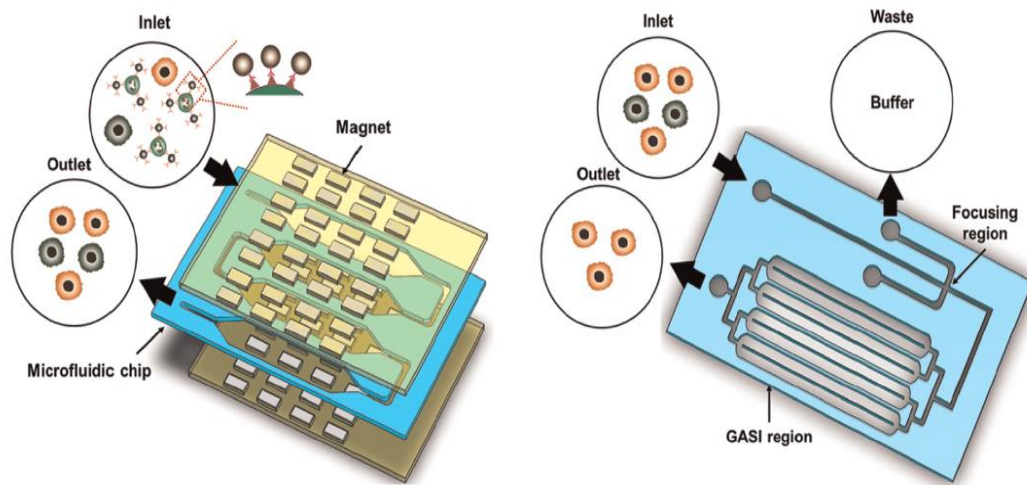


Figure 2.5. The schematic illustration of the two-stage microfluidic system (Hyun *et al.*, 2015).

Other than CTCs, different tumor cell line like human histiocytic leukemia cells were investigated via the application of dielectrophoresis (DEP) combined with the environmental scanning electron microscopy (ESEM). The designed microfluidic device had curved microelectrodes, which were produced via chrome/gold deposition on glass piece. PMMA polymer was used to create the separable microculture chamber of 2mm height on the glass substrate along with the electrode arrays. 3D surface topographical information can be obtained via ESEM images instead of flat or reconstructed images produced by confocal imaging. Since very low number of cells were used in this system, rare cell studies can be conducted via this system due to its good performance (Khoshmanesh *et al.*, 2011). The amount of ovarian cancer cells (SKOV3) in the blood was determined by an electrochemical Lab-on-a-Disc (eLoaD) system.

The device sensitively allowed blood decomposition and cancer cell separation from plasma by applying label-free electrochemical impedance. In order to make detection, gold electrodes were coated with anti-EpCAM. The device consisted of 3 PMMA and 2 adhesive layers. The capture efficiency of the device was 87% at the AC amplitude of 50mV. Five different assays can be done in parallel within the device. By using gold electrodes, SKOV3 cells were detected and separated successfully (Nwankire *et al.*, 2015). A centrifugal-force-based size-selective CTC isolation microfluidic device was produced to separate the CTCs from blood and to count them. The device includes PC membranes of  $8\mu\text{m}$  pore sizes. MCF-

breast cancer cell line was used and 61% capture efficiency was obtained depending on the several dilution factors and flow conditions (Lee *et al.*, 2014).

### 2.2.5. Separation/Isolation of Other Cells

Male reproductive cell (sperm) isolation was conducted in a PMMA made microfluidic device. This device was capable of separating the healthy, motile and morphologically normal sperms without the centrifugation of unprocessed semen. Microfluidic sperm sorter (MSS) had macroreservoirs with micropores which allowed most motile and functional sperms. The bottom chamber (50mm × 30mm) was bonded to a glass slide with double sided adhesive (DSA), and PC membrane filters were placed on the bottom chamber.

The top chamber (30mm × 30mm) was attached to the bottom chamber. By using this chip, lesser ROS and DNA fragmentation were observed than that of the conventional swim-up method (Asghar *et al.*, 2014). A lensless charge-coupled device (CCD) that facilitated the monitoring of large field of view (FOV) and made the recording automatically, was integrated into a microfluidic platform to sort and track the sperms inside the channel. The height and the width of the channel was 50µm and 4mm, respectively. The sperm cell solution was loaded through the inlet via pipetting; the images were taken with CCD in both horizontal and vertical configuration. Tracing the shadow paths of the individual sperm was used to reveal the sperm motilities. This technique will be useful while working with the oligozoospermic and oligospermaesthenic samples in which the most motile sperm need to be isolated (Zhang *et al.*, 2011).

A microfluidic sperm-sorting (MFSS) device was fabricated using COP polymer instead of commonly used PDMS or quartz. Two separate inlets were designed for channels (medium inlet and semen inlet) to separate the motile and nonmotile sperms. Two microfluidic channels of different dimensions (chip A: 0.3 × 0.5mm and chip B: 0.1 × 0.6mm) were fabricated and the fluids moving through the outlets should move parallel to each other. The sperm separation efficiency changed depending on the position (bottom-center-top) of the sperm and the height of the channel. In chip A, the linear velocity distribution was higher than that in chip B and the highest amount of motile spermatozoa was monitored at the bottom of the channel. In order to increase the recovery of spermatozoa

at higher velocity, the width of the channels should be increased (Matsuura *et al.*, 2012). By using microfluidic devices, separation/isolation of living and non-living cells can be conducted in a more controlled manner with increased efficiency. Several processes such as lysis, amplification and detection can be carried out in a single device without any need for conventional methods. Beads are generally placed in the devices to facilitate the separation. Complex samples (including more than one species) can be sorted and isolated without damaging them. Higher clinical yield and better purity can be attained and sequential operations such as isolation of the cell and further analysis can be done successfully.

### **2.3. Detection and Analysis**

Cell division, differentiation, maturation and death are the parts of the cell cycle of living organisms. Detection and characterization of a cell are among the most popular areas in scientific research for diagnosis and therapy. There are several methods to detect the cells, and Raman spectroscopy, biosensing, electro-based detection are some of the examples (Pantel and Alix-Panabières, 2012).

#### **2.3.1. Electro-based Detection**

Detection of bacterial cells via electro-based detection systems is widely used in microfluidic devices. In 2002, Yang *et al.* operated a stacked microfluidic chip capable of making electric-driven immunoassay and DNA hybridization. The device has a patterned polyimide layer with a flip-chip bonded CMOS chip, a pressure sensitive acrylic adhesive. PMMA layer and a glass cover layer. The device had  $76 \times 76\text{mm}^2$  dimension and the channel in the device had 1.27mm width, 0.304mm height. The detection of *E. coli* bacteria and Alexa-labeled protein toxin staphylococcal enterotoxin B (SEB) was conducted via electric-field-driven immunoassays. Shiga-like toxin gene (SLT1) from *E. coli* cells was also identified by using strand displacement amplification (SDA) module (Yang *et al.*, 2002). In another microfluidic device, *E. coli* and *S. cerevisiae* cells were used to study the electrokinetic transport. The devices were made of UV-modified PMMA and PC having  $50\mu\text{m}$  width  $\times$   $80\mu\text{m}$  height  $\times$  4cm length in dimension. Apparent mobility ( $\mu_{\text{app}}$ ) of the cells showed around 10% differences from chip to chip. Since yeast cells have smaller electrophoretic mobility than the electroosmotic flow (EOF), they moved towards the cathode of the devices.

In contrast, *E. coli* cells went towards the anode in 0.5mM and 1mM PBS due to their higher mobility than EOF. In 20mM PBS *E. coli* cells migrated to the cathode due to higher ionic strength (Witek *et al.*, 2004). Jezierski and his group fabricated a microfluidic free-flow electrophoresis ( $\mu$ FFE) chip to perform separation and biosensing experiments with adherent HEK cells. Fluorescent calcium indicators were loaded with HEK 293 cells to detect the ATP, which is a nonfluorescent active molecule with high electrophoretic mobility. The chips were made of either PMMA or COP or bought from ChipShop. Electrophoretic separation of ATP stream in the  $\mu$ FFE chips loaded with HEK 293 cells were visualized by the fluorescence imaging of sensing cells. This system was capable of the on-line detection of native and unlabeled compounds (Jezierski *et al.*, 2013).

In another study, the identification and quantification processes of bacterial cells and spores were adapted into an electronic microfluidic device. The device was capable of immune-localization of spores, which were captured by the membrane filter within the chip. Analyte signal was recorded, and collective response or detection and counting of individual spores and particles were done. The device was made of PMMA and Nuclepore membrane, and stainless steel tubing (19.5 gauge in outer diameter) was inserted via drilling into the PMMA for fluid passage. The limit of detection of the chip was around 500 *Bacillus globigii* (Bg), which is a stimulant for *Bacillus anthracis* (Ba) (Floriano *et al.*, 2005). In 2008, an electrochemical impedance spectroscopy (EIS)-based microfluidic device was developed to study the adhesion of bacteria cells onto semiconducting indium tin oxide (ITO) plate with the aim of electrochemical detection and characterization. *Pseudomonas stutzeri* (PS) and *Staphylococcus epidermidis* (SE) bacterial strains were used in this system to compare the adhesion behavior and charge transporting property of these cells. Impedance variations were measured both at low and high frequencies for electrical detection and electrical characterization, respectively. The flow chamber was made of two parallel PMMA sheets, and a silicone membrane was put in between these sheets. ITO plate was located at the bottom sheet of 22mm  $\times$  22mm dimensions, and a circular chamber of 14mm in diameter and 1.8mm in height was placed on the upper sheet for bacterial suspensions. As the number of adhered cells increased, the intensity of the impedance decreased exponentially. First PS cells, then SE cells were identified electrically and PS cells were more prone to make charge transfer to the electrode than SE cells (Bayouhd *et al.*, 2008). Similarly, protein digestions was performed in an electrokinetically-driven solid-phase trypsin microfluidic

device integrated with matrix-assisted laser desorption/ionization time-of-flight mass spectrometer (MALDI-TOF MS). The microbioreactor included a microchannel of 4cm length, 200 $\mu$ m width and 50 $\mu$ m height, and the micropost system (50 $\mu$ m diameter) was located in that channel. Several proteins were employed in the system and cytochrome c digestion was the most efficient one with 97% sequence coverage for protein identification. Bovine serum albumin (BSA) with 46%, phosphorylase b with 63% and  $\beta$ -casein with 79% sequence coverages were detected in the device. E.coli cells were also used for fingerprint analysis of intact cells (Lee *et al.*, 2009).

Vila and his colleagues operated an optical analysis for the determination of environmental pollution. The system included PMMA optofluidic arrangement, comprising of light emitting diodes (LEDs) and detectors, and they managed optical measurement and elimination of ambient light interference via an electronic circuit. The device included 4 layers of PMMA with distinct patterns and optical and fluidic aspects. The system was applied to the detection of water toxicity. In these toxicity tests, bacterial reduction kinetics of ferricyanide was used, where ferricyanide collaborated with the membrane proteins of E. coli, and simple, precise and reliable water toxicity determination was enabled (Pujol-Vila *et al.*, 2016). Recently, electrical sensing of bacterial lysate was used to detect the *Pseudomonas aeruginosa* and *Staphylococcus* bacteria cells that cause keratitis.

The device included PMMA wells (2mm  $\times$  2mm  $\times$  1.5mm) and electrodes of 10 $\mu$ m width and 20 $\mu$ m spacing. A statistically remarkable impedance change was obtained for 10 CFU/mL diluted bacteria samples (Pandya *et al.*, 2017). The electroporation chips have been produced to eliminate the limit in the amount of target cells to be detected, potential risk of using high voltage and the undesired effect of temperature rising encountered in conventional systems. One such device included a channel of 5mm width, 0.2mm height and 25mm length. Electrical square pulses were applied through the channel, and the mixture of Huh-7 cells lines and reporter genes were sent into the channel. In order to see the cells under the fluorescent microscope (BX60, Olympus, Japan), trypan blue was used for staining. Transfection was successfully accomplished in the device and the cell survival rate was increased when the low pulse frequency and high flow speed were employed (Lin *et al.*, 2001). Optical fibers, mirrors and electrodes were used to make cytometric analysis of blood cells in three-dimensional microfluidic devices. In the study of Kummrov *et al* (2009),

erythrocytes and thrombocytes were distinguished via forward light scatter. The fluorescence imaging was used to monitor the two dimensional focusing of sample flow and the results were confirmed by the finite element calculations. The sample fluid channel had  $125\mu\text{m}$  width  $\times$   $125\mu\text{m}$  height  $\times$   $4\text{mm}$  length. In this study, T-helper cells labelled by fluorescent monoclonal antibodies were also determined (Kummrow *et al.*, 2009).

### 2.3.2. Magnetic Field Based Detection

Nowadays, the creation of magnetic field in microfluidic devices for cell detection is heavily used. For *E. coli* detection, Laczka *et al.* benefited from immunomagnetic capture and amperometric detection techniques. The combination of horseradish peroxidase (HRP), hydrogen peroxide ( $\text{H}_2\text{O}_2$ ) and hydroquinone (HQ) was used for electrochemical monitoring. An incubation micro-chamber, which had magnetic particles (MPs), was employed for the enzymatic reactions. The microelectrodes was used to monitor the enzyme product, which flowed in the microchannels of  $500\mu\text{m}$  width and  $150\mu\text{m}$  height. PC polymer formed the bottom of the chip, where two magnets, necessary for keeping the MP upstream from the electrode, and a pocket for housing the chip were located. The experiment took 1h and the bacterial cells were identified with a limit of detection of  $55\text{ cell ml}^{-1}$  (Laczka *et al.*, 2011). In another study, polymerase chain reaction (PCR) of bacterial cell culture was conducted in a magnetically functionalized closed-loop PCR microfluidic device. A ferrofluid plug was employed as the valve and actuator to prevent the liquid flow in the device. There was a circular channel of  $20\text{mm}$  diameter,  $0.375\text{mm}$  width and  $0.3\text{mm}$  height, and the overall volume was around  $7\mu\text{L}$ .

The loaded sample visited all the sections of the device to accomplish the PCR amplification, the thermal lysis, and the denaturation of the PCR mixture. The limit of detection was found as four bacterial cells. This device was capable of shortening the reaction time compared to conventional thermocycler systems, and the results were comparable (Lok *et al.*, 2012). Spinning magnets were employed to handle the sample manipulation, mixing and controlled target release in the microfluidic device called MagTrap, which was used for detection of *E. coli* cells. MagTrap consisted of magnets, which were placed in a rotating wheel and microfluidic channels. The height of the channel was  $125\mu\text{m}$ , the width was  $500\mu\text{m}$  at the top and  $355\mu\text{m}$  at the bottom. In this system, strip

magnet design was used, and the detection procedure was first binding of *E. coli* to antibody coated superparamagnetic fluorescently-coated beads, and then releasing them into the microchannel. As the wheel rotated, the beads were trapped and separated. MagTrap was successful in detecting the bacterial cells (Verbarg *et al.*, 2012). In 2013, Verbarg and his group have combined their MagTrap device with another device to do cytometry experiments using *E. coli*, *Salmonella*, and *Shigella* bacteria cells. Again, target-specific magnetic beads were used in the MagTrap and rotational movements of the device (forward and backward) conducted reagent processing in MagTrap. The MagTrap device was made of PMMA and consisted of trapezoidal channel of 500 $\mu$ m top width, 355 $\mu$ m bottom width, 125 $\mu$ m height and 6cm length. In order to activate the magnetic wheel for bead manipulation, a motor was used. PDMS microflow cytometer was connected to the outlet of the MagTrap to accomplish the cytometry experiments (Verbarg *et al.*, 2013). In 2013, the combined MagTrap and cytometer system was used to identify the particles in the microfluidic system as well as to obtain sample-to-answer diagnosis.

Fluorescently stained microspheres grabbed the target molecules, and these molecules were taken out of the sample matrix. These grabbed molecules were exposed to biotinylated tracer molecules and streptavidin-labeled phycoerythrin, respectively. Finally, these molecules passed through the microflow cytometer for color analysis. In order to detect the *E. coli* cells, three sets of MagPlex microspheres were prepared, and the concentration of  $1 \times 10^4$  cells/ml can be recognized via MagTrap (Golden *et al.*, 2013).

### **2.3.3. Chemical Detection**

Daunert and her group produced a microfluidic device having a chemical detection system. Arsenite and antimonite were used as the target analytes to be sensed by the *Escherichia coli* cells, which included plasmid pSD10. The microfluidic platform was able to recognize the regulatory protein ArsR fused with GFPuv, which is a reporter protein. The GFPuv in the cells was capable of fluorescence emission, enabling arsenite and antimone detection. The device consisted of 2 reagent reservoirs, a mixing channel and a detection reservoir. Whole-cell biosensing system was successfully accomplished, and the response time was shortened compared to conventional systems (Rothert *et al.*, 2005). Later, the same group improved their design, and they introduced two different spore-based whole-cell

sensing portable microfluidic systems to detect arsenite and zinc. The detection limit of the system in both serum and water media was  $1 \times 10^{-7} \text{M}$  for arsenite and  $1 \times 10^{-6} \text{M}$  for zinc, respectively. The first platform (CD 1) was used for zinc detection (left) and the second platform (CD 2) was employed to detect the arsenic (right). During the experiments, all the luminescence measurements were conducted via spectrophotometer that had fiber optic probe. This probe was placed 2mm above the detection chamber perpendicularly, and all the measurements were taken at 20min intervals. In this sensing systems, *Bacillus subtilis* strain was used for arsenic detection and *Bacillus megaterium* cells was used for the zinc detection (Date *et al.*, 2010). *Artemia franciscana* (Artoxkit MTM) cells were used to test the aquatic toxicity in a microfluidic system. In order to determine the outcomes of the reference toxicant on the identified behavioral parameters, fully automated time-resolved video data analysis was carried out. Continuously microperfused microfluidic system was used to monitor the free-swimming actions of *Artemia* sp. nauplii cells. CorelDraw X3 CAD and SolidWorks programs were used to model the device in 2D and 3D, respectively.

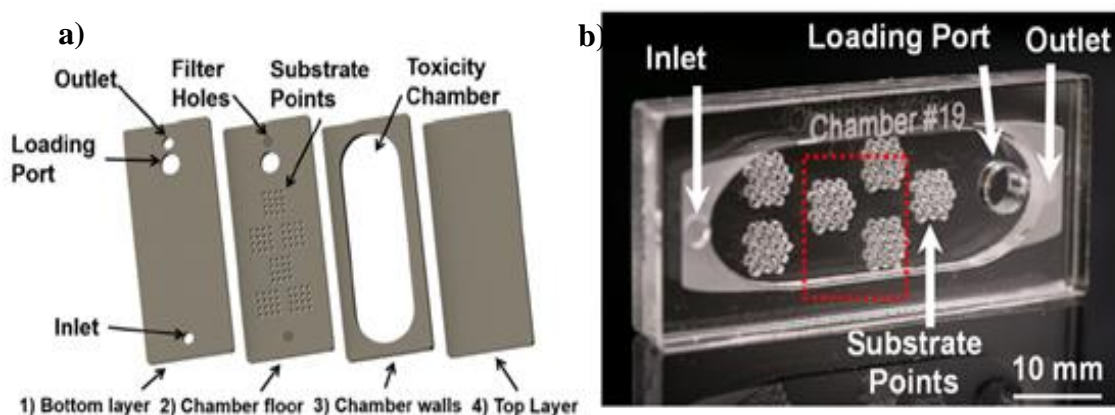


Figure 2.6. (a) The layers of the microfluidic system. (b) Assembled chip microphotograph (Cartlidge *et al.*, 2017).

The device included circular caging chamber of 10mm in diameter and 1.5mm in height for larvae free swimming. 10 microchannels of 0.2mm height were placed in between the inlet/ outlet and caging chamber. Several chemical stressors were applied through the system and the behavior of the cells were followed. Hyperactivity and hypoactivity syndromes were analyzed in response to chemical stressors (Huang *et al.*, 2016). In another study, *Allorchestes compressa* marine amphipod was used to monitor the sublethal behavioral

toxicity by employing a microfluidic device capable of continuous perfusion. The toxicants were perfused through the device, and automated behavioral tests were done. 2D and 3D versions of the device were designed via CorelDraw  $\times$  3 and SolidWorks 2015 software, respectively. COMSOL Multiphysics 4.4 was used to study the fluid dynamics inside the device (Figure 2.6). There is an elliptical chamber of  $54\text{mm} \times 17\text{mm} \times 3\text{mm}$  dimensions in the chip. Detection and automatic analysis of swimming behavior of the *A. compressa* cells were done successfully (Cartlidge *et al.*, 2017). In a study on drug delivery, lectins were attached on the inner surface of PMMA made microfluidic device to target cells in the gastrointestinal tract. Aminolysis was used to obtain amine-terminated surfaces. The device contained reservoirs of  $80\mu\text{m} \times 80\mu\text{m} \times 1.5\mu$  dimension and Caco-2 cell lines were employed in the experiments. Avidin molecules were bound to the PMMA surfaces rendering PMMA cytoadhesive. This system demonstrated strong potential for use in drug delivery (Tao *et al.*, 2003).

#### **2.3.4. Biosensing/Biosensor Based Detection**

Enteropathogenic *E. Coli* (EPEC) cells, which caused several gastroenteric illnesses, were investigated in a special microfluidic system. Fabry-Perot (FP) cavity-based biosensing platform was employed to detect the EPEC in 5min. Micro-thin double sided adhesive tape and two semi-transparent FP mirror plates were used for the construction. In order to measure the spectral changes, optofluidic FP cavity was employed, and the channel of 2mm width was cut via CO<sub>2</sub> laser. Capillary force was applied through the system to fill the channel, and then the transmission spectra was detected in order to arrange the adhesion time of cells on the functionalized surfaces. Surface functionalization was conducted by translocated intimin receptor (TIR). Four taxonomically or distantly related bacterial strains were specifically recognized by TIR surfaces. The efficiency of trapping on the functionalized gold mirrors was determined by confocal optical imaging via SEM (Ivanova *et al.*, 2012). In another study, electrokinetic capture was employed to detect *E. coli* cells via a cantilever biosensor combined with electrodes for piezoelectric actuation. PiezoMUMPs process was used to create the biosensor consisting of four layers; a silicon structural layer ( $10\mu\text{m}$ ), a silicon oxide insulating layer ( $1\mu\text{m}$ ), an aluminum nitride piezoelectric layer ( $0.5\mu\text{m}$ ) and a gold electrode layer ( $0.52\mu\text{m}$ ). The microfluidic platform responsible for sample/solution delivery to biosensor was made of PMMA and PDMS. The two PMMA

sheets of  $45 \times 20 \times 1.6\text{mm}^3$  dimensions hosted the inlet and outlet holes, and a PDMS gasket of  $10 \times 10 \times 0.15\text{mm}^3$  dimensions was used for sealing in between the outlet and the chip. When the sample concentration was 107 cells/ml, the signal to noise ratio was 82 within 10 min; and when the sample concentration was 105 cells/ml, this ratio was 26. Therefore, *E. coli* cells were successfully detected via the cantilever biosensor (Leahy and Lai, 2017). High-throughput centrifugal microfluidic device was designed to make colorimetric analysis of foodborne pathogen. A sample reservoir of 1.2mm height and 5mm radius, a spiral shaped sample injection microchannel of 550 $\mu\text{m}$  height and 2mm width, 24 aliquoting chambers of 2.5 $\mu\text{L}$  volume, cross capillary valves and 24 reaction chambers of 2.5 $\mu\text{L}$  volume were placed in the device (Figure 2.7). The microfluidic system was made of PMMA using pressure sensitive adhesive (PSA). Loop mediated isothermal amplification (LAMP) was employed to identify *E. coli*, *Salmonella typhimurium* and *Vibrio parahaemolyticus* pathogens and all of the genetic analytical process was finalized within 1h (Seo *et al.*, 2017).

Gold nanorods (AuNRs) were used to detect the orchid viruses in the fiber optic particle plasmon resonance (FOPBR) immunosensor system. A near infrared sensing window was generated by the AuNRs to make direct sensing. Cymbidium mosaic virus (CymMV) and Odontoglossum ringspot virus (ORSV) were identified by the antibodies present on the AuNRs by unclad fiber core surface. The AuNR-FOPPR sensing window was established in the microfluidic channel, which was made of PMMA, and the channel had 15 $\mu\text{L}$  volume. The limits of detection (LOD) of the microfluidic system was compared with that of the ELISA test and the results confirmed that this microfluidic system has better performance. The immunosensor achieved faster analysis, better reproducibility and lower detection limits compared to ELISA. In addition, this sensor was capable of categorizing the healthy and infected orchids, and also displayed the infection level (Lin *et al.*, 2014).

A micromixer, including a microballoon, was fabricated for creating 3D reciprocating flow and to detect dengue virus. The system was capable to expand and contract and hence to change the flow dynamics. Two different CD-like designs were constituted, where Design A was used to evaluate the mixing in the microballoon, to make comparison with the stopped-flow mixing method and to theoretically analyze the rotational frequencies. Design B was used to see the effects of microballoon as well as the stopped-flow mixing technique on the ELISA results. Two loading reservoirs, mixing chamber and two microchannels were

located on both designs A and B. Biomolecule reaction rate and detection sensitivity of the dengue viruses were increased compared to the conventional methods (Aeinehvand *et al.*, 2015). In the study of Morant-Minana *et al.* (2015), the detection of *C. Camplyobacter* spp. in real food samples was performed by using a biodevice integrated with a DNA sensor. For the detection, electrochemical geosensor based on thin-film gold electrodes was deposited onto COP surface. The feasibility and sensitivity of the biosensors developed in this study were tested by atomic force microscopy (AFM), X-ray diffraction (XRD), Fourier Transform Infrared spectroscopy (FTIR), Cyclic Voltammetry (CV) and Square Wave Voltammetry (SWV), and the detection of PCR amplicon of *C. Camplyobacter* spp. concentration was successfully performed. Photolithography and sputtering were used to create the electrodes on COP. The device presents an integration of electrochemistry and microfluidics for real time detection and analysis of microorganisms in food.

The amplification of bacterial genomic DNA in a short time by using electrochemical biosensor technology on COP polymer made microfluidic device showed that it can be used for further diagnostic studies in the food sector (Morant-miñana, and Elizalde, 2015). Dong and Zhao (2015) designed a PS made biochip; i) to determine the specific pathogen among 13 types of uropathogenic microbes, that cause urinary tract infections (UTIs) by employing immunosorbent ATP-bioluminescence assay (IATP-BLA) and ii) to find the relevant antibiotic for patient according to detected microbial organism. The biochip consisted of 5 layers, two glasses as cover, two PS sheets of 2-mm thickness with 384 vertical reaction chambers as sample layer (urine and oxygen/air) or culture layer (microbes and other reagents) and fiberglass membrane, in which 8 different types of antibodies were immobilized, fixed between two PS sheets to target and capture microbes. The immobilized antibodies captured the specific microbes in loaded urine sample. Calcium alginate gel was used to encapsulate the captured cells and these encapsulated cells were evaluated by ATP-BLA in a microplate reader by using different methods for different channels. As a result, the biochip decreased the detection time of the pathogens from days to minutes and can be a model for the diagnosis of other diseases (Dong, and Zhao, 2015). Human embryonic kidney cell line (HEK-293) is widely used in cell biology studies. Since many neuronal proteins can be expressed by this cell line, it is accepted that, this cell line was generated from embryonic neural cells (Madhusudana *et al.*, 2010). A portable ion channel biosensor (4 channel incubation type planar patch clamp biosensor) was developed, and the channel

rhodopsin wide receiver (ChRWR) expressed by HEK293 cells was used to evaluate the performance of the microfluidic system. The system consisted of a cell trapping area and a pipette solution well. The thickness of the thin film region between these parts was around 10 $\mu\text{m}$ . A micropore (1.5 $\mu\text{m}$  to 2 $\mu\text{m}$  diameter) was created in the middle of the round area to achieve the cell trapping. The biosensor's surface was coated with ECMs of poly-L-lysine and the cells were fed through this coated chip.

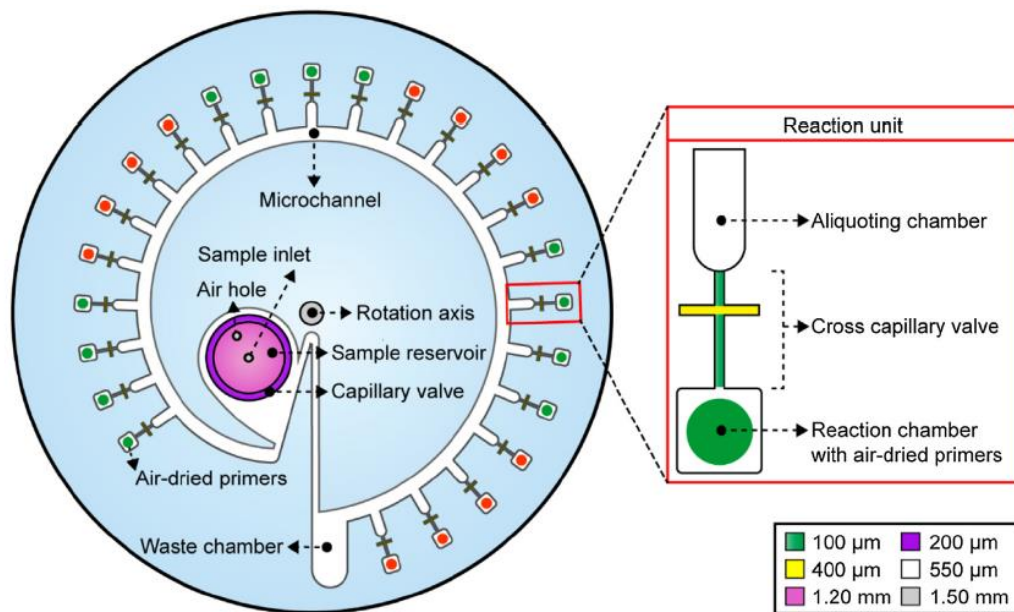


Figure 2.7. The design of the centrifugal LAMP microdevice (Seo *et al.*, 2017).

During the experiments, laser-evoked channel current of the cells was recorded via patch-clamp amplifier. This system can safely be used for high throughput screening of neural cells (Wang *et al.*, 2012). In order to conduct immunostaining-based cytometry, a microfluidic device was developed, where antibodies were placed in a gelatin layer. The chip included flow chambers of 4.8mm  $\times$  61mm dimensions and counting chambers of 15mm  $\times$  9mm on laminating adhesive, and was sandwiched in between the PMMA layers. Inkjet printing was used to establish the gelatin/antibody layer. A homogeneous antibody distribution was accomplished in the device due to long maturation process of gelatin, and the antibody release was done by heating up the gelatin layer. In the experiments, CD4 positive (CD4<sup>+</sup>) T-lymphocytes were used to perform on-chip immunostaining to the whole blood, and cell counting was done effectively. The temperature-switch antibody release from gelatin/antibody layers was successfully completed (Zhang *et al.*, 2016).

### 2.3.5. PCR Based Detection Systems Based on Genetic Material

Creating a new strand of DNA complementary to a template strand is called polymerase chain reaction. Several organisms' DNA can be copied or reproduced by using this technique. Tumor virus identification via DNA manipulation was conducted in a microfluidic device, in which micro-reverse transcription polymerase chain reaction ( $\mu$ RT-PCR) was carried out. PMMA with SU-8 was used as the construction material of the device, that integrated sample reservoirs, RT-PCR meanders and capillary electrophoresis (CE). The device design was simulated via ANSYS, CFD-RC and IntelliSuite softwares, and then validated by the experiments. Heat transfer, reaction temperature control and fluid flow clogging preclusion were successfully accomplished in this device (Tsai, and Sue, 2006.). In another study,  $\mu$ RT-PCR, CE and on-line detection with buried optical fibers were combined in the microfluidic platform to detect Piscine nodavirus cells in a fast, sensitive and automated way. PDMS, PMMA and soda-lime glass were used to fabricate the device of the dimensions  $4.5\text{cm} \times 6.5\text{cm}$ . By using this system, virus cells were successfully detected from fish samples and the detection limit was  $12.5\text{ copies}/\mu\text{L}$  (Lee *et al.*, 2007).

In 2015, the detection of Human papilloma virus (HPV) 16 was accomplished by a biomicrosystem employing PCR based detection system. The device included 98 biosensors, and the monoclonal antibody (mAb) 5051 immobilization was done on the PMMA substrate with gold layer. Electrochemical impedance spectroscopy, cyclic voltammetry, impedance measurements, AFM and SEM were used to define the system. The wells of 2mm in diameter were located on the PMMA substrate for detection. The comparison of the results of HPV 16 detection with those of the standard PCR tests confirmed the effectiveness of this biomicrosystem (Urrego *et al.*, 2015). A COP made microfluidic device was developed to achieve a rapid genetic testing system, such as the detection of the point mutation of FGFR3 gene. This microfluidic device had a serpentine channel of  $400\ \mu\text{m}$  depth and  $400\ \mu\text{m}$  width with 80 loops, was covered with a thin pressure sensitive adhesive transparent film, and consisted of two temperature zones for denaturation and annealing reactions. The rapid thermal cycling was performed by continuous flow of PCR, the solution was thermally cycled through the created multiple local temperature zones in the microfluidic channels. Due to the high surface area to volume ratio, the fast heat conduction to the solution was obtained via channel walls as an advantage of this process. A point mutation of FGFR3 gene

was detected in 6.5 min by using *Bacillus subtilis* spores. As the genetic mutation of FGFR3 gene is related to bladder cancer, this study is a promising one for rapid genetic testing of various diseases (Nagai, and Fuchiwaki, 2015).

### **2.3.6. Miscellaneous Detection Systems for Diseases**

2.3.6.1. Fluorescence Based Detection for HIV Point of Care Testing Systems. Acquired Immunodeficiency Syndrome (AIDS) disease is caused by Human Immunodeficiency Virus (HIV). This disease can be spread via sexual contact, infected blood or mother-to-child interaction (Girard *et al.*, 2011). HIV and AIDS studies have also been conducted in microfluidic platforms. For example, the anti-gp120 antibody was immobilized into the microfluidic device for capturing and imaging of HIV from untreated HIV-infected blood sample. The quantum dots (Qdot525 and Qdot655) were employed to label the envelope of gp120 glycoprotein and high-mannose glycans of captured HIV, respectively. The virus images were counted via fluorescence microscope. PMMA, double sided adhesive film (DSA) and glass were used to build the microfluidic device, which included 25mm length  $\times$  4mm width fluidic channels. The device was capable of identifying HIV in less than 10min from a fingerprick volume of blood. Here, Qdots implemented a new and effective tool for analyzing the HIV molecules without any need for pre-processing (Kim *et al.*, 2009). Detection of CD4+ T-lymphocytes was done in a microfluidic device with lensless imaging for HIV point-of-care testing. Anti-CD4 antibody was immobilized in the device for capturing of CD4+ T-lymphocytes from the blood. Charge coupled device (CCD) sensor was employed to make the identification of the captured cells, and the gray scale images were obtained via this lensless imaging CCD sensor. An automatic cell counting software was used to enumerate the cells, and a fluorescence microscope was also used for manual counting. The device was made of PMMA with double sided adhesive film (DSA), and included 24mm long  $\times$  4mm width microfluidic channel, which was created on the DSA film. This microfluidic system had  $70.2 \pm 6.5\%$  capture efficiency and  $88.8 \pm 5.4\%$  capture specificity for CD4+ T-lymphocytes (Moon *et al.*, 2009).

2.3.6.2. Sensors for Detection and Analysis of Cancer. In recent years, it was observed that the cancer risk is increasing in industrialized communities/societies (Climent *et al.*, 2017). There are many studies on cancer treatments, and the detection of cancer cells can be done

in microfluidic devices. Weigum *et al.* produced a cell-based sensor for the detection of oral cancer biomarkers via epidermal growth factor receptor (EGFR). The device included track-etched membrane served as a micro-sieve for capturing and enriching the cells from the biological sample. Automated microscopy and fluorescent image analysis were used to monitor the presence and isotype of the captured cells on membrane, and the EGFR tests were conducted in less than 10min via this biosensor. The cell-based lab-on-a-chip (LOC) sensor was made of PMMA and PC membrane of 0.4 $\mu$ m pores. The device consisted of a microchannel of 1mm width, 125 $\mu$ m height, 8.2mm length and a circular membrane capture area with imaging window of 200 $\mu$ m in diameter, resulting in a volume of 3.9 $\mu$ L. EGFR expression in cancer cells was found to be higher than that of the control cells, which had EGFR expression similar to normal squamous epithelium. The LOC sensor can thus be used to detect the oral cancer biomarkers as well as to characterize the EGFR over-expression in oral malignancies reliably (Weigum *et al.*, 2007). Chemotaxis assay study was done in a microfluidic chamber by using breast cancer cells. In order to fabricate the microchannels for chemoattractant transportation and barriers/conduits for flow diversion, the photolithography method was employed. The device consisted of three layers; the bottom layer was glass including a microchannel of 20  $\times$  20 $\mu$ m dimension, the middle layer was made of PDMS to seal the reservoir and the top layer was made of PMMA connected to a pressure regulator. The directionality and instantaneous speed of cell protrusion were studied in this platform. In the presence of epidermal growth factor receptor, breast cancer cells answered more directionally and fastly than the uninduced cells (Fok *et al.*, 2008). A prostate-specific membrane antigen (PSMA) was used as an indicator of the prostate tumor cells. The antibodies and aptamers can bind to PSMA. High-throughput micro-sampling unit (HTMSU) was made of PMMA, and it consisted of immobilized anti-PSMA aptamers for capturing the circulating prostate tumor cells from the peripheral blood. The device included 51 curvilinear microchannels of 150 $\mu$ m height and 30 $\mu$ m width. The reason for using curvilinear channel was to increase the cell capture efficiency. During the experiments, 90% of the LNCaP cells (prostate cancer cell line) were captured. In order to reinforce the detection and efficiency, a conductivity sensor was combined with the HTMSU for cell counting (Dharmasiri *et al.*, 2009). Microfluidic flow cytometry ( $\mu$ FCM) technology was developed to observe the caspase-dependent cell death in a user-friendly chip-based system. This system included off-chip electronic interface and was capable of making multivariate analysis using small amount of sample (10 $\mu$ L).

Human leukemia U937 and THP1 $\alpha$  cells were used to conduct 2D hydrodynamic cell focusing of cells in the PMMA made microfluidic device. Two solid-state lasers (blue: 473nm and red: 640nm) and four photomultiplier tube-based (PMT) detection channels with band-pass filters were placed on the off-chip hardware system in order to catch the fluorescent signals. The chip included sheath fluid reservoir (of 2ml volume), a microchannel for cell focusing (75 $\mu$ m width and 50 $\mu$ m height) and sheath fluid gathering chambers (2ml). This device enabled the analysis of the DNA, the recording of the pharmacologically-induced activation of caspases and the dissipation of mitochondrial inner membrane potential in living cells (Akagi *et al.*, 2012).

Point mutations can be detected with the application of capillary electrophoresis assay, polymerase chain reaction (PCR) or ligase detection reaction (LDR). A microfluidic device for the detection of circulating tumor cells (CTCs) was developed. This system had electrokinetic enrichment ability to reveal the mutations within the DNA of the CTCs. SW620 and HT 29 cells in the blood samples were used because these cells can overexpress the integral membrane protein EpCAM. The wall of the microfluidic device was coated with the anti-EpCAM antibodies to detect the cells. The rectangular channels had 80 $\mu$ m width and 100 $\mu$ m height. In the electromanipulation unit, 125 $\mu$ m diameter Pt wires were used as the electrodes to perform the conductivity-based enumeration, following the release of the CTCs from the antibody selection surface.  $96 \pm 4\%$  efficiency was attained during the CTC selection (Dharmasiri *et al.*, 2011). The detection of circulating tumor cells (CTCs) was further conducted in the label-free reflectometric interference spectroscopy (RIFs) functionalized microfluidic biosensor system. RIFs sensing structure was created by anodic aluminium oxide (AAO), which was produced by the electrochemical anodization. This AAO surface was coated with biotinylated anti-EpCAM antibody to bind the human cancer cells of epithelial origin. The device had two microfluidic channels with simple mixers for sending the fluid evenly through the AAO sensing platform. This system did not require any bonding procedure, the PMMA layers were just clamped to each other. In addition, this detection method did not need any fluorescence tagging or pre-enhancement processes; the samples were simply sent through the system, and the cells were detected via AAO RIFs sensor. The device successfully detected around 1000-100,000 cells/mL in a 5min response time for 50 $\mu$ L sample (Kumeria *et al.*, 2012).

In order to fight against cancer cells, many scientists have been struggling to develop therapies that strengthen the immune system and cure the disease (Minn, and Wherry, 2016). In order to get insight on the biological behavior of the myeloma tumor cells after mechanical stress, a microfluidic device was developed and optimized. A microgear pump was fabricated via deep X-ray lithography (DXRL) method by using PMMA sheets of 500 $\mu\text{m}$  thickness.  $1 \times 1\text{mm}^2$  magnet was placed in the device for actuation and solvent bonding technique was used for sealing. The gear included 20 teeth (of 3mm external diameter). The cell suspension was fed to the system; pumped for a determined time, and the local head pressure difference was recorded. As the stress increased, the cell viability was found to decrease (Matteucci *et al.*, 2007). Mechanical dissociations of digested tumor tissue and cell aggregates into single cell experiments were done in polyethylene terephthalate (PET) made microfluidic devices to enhance the quality of the results obtained.

Several sized (millimeters to microns) channels were placed in the device to create well defined high shear force regions to increase the dissociation of clusters into single cells. HCT 116 colon cancer cells were used in the experiments and by using this microfluidic device, cell recovery, cell viability and process time were improved (Qiu *et al.*, 2015). 3D micro-chambers for cell capturing and analysis was fabricated by COC. The device was capable of creating high flow velocity in 3D microchannels to provide selective cell immobilization. The performance of the device was tested via immune-fluorescence labeling and Fluorescence in Situ Hybridization analysis on cancer cell lines and on a patient pleural effusion sample. This device, fabricated at low cost, can be used for medical diagnostics (Mottet *et al.*, 2014).

#### 2.3.6.3. Morphology Based Detection and Analysis Systems for Diagnostic Purposes.

Several studies on red blood cell detection have been conducted in microfluidic devices. The quantification of blood was handled in the microfluidic device using the impedance analysis technique. Ansys Fluent 12.1.4 simulations were performed to evaluate the diffusive mixing practices. The microfluidic system used in this study had the microfluidic lysis block, the impedance analysis chip, the electronic detection and data collection processing parts. The microfluidic system was made of PMMA and the height and channel widths were 100 $\mu\text{m}$  and 200 $\mu\text{m}$ , respectively.

As the cells flowed in this impedance chip, the electrical cell volume and cell membrane capacitance were measured by applying two different sinusoidal voltages through the electrodes. The results obtained from the red blood cell (RBC) lysis experiments conformed to those in the conventional hematology devices (Han *et al.*, 2012). The red blood cells, which have concave surfaces, have been used to reveal their shapes for diagnostic purposes. The particular microfluidic device used for RBC analysis was made of PMMA, and it has  $1000\mu\text{m} \times 200\mu\text{m}$  (width  $\times$  height) dimensions. In order to hold the RBCs in the channel, optical traps were used, and by using laser power the cells were rotated. During the rotation, the images of the RBCs were taken from several viewpoints and recorded. It was proven that the system was capable of revealing the holographic images of the RBCs. Therefore it is possible to apply this system for diagnostic analysis without any labeling (Memmolo *et al.*, 2014). Alapan *et al.* developed a biochip for Sickle cell disease (SDC) and made quantitative evolution of red blood cells (RBC) in a microfluidic system with the help of protein coated microchannels. By using SDC biochip, the relation between the RBC adhesion to fibronectin (FN) and laminin (LN) proteins as well as the features of RBCs were revealed. The SDC chip contained FN or LN coated glass slide at the bottom, and PMMA substrate including inlets and outlets at the top. The adhered RBCs were monitored and classified as deformable and nondeformable by considering their morphology. SDC biochip is a promising tool for quantitative assessment of RBCs and for observing the disease progression and vaso-occlusion (Alapan *et al.*, 2016).

By using microfluidic devices, several detection experiments such as pathogen detection or disease detection can be done. Micro-nano particles or magnets can be used as assistant elements in these device to enhance the quality of detection. Two microfluidic devices can be combined to make consecutive experiments. For example, first detection of cells in one device then enumeration of detected cells can be done in another device. Moreover, environmental stress is an important factor for living organisms. Microfluidic devices give opportunities to monitor the changes in cells instantaneously. Taxonomically or distantly related cells can be observed in one single device. In developing countries, disease diagnosis is very difficult. Healthcare services are deprived of advanced medical devices. Therefore, microfluidic devices are seen as savior for disease identification in these countries, enabling the detection in a short and easy way.

## 2.4. Reaction: Microbial Fuel Cells

Fossil fuels, renewable sources and nuclear sources are the energy sources of the life. Fossil fuels satisfy considerable amount of energy need in the world. In this regard, microbial fuel cell (MFC) studies have gained great attraction since the early 20th century. MFC field combines different scientific and engineering knowledge, and MFCs were produced to benefit from small volume and high output power density (Logan *et al.*, 2006), (Rahimnejad *et al.*, 2015), (Chaturvedi, and Verma, 2016). A mini-MFC included one chamber of 25 $\mu$ L volume, and a plate-shaped (instead of stripe-shaped) gold anodic electrode was operated to obtain higher electrochemical activity. *Shewanella oneidensis* MR-1 cells were used to create the biofilm on the gold electrode. The gold anodic electrode layer was fabricated on the glass and 8 wells of 4mm in diameter were located on the PMMA made anode well layer. The mini-MFCs contained 2mm thick PMMA supporting layer, and PEM layer carried the nafion membrane (proton-conductive polymer film) with 8 Pt/C electrodes (Figure 2.8). The biofilm formation on gold electrodes was attained after one day operation that increased the electricity production. 29mW/m<sup>2</sup> power density and 2148mA/m<sup>2</sup> current density were collected via this mini-MFC (Chen *et al.*, 2011). Two years later, monitoring of electrochemically active bacteria was conducted in five layers microbial fuel cells (MFCs). An anode electrode layer made of Cr/Au on PMMA, an anode chamber layer (gasket) of 1.5 $\mu$ L volume, a proton exchange membrane (PEM), a cathode chamber layer (gasket) of 1.5 $\mu$ L volume and a cathode electrode layer made of Cr/Au on PMMA layers constituted the MFC from bottom the top. The electricity generation capacities of bacterial cells, wild-type *Shewanella oneidensis* (*S. oneidensis*) and *Pseudomonas aeruginosa* (*P. aeruginosa*) along with the isogenic *nirS*, *lasI*, *bdIA* and *PilT* mutants were compared, and they were found to perform different efficiencies of extracellular electron transfer. 6 different MFC showed only 1.4% difference among each other (Mukherjee *et al.*, 2013). In 2016, Mardanpour and Yaghmaei investigated nickel based microfluidic microbial fuel cell (MFC) and *Escherichia coli* cells were used as the biocatalyst. Bioelectricity generation from glucose and urea of human blood and urine, respectively, was accomplished by using MFC as a power production. The device was made of PMMA and included a microchannel of 1mm height, 1mm width and 8cm length. The MFC can be operated in both fed-batch and continuous modes.

Glucose-fed and urea-fed MFCs can have  $5.2\mu\text{W cm}^{-2}$  and  $14\text{Wm}^{-3}$  power densities, respectively, providing high power density, self-regeneration, waste management and low production cost instead of conventional methods (Mardanpour, and Yaghmaei, 2016). Cyanobacterial photosynthetic and respiratory processes are capable of electricity production in all day. Nine bio-solar panel microsystem, having PMMA energy capturing layer, an anodic PMMA chamber layer ( $140\mu\text{L}$  volume), proton exchange membrane (PEM) and a bottom PMMA layer for exposing air-cathode to oxygen, was fabricated. *Synechocystis* sp. PCC 6803 cells produced  $5.59\mu\text{W}$  maximum power and  $1.28\text{V}$  energy. This study can be a progression in bio-solar cells to promote high energy production (Wei *et al.*, 2016).

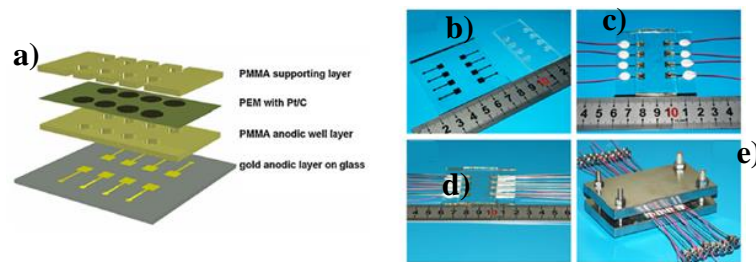


Figure 2.8. (a) mini-MFC schematic illustration (b) Gold anodic layer on glass and PMMA anodic well layer (c) Image of the bonded PMMA anodic well layer on glass substrate (d) Metal straw sealed by silicon rubber to the anodic layer (e) Assembled mini-MFC (Chen *et al.*, 2011).

Very recently (2017), a microbial electrolysis cell (MEC) was fabricated to produce biohydrogen for medical applications. *Escherichia coli*, non-pathogenic bacteria cells, were used to bioxidate the human excreta in MEC to generate the biohydrogen.  $0.94\mu\text{L}$  hydrogen ( $\mu\text{L}$  urea)-1day-1 from urea and  $0.84\mu\text{L}$  hydrogen ( $\mu\text{L}$  glucose)-1day-1 from glucose were attained. The device was made of PMMA and included a microchannel of  $7\text{cm}$  length,  $1\text{mm}$  width and  $1\text{mm}$  depth. Chemotaxis phenomena was also investigated in MEC device and the results were found to be compatible with the real conditions (Mardanpour, and Yaghmaei, 2017). Integrable and scalable power source of MFC, based on laminar-flow, was produced, where the device was operated without any physical membrane in it, and the virtual membrane was created to harvest the electricity.

Y-shaped microfluidic chambers were located in the device, and the size of the array was  $5.5\text{cm} \times 7\text{cm}$  with 4 MFC units of 8mm length, 3.8mm width and  $102\mu\text{m}$  height. Wild type *Pseudomonas aeruginosa* PAO1 cells were used in the system, and a power density of  $60.5\mu\text{W}/\text{cm}^2$  was obtained using  $100\text{k}\Omega$  load power output (Yang *et al.*, 2017). The manufacturing of products having importance on human life like biological hydrogen production from renewable resources can be accomplished in the thermoplastics made devices, as they are hard and durable to certain reactions.

## 2.5. Conclusion/Future Directions

This study provides an overview of recent advances in microfluidic devices made from PMMA, PS and COP that have been used in biological applications. Different aspects related to the cultivation, separation/isolation, detection and reaction experiments in microfluidic devices have been discussed and an overview of these studies carried out since 2000 to today is given. The main conclusions are as follows: (1) High-throughput analysis at low cost can be done in a single device that is capable of conducting parallel experiments. (2) More detailed results can be obtained by integrating imaging technologies. (3) Experiments can be conducted in a stable, well defined and biologically relevant culture environments. (4) Multi-organ microphysiological systems can be constituted by mimicking the real conditions. (5) More than one process such as lysis, amplification and separation can be accomplished in a single device.

Microfluidic systems technology continues to evolve and progress in every field. However, more economical, environmentally friendly and portable devices should be fabricated. Scientists should be more interested in real-world problems, such as epidemic illnesses etc., and serious steps should be taken to solve these problems. Many of the developing countries are short of healthcare facilities and medicine. Devices for point-of-care diagnostics can be fabricated for pathogen or disease detection and this can be life saver in these countries. With many devices in or under development, innovative designs, improvements in processes and growth in consumer applications will lead mems products to have a market share of 24 billion US dollars in 2020. The breakthrough technologies in bio-mems will overcome the challenges encountered so far and make room for new mems applications in multiple markets.

### 3. DESIGNING AND FABRICATION OF A THERMOPLASTIC MADE MICROBIOREACTOR FOR YEAST CULTURING

Microfluidic platforms have become popular for experimental cell studies in recent years since they enable less material/volume consumption, fast result acquisition and single cell tracking. In conventional bioreactor experiments, average properties of cell populations inside a specific volume are measured, while in microfluidic devices the same cell can be monitored from the beginning to the end of the experiment under continuous flow. Performing single cell study in a microfluidic system is a robust and sensitive method to track cell-to-cell variations. Being a closed system and maintaining a controlled environment, risk of contamination is minimized in microfluidic bioreactors. Real-time monitoring of cells in response to input feeding is possible.

Cell division, volume change and fluorescently tagged specific protein expression can be monitored on single cell basis. The perturbations like drug or inhibitor applications to microbial cells often prolong the cell cycle and experiment time. Thus, when working with these cells, the materials used to fabricate microfluidic devices (microbioreactors) must be durable. One of the well-known and mostly used material for microfluidic studies is polydimethylsiloxane (PDMS). PDMS is biocompatible, transparent and it has low auto-fluorescence (Bélanger and Marois, 2001), (Piruska *et al.*, 2005). However, absorption of hydrophobic molecules by PDMS is one of the main drawback of this material. Working with drug solutions or biomolecules for extended hours is difficult in PDMS devices (Toepke and Beebe, 2006). Surface treatment of PDMS is also necessary to eliminate its hydrophobicity (Trantidou *et al.*, 2017).

Due to the mentioned disadvantages of PDMS, thermoplastic made microfluidic chips have been developed as alternatives (Gencturk *et al.*, 2017). Thermoplastic materials can be softened via heat and pressure and they harden after cooling, taking the shape of the desired device without going through any chemical modification (Odabasi *et al.*, 2018). Among several thermoplastics, cyclo-olefin polymer (COP) is selected as the material for the fabrication of the microbioreactors because it is biocompatible for biological studies and transparent for visualization. It has low auto-fluorescence and high dimensional stability.

Moreover, COP is suitable for mass manufacturing process and it is durable for long-hours of cell culture experiments (Puza et al. 2017). *Saccharomyces cerevisiae* (*S. cerevisiae*) is a widely used eukaryotic model organism in molecular and cell biology studies due to its complex genetic structure, rapid growth ability in optimum conditions and easy replication properties (Sherman 1997). Ease of manipulation and genetic tractability make yeast cells more attractive for mammalian cell protein analysis. 31% of proteins encoded by yeast genes have human homologs and vice versa.

Therefore, yeast is a valuable predictor of human gene functions, and has increased the knowledge of the principal pathways in humans and has promoted the awareness of many disease genes (La Ferla *et al.*, 2015), including ribosomopathies, the human disease that influences ribosome biogenesis (Woolford and Baserga, 2013). In the literature, there are several works conducted with yeast cells in microfluidic platforms. High-throughput microfluidic imaging system for single yeast cell tracking was performed over multiple generations (Falconnet *et al.*, 2011, Hansen *et al.*, 2015). More recently, microfluidic devices were developed to investigate various biological issues like spatial variation in yeast cell growth in heterogeneous environment, the formation of gene expression landscapes (Marinkovic *et al.*, 2019), protein dynamics during sporulation of yeast cells (Zhao *et al.*, 2019), long term imaging of yeast cells under constant or changing environment,

DNA damage using of genotoxic chemicals (Schmidt *et al.*, 2018), and isolation of cells in an automated system (Yu *et al.*, 2018). Microfluidic impedance cytometry was used to combine cell impedance with yeast cell morphology (Haandbæk *et al.*, 2016). There are also review papers about yeast cells in microfluidic devices with several applications (Dusny and Grünberger, 2020), (Jo and Qin, 2016). In the present part, we designed a new microfluidic chip and fabricated it using COP substrates. With the new design, it is now possible to conduct two different experiments at the same time unlike the previous designs (Odabasi *et al.*, 2018), (Puza *et al.*, 2017).

Two different strains in one medium or two different media with single strain can be operated in this platform. Comsol 5.2 software with microfluidics module was used to determine the system dynamics of the designed device. Here, our focus is to show the benefit of our dual purpose design of new microfluidic chip in experimentation.

### 3.1. Materials

The strain used in this study is *Saccharomyces cerevisiae* (EY0987 genetic background  $\text{Mat}\alpha$   $\text{his3}\Delta 1$   $\text{leu2}\Delta 0$   $\text{lys2}\Delta 0$   $\text{ura3}\Delta 0$  (S288C)) with the RFP tagged YLR197W (Nop56p) gene, kindly provided by Peter Arvidson from Harvard University, HHMI. Cyclo olefin polymer (COP) (Product code: Zeonor 10-0672-0349-1.0-05) was purchased from Microfluidic ChipShop Company (Jena, Germany).

Polyethylene tubing (Product code: BB31695-PE/6) and epoxy (5min epoxy) are products of Scientific Commodities Inc. SCI (Lake Havasu City, AZ 86406, The USA) and BISON (Rotterdam, The Netherlands), respectively. All the chemicals and reagents (including HU, HMF and temsirolimus) used for medium preparation were purchased from Sigma-Aldrich (Taufkirchen, Germany) and metformin was purchased from a local pharmacy under the brand name of Diaformin.

### 3.2. Design of the Microfluidic Device

The experimental setup is shown in Figure 3.1. The new design used in this study was improved considering the shortcomings of the devices used in the previous studies (Odabasi *et al.*, 2018; Puza *et al.*, 2017). Working with single strain and single medium was one of the most cumbersome aspects of the previous design, consuming time and energy (work power). The chambers are now placed in parallel fashion instead of series arrangement. This allowed the cells to be evenly distributed throughout each chamber and eliminated residues coming from the front chamber affect the rest of the chambers in series configuration.

The present microfluidic device includes two different segments, each having 8 chambers with C-shaped regions, which are placed along the channels to trap the yeast cells (Figure 3.1a). This design enables the cultivation of two different strains in one type of nutrient medium or the cultivation of one strain in two different nutrient media, i.e. there is no need for the exchange of cell culture and nutrient flows. The dedicated lines for yeast cells (2) and the nutrient medium (1 & 3) prevent any contamination among the channels (Figure 3.1a). In addition, every chamber within the device act like an independent microbioreactor. Thus, two different experiments are repeated for 8 times.

### 3.3. Device Fabrication

#### 3.3.1. Computational Fluid Dynamics (CFD) Simulations

Various fluid dynamics simulations were performed to reach the optimum design for cell trapping. The main purpose of the simulation is to analyze design alternatives to achieve cell trapping in all C-shaped regions of 16 parallel microfluidic channels. In order to achieve this, two main modules (spf and fpt representing laminar flow and particle tracing for fluid flow, respectively) and a multi-physics module (fluid-particle interaction) were created and simulated in COMSOL 5.2.

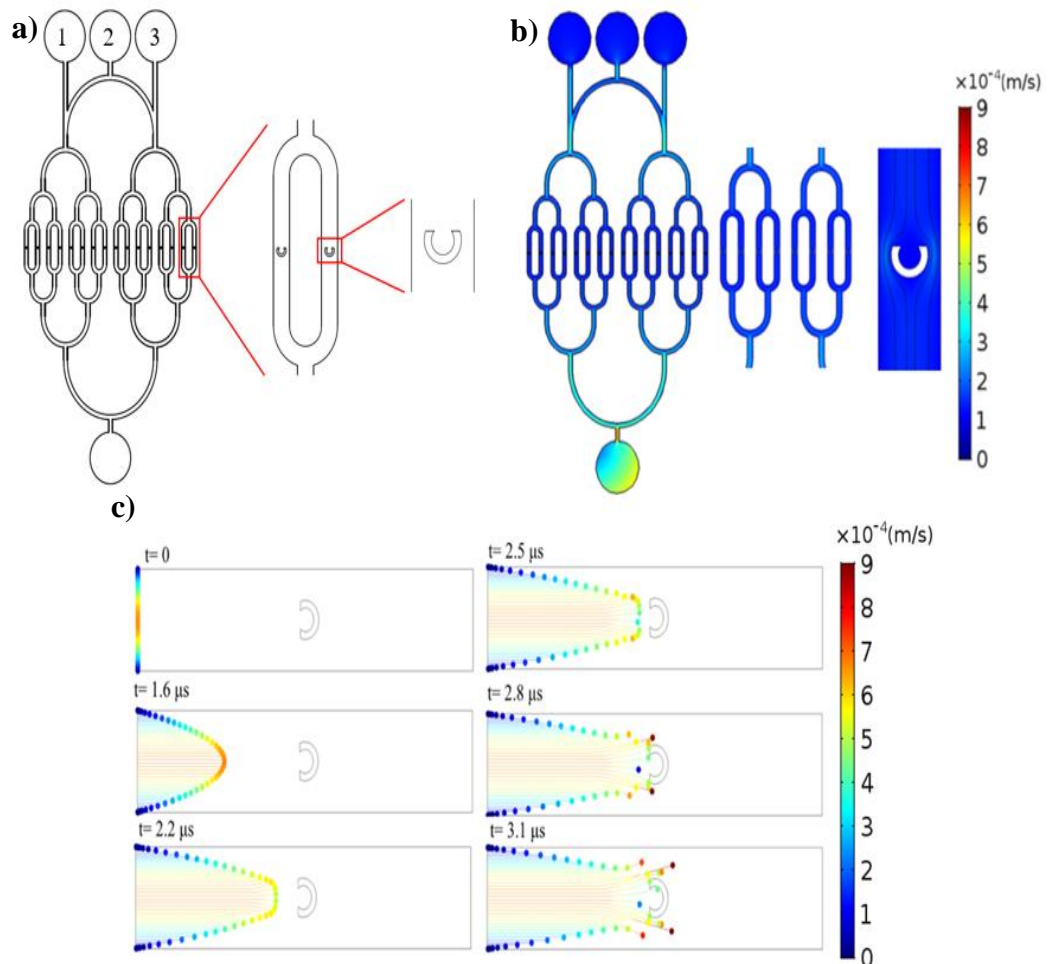


Figure 3.1. (a) Schematic illustration of the device design (b) Simulation of trapping mechanism with parallel channel designs showing 16 equivalent stagnation points in C shaped regions (c) Particle tracing at different time points.

The design effort is based on creation of stagnation points in each channel inside the c shape. For this purpose, spf module was used to analyze the flow rates and directions in the channels. Fpt plays an important role to analyze particle movement under laminar flow condition that is solved by the multi-physics module. Mesh analysis is based on independent solver that allows us to observe same results on coarse, normal, fine and extra fine mesh designs. The simulation of trapping mechanism with parallel channel designs enables equal 16 stagnation points in C shaped regions.

Due to the laminar flow, the stagnation point is observed inside the C shape and high velocity profile between the C shape and channel walls. Figure 3.1b shows velocity profile in the microfluidic channel with velocity field streamlines that also prove the stagnation point. After implementation of spf module of Comsol 5.2, fpt was implemented with the time dependent solver that enables to observe the trapping mechanism with different time scales. It can be clearly seen that every particle has unique speed because of its location, and particles follow the velocity profile of laminar flow. As the particle has higher velocity in the middle of the channel, it moves directly towards the stagnation point, other particles on the sides continue to move from the edge of the C shape to the outlet. Finally, several particles can be observed in the C shape in Figure 3.1c.

### **3.3.2. Mold Preparation**

3.3.2.1. Photolithography. The design was drawn on AutoCAD software. The flow rate required for cell trapping in the c-shaped chambers was arranged. Finalized design was transferred to the acetate paper to be used in the photolithography process. 1 mm thick stainless steel substrate was employed for the photolithography process. Here, the aim is to transfer the design on the acetate paper to the stainless steel substrate. Stainless steel substrate was cleaned with baby shampoo, acetone, isopropyl alcohol (IPA) and distilled water, respectively. It was dried with nitrogen gun to leave no dust on wet stainless steel. Sanitized steel was located in the spin coater and PR-1828 photoresist was coated on it to obtain an average photoresist layer thickness of 5  $\mu\text{m}$ . Soft baking process was implemented for 2 min at 95  $^{\circ}\text{C}$  on hot plate to the photoresist coated steel. Acetate paper with design was superimposed on the coated steel and UV light (490 nm) was sent for 3 min. UV light

exposed photoresist on the steel was removed by dipping into the developer solution. The design made of photoresist on the stainless steel substrate was cleaned with distilled water and dried. The shape of the design was checked under the microscope and photoresist layer was hard baked on the hot plate for 3 h at 110 °C.

3.3.2.2. Electrochemical wet etching. In order to have a positive stainless steel mold, electrochemical wet etching process was used (Gokdel *et al.*, 2010). Once the master mold is created, it can be used both fabrication of thermoplastic chips with and without electrodes. NaCl : Distilled water solution was prepared in a ratio of 1 : 4 (w/w). Photoresist coated steel and a blank steel were placed in the container facing each other and NaCl solution is poured in it. Blank steel was used as cathode while photoresist coated steel was used as anode. DC current of 60 A was applied between the steels for 20 s, resulting in an etch depth of around 12 µm. The stainless steel positive master mold containing the chip design in all details was obtained.

### **3.3.3. Drilling Inlet-Outlet Reservoirs and Planarization**

Blank COP substrate of 75.5 mm x 25.5 mm x 1 mm (L x W x H) dimension is placed on the stage of computer numerical control (CNC) machine and the inlet and outlet holes are drilled automatically according to the coordinates of the design. The drilled COP piece is put into ultrasonic bath for 15 min and dried with N<sub>2</sub> gun. Burrs around inlets and outlet are cleaned via craft knife to have smooth surface for proper bonding. This COP sample is then pressed with the help of 2-mm-thick blank glass pieces using a hydraulic press machine. Glass pieces and COP are cleaned using baby shampoo, acetone, isopropyl alcohol (IPA) and distilled water, respectively. They are dried with N<sub>2</sub> gun.

After this cleaning process, all of the pieces are stacked in the order of glass-COP-glass, covered with aluminum foil and placed on the hot plate of the hydraulic press machine, which was set to 130 °C. The system is warmed up for 10 min and then 35 bar pressure is applied for another 10 min. Finally the pieces are left for cooling to 60 °C for 1.5 h under pressure. The purpose of this pressing step is to remove any further bumps or burrs remaining on the surface after drilling.

### **3.3.4. Hot-embossing**

Hydraulic press machine was set to 130 °C. Glass transition temperature of the COP is 136 °C. While hot embossing was selected close to the glass transition temperature, a lower temperature was preferred for the thermo-compression bonding process. The stainless steel mold, pressed COP and a glass pieces were cleaned with baby shampoo, acetone, IPA and distilled water, respectively. Nitrogen was used for drying of all parts, dust-free napkin was employed for removing the traces on the surfaces and nitrogen was used again to clean out residual dusts. Pressed and cleaned COP was superimposed on the mold, and glass was put onto them. All of the pieces were placed on the hot plate of the hydraulic press machine, and a piece of aluminum foil was used to cover all of the parts. The hot plates of the press machine were brought close together, and pieces (the stainless steel mold, COP and glass) were warmed up for 10min. 35 bar pressure was applied for 10min subsequent to warming up. The system was left for cooling to 60 °C, under pressure for 1.5 h.

### **3.3.5. Thermo-compression bonding**

In this step, hot embossed COP piece and a blank COP piece are bonded together. Bonding process should be conducted below the glass transition temperature of the polymer to prevent the deterioration of the patterns on the hot embossed piece. The glass transition temperature of the COP is 136 °C and the temperature for bonding process is optimized as 125 °C. COP pieces are placed between glass ones and covered with a piece of aluminum foil. The cleaning procedure is carried out as described in previous sections. After pieces are thermally stabilized at the set temperature value, 25 bar pressure is applied for 45 min to start bonding. After this step, the temperature controller of the hydraulic press machine is set to room temperature to cool under pressure. Cooling process takes 3 h and glass pieces are separated from the bonded pieces carefully without damaging. Figure 3.2c shows the fabricated device.

## **3.4. Medium Preparation and Microscopy**

Yeast nitrogen base (YNB) (2% glucose, yeast extract, nitrogen base) media were used during the experiments. YNB medium including 2% glucose, 1.7g/L YNB, 5g/L ammonium sulfate, 0.1g/L leucine, 0.02g/L histidine, 0.03g/L lysine and 0.02g/L uracile was prepared

for yeast cells (Nop56:RFP). HU, HMF and temsirolimus were added dry to final concentration of 200 mM, 4g/L and 0.2 $\mu$ g/mL (prepared from powder form and not sterilized), respectively. The optical density (OD) of the preculture loaded to the microfluidic device was 0.5 (600 nm). 1.25 g metformin in powder form was dissolved in 100 ml DMSO. 2 ml of metformin-DMSO solution was added to YNB medium and final concentration of metformin was 0.025%.

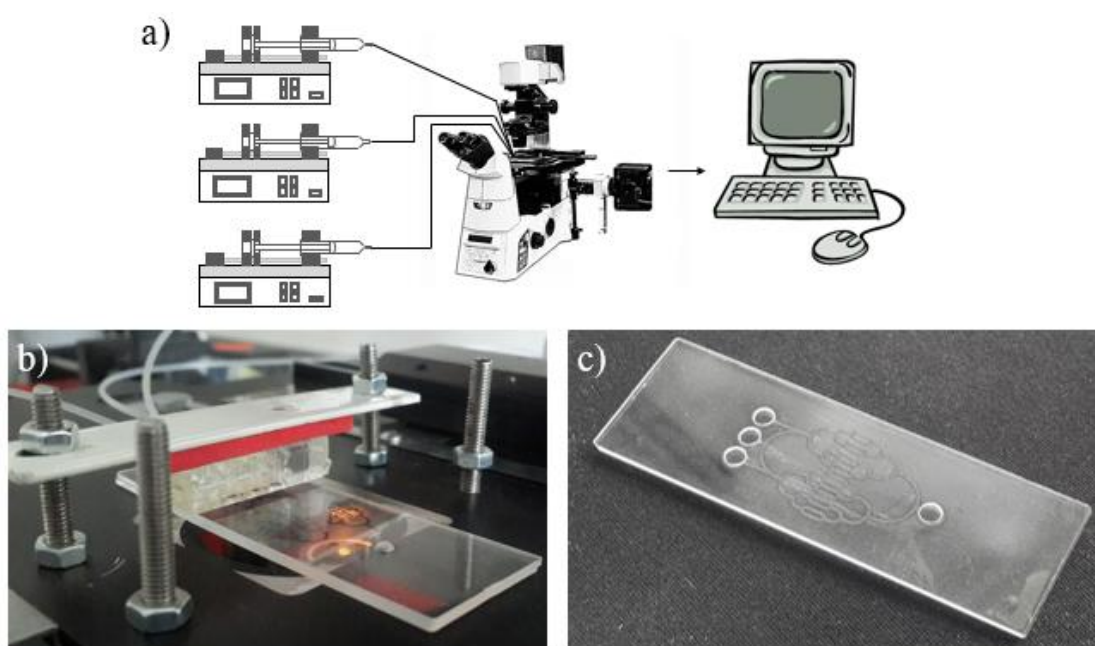


Figure 3.2. (a) Experimental setup (b) In-house fabricated microbioreactor placed on microscopy stage with external tubing connections (c) Fabricated microfluidic device.

Nikon Ti-E inverted fluorescence microscope with Nikon DS-Ri2 detector and Texas Red filter were used to detect Red Fluorescent Protein RFP:Nop56 tagged yeast cells. Brightfield and fluorescence microscopy images of the cells were taken during the experiments and ImageJ (NIH, Bethesda, MD) software was used to process the acquired images. Several filters and Otsu thresholding were applied to obtain cell count and perimeter values. Moreover, red channel was used to analyze fluorescence microscopy images of the cells in accordance to their RFP tagging. Figure 3.2a and Figure 3.2b shows the experimental setup illustration and microbioreactor chip placed on the microscopy stage with established external tubing connections, respectively.

### 3.5. Microfluidic Device Operation

First, the priming step of the microfluidic device with YNB medium was performed and then, yeast cells grown in the YNB medium were loaded into the device. Cells were trapped in the c-shaped regions of the chambers, and fresh YNB medium was sent through the device for 3-6 h. Thereafter, the drug administration was started, that lasted for another 3 h. Subsequently, fresh YNB medium was fed for the next 10 h for the recovery of cells until the end of the experiment. During these operations, the cells were monitored by using Nikon Ti-E inverted fluorescent microscope, brightfield and fluorescence microscopy images (60X lens) were taken every 9 – 15 minutes and luminescence of Nop56:RFP was followed. A sequence of captured brightfield images of a trapped cell showing its budding process can be seen in Figure 3.3 as an example. When cells were trapped inside the device, their morphological changes and cell cycle can be tracked. Variation in budding times and cell status before and after drug treatment can be observed.

### 3.6. Results and Discussion

Cell cycle is the series of events happening in cell with the DNA duplication, organelles to produce two daughter cells and cytoplasm division. G1, S, G2 and M are the 4-phases of cell cycle (Figure 3.4). Actively dividing eukaryotic cells undergo these phases and the cell grows and divides into two identical cells. In the G1 phase, cell size increases and cellular components double. DNA replication (replication of chromosomes from 23 to 46) occurs in S phase. In the G2 phase cells prepare themselves for cell division and in the M phase cytokinesis (cytoplasm division) takes place. At the end of this process two identical daughter cells form (Han-Shu *et al.*, 2019).

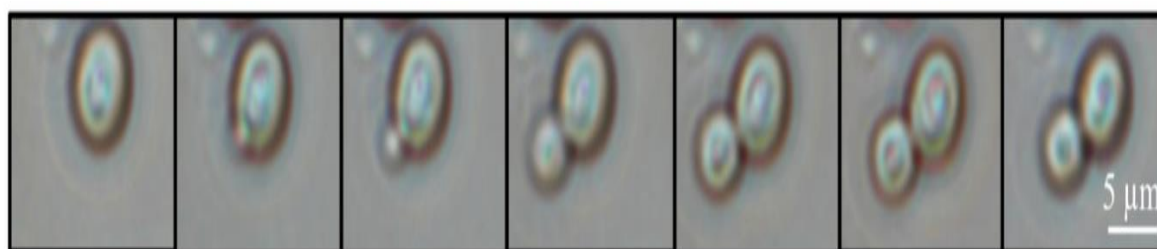


Figure 3.3. Microfluidic device used for single cell tracking.

In yeast, the cell division is affected by ribosome biogenesis, which starts at the nucleolus and is related to ribosome production. It is a complicated and tightly coordinated process (Bernstain *et al.*, 2007), (Lempiäinen and Shore 2009), (Leary and Huang, 2001), (Gomez-herrerros *et al.*, 2013), (Ebersberger *et al.*, 2014), (Thomson *et al.*, 2013). When cells pass through START mechanism in late G1 phase, cell division process begins (Polymenis and Aramayo, 2015).

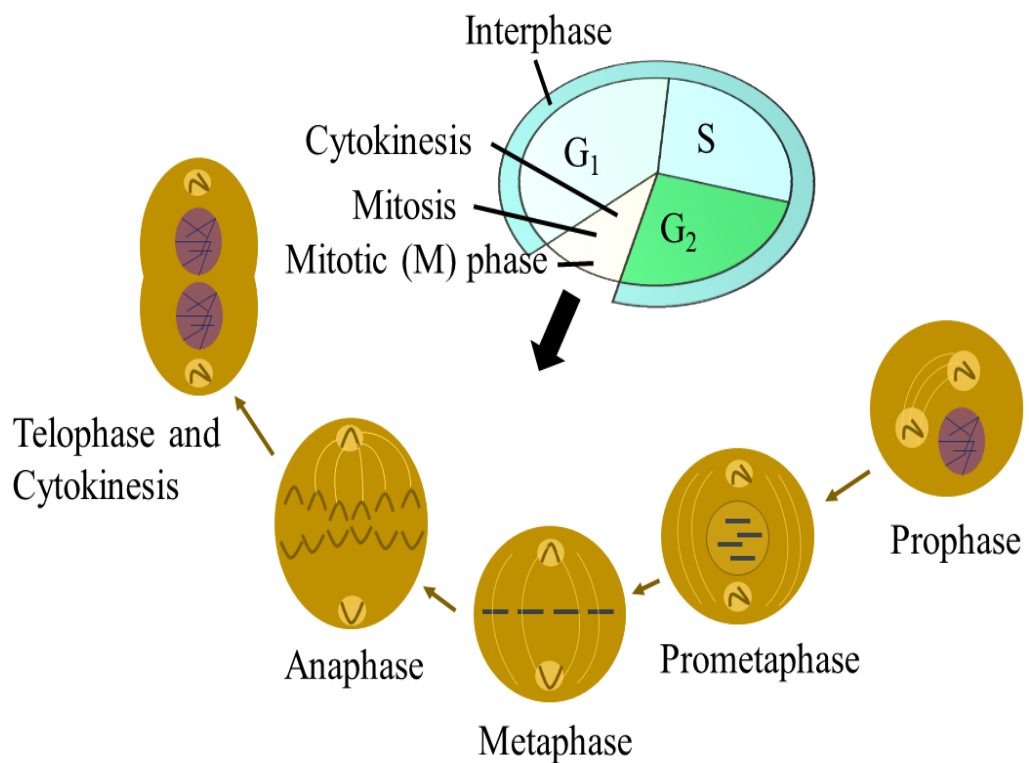


Figure 3.4. Schematic representation of cell cycle phases and checkpoints.

The size of the cell at division and the ribosome numbers are related to the growth rate. Although up to date studies have implied various interactions between cell cycle and ribosome synthesis in cells (Bernstain *et al.*, 2007), (Dez and Tolvervey, 2004), there are still gaps of knowledge of that relationship. In order to observe the changes in ribosome assembly/pre-processing and cell cycle in response to the growth inhibitory drugs, RFP tagged Nop56 nucleolar protein is selected. Nop56 is an essential evolutionarily-conserved nucleolar protein, and is required for ribosome synthesis (Lafontaine and Tollervey, 2000). Nop56 expression as well as the critical cell size for budding of yeast cells are followed in in-house fabricated dual purpose microfluidic bioreactor system.

### 3.6.1. Effect of Hydroxyurea on Yeast Cells

The changes in cell cycle as well as in protein synthesis within the yeast cells were followed under the application of the anti-tumor agent HU applied to the one side of the chip. In Figure 3.5, the expression of RFP tagged nucleolar Nop56 gene product can be tracked in single live cells before, during and after HU treatment. Before HU application, each cell continued its normal life cycle. The cells' luminescence was significantly decreased during HU treatment period, as the DNA replication was inhibited by HU treatment (Figure 3.5). When the HU feeding was stopped and fresh nutrient medium was flown through the microbio reactor, the cells recovered themselves slowly and luminescence increased.

Figure 3.6a shows stable cell count in yeast population under steady state conditions including the HU treatment period. There was neither proliferation nor cell death in between the 435th and 610th minutes (Figure 3.6a). After the HU treatment, cell count increased gradually (from 55 to 70 cells) towards the end of the experiment. When the total cell perimeter was considered as a representation of biomass synthesis rate, there was a decrease in dimensions of the cells during HU feeding period. However, after the HU treatment, the cells were able to recover, and increase in size was observed through the end of the experiment (Figure 3.6b). The total fluorescence intensity of the cell population was decreasing in a certain time interval before the HU treatment period (Figure 3.6c). That time might coincide with the mitosis phase (M phase) of the cells where the protein synthesis slows down. During HU treatment, the fluorescence intensity got closer to zero at some points, indicating suppression of Nop56 expression or inviability. The reason for this might be that, HU slows down the S-phase of the cell cycle and it suppresses the cell proliferation event. Consequently, the protein synthesis, which should follow Nop56 protein expression, did not take place within the cell. Since HU is a DNA synthesis/replication inhibitor, it affects the progression of S-phase. HU treatment causes S phase to continue in slow motion but does not cause to stop the cell cycle. Cells probably maintained their regular evolution, as increasing trend in the fluorescence intensity was observed after the release of HU through the end of the experiment, where protein synthesis seems to be the dominating process compared to proliferation. We may speculate that, after the release of HU, the cells are maintaining themselves and during this maintenance step Nop56 protein might have a role in DNA repairing.

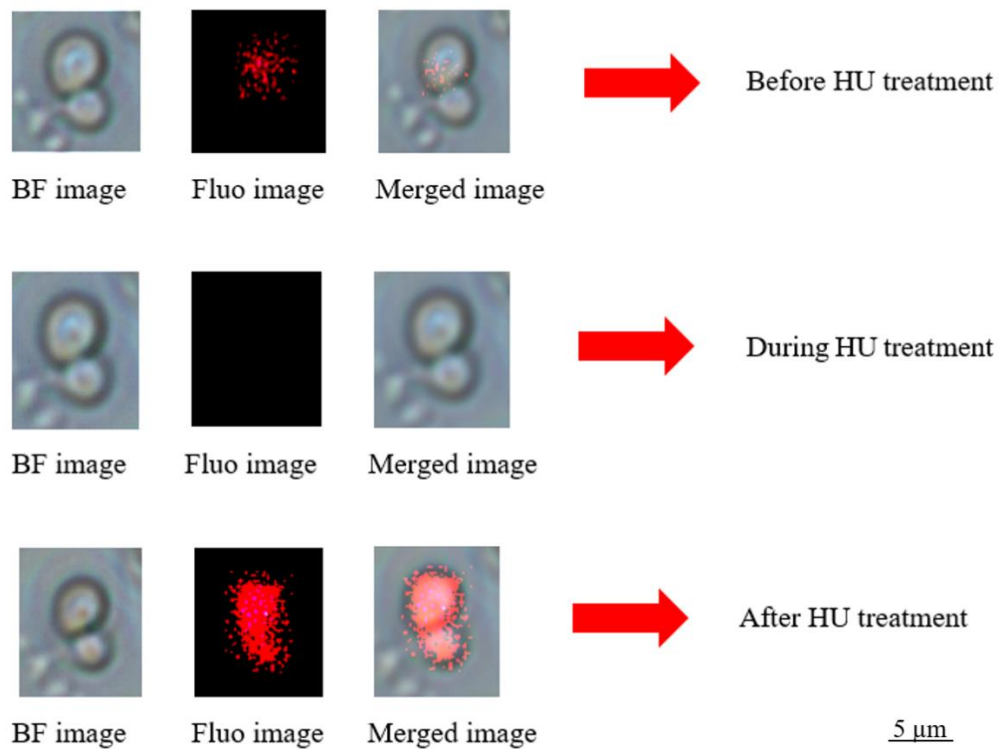


Figure 3.5. The brightfield (BF), fluorescence (Fluo) and merged microscopy images of yeast cells before, during and after hydroxyurea (HU) treatment.

The role of nucleolar protein Nop56p in DNA replication has already been reported (Bogomolnaya *et al.*, 2004). Nop56 is used before the initiation of DNA replication, shortening the duration of G1 phase of the cell cycle (Bogomolnaya *et al.*, 2004). In our experiments, the duration of G1 phase took 26.5 min on average (Figure 3.6d), and the cell cycle duration took 112 min before HU administration. However, after HU treatment, the cell cycle duration changed to 131 min. When the data at 900th minute were considered, all of the cells recovered themselves. This result proves that, although HU slows down the cell cycle mechanism, it does not kill the cells. As also observed by the time profile of perimeter, the biomass synthesis rate is sustained after the cessation of HU application. The typical examples of single cells obtained in the experiments are discussed below in terms of the effects of HU inhibitor on cell cycle, cell dimension and Nop56 expression (protein synthesis). In the presence of HU, elongated ellipsoidal yeast cells were observed in YNB medium (Figure 3.7a) and the Nop56 gene expression was repressed. HU might have suppressed ribosome biogenesis proteins and generated elongated cell morphology. Similarly, in literature, it was reported that the repression of most of the ribosome biogenesis

proteins (20S and 60S proteins) caused an excessive extension in the buds of the yeast cells (Thapa *et al.*, 2013). In YNB medium, if HU was not present in the medium, G1 phases of the single cells took  $32 \pm 11$  min, in agreement with literature.

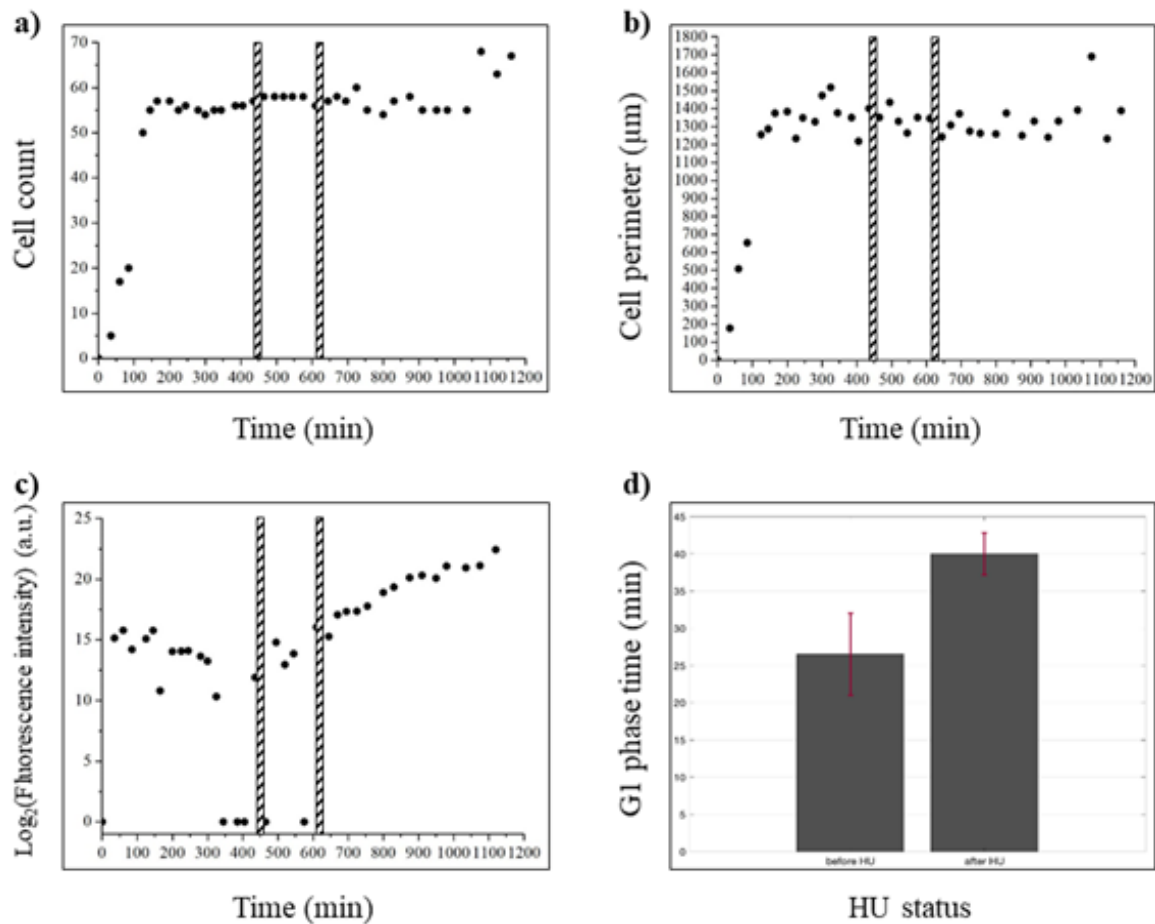


Figure 3.6. (a) Time profile of the cell count. (b) Time profile of the cell perimeter (population). (c) Time profile of the fluorescence intensity (Vertical lines indicate the start and end of HU application) (d) Duration of G1 phases before and after HU treatment.

The doubling times were around 112 and 131 min, before and after HU treatment (in fresh nutrient medium), respectively. In the presence of HU, for example, Cell 4 and Cell 9 started budding after 233 min of coming to the chamber, i.e. G1 phase of these cells actually took more time than 233 min. Similarly, in literature reports, suppressing the synthesis of most 40S ribonucleoprotein subunit proteins led to the arrest of the cell cycle at G1 phase or dramatically slowed down the G1 phase (Thapa *et al.*, 2013). It was highly probable that the yeast cells exposed to HU at high concentration had slightly higher critical volume to divide

as shown in Figure 3.7b. The fluorescence intensity of some single cells fell to almost zero after HU application as shown in Figure 3.7c. On the other hand, at the end of the experiment, the cells' integrated fluorescence density increased indicating cell viability and recovery. In order to complete the cell cycle, protein synthesis is necessary. We observed that the ribosomal protein Nop56 was extensively expressed when the single cell perimeter is around 14-16 micrometers. This can be seen in Figure 3.7c, where fluorescence density is plotted versus cell perimeter. This corresponds to G1 phase of the cell cycle. Nop56 expression was significantly decreased when the live single cell's perimeter increased to more than 20 micrometers, i.e. at the end of cell cycle, probably the M phase. Cells require a rapid protein synthesis during G1 to create crucial regulatory proteins. Moreover, protein synthesis is also needed to complete the G2 phase and enter mitosis (Burke and Church, 1991). In budding yeast cells; a conserved transcriptional activation of ribosome biogenesis was reported before the cells started a new round of cell division, i.e. at G1 phase (Blank *et al.*, 2017).

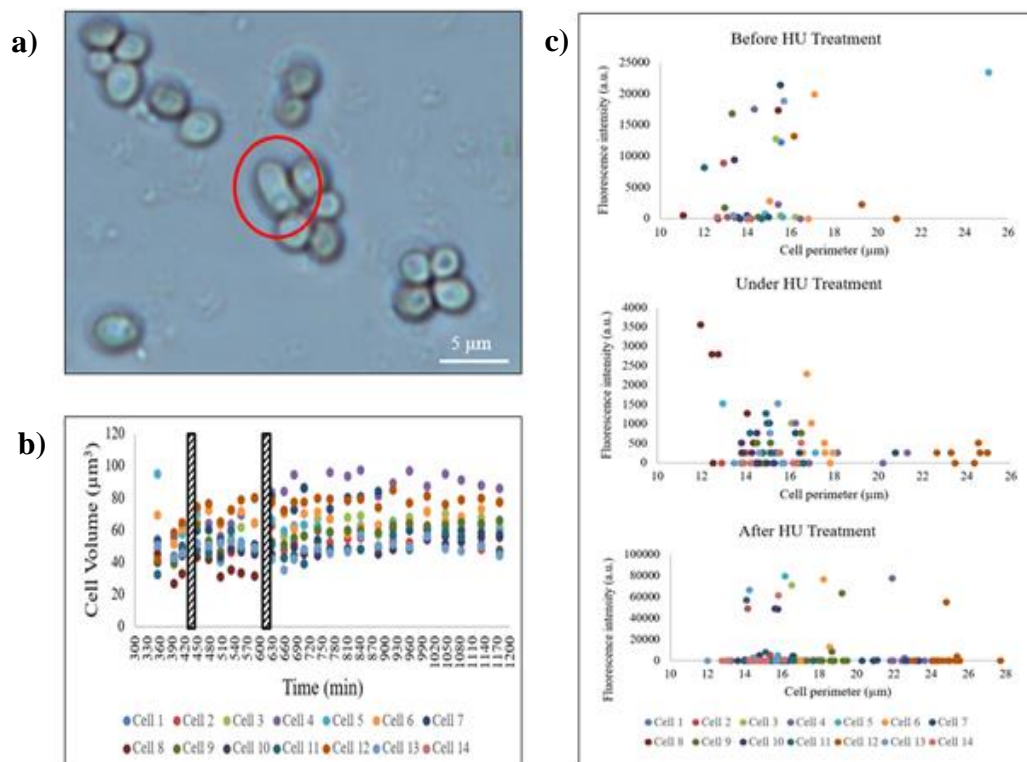


Figure 3.7. (a) Long spheroidal shape of yeast cell during YNB HU experiment (Chamber 2) (b) Time profile of single cell volume during YNB HU experiment (Chamber 1) (c) Time profiles of single mother and daughter cells integrated fluorescence density and perimeter before, during and after YNB HU experiment (Chamber 1).

HU treatment causes inhibition of ribonucleotide reductase (RNR), inhibition of the ribonucleoside diphosphate reductase (Madaan et al. 2012) and subsequent deoxyribonucleoside triphosphates (dNTPs) production (Dubacq et al. 2006; Alvino et al. 2007; Koç et al. 2004). dNTPs appear when cells enter S phase and induce an S-phase checkpoint response, which results in transcriptional activation of RNR genes and prevention of cell-cycle progression (Dubacq et al. 2006). HU, thus, interferes with the S phase progression and engages the checkpoint to prevent the passage into a catastrophic mitosis throughout the cell cycle. Although, many studies stated that, HU does not affect protein synthesis (Alvino et al. 2007), it might have an effect on ribosome biogenesis (Kihlman et al. 1966; Johnston 1980; Scala et al. 2016). If ribosome biogenesis is hindered, an Rb-like protein (Whi5)-dependent mechanism restrains cell cycle commitment event (START) (Lempiäinen and Shore 2009). Thus, ribosome biogenesis and protein synthesis are the major steps of cell proliferation. Ribosomes direct the G1-S phase transition, hence control the cell cycle progression.

### **3.6.2. Effect of Metformin on Yeast Cells**

Cell growth comprising of transcription, translation, protein degradation etc. is regulated by the target of rapamycin (TOR) pathway. The proteins in the mammalian TOR family are conserved from yeast to man (Mayer and Grummt, 2006). Transcription, protein synthesis, ribosome biogenesis, nutrient transport and mitochondrial metabolism are the anabolic processes governed by the TOR. On the other hand, mRNA degradation, ubiquitin-dependent proteolysis, autophagy and apoptosis are the negatively regulated catabolic processes by TOR (Hall 2008). Stalling of cell growth and release of autophagic processes are the results of the absence of mTORC1 signaling. In this part of the work, the response of yeast cells to mTOR inhibitor, the drug metformin, was investigated to reveal the role of mTOR signaling in ribosome biogenesis/synthesis and cell proliferation on the other side of the chip while the cells on the previously mentioned side of the chip were under the influence of the anti-tumor agent HU. Under the experimental conditions of metformin, the cell count increased in the first 500 min including the drug treatment period (Figure 3.8a). Total cell perimeter also increased continuously until the drug application. However, it slightly decreased due to metformin effect on the cells, in spite of the increase in cell count during the metformin application period (Figure 3.8b). Cell growth is identified as an increase in

cell size rather than an increase in cell number which is the outcome of the cell division (Hall 2008). Since metformin acts as the cell growth inhibitor, a decrease in cell size is a reasonable outcome. Since metformin is used to regulate the insulin level, the glucose uptake mechanism of cells might be disturbed. Cells continued to cell division, so cell count increased, but their dimensional growth (cell size) decreased due to metformin effect on cells.

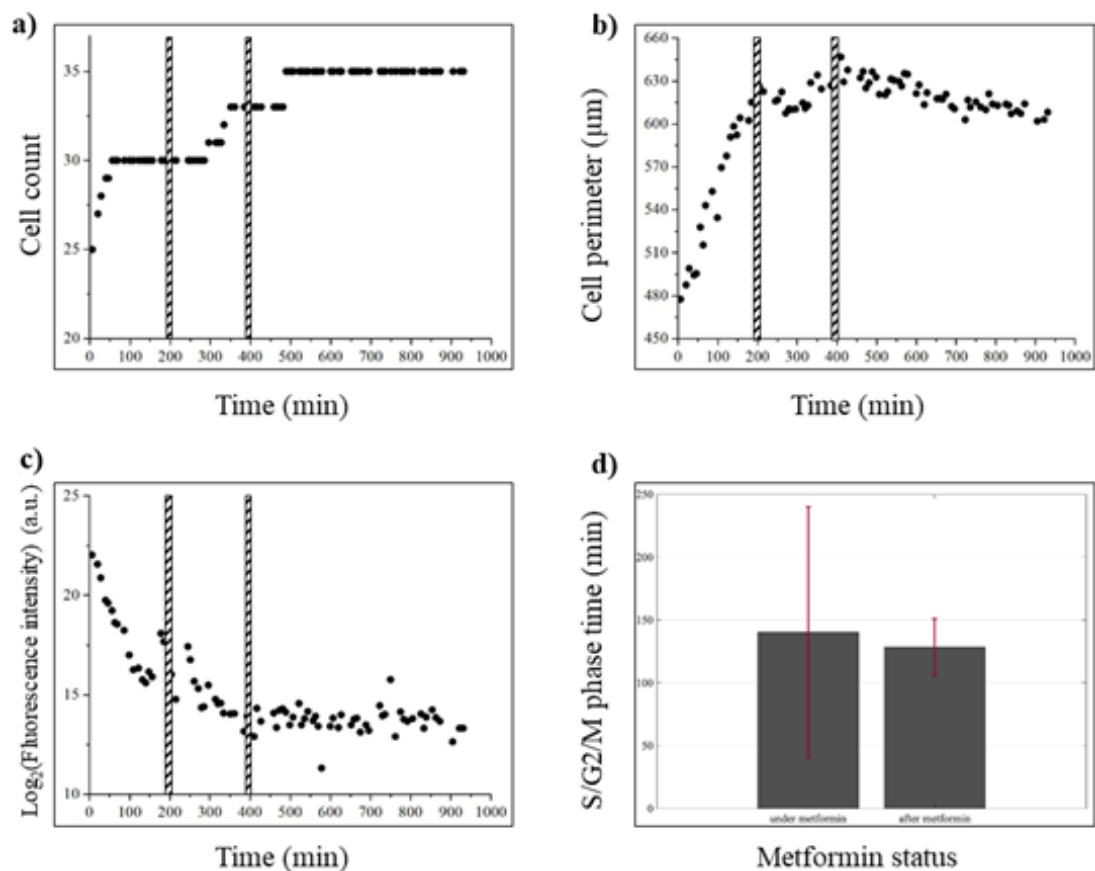


Figure 3.8. (a) Time profile of cell count (b) Time profile of cell perimeter (population) (c) Time profile of the fluorescence intensity (Vertical lines indicate the start and end of metformin application) (d) Duration of S/G2/M phases before and after metformin treatment.

The Nop56 protein expression of the total cells (population) is displayed in Figure 3.8c. In the first 100 min, the fluorescence intensity of the cells was very high but decreasing. During the metformin application period, this decreasing trend of the fluorescence intensity continued. There is an increase in the intensity concomitant with the decrease in cell size at

the 250th min. However, as the drug supply continued, a decrease in the fluorescence intensity was seen, followed by its stabilization. This result is in agreement with the reports on another mTOR inhibitor, rapamycin, which inhibited the gene expression of r-proteins (Kakihara *et al.*, 2014), (Sinclair 2005). Moreover, there is an extension in the time of S/G2/M phase due to metformin application (Figure 3.8d).

In order to capture cell to cell variations, each cell was individually analyzed in the metformin treatment experiment. The perimeter change of every cell at the given time intervals (before, during and after metformin exposure) can be seen in Figure 3.9a. Although the perimeters of many single cells were decreasing towards the end of the experiment, these cells continued their proliferation during and after the drug application. The dimension of the first daughter increased before the drug application, but a decreasing trend can be seen during the drug treatment period (Figure 3.9b). During metformin application, Nop56 expression in mother cell increased in parallel to the increase in single cell perimeter, i.e. highest during the S/G2/M phase of cell cycle (Figure 3.9b), but decreased significantly towards the end of the cell cycle, most probably during mitosis phase. The daughter cells had comparable levels of Nop56 expression with their mother. Under normal conditions, yeast cells complete their cell cycle at around 80 – 110 min. However, under metformin treatment, it took 220 min to have the daughter cell. i.e., metformin caused the prolongation of the cell cycle. Moreover, if the daughter cell were born after the metformin application, it could never bud again. TOR pathway is necessary for RNA transcription, and it takes part in the regulation of RNA polymerase I and II. The gene expressions related to r-proteins were reported to be inhibited by mTOR inhibitor rapamycin (Powers and Walter, 1999). TOR signaling pathway was deactivated by rapamycin and yeast cells behaved like at starvation conditions, and the core proteins of C/D box were transferred from the nucleolus to nucleoplasm (Kakihara *et al.*, 2014). Rapamycin also induced sporulation of diploid yeast cells under suitable conditions (Powers and Walter, 1999). Our findings obtained in this 0.14 nL volume microfluidic bioreactor are in agreement with these literature results, which were obtained in shake flasks or macroscale systems. In the last decade, the relation between metformin and cancer is also examined, where metformin treatment of type2 diabetes (T2D) patients led to a decreased risk of cancer (Kasznicki et al. 2014). High levels of circulating insulin/IGF1 and upregulation of insulin/IGF receptor signaling pathways participate in the generation of cancer cells.

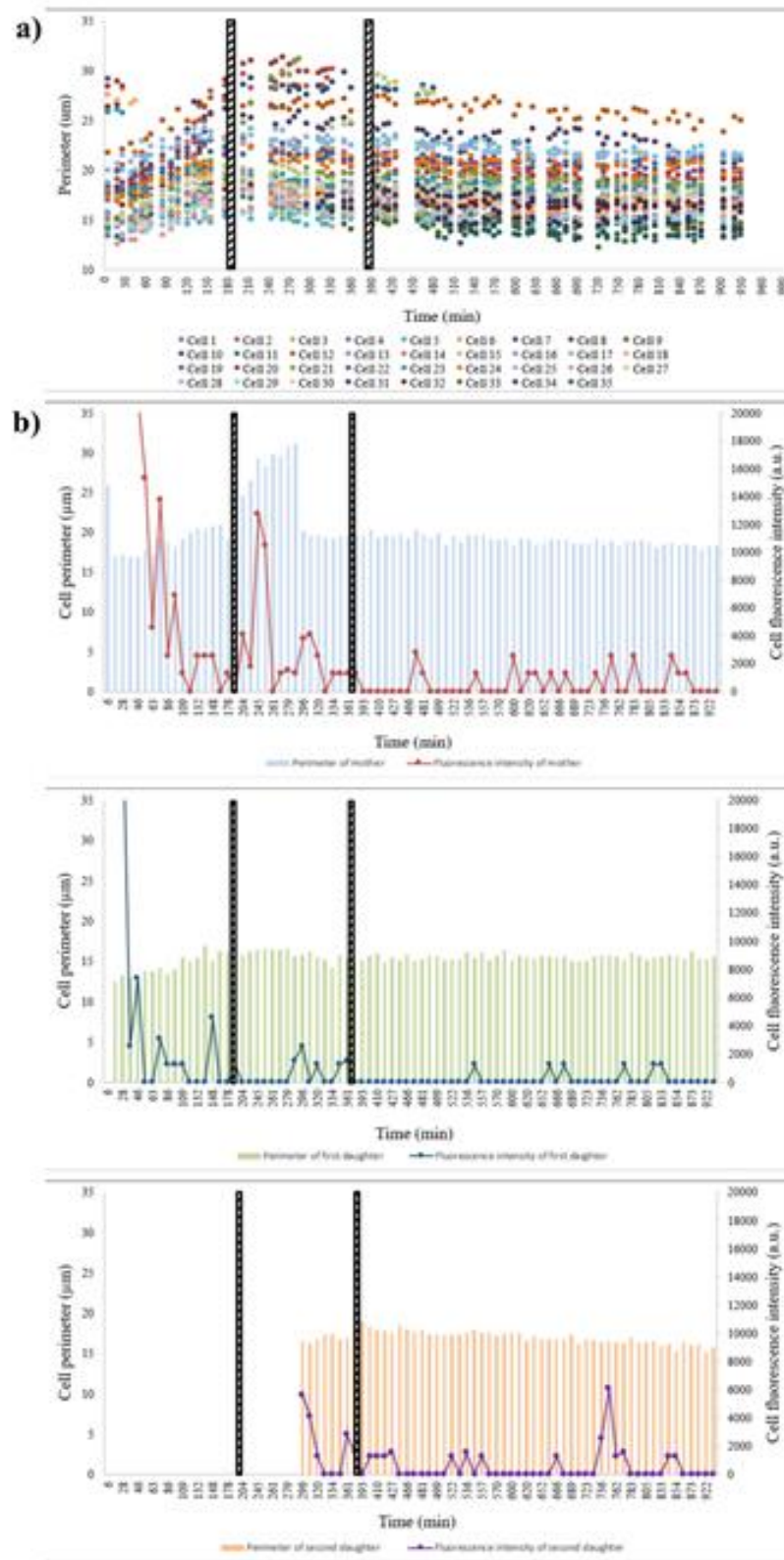


Figure 3.9. (a) Time profiles of the single daughter cells (b) Time profiles of single mother and daughter cells integrated fluorescence density and perimeter before, during and after metformin experiment.

Thus, metformin is used to adjust the insulin level, inactivate insulin/IGF signaling pathways and adapt cellular survival (Kasznicki *et al.*, 2014). Insulin/IGF-1 is responsible for the adjustment of glucose uptake and carcinogenesis via upregulation of insulin/IGF receptor signaling pathway. Excess amount of food consumption results in increased production of IGF-1, which binds to IGF-1 receptor and insulin receptor. Subsequently, insulin receptor substrate (IRS) transmits the signal to phosphoinositide 3-kinase (PI3K) and Akt/protein kinase B (PKB), which triggers mTORC1. So this pathway need to be suppressed in order to cope with T2D and consequent cancer. The emergence of mTOR inhibitors as anticancer agents has been largely preceded by rapamycin analogs (Zheng and Jiang, 2016). Currently these analogs include temsirolimus, everolimus, ridaforolimus and deforolimumustan. mTOR inhibitors have been highlighted for their safety and efficacy in cancer patients.

### **3.6.3. Effect of Temsirolimus on Yeast Cells**

Cell growth, which is controlled by TOR complex, is upregulated by anabolic processes such as protein, lipid and nucleotide synthesis and downregulated by catabolic processes such as autophagy (Kim and Guan, 2019). Moreover, mTOR has role on phosphorylation and then activation of p70 S6 kinase that contributes to enhanced translation of certain ribosomal proteins and elongation factors. In the present experiment, the effect of temsirolimus, a soluble ester of rapamycin (Rini 2008), on yeast cell growth and ribosome biogenesis was investigated in a microfluidic platform. Fresh nutrient medium was continuously passed through the microbioreactor for 3 hours, and then temsirolimus containing nutrient medium was sent for the 3 hours. After the cessation of the drug treatment, fresh medium was again sent for the next 10 hours. The analyses of the brightfield and fluorescence images taken during the experiment showed that the increase in cell count continued until the middle of the temsirolimus application period (Figure 3.10). From that point onwards, there was no further proliferation until the end of the experiment (Figure 3.10a). Similarly, in literature, temsirolimus is reported to cause G0/G1 cell-cycle arrest and decrease in the amount of cells that progress in S and G2/M phases for mantle cell lymphoma (MCL) and human prostate carcinoma cells (Yazbeck *et al.*, 2008), (Fagone *et al.*, 2013). Figure 3.10b and 3c show the cell perimeter/cell count and single cell perimeter results, respectively. Yeast cells increased their dimensions until the drug application and a sharp

decline in the dimension can be seen in the period of temsirolimus treatment. In the microfluidic study, temsirolimus affected both Nop56 expression and cell growth and proliferation, in agreement with literature reports. Indeed, Nop56 is a tightly regulated protein. When Nop56 levels were low, pre-rRNA biogenesis was compromised with a 3-fold increase in apoptotic cells (Figure 3.10d). Conversely, when Nop56 was overexpressed for 24 hr, fewer cells in apoptosis or S-phase and an -2-fold increase in the number of cells in G2/M-phase were observed (Mills and Green, 2017), (Russo and Russo, 2017). Hence perturbations in Nop56 levels lead to altered ribosome biogenesis, localization, and cellular fitness.

The defects in ribosome production can activate the central tumor suppressor p53 causing cell-cycle arrest and apoptosis (Mills and Green, 2017), (Russo and Russo, 2017). Moreover, the activation of mammalian Tor (mTOR) pathway is organized by a series of complex signaling interactions including growth factor receptor signaling and other stimuli such as activations in phosphatidylinositol 3-kinase and Akt/protein kinase B pathways. mTOR is also a key regulatory protein in cancer that remembers the stress signals, such as nutrient and energy deficiency, oxidative or hypoxic stress and proliferative and survival signals, via the phosphoinositide 3-kinase (PI3K)-Akt pathway. When the tumor cells are treated with temsirolimus, G1 growth arrest is seen due to the inhibition of mTOR activity (Klümper *et al.*, 2010).

#### **3.6.4. Effect of 5-hydroxymethylfurfural on Yeast Cells**

The furan derivatives 5-hydroxymethylfurfural (5-HMF or HMF) and furfural are the degradation compounds of hexoses and pentoses, respectively. HMF and furfural influence the ethanol yield, and ethanol productivity by inhibiting enzymes such as alcohol dehydrogenase, aldehyde dehydrogenase, pyruvate dehydrogenase and glycolysis (Almeida *et al.*, 2008). The most striking effect of these chemicals on the livings is that they interfere with the microbial growth and they are considered as the most potent inhibitors in bioethanol production (Hasunuma *et al.*, 2014). HMF and furfural decrease enzymatic biological activities, break down DNA, inhibit protein and RNA synthesis, damage cell structure, generate cellular reactive oxygen species (ROS) and reduce the specific cell growth rate (Almeida *et al.*, 2008), (Liu *et al.*, 2008), (Ma and Liu, 2010), (Liu *et al.*, 2009), (Park *et al.*, 2011). In order to generate the industrial bioethanol, *Saccharomyces cerevisiae* (S.

cerevisiae) is the most widely employed microorganism; it is well-known food-grade yeast with a long history on alcohol fermentation from various raw materials. The yeast cells are able to decrease HMF and furfural into less harmful compounds.

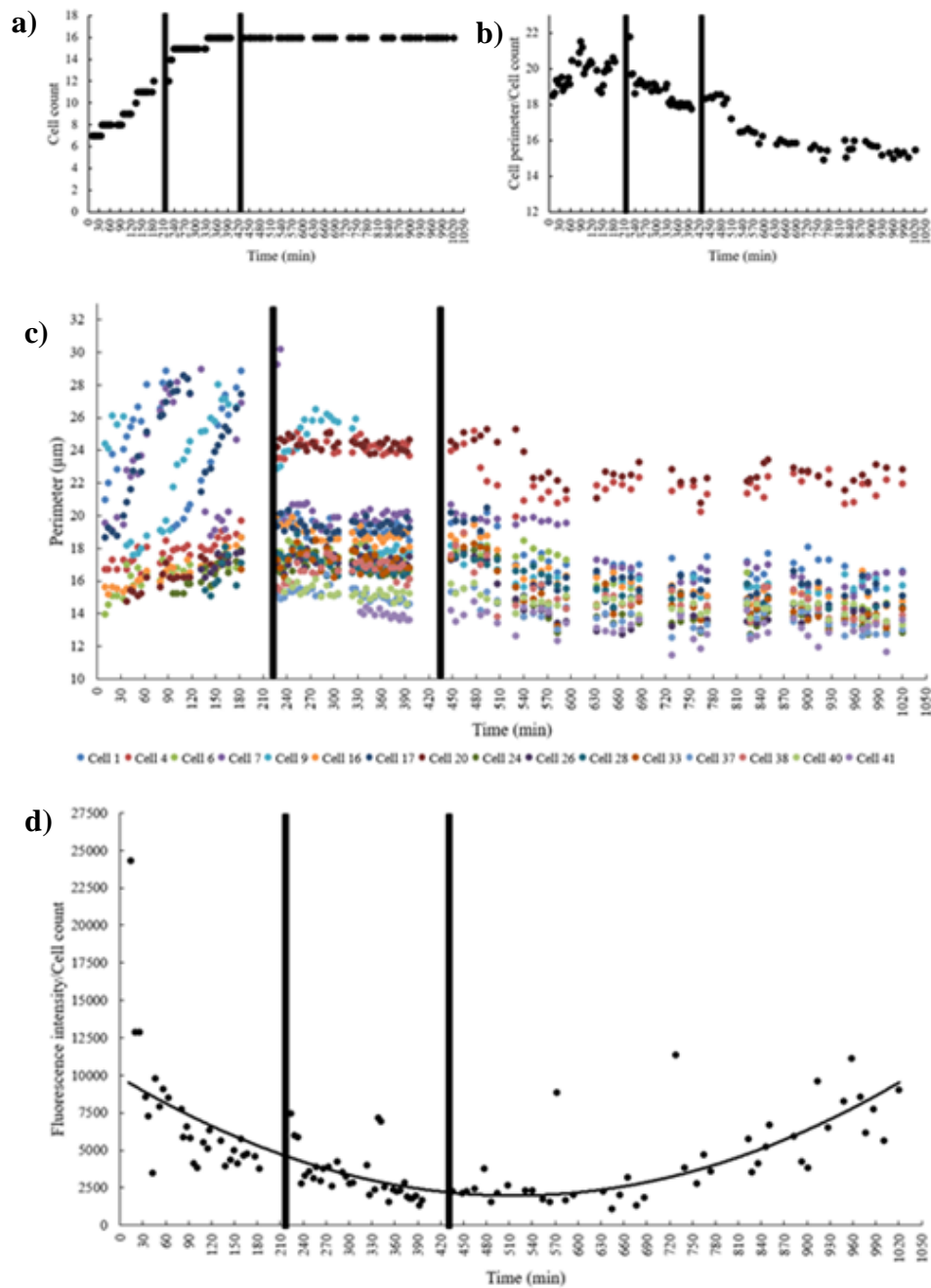


Figure 3.10. (a) Time profile of cell count (population) (b) Time profile of cell perimeter/cell count (population) (c) Time profile of single cell perimeter (d) Time profile of fluorescence intensity/cell count (population) (Vertical lines show the interval of temsirolimus treatment).

2,5-bis-hydroxymethylfuran [furan-2,5-dimethanol (FMD)] and 2-furanmethanol (FM) are the reduced chemicals of HMF and furfural under anaerobic conditions, respectively. Moreover, NAD(P)H and NAD(P)<sup>+</sup> usage are necessary for furfural and HMF detoxification, respectively (Figure 3.11) (Almeida *et al.*, 2008), (Park *et al.*, 2011). When HMF and furfural concentration decrease to a lower concentration, a recovery of cell growth can be observed. Thus, it was proposed that, genomic adaptation might occur during the lag phase (Ma and Liu, 2010), (Sehnm *et al.*, 2013). However, cellular stress response caused by HMF is not fully understood in yeast cells.

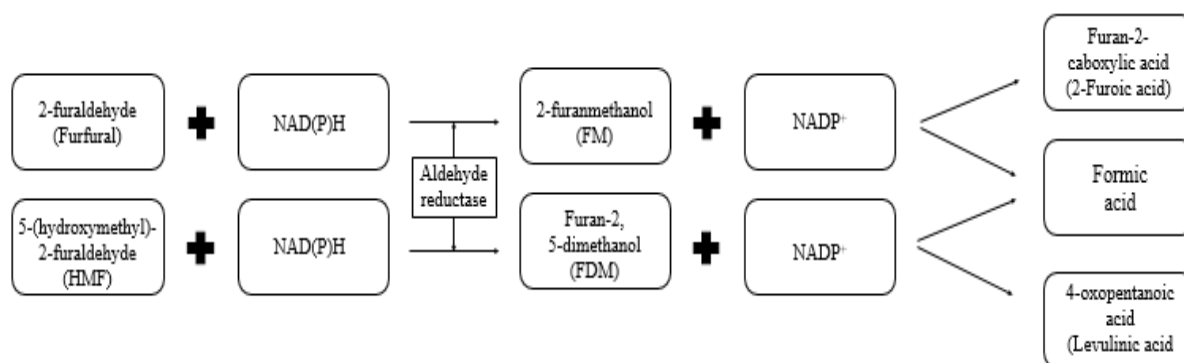


Figure 3.11. Conversion pathways of furfural and HMF.

In order to understand the link between growth and HMF inhibition, the response of RFP:Nop56 yeast cells upon HMF treatment was followed in a microfluidic platform. At first, YNB medium was sent through the microfluidic bioreactor for priming step. Then, yeast cells were loaded and trapped in the c-shaped regions of the chambers. After cell loading, fresh YNB medium was sent for 3h followed by HMF solution for another 3 h. Finally, fresh YNB medium was fed for 10 h till the end of the experiment. Cell count increases gradually throughout the experiment till the end of the HMF treatment period (Figure 3.12a). When the HMF feeding is ceased, no proliferation is observed until the end of the experiment. Yeast cells continue growing and increasing in dimension including the HMF treatment period. Around the 720th minute, there is a decreasing trend in the total cell perimeter (Figure 3.12b). Each cell is also treated separately and the response is monitored, capturing cell to cell variations (Figure 3.12c). The initial increase and subsequent decrease

in cell size during the HMF treatment period can be seen more clearly on single cell basis. Towards the end of the experiment, the cells are able to recover themselves without losing their viability.

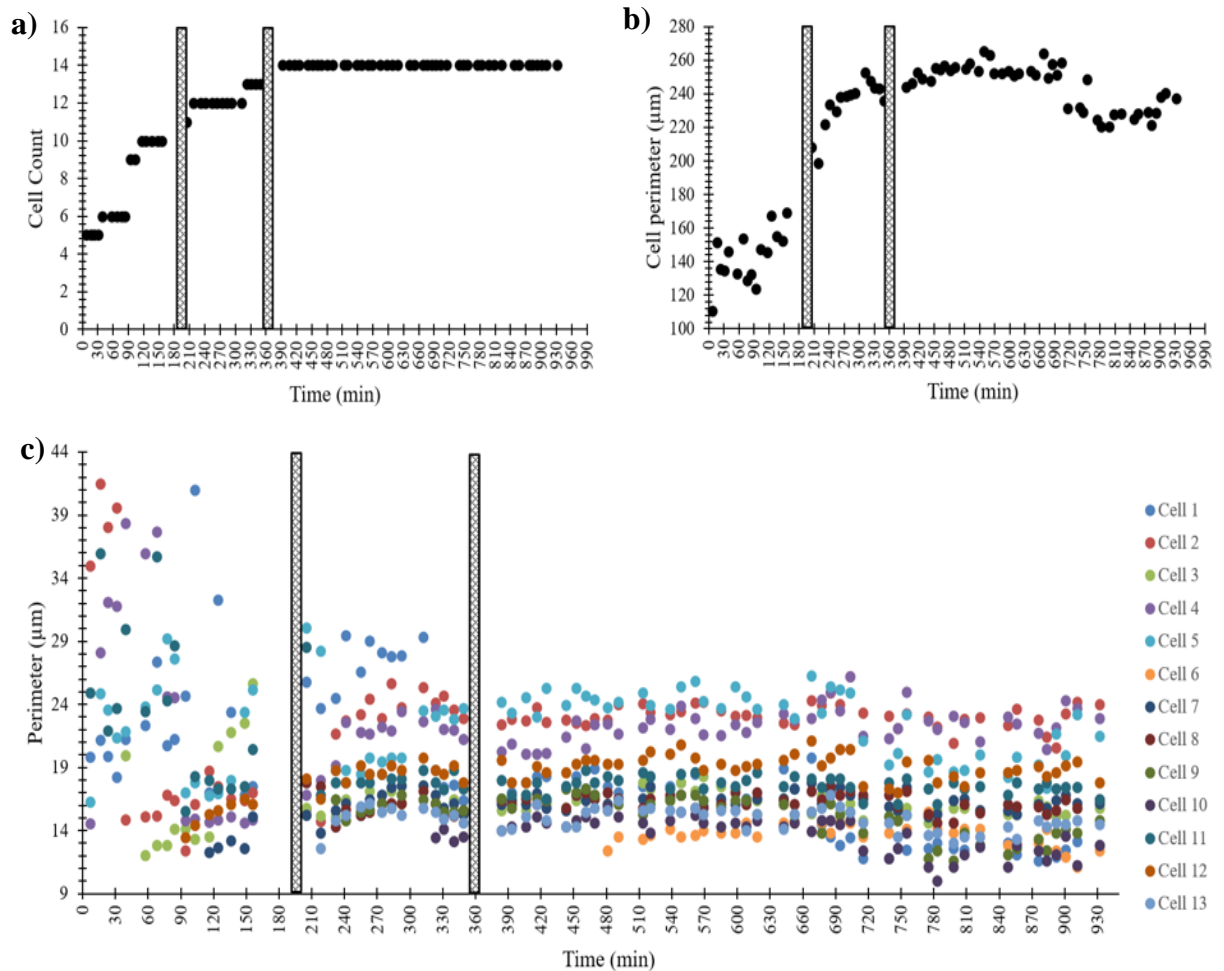


Figure 3.12. (a) Time profile of cell count (b) Time profile of total cell perimeter (c) Time profile of single cell perimeters (Vertical lines on the graphs shows the HMF feeding period).

RFP tagged Nop56 expression is analyzed to observe the changes in protein expression within the cells. In the first 150 min, the fluorescence intensities of the cells are very high, as shown in the inset graph of Figure 3.13. During the HMF treatment, the fluorescence intensity has a decreasing trend, i.e. Nop56 expression is suppressed by the HMF. After the HMF treatment, the fluorescence intensity continues to decrease for a while, however through the end of the experiment, under the fresh nutrient medium, the cells fluoresce at an

increasing trend. Since Nop56 has a role in ribosome biogenesis and ribosome biogenesis is closely linked to cellular activities like growth and division (Nissan *et al.*, 2002), we can speculate that the cells are trying to regain their cellular functions and recover themselves.

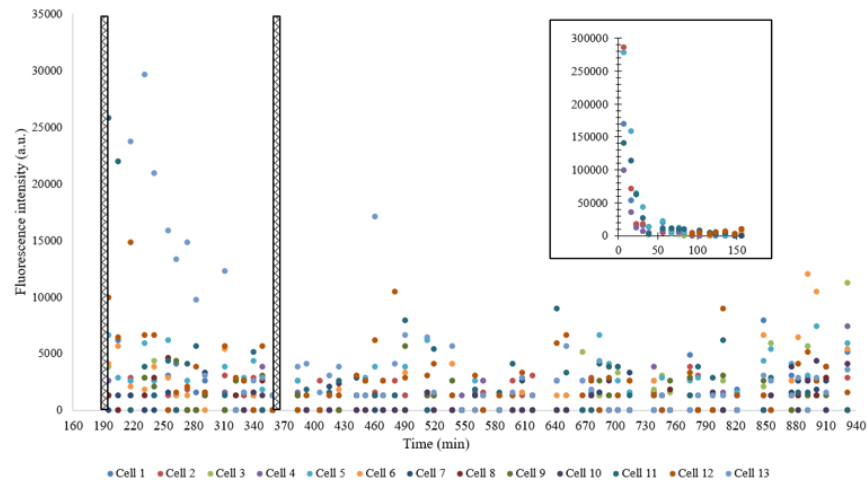


Figure 3.13. Time profile of fluorescence intensity at single cell level (inset shows the fluorescence intensity in the first 150 min).

Figure 3.14 shows the time profiles of the perimeter and fluorescence intensity of mother and its daughter cells. M defines the mother cell and the numbers next to M show the daughter and granddaughter cells. For example, M1 is mother cell 1, M1-2 is second daughter of the M1 and M1-2-1 is the daughter cell of second daughter of M1. Before the HMF treatment, all mother cells continue their normal life cycle and proliferated. The doubling time of the cell was 70-80 min before the HMF treatment. During the exposure to HMF, all of the mother cells still continued proliferation, however the doubling times of these cells are extended, ranging between 124 and 207 minutes depending on the exposure time of the individual cells to HMF, confirming cell to cell variation in the population (Figure 3.14a-d). For example, M4 entered G1 phase 22 min before the M1 that is more exposed to HMF than M4. Moreover, if the daughter cell was born before the HMF treatment, it can make a new bud despite the presence of HMF. But, if the daughter cell was born after the HMF treatment, it could not bud. In order to see clearly the rises and falls of fluorescence intensity of the cells, some noisy data at the beginning are discarded. Before HMF treatment (in fresh medium) there is sharp peak of the expression of Nop56 in G1 phase as well as in budding phase. If a daughter cell appears towards the end of the HMF treatment period, Nop56

expression is not seen, probably due to the HMF suppression (Figure 3.14). However, if the cell division occurred within 20-30 min of HMF application period, Nop56 expression was seen in both G1 and budding phases of cell cycle, however at the end of the M phase Nop56 fluorescence (expression) disappears. Finally, if the cell is divided after HMF treatment, it behaves as if it were in fresh medium at the beginning of the experiment, and Nop56 expression was seen (Figure 3.14c).

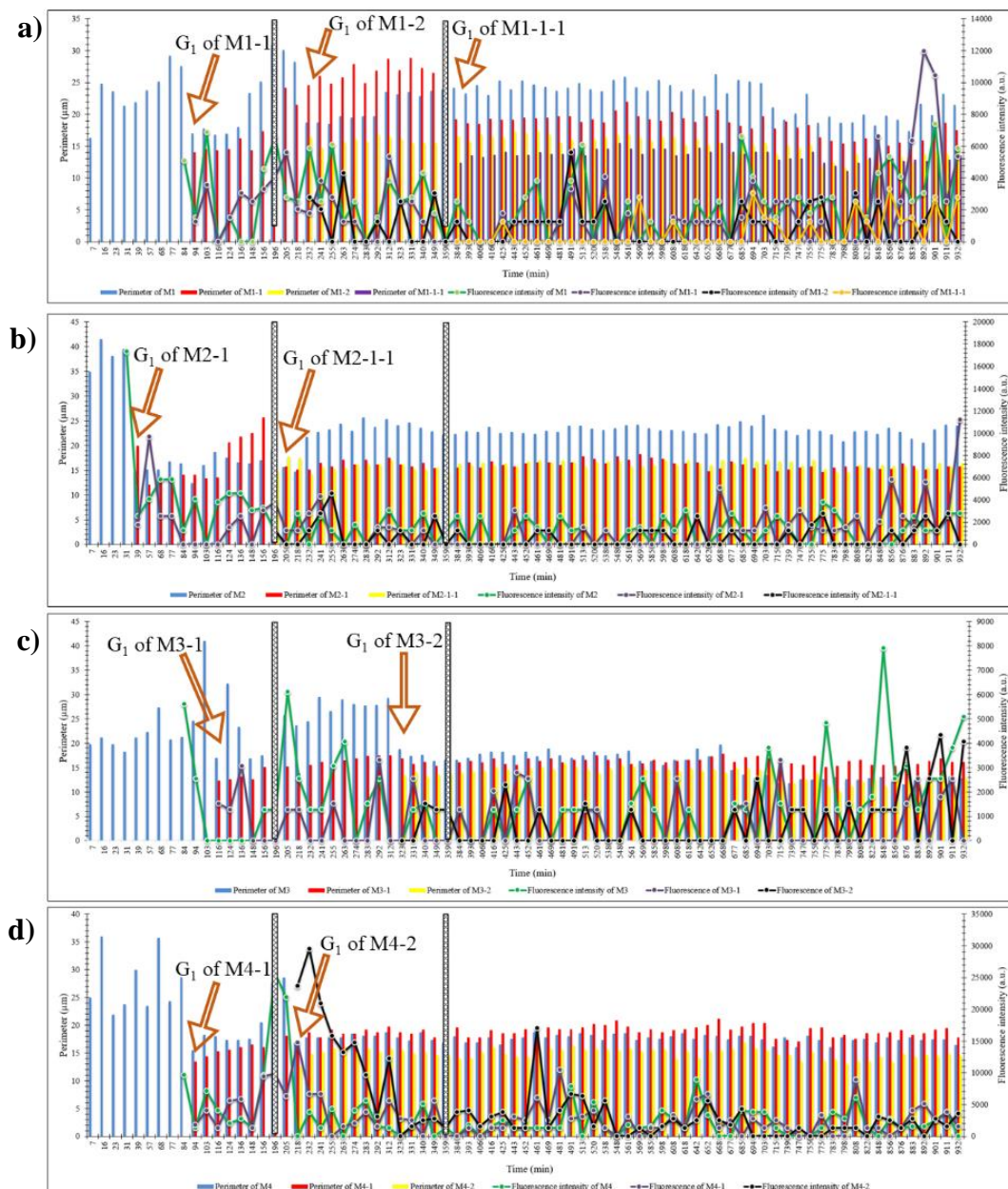


Figure 3.14. Time profile of perimeter and fluorescence intensity of individual mother and daughter cells.

The relationship between growth and HMF, which has negative effects on cells like break down of DNA, inhibition of protein and RNA synthesis, is studied in continuous flow single phase microfluidic device for the first time. In cells, the snoRNAs have two main functional groups; one of them is the box C/D snoRNAs that manages the methylation of ribosyl-2'-hydroxyl groups and the other one is the H/ACA snoRNAs that direct the conversion of uridine to pseudouridine (Mitchell *et al.*, 2003). Nop56 is an essential evolutionary-conserved nucleolar protein, and it is found as the member of the box C/D snoRNP complexes. Nop56 is involved in the early to middle stages of 60S ribosomal subunit biogenesis, required for the assembly of 60S ribosomal subunit and joined in pre-RNA processing. Yeast cells with RFP tagged Nop56 gene product were used to observe the changes in protein and ribosome syntheses along with their link to growth within the microfluidic device.

During the HMF treatment, the cell proliferation continued but HMF slowed down the cell cycle, and the budding of cells stopped after the HMF treatment period (Figure 3.12a). However, the yeast cells did not lose their viability, and recovered in 6 hours by the addition of fresh nutrient medium after the HMF treatment (Figure 3.12b). Thus, 4g/L HMF treatment suppresses normal functioning of cell cycle but it does not cause cells to die. In order to observe the single cell behavior, each cell in the experiment was individually analyzed. As previously stated for the population, the individual cell proliferation continued during the HMF treatment and new cells (daughter cells) joined the culture. Since HMF inhibits protein and RNA synthesis, there is a sharp decrease in the intensity of Nop56 fluorescence during the HMF treatment, and that decreasing trend continued till the 600th minute. However, the fluorescence intensity increased towards the end in fresh nutrient medium, and the cell recovery can be seen clearly.

### 3.7. Conclusion

Microfluidic systems continue to be applied to cell biology. They try to show behavior of individual cells, confirm existing chemical and biological pathways or unveil new ones. Similarly in this work, we used COP based microfluidic bioreactor to perform cell biology experiments successfully. It provided several advantages such as; real time observation of the yeast cells, suitability for single cell studies, conduction of two different experiments at

the same time under equal conditions and being durable to long-lasting experiments. The brightfield and fluorescence (tracking RFP:Nop56) microscopy images of the yeast cells trapped into the C-shaped regions were successfully recorded during the experiments. DNA inhibitor HU and mTOR inhibitor metformin were used for the first time in a microfluidic study, and their effects on the single yeast cells were investigated under continuous flow. The results obtained in this microfluidic system are in agreement with those at macroscale: While HU inhibited DNA replication due to the disturbance of S-phase, metformin slowed down cell growth. Moreover, in the present study, the expression of the nucleolar protein Nop56 of ribosome assembly and synthesis was densely observed during G1 phase of cell cycle, where the single cell perimeter representing the biomass synthesis rate was around 15 micrometers, and later towards the end of cell cycle, probably during M phase, the ribosomal protein expression slowed down. Under metformin treatment, the perimeters of single cells were observed to decrease, implying a decrease in biomass growth; however these cells continued their proliferation during and after the drug application. Moreover, Nop56 expression was observed both in G1 phase as well as in S/G2/M phases. Thus, these findings indicate that metformin extends the lifespan of the cells as expected despite the dimensional changes. The relation between ribosome biogenesis and cell cycle was successfully investigated on single cell basis, capturing cell-to-cell variations, which cannot be tracked at regular macroscale bioreactors. As the heterogeneity of cell populations is an important issue in tumor cells, the present microfluidic platform can effectively be used for studying the drug effects on tumors and may shed light on the putative treatment strategies towards cancer. Dominating the biological activity of the cells, HMF caused a decrease in cell dimensions, however, yeast cells did not lose their viability. Despite the deceleration in the rate of yeast cell proliferation, an increase in the number of cells was later observed in fresh nutrient medium following the HMF treatment. In addition to examining the collective (total) behavior of the yeast cells, each cell was separately examined in the fabricated microfluidic bioreactor and Nop56 expression phases of the cells were determined, which helped us understand the protein and ribosome synthesis cycles along with their link to growth. The information gained from this microfluidic study may help us develop new microbial strains, which are engineered towards optimizing growth coupled with the production of biochemicals of industrial value. By metabolic engineering tools, one can use strain engineering strategies, like deletion of specific gene(s) or removal of metabolic reactions that are capable of uncoupling cellular growth from chemical production, and hence the

metabolic network regulated by internal cellular objectives can lead to the elimination of toxic by-products and/or overproduction of chemical compounds of interest. According to the experimental study on yeast cells with the microfluidic platform using the drug temsirolimus, Nop56 appears to have a role in ribosome biogenesis whose expression is normally seen in the G1 phase of the cells to make preparations for budding. Nop56 levels have to be tightly regulated, as its depletion or overexpression leads to defects in ribosome biogenesis and localization. In our study, no proliferation was observed under and after the application of temsirolimus to the yeast cells, indicating that the cell cycle did not sustain and the cells remained in phase G0/G1 phase as it was the case in macro-systems. Thus, the increased fluorescence intensity of Nop56 after the drug treatment can be explained by the G1 phase arrest of the cells.

#### 4. DECIPHERING THE EFFECT OF 5-HYDROXYMETHYLFURFURAL (HMF) ON BIOMASS GENERATION AND ETHANOL PRODUCTION

Systems biology is a biomedical research field and used to understand the living creatures by collecting the pieces together. It is rapidly growing and based on construction and validation in silico models of biological systems employing a vast majority of experimental data (Bork 2005). In order to find out the cellular behavior of an organism, tissue or cell, several models are handled via creating novel, testable and quantitative predictions.

Cellular process models, including signal transduction (Papin *et al.*, 2005), transcriptional regulation (Covert *et al.*, 2004), (Brynildsen *et al.*, 2005) and metabolism, are constituted with the genome-scale network reconstruction efforts (Reed *et al.*, 2006). Biochemical reactions appearing in a cellular system and the relations between these reactions and relevant proteins, transcripts and genes is identified as reconstruction. Reconstruction is adopted to generate the model by adding the assumptions required for computational simulation such as maximum reaction rates and nutrient uptake rates. Models are used to find the answers of biological questions and to learn the living things (Becker *et al.*, 2007).

Constraint-Based Reconstruction and Analysis (COBRA) is a MATLAB software supported toolbox and works in the field of metabolic engineering including transcriptional and signaling networks. There are several COBRA methods investigated in the literature and genome-scale features of metabolic networks and their phenotypic states are characterized via this toolbox. Operating physicochemical, data-driven and biological constraints for calculation the set of appropriate phenotypic states of a reconstructed biological network in a determined condition is the aim of COBRA. Moreover, compartmentalization, mass conservation, molecular crowding and thermodynamic directionality are the types of constraints. COBRA methods do not give only a unique solution, it proposes a reduced set of solutions for a hypothesis suggested (Schellenberger *et al.*, 2011), (Ebrahim *et al.*, 2013). In the present part, IMM904 model is employed to make analysis about biomass generation and ethanol production within the *Saccharomyces cerevisiae* cells w/o HMF treatment.

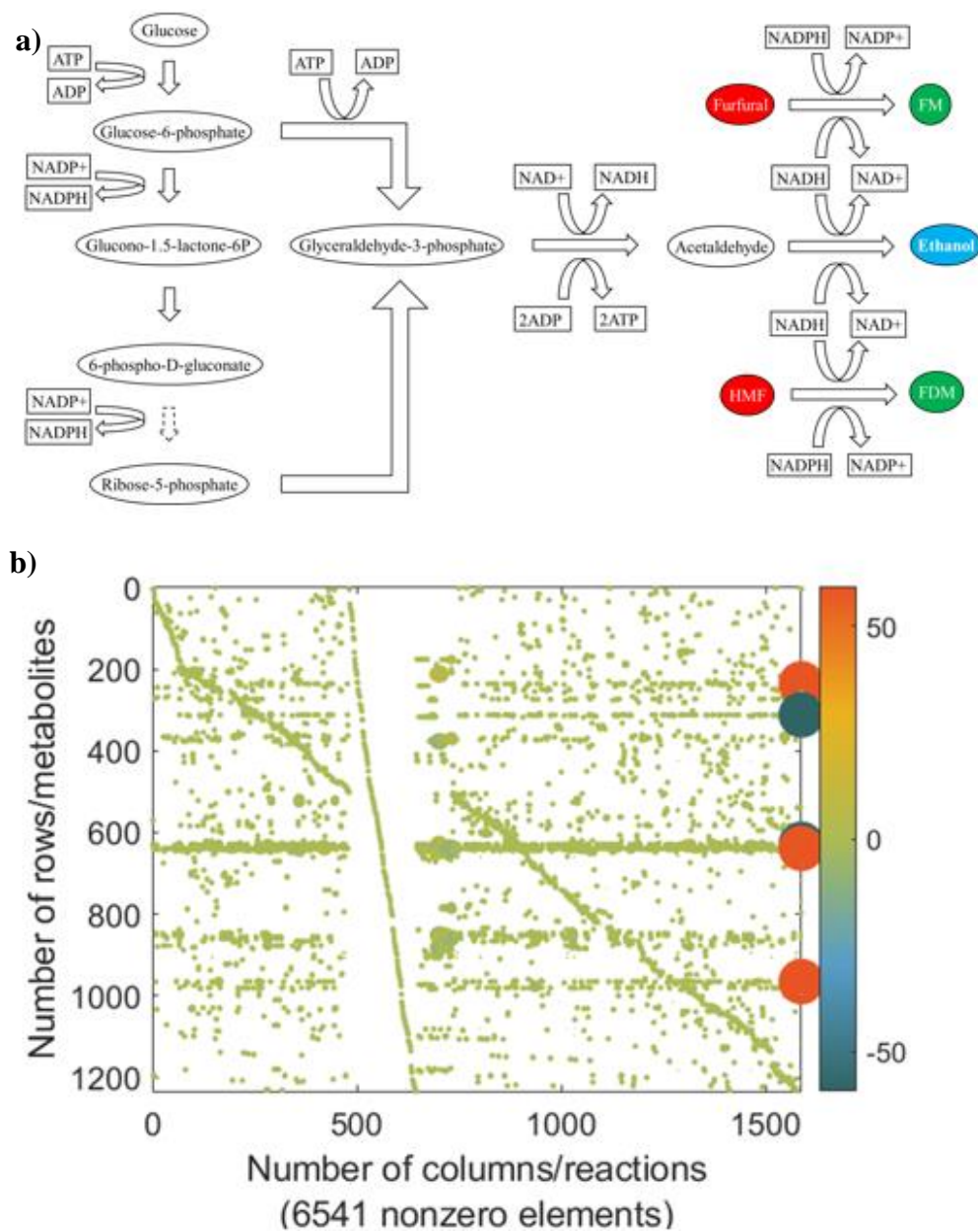


Figure 4.1. (a) Ethanol production pathway under HMF effect (b) Stoichiometric matrix of the model.

In this computational part, two types of models are handled; one of them is used as a control model (without HMF treatment) and the other one is used as a modified model (with HMF treatment). Modified model includes HMF degradation reactions and related pathways (Figure 4.1a) as explained within the results and discussion section. Here, our aim is to reveal the differences between the models and increase the ethanol production while generation of biomass.

## 4.1. Methods

### 4.1.1. Computational Tools and Model

Computational methods are implemented using Matlab R2020a software. Constraint-Based Reconstruction and Analysis (COBRA) Toolbox (version 3.0) and Reconstruction, Analysis and Visualization of Metabolic Networks (RAVEN) Toolbox (version 2.0) are operated for the series of analysis. Cytoscape 3.8.0 is utilized for the visualization. The stoichiometric matrix (S) is the building block of a metabolic model. This matrix includes all of the information about the metabolic transformations. Each metabolite is represented in a row and each reaction in a column (Palsson 2015). The stoichiometric coefficients of a metabolite, whether consumed (negative) or produced (positive) in the reaction, constitute the elements of the matrix and it is a mathematical depiction of the network that, in turn, shows curated and organized biological knowledge about a target organism (Palsson, 2015) Figure 4.1b shows the visual demonstration of S matrix for the modified iMM904 model.

### 4.1.2. Flux Balance Analysis

Flux balance analysis (FBA) determines the metabolic states via computing expected reaction rates in complex metabolic networks. The basic strategy of FBA is to equalize the sum of incoming fluxes to the sum of outgoing fluxes for each metabolite. FBA gives steady state metabolic fluxes which accomplish a set of constraints and maximize/minimize a given objective function. In this method, biomass production flux is maximized by linear programming. The achieved maximum value is assigned as the growth rate and the production rate of each metabolite is predicted with the assumption of maximized growth rate (Orth, *et al.*, 2011), (Reznik *et al.*, 2013). The upper bound of glucose uptake is 20 mmol gDW<sup>-1</sup>h<sup>-1</sup>, and the ATP maintenance demand is 1 mmol gDW<sup>-1</sup>h<sup>-1</sup>.

### 4.1.3. Flux Variability Analysis

Flux variability analysis (FVA), a variant of the FBA, is another analysis method for constraint-based modeling. Flux span of each reaction is calculated within a given range of the acceptable predicted growth rate. Unlike FBA, which gives only one flux, FVA

demonstrates the minimum and maximum flux values of reactions. FVA enforces the metabolic network to obtain a minimum amount of flux through an objective function and optimizes for the flux through each reaction (Rawls *et al.*, 2019), (Lewis *et al.*, 2010). Reaction classification is accomplished based on the FVA. “Hard-coupled reactions” are those ensuring a certain flux to maintain the optimal objective. If reactions do not carry a flux to provide at least 90% of the maximum target, they are classified as “zero-flux” reactions. “Partially-coupled reactions” include non-zero flux reactions but these can change their flux to maintain at least 90% of the maximum flux distribution. Finally, “Not-coupled reactions” contain zero or non-zero flux values (Lewis *et al.*, 2010).

#### 4.1.4. Flexibility of the Network

Flux variability spectrum can be recognized as the maximum and minimum value of each reaction fluxes and flux span is defined as the difference between them (Palsson 2015). Flexibility of the network is based on the average of all flux spans (Equation (4.1)):

$$Flexibility = ave(maxFlux_i - minFlux_i) \quad (4.1)$$

where  $i$  represents the reactions. Minimum and maximum flexibility scores are also found as Equation (4.2) and Equation (4.3):

$$FlexibilityMin = ave\left(\frac{minFlux_i}{Flux_i}\right) \quad (4.2)$$

$$FlexibilityMax = ave\left(\frac{maxFlux_i}{Flux_i}\right) \quad (4.3)$$

#### 4.1.5. Flux Coupling and Regulation

Functional relatedness based on coherent usage of reactions in the metabolic network is described by flux coupling via unbiased mathematical methods (Szappanos *et al.*, 2011), (Montagud *et al.*, 2011), (Notebaart *et al.*, 2008). Besides the steady-state flux distributions of the network, the coupling relations between the reactions are revealed with the help of stoichiometric and thermodynamic constraints.

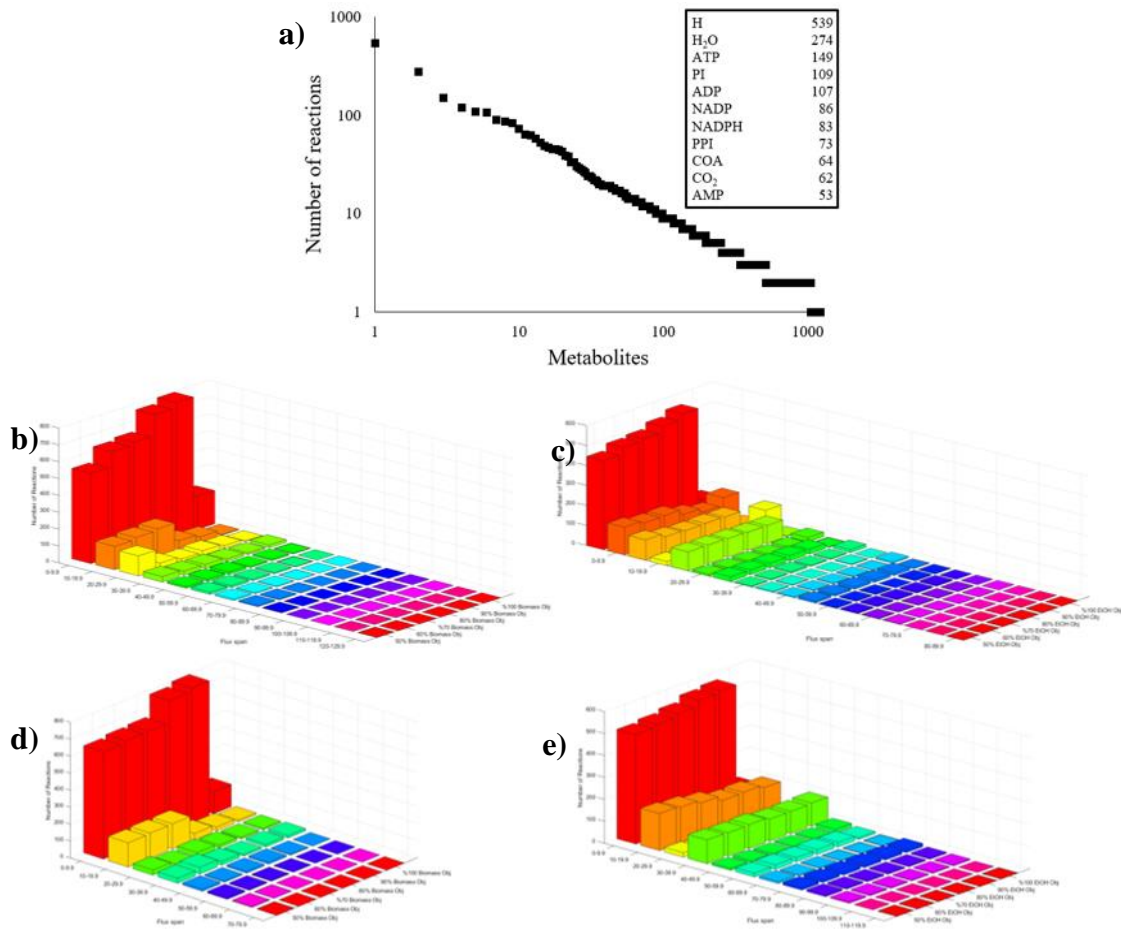


Figure 4.2. (a) The number of reactions in which each of the metabolite involved in the network Frequency for different ranges of flux span at growth limited by oxygen uptake rate: (b) Objective: Biomass for control model (c) Objective: Ethanol for control model (d) Objective: Biomass for HMF model (e) Objective: Ethanol for HMF model.

The algorithm, F2C2, is used which has two main assumptions: reducing the stoichiometric model and minimization of the number of linear programming problems. Uncoupled, fully coupled, partially coupled and directionally coupled reactions are identified (Larhlmi *et al.*, 2012). In the regulation part, gene expression data (GSM566436 and GSM566429) are integrated with flux data and sampling is done. Averages and standard deviations of the metabolic fluxes in the GEM are calculated and this gives the regulation type. Significantly correlated change both in flux and expression level is denoted as transcriptional regulation, significant change in expression but not in flux is called post-transcriptional regulation and significant change in flux but not in expression is called metabolic regulation (Bordel *et al.*, 2010).

#### 4.1.6. Flux Scanning Based on Enforced Objective Flux

Flux scanning based on enforced objective flux (FSEOF) method is built on the amplification of gene targets. The distinction in the metabolic fluxes in consideration of the enforced fluxes directed through the target product (etoh) is first scanned and selected. The flux values, which increased or decreased in response to the enforced fluxes toward the target metabolite, are determined and amplification targets are selected. In short, all metabolic fluxes are examined to reveal the reactions that increase/decrease when product flux is forced (Choi *et al.*, 2010), (Park *et al.*, 2012).

#### 4.1.7. Knocking Out Reactions and Genes

In order to maximize the desired target metabolite production, several reaction/gene deletions within the metabolic network is performed. OptKnock is one of the well-designed method to create an optimal deletion scenario. Bi-level linear optimization via mixed integer linear programming is used by OptKnock method and the production of the desired metabolite is specified as a required byproduct of growth (Tamura 2019). Apart from OptKnock, manual reaction deletion strategies have been developed based on FSEOF results and, single and double gene deletion studies are also conducted using COBRA software. The production envelopes are drawn to see the gene deletion effects on ethanol production.

## 4.2. Results and Discussion

In order to understand the link between ethanol production and growth under HMF supplied nutrient conditions computational studies is conducted and the computational study is done with COBRA and RAVEN Toolboxes in MATLAB environment. The yeast metabolic network is defined by chemical equations according to gene-protein-reaction associations. *Saccharomyces cerevisiae* iMM904 model has 1226 metabolites and 1577 reactions. In order to investigate the response of yeast cells under HMF treatment, additional metabolites and reactions are integrated to the iMM904 model and finally, the modified model (HMF model) with 1234 metabolites and 1587 reactions is obtained. Highest to the lowest degree of participation of metabolites in HMF model are rank ordered in Figure 4.2a, where hydrogen (539), water (274), ATP (149), phosphate (109) and ADP (107) are the

metabolites that are involved in most of the reactions. While the modified model shows the HMF applied results, the basic yeast model iMM904 (control model) is used for control purposes.

#### 4.2.1. FBA, FVA and Flexibility of the Network

Flux balance analysis is used to predict the optimum steady state rates/fluxes of intracellular metabolic reactions in a metabolic network. The impositions of the set of physicochemical/thermodynamic/exometabolomic constraints and the maximization (or minimization) of the objective function is the fundamental strategy of FBA (Reznik *et al.*, 2013), (Orth *et al.*, 2011). In the present study, lower bounds of glucose and oxygen are set to -20 and -2.5 mmol gDW<sup>-1</sup>h<sup>-1</sup> for both of the modified and control models. Lower and upper bounds of HMF, acetate and furfural are set to 2.5, 2.5 and 0 mmol gDW<sup>-1</sup>h<sup>-1</sup> in the modified model, respectively. The objective is to increase either biomass or ethanol production for both models. FBA gives the growth rate as 0.539 and 0.412 h<sup>-1</sup> (doubling time of 1.68 h) and ethanol production as 40.0 and 37.917 mmol gDW<sup>-1</sup>h<sup>-1</sup> for control and HMF models, respectively. The toxic effects of HMF on cells can also be witnessed from the FBA results. Alcohol dehydrogenase, aldehyde dehydrogenase, pyruvate dehydrogenase and glycolysis enzymes regulate the ethanol productivity and ethanol yield but the presence of HMF and furfural influence the yield and productivity by inhibition (Almeida *et al.*, 2008).

These chemicals (HMF and furfural) also affect the microbial growth and they are considered as the most potent inhibitors in bioethanol production (Hasunuma *et al.*, 2014). To get further insight on the admissible range of each intracellular flux under HMF supply, flux variability analysis (FVA) is performed in the metabolic network. The reactions are grouped according to their flux span value and 6 different percentages of maximal possible biomass and ethanol production capacities are considered in order to give flexibility to yeast metabolism. Figure 4.2b, c, d and e show the overall metabolic flux spans of the control and HMF models under oxygen limited environment where the objective is either biomass or ethanol production. The number of reactions is highest for 0 – 9.9 flux span for both objective functions (biomass and ethanol productions) and both models (control and HMF). At this flux span, when the objective is biomass formation for both models, the number of reactions increases up to 800, while the number of reactions increases to 600 when the objective is

ethanol production. The number of reactions involved and the flux span are higher in the control model than the HMF model with the biomass as the objective function. Therefore, HMF obviously affected the intracellular reaction mechanism of yeast towards growth and has a lethal/inhibitory effect on the cell (Fig 4.2b and d).

#### **4.2.2. Classification of Reactions (in terms of coupling) Functioning towards Growth or Ethanol Production**

The intracellular reactions are classified by FVA using six different percentages of maximal possible biomass and ethanol production capacities of yeast (Figure 4.3). Blocked reactions which do not carry flux under the given conditions are eliminated from the model. The number of partially coupled reactions to biomass (Figure 4.3a and c, about 145-200 reactions) are more than those obtained when the objective function is ethanol maximization (Figure 4.3b,d, about 8-14 reactions) in both of the models. Since partially coupled reactions carry non-zero flux and process towards fulfilling and maintaining the objective function, this result demonstrates that the cell attaches more importance to biomass generation than ethanol production. As in the previous results (Figure 4.2b, c, d and e), yeast cells mostly concentrate on the biomass generation. Since yeast cells have to eliminate the HMF by decreasing it into less harmful compounds, more reactions may have been required to sustain biomass production (Almeida *et al.*, 2008), (Park *et al.*, 2011). The not-coupled reactions do not contribute to production of objective, which is either biomass or ethanol production. In the case of HMF model, there are too many reactions that do not contribute to ethanol production (more than 800 not-coupled reactions). The number of hard-coupled reactions ranges from 1 to 6 while keeping growth between 50% to 100% of the maximum (Figure 4.3a and c). Maintaining 50% of the maximum growth rate decreased the number of hard-coupled reactions to 1. Growth rate normally declines if the hard-coupled reactions decrease (Lewis *et al.*, 2010). In the case of ethanol production, the number of hard coupled reactions is only 1 in the HMF model.

#### **4.2.3. Flexibility of Reactions (in terms of subsystems)**

The flexibility of the yeast network has also been examined on the basis of subsystems by FVA. The flux span average of the control and HMF model is given in Figure 4.4 to

Figure 4.11 for 50% to 100% maximum objective function values of both biomass generation and ethanol production.

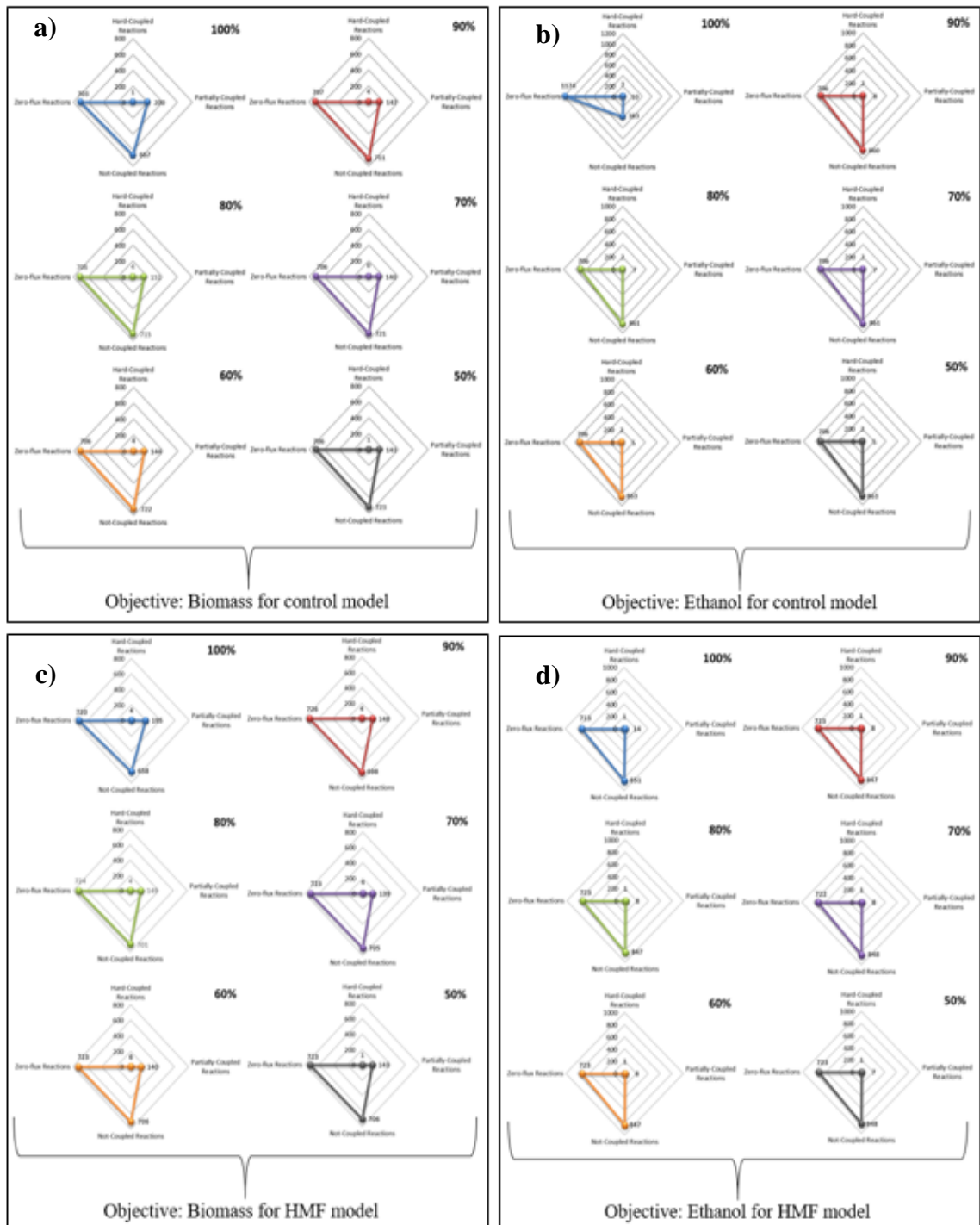


Figure 4.3. Reaction classifications (a) Objective: Biomass for control model (b) Objective: Ethanol for control model (c) Objective: Biomass for HMF model (d) Objective: Ethanol for HMF model.

In general, the number of subsystems involved in the generation of biomass is much higher than those towards ethanol production. In accordance with the previous results in Figure 4.3, where fewer reactions are involved in the production of ethanol, the participation of less subsystems in the production of ethanol (Figure 4.10 and Figure 4.11) by FVA analysis also reveals the accuracy of the results. Sterol metabolism, extracellular transport, glycerolipid metabolism and mitochondrial transport appear to be the subsystems with the highest flexibility for all ranges (50% to 100%) of biomass generation in the control model (Figure 4.4 to Figure 4.9). In fact, both control and HMF models indicate that yeast cells have a highly active extracellular transport system (Figure 4.4 to Figure 4.9). Although yeast cells are eukaryotes, having a thick cell wall is the distinctive characteristic of them. Due to this key difference, yeast cells have specific and complex secretion systems (Oliveira *et al.*, 2010a), (Oliveira *et al.*, 2010b). Using post-Golgi vesicles is a conventional method of secretion in eukaryotes including yeast cells. Moreover, there is a trans-cell wall secretion system in fungi and this system is a relatively unknown cellular event. Enzymes which are found in the periplasm are continuously secreted by yeast cells via trans-cell wall secretion (Oliveira *et al.*, 2010a).

Another common subsystem in the control and HMF models with high flexibility is glycerolipid metabolism whose components are usually represented as biomass constituents in GSMMs. The enzymes associated with cytosol, endoplasmic reticulum, mitochondria and lipid droplets can be employed for the synthesis of glycerolipids and their precursors. Cell signaling, membrane trafficking and anchoring of membrane proteins in addition to membrane structure are the missions of glycerolipids. Growth stage and nutrient opportunity determine the expression of glycerolipids (Henry *et al.*, 2012). This literature information reveals the importance of both subsystems (extracellular transport system and glycerolipid metabolism) and that they are necessary for the continuity of the cell. It is therefore plausible that they are active in both biomass generation and ethanol production. When there is 5-HMF in the environment, the pentose phosphate pathway and purine, pyrimidine biosynthesis stand out among other subsystems having high flux spans in biomass generation (Figure 4.4). Yeast survival, growth rate, cell budding, ethanol yield, biomass yield and biochemical enzyme activity are affected by the HMF. Yeast cells are able to eliminate the HMF by reduction (Gorsich *et al.*, 2006). Once concentration of HMF is lowered, glucose consumption starts to increase in yeast. This is explained as genomic adaptation and pentose

phosphate pathway is important for glucose metabolism/consumption to contribute energy and metabolites for biomass synthesis and ethanol production.

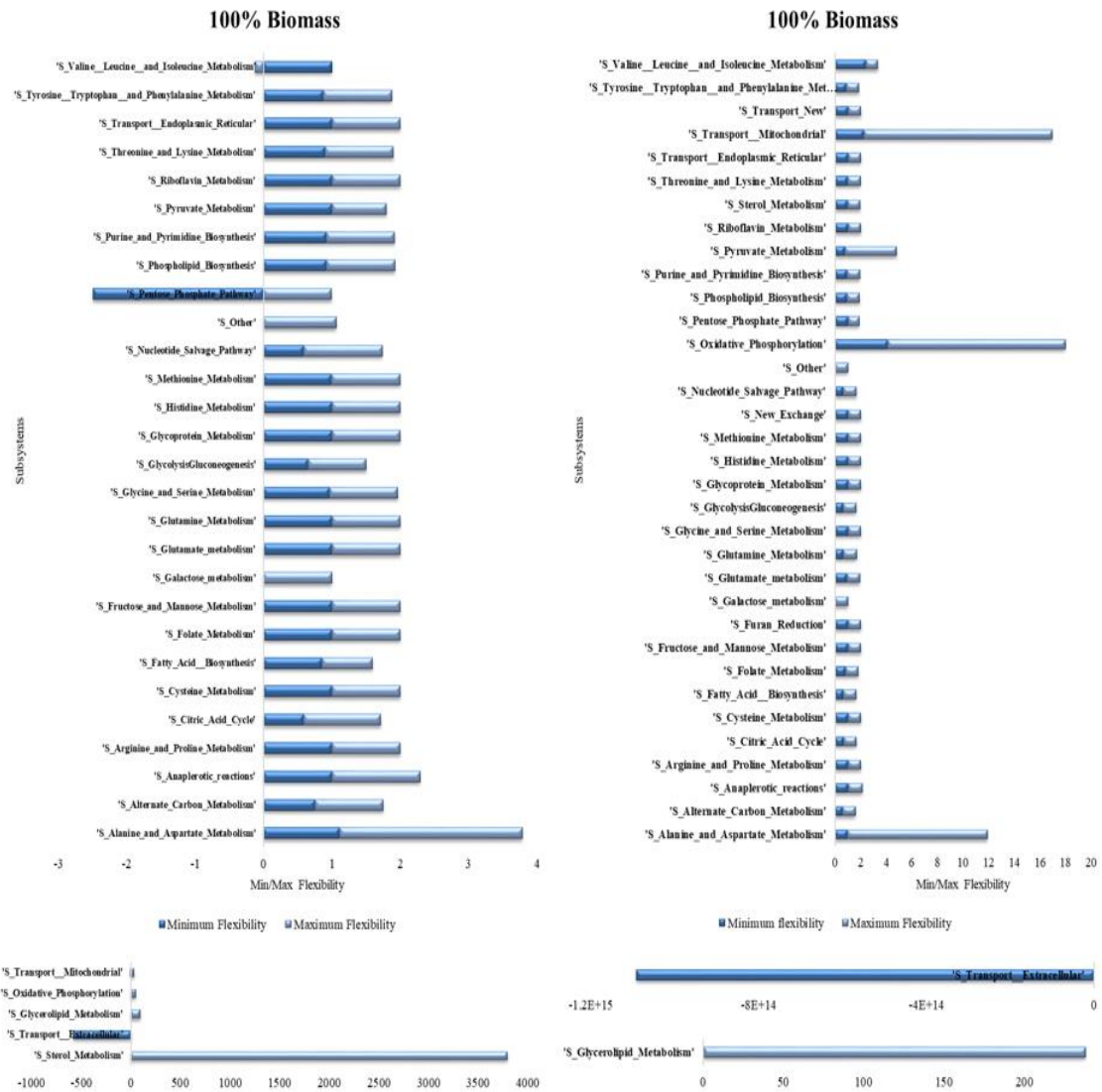


Figure 4.4. Flexibility of network based on subsystems for 100% maximum objective. Control model (left) and HMF model (right) for biomass generation.

Moreover, in yeast cells, purine metabolism has also significant roles to proceed the cellular functions such as energy carriage. Adenine requiring genes (ADE1, ADE13 and ADE17) engage in the de novo purine synthesis pathway. Among the ADE genes, ADE17 has role to enhance the tolerance to HMF in yeast cells and this gene also helps to increase the ethanol fermentation in the presence of inhibitors (Zhang *et al.*, 2019), (Chen *et al.*, 2019).

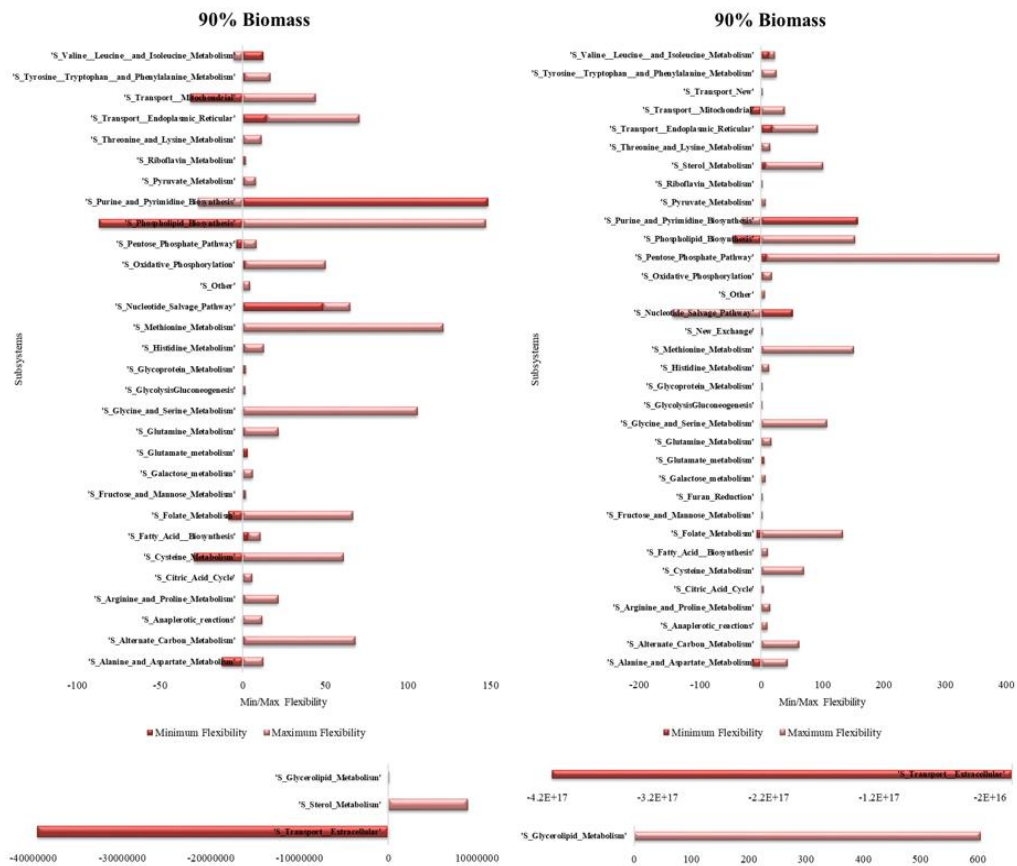


Figure 4.5. Flexibility of network based on subsystems for 90% maximum objective. Control model (left) and HMF model (right) for biomass generation.

When 90% biomass generation is aimed to give flexibility to internal flux distribution, pentose phosphate (PP) and nucleotide salvage pathways have wide flux spans (Figure 4.5). In addition to previous information pentose phosphate pathway has two main missions within the cell. One of them is the reduction of equivalents in the form of NADPH for lipid and other biosynthetic purposes. The second one is the contribution of pentoses for the generation of nucleic acids, glycoproteins, etc. (Steel *et al.*, 2001) and supporting the biomass accumulation (Stincone *et al.*, 2015) (Dutt *et al.*, 2018). Since PP pathway is used for NADPH production, this pathway contributes indirectly to growth. Moreover, nucleotides have significant role in cell growth and replication (Berg and Jørgensen, 2006). Free purine and pyrimidines are converted to nucleotides with the help of salvage reactions. These nucleotides are the key elements of the construction of DNA and RNA, the building blocks of the cell (Fasullo and Endres, 2015). The completion of many activities such as cell growth, reproduction, nourishment and so on takes place through DNA and RNA activity.

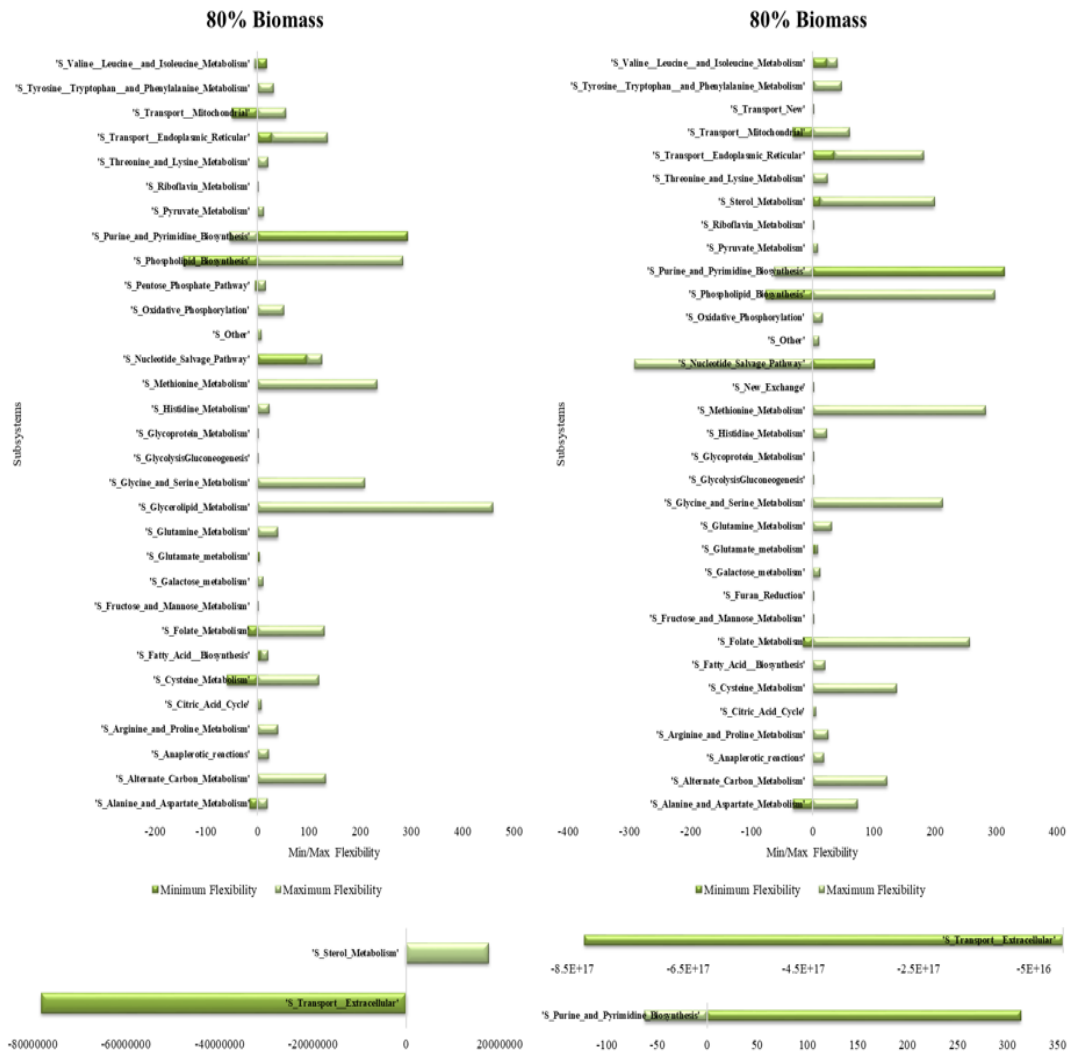


Figure 4.6. Flexibility of network based on subsystems for 80% maximum objective. Control model (left) and HMF model (right) for biomass generation.

Since the continuity of the cell depends on nucleotides, the nucleotide salvage pathway has an important flux span in biomass generation. Purine and pyrimidine biosynthesis, nucleotide salvage, phospholipid biosynthesis and folate metabolism are prominent subsystems while the objective value of biomass generation is at 80% or 70% of maximum in the model. Purines and pyrimidines present various and fundamental tasks in the cells. They are precursors to DNA and RNA and in charge of maintaining energy source. De novo synthesis and salvage pathways are used to provide purines and pyrimidines. These nitrogenous bases of nucleotides are nitrogen-rich molecules and can serve both as nitrogen and carbon sources for growth in yeasts (Berg and Jorgensen, 2006).

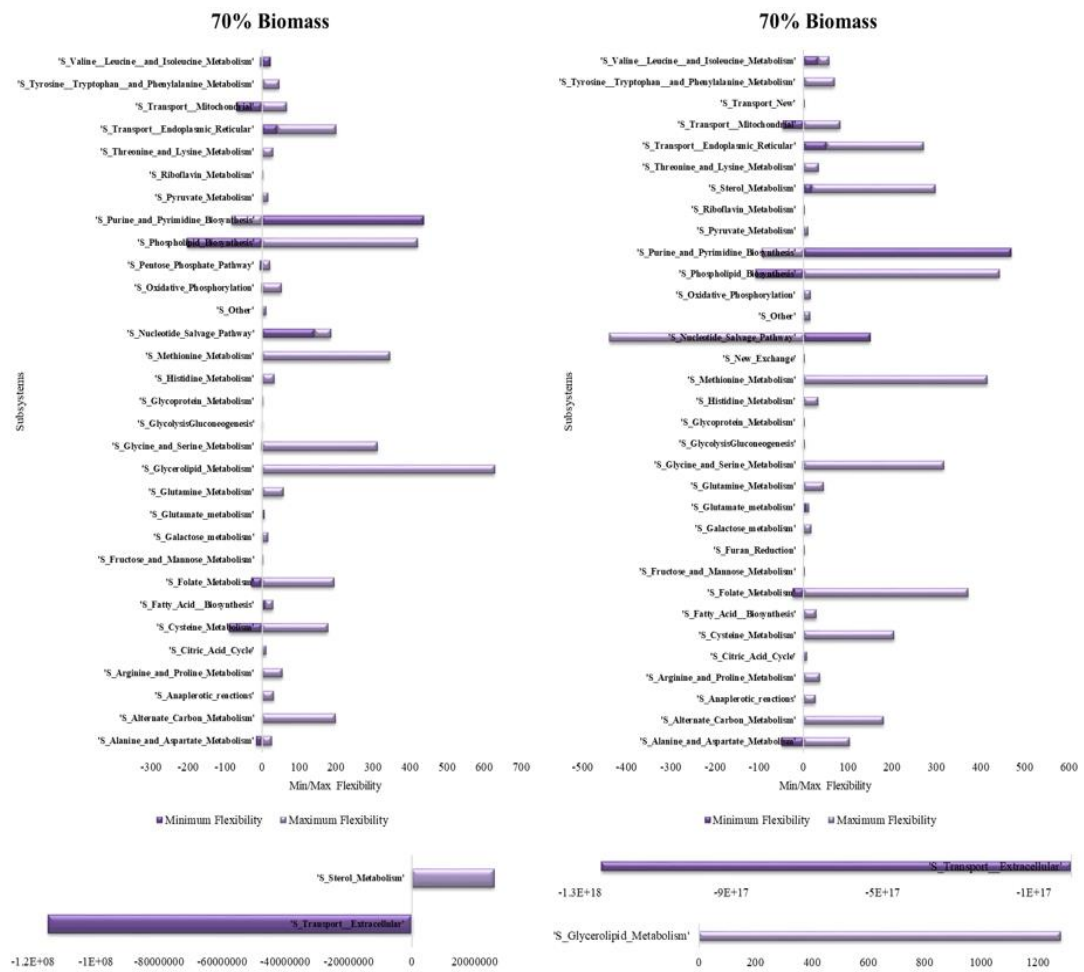


Figure 4.7. Flexibility of network based on subsystems for 70% maximum objective. Control model (left) and HMF model (right) for biomass generation.

The other important subsystem is the phospholipid biosynthesis. The phospholipids are also major components of cells and essential for vital cellular processes. In yeast cells, phospholipids are produced by several pathways and generally common to those found in higher eukaryotic organisms. The syntheses of phospholipids are dependent on the multiple factors such as nutrient availability, growth stage, pH or temperature (Carman & Henry, 1999), (Carman and Han, 2011). Organization and dynamics of membranes are regulated by phospholipids to control budding, membrane trafficking, domain formation and arrangement of protein-protein and protein-lipid complexes (Renne and Kroon, 2018). The last important subsystem is folate metabolism. Foliates belong to vitamin B family and are water-soluble compounds. They are necessary cofactors for one-carbon transfer reactions in cells. Methionine and purines can be produced with the help of folates and they are used as an

interconversion between serine and glycine, hence vital for replication and growth (Hjortmo *et al.*, 2008). This vitamin cannot be synthesized by animals and animals need to access it through the diet. Since folates join the important metabolic pathways, its deficiency might result in megaloblastic anemia, neural tube defects, cardiovascular diseases and cancer (Revuelta *et al.*, 2018).

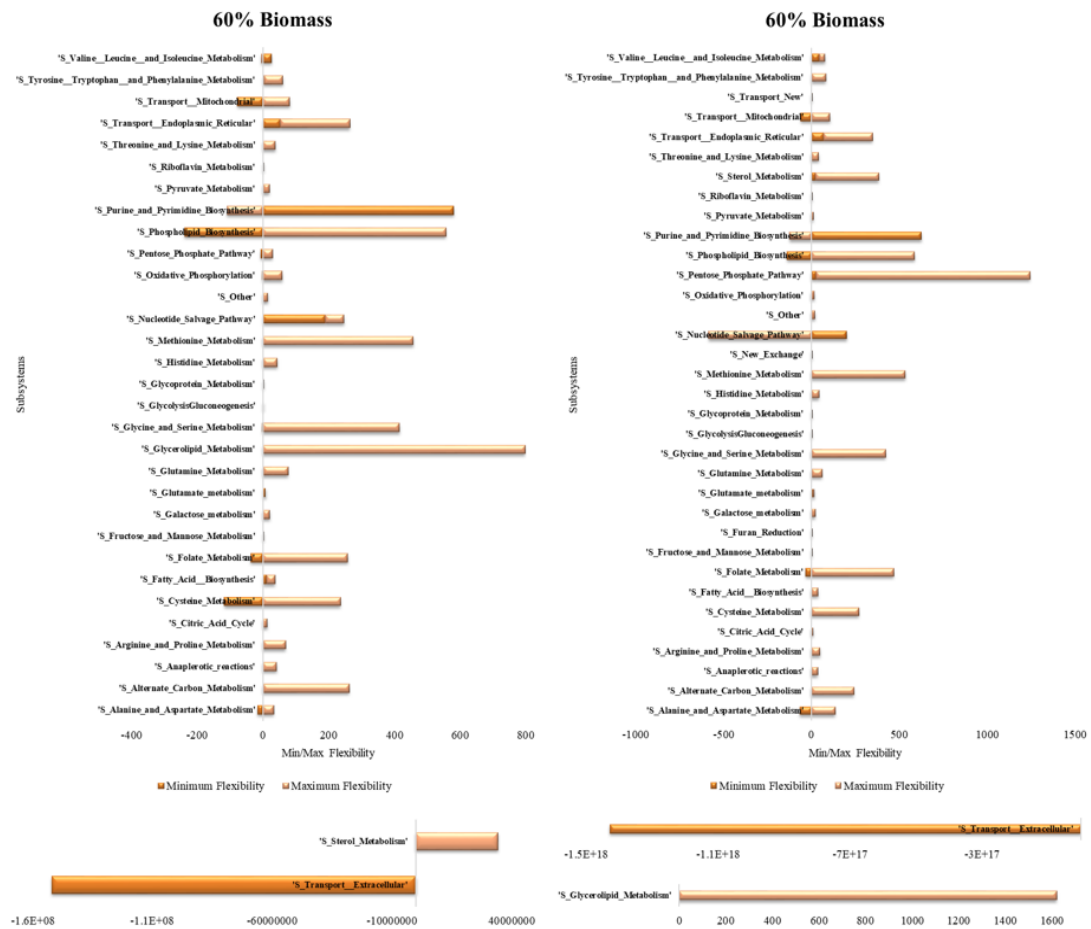


Figure 4.8. Flexibility of network based on subsystems for 60% maximum objective. Control model (left) and HMF model (right) for biomass generation.

It can be inferred from the results that pentose phosphate pathway, glycerolipid metabolism and purine and pyrimidine biosynthesis are the subsystems which have wide flux span at the objective values below 90% of the maximum biomass. These subsystems are linked with each other in terms of replication, growth and biomass. This reveals the reliability of the model (Figure 4.4 to Figure 4.9). The subsystems of mitochondrial transport, oxidative phosphorylation and alanine and aspartate metabolism are very active in

biomass generation (the maximum objective values is 100%) in the HMF model. The energy management is very important for cells to maintain their lives and mitochondrial metabolites are necessary to form biomass (Agostini, *et al.*, 2021), (Spinelli and Haigis, 2019).

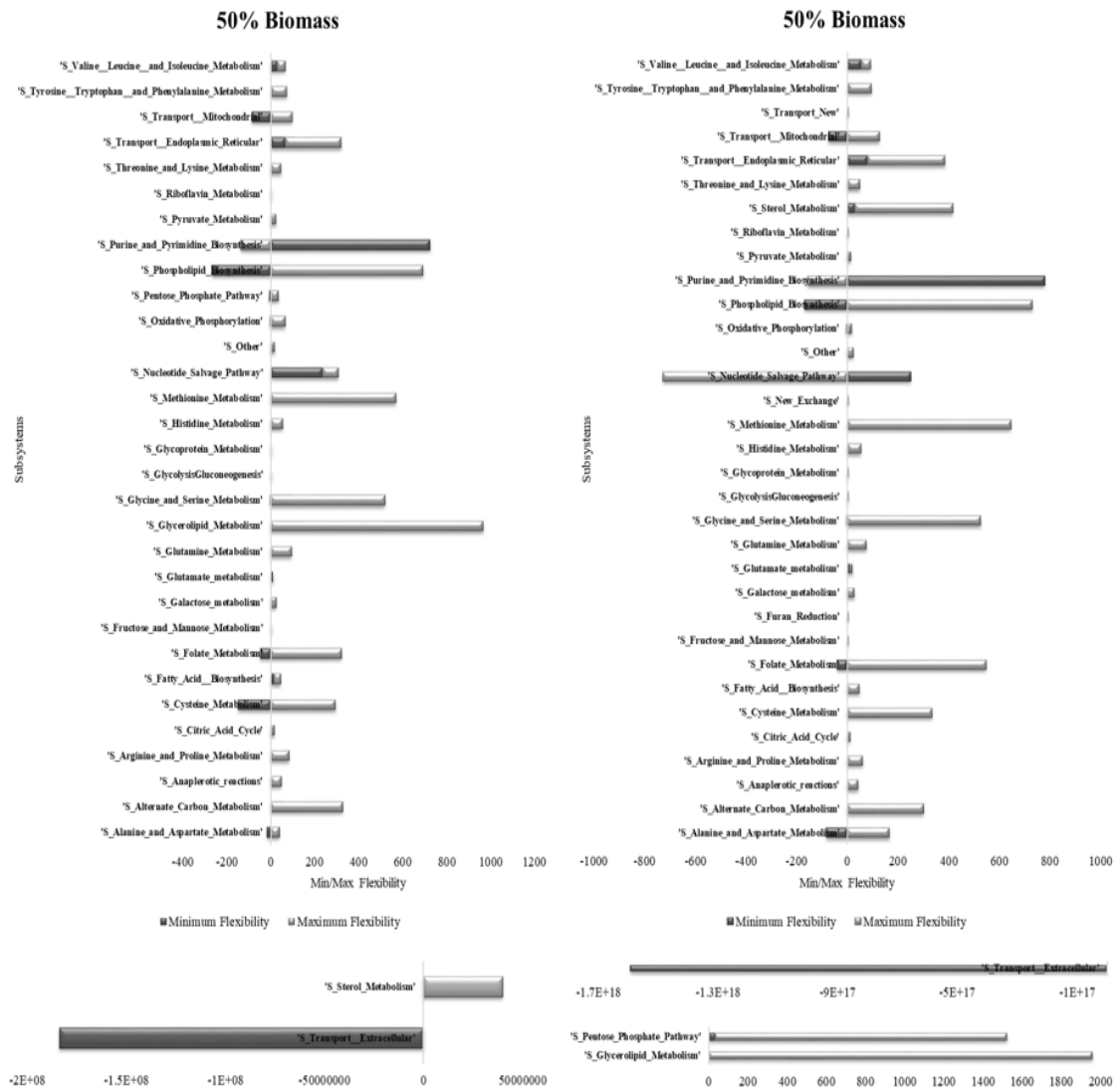


Figure 4.9. Flexibility of network based on subsystems for 50% maximum objective. Control model (left) and HMF model (right) for biomass generation.

When the objective function is maximization of ethanol, completely different subsystems have roles on ethanol production. While the nucleotide salvage pathway predominates for all percentages of the control model (Figure 4.10, 4.11, 4.12, 4.13, 4.14 and 4.15), the sterol metabolism in the HMF model has great flexibility (Figure 4.10, 4.11, 4.12, 4.13, 4.14 and 4.15). Sterols are generally found in membranes of the several species.

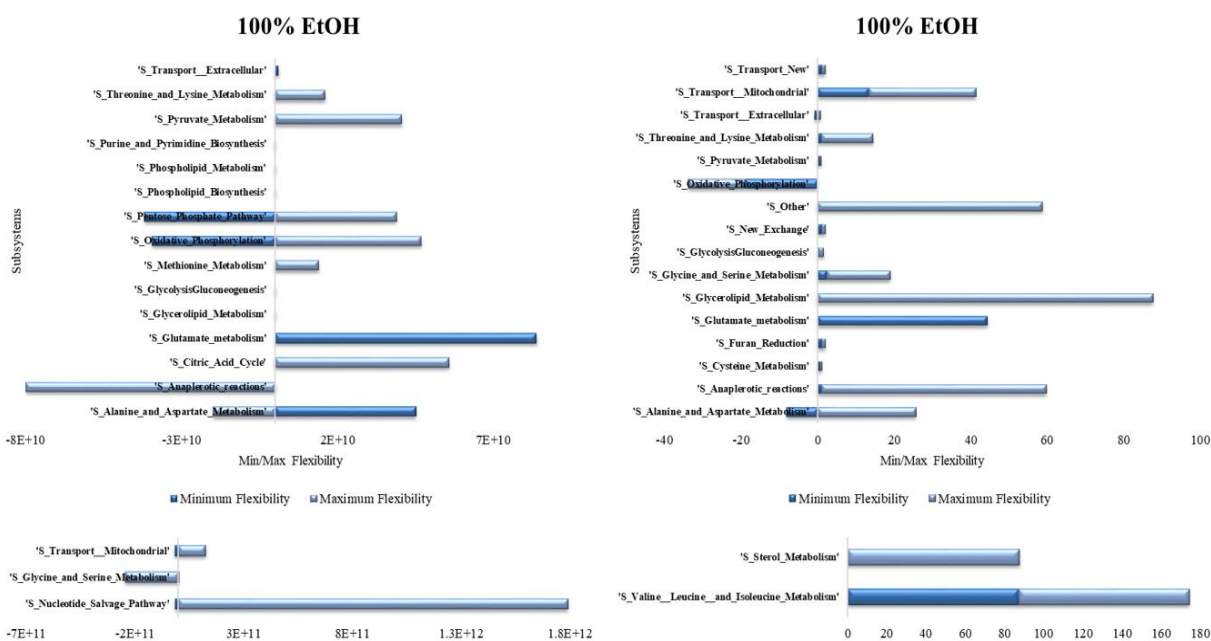


Figure 4.10. Flexibility of network based on subsystems for 100% maximum objective. Control model (left) and HMF model (right) for biomass generation.

While the most abundant sterol is cholesterol in mammalian cells, ergosterol and phylosterol are mostly found in fungi and plant cells. Maintaining the stability, fluidity and permeability are the responsibilities of sterols (Dupont *et al.*, 2011). Under normal conditions, without HMF, sterols work for transportation of nutrients and biological wastes. In this case, it is reasonable to have wide range of flexibility in the sterol metabolism and extracellular transport in the control model because the cell needs these subsystems to continue its life. The remarkable part here is that sterol metabolism has high flexibility in biomass production of the control model and ethanol production of the HMF model. From this, it can be concluded that sterol metabolism works purposefully in the HMF stressed or non-stressed environment.

In addition to the reactions in sterol metabolism, glycerolipid metabolism and anaplerotic processes have also been found to have a serious flux span in HMF model, when the objective is maximization of ethanol production. Moreover, oxidative phosphorylation has also wide flux span for both biomass generation and ethanol production. This subsystem is related with mitochondrial transport because the common point here is the energy. Energy generation and consumption are essential processes for understanding the metabolism and

for modelling the growth. Growth is both dependent on the energy requirements for biomass synthesis and the ATP yield by respiration (Zeng *et al.*, 1990), (Queiroz *et al.*, 1993).

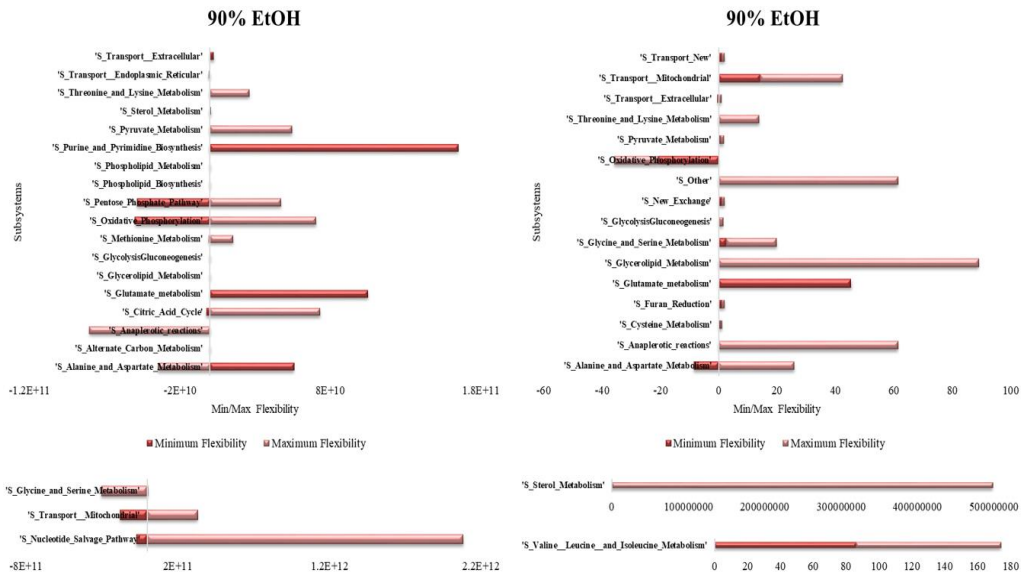


Figure 4.11. Flexibility of network based on subsystems for 90% maximum objective. Control model (left) and HMF model (right) for biomass generation.

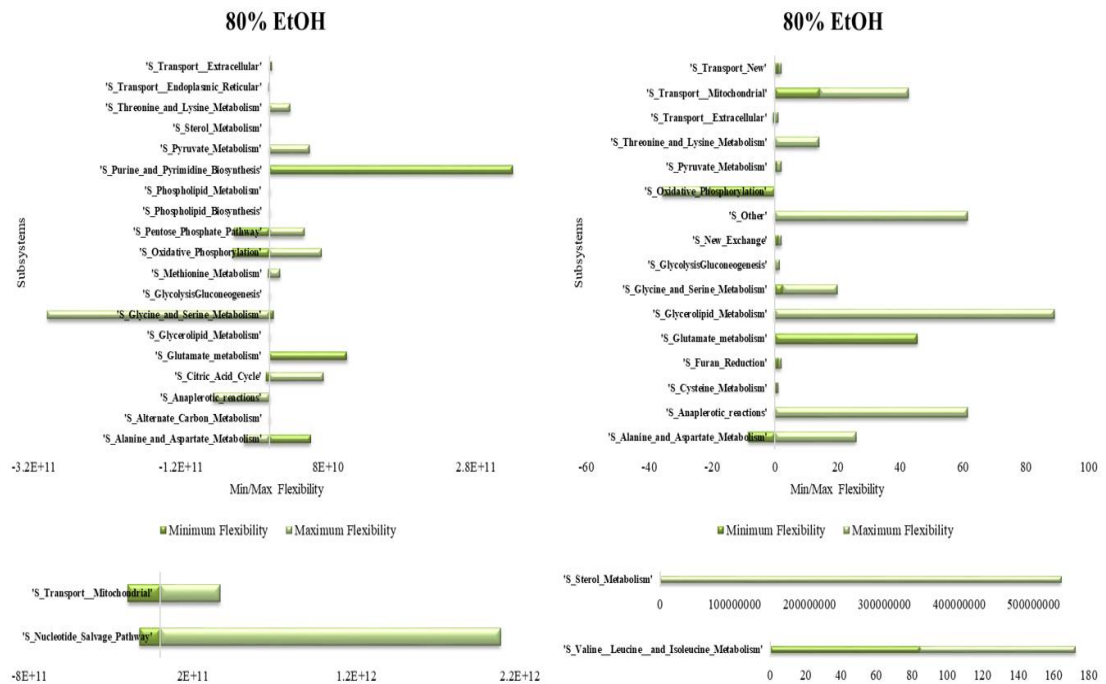


Figure 4.12. Flexibility of network based on subsystems for 80% maximum objective. Control model (left) and HMF model (right) for biomass generation.

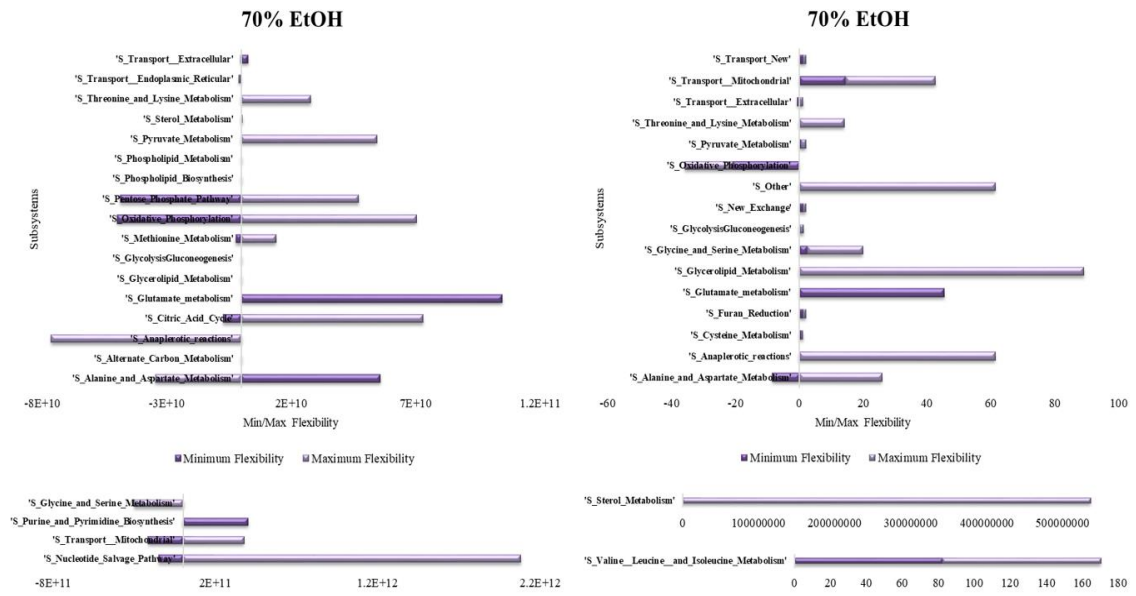


Figure 4.13. Flexibility of network based on subsystems for 70% maximum objective. Control model (left) and HMF model (right) for biomass generation.

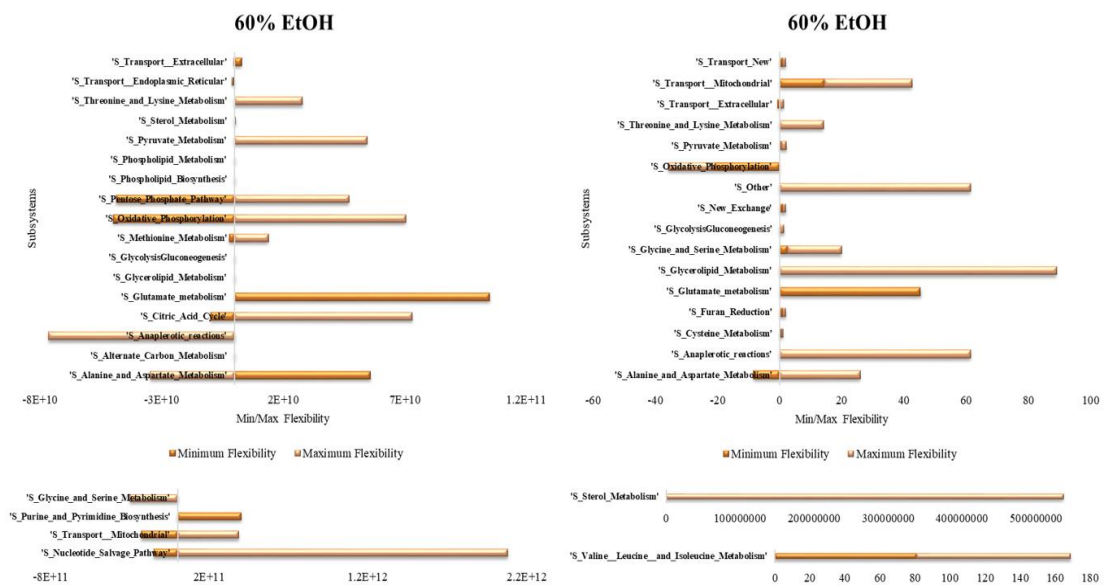


Figure 4.14. Flexibility of network based on subsystems for 60% maximum objective. Control model (left) and HMF model (right) for biomass generation.

When the ethanol production is considered, the metabolism of ethanol through alcohol dehydrogenase (ADH) prepares cytosolic NADH, which is oxidized indirectly by mitochondrial electron transport (Hoek *et al.*, 2002). Thus, the biomass generation and

ethanol production both require oxidative phosphorylation, as shown in Figure 4.4 to Figure 4.9. In the ethanol production case for the HMF model, lipids come into prominence under 100% maximum objective conditions. In eukaryotic cells, lipid transport takes an important place. They can be synthesized by certain organelles and they are the constitutive elements of all membranes (Zinser *et al.*, 1993). Lipids are organic elements and can be categorized by their structure and function. Fatty acids, glycerolipids, glycerophospholipids, sterols and sterol derivatives, sphingolipids, prenol lipids, glycolipids and polyketides belong to lipid family. They are used as energy source and are mediators of membrane fusion and apoptosis (Klug and Daum, 2014). The alterations in the plasma membrane content (due to ethanol production) affect the membrane fluidity in order to compensate for the disruption caused by ethanol.

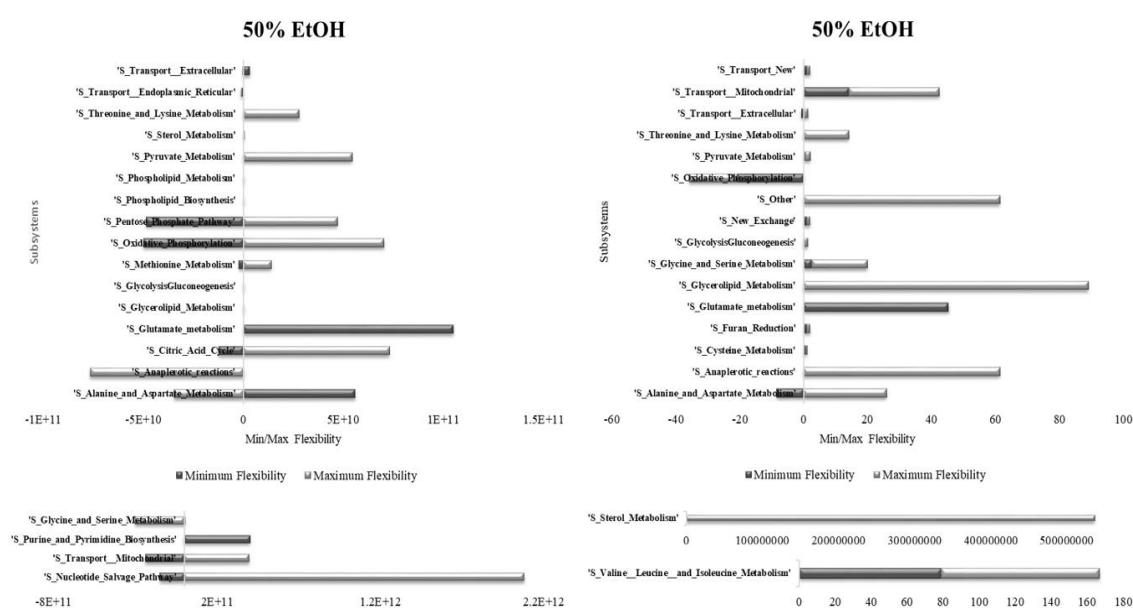


Figure 4.15. Flexibility of network based on subsystems for 50% maximum objective. Control model (left) and HMF model (right) for biomass generation.

Since sterols have role on sustaining the order of the membrane, sterol metabolism might be more active in the ethanol production (Vanegas, *et al.*, 2012), as also indicated by Figure 4.10, 4.11, 4.12, 4.13, 4.14 and 4.15. Glycerolipid metabolism (represented as biomass constituents in GSMMs) is one of the subsystems that has a significant impact on ethanol production. Monoacylglycerol, diacylglycerol and triacylglycerol can be found in glycerolipid metabolism and these molecules contribute to the ethanol production via Acyl

CoA (Vinayavekhin *et al.*, 2020). When the target of the HMF model is to produce ethanol and make the objective values below 90% of maximum, valine, leucine and isoleucine and glycerolipid metabolisms come to the forefront (Figure 4.6b). Valine leucine and isoleucine are also known as the branched chain amino acids (BCAA) and they must be obtained from the extracellular nutrient medium or the diet in human cells. Besides being a building block for tissue protein, BCAA has also metabolic functions. Among the three BCAA, leucine has a specific role in activation of mTOR signaling pathway. Moreover, BCAA enhance the secretion of insulin and eventually might cause insulin resistance or type 2 diabetes in human (Zhang *et al.*, 2017a). In the control model, on the other hand, glutamate metabolism appears to have high flexibility towards ethanol production (Figure 4.6a). Yeast cells can utilize variety of compounds as a source of nitrogen. Molecules including nitrogen are converted into ammonia, glutamate and glutamine within the yeast cells to use them as amino donors for several biosynthetic reactions (Guillamon and Giuseppin, 2001). In addition, glutamate plays important role in protein synthesis and promotes the cell growth (Huang *et al.*, 2017). In this control model, since the yeast cell is forced to produce ethanol without consideration of biomass generation, the reason for the high flexibility of glutamate metabolism may be to maintain vitality in the cell. In order to generate the biomass or produce ethanol, extracellular transport and glycerolipid metabolism are common and important subsystems for both of the control and HMF model. Although the number of reactions participated in the models are almost the same, there is a serious difference in number of subsystems appeared in the results. When the objective function is ethanol production, most of the subsystems are discarded by the COBRA toolbox and only ethanol related reactions and subsystems are presented.

#### 4.2.4. Flux Coupling and Regulation

In a genome-scale metabolic model constraint with stoichiometric and thermodynamic parameters, some reactions are unable to carry flux at steady state or a non-zero flux through a reaction might cause a non-zero flux through another reaction. This dependency between reactions is identified as coupling. In order to determine the dependencies between reaction fluxes of a metabolic network at steady state flux coupling analysis (FCA) is used (Larhlimi *et al.*, 2012).

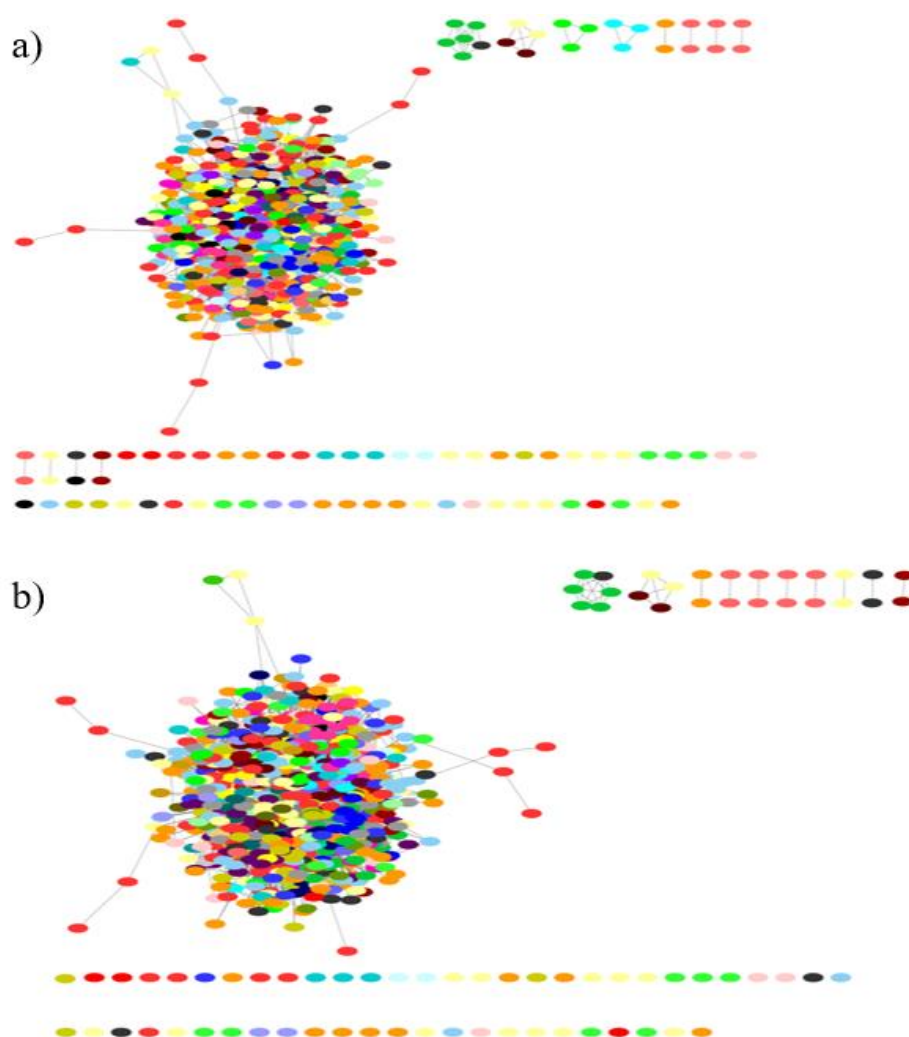


Figure 4.16. Flux coupling network of (a) control and (b) modified models. Nodes show the reactions and colors are based on subsystems.

In this study, F2C2, a fast tool for the computation of flux coupling is employed according to our constraints in both of the models (control and HMF models). Blocked reactions were eliminated from the network and uncoupled, fully coupled, partially coupled and directionally coupled reactions are identified. The reason for the elimination of blocked reactions from the network is mainly the incomplete explanation of the biomass composition and medium composition indicated in simulation (Montagud *et al.*, 2011). In the HMF model; 656 pairs were classified as fully coupled, 10 pairs partially coupled, 3724 pairs directionally coupled, and the remaining ones were classified as uncoupled. The number of fully coupled pairs is 655, partially coupled pairs is 6 and directionally coupled pairs is 3712 in the control model. The coupled Extracellular transport subsystem is commonly dominant

in the biomass generation case of both control and HMF models when the 100% maximum objective was attained (Figure 4.16a and Figure 4.16b). In this subsystem, glucose transport unit (GLCt1) reaction is involved in many of the coupling pairs. This reaction is generally directionally coupled with other reactions. GLCt1 helps the transportation of glucose in the cell and this process is known as facilitated diffusion. Since glucose is fundamental energy source, these transporters are significant (Maier *et al.*, 2002). In addition, ATPS reaction is also found in extracellular transport subsystem. Its importance is also mentioned in the FVA part and this reaction is directionally coupled with D-Glucose exchange (EX\_glc\_\_D\_e) and GLCt1. As this part is common to both of the models, it can be said that biomass generation reveals the mutual aspects of the models. In HMF model (Figure 4.16b), when the maximum objective value is set to 100% of biomass generation, the reactions in mitochondrial transport subsystem have several coupling types.

The metabolites, nucleotides and cofactors across the inner mitochondrial membrane are carried via mitochondrial transport subsystem (Todisco *et al.*, 2006). The acetate transport mitochondrial (ACtm), CO<sub>2</sub> transport diffusion (CO<sub>2</sub>tm), O<sub>2</sub> transport diffusion (O<sub>2</sub>tm) and NH<sub>3</sub> mitochondrial transport (NH<sub>4</sub>tm) reactions are directionally coupled with EX\_glc\_\_D\_e and GLCt1 reactions. ACtm reaction belongs to ethanol metabolism pathway and CO<sub>2</sub>tm reaction is the part of TCA cycle. These two reactions contribute to glycolysis pathway via coupling with GLCt1 reaction. CO<sub>2</sub>tm reaction has also directionally coupled with acetolactate synthase mitochondrial (ACLSm) and pyruvate dehydrogenase (PDHm) catalyzed reactions. While NH<sub>4</sub>tm reaction appears as directionally coupled with glycine cleavage system mitochondrial (GLYCLm) reaction, it is fully coupled with glycine hydroxymethyltransferase reversible mitochondrial (GHMT2rm) reaction and partially coupled with glycine mitochondrial transport via proton symport (GLYt2m) reaction. O<sub>2</sub>tm reaction is fully coupled with cytochrome c oxidase mitochondrial (CYOOm) and directionally coupled with D-lactate dehydrogenase cytosolic mitochondrial (D\_LACDcm) reactions.

Sterol metabolism is encountered with both when 100% biomass generation is objected in the control model and when 100% ethanol production is objected in the HMF model (Figure 4.16a & 4.16b). In this subsystem, hydroxymethylglutaryl CoA reductase (HMGCOAR) reaction makes several couplings with other reactions in both of the models.

Acetyl-CoA C-acetyltransferase (ACACT1r) reaction is directionally coupled with HMGCOAR and dimethylallyltranstransferase (DMATT), O<sub>2</sub> transport endoplasmic reticulum (O<sub>2</sub>ter) and H<sub>2</sub>O endoplasmic reticulum transport (H<sub>2</sub>Oter) reactions are fully coupled with the same reaction. These coupling types of HMGCOAR is prevalent to both models. However, in the HMF model (for ethanol production case), HMGCOAR is directionally coupled with cholesterol delta isomerase lumped reaction (CHLSTI), oxygen exchange (Ex\_o2\_e) and oxygen transport diffusion (O<sub>2</sub>t). These reactions might have roles in the production of ethanol under the sterol metabolism and due to basic difference in between the biomass generation and ethanol production, they might not create any coupling types with HMGCOAR in the control model. In addition to sterol metabolism for ethanol production (100%), valine, leucine and isoleucine subsystem has high flexibility in the presence of HMF, as stated previously (Figure 4.16b).

Among the reactions within the valine, leucine and isoleucine subsystem isoleucine transaminase (ILETA) is fully coupled with 3 Methyl 2 oxopentanoate transport diffusion mitochondrial (3MOPtm), isoleucine transaminase mitochondrial (ILETA<sub>m</sub>) and isoleucine transport from mitochondria to cytosol (ILET<sub>mi</sub>) reactions. ILETA reactions are found in the family of transferases to transfer nitrogenous groups. They have roles in valine, leucine and isoleucine degradation and biosynthesis and pantothenate and coa biosynthesis (Aki *et al.*, 1968), (Ikeda *et al.*, 1976). In the control model, on the other hand, Nucleotide salvage pathway is the main subsystem containing the reactions coupled to the production of ethanol (Figure 4.16a, b). This pathway includes several reactions and one of them is ATP diphosphohydrolase (ATPH1). ATPH1, also known as apyrase, manages the hydrolysis of phosphoanhydride bonds of ATP with divalent cations. Apyrase can be encountered in many reactions to further sustain/enhance the cellular activities (Nourizad *et al.*, 2003), however it has only directional coupling relation with Ex\_glc\_\_D\_e and GLCt1 in this case.

This may be because the model contains insufficient information on this subject. The reactions catalyzed by 4HGLSD<sub>m</sub>, CYSTGL, G5SAD<sub>rm</sub>, PYR5CD<sub>m</sub>, SHSL1 and SHSL4<sub>r</sub> enzymes joined the coupling network in the control model (Figure 4.16a) but they are not found in the HMF model. Due to the destructive effect of HMF on the yeast, the cell may have forsaken a number of reactions in order to survive and reduce the HMF concentration. By looking at the partially coupled category, it was found that there was a small amount of

coupling in both models. The reactions catalyzed by FAS100COA, FAS120, FAS120COA, FAS140 and FAS80COA\_L (belongs to fatty acid biosynthesis subsystem) are partially coupled in both control and HMF models (Figure 4.16a and Figure 4.16b). Apart from the partially coupled pairs that are common with the control model, there are 2 more pairs in the HMF model. GLYt2m reaction in mitochondrial transport subsystem and GHMT2rm reaction in glycine and serine metabolism subsystem are partially coupled with each other. GLYt2m is also partially coupled with NH4tm in the mitochondrial transport subsystem.

#### 4.2.5. Transcriptional vs Metabolic Regulation

In order to understand the cellular functions in detail, the correlation between the gene expression and metabolic flux is decisive. Thus, an analysis workflow (Bordel *et al.*, 2010) is used to discover the regulation types (transcriptional, post-transcriptional and metabolic) in the metabolic network. The conversion from DNA to RNA (transcription) and coordinating the gene activity is explained via transcriptional regulation. Cell and organism development, complexity and homeostasis are orchestrated via transcriptional regulation, and transcription is the first step in the universal pipeline of biological information flow from genome to proteome (Madigan *et al.*, 2018), (Polouliakh 2019). The harmony in between the substrate and product of enzyme catalyzed reactions is coordinated by metabolic regulation, thereby developmental requirements and environmental changes can be organized with the help of ordered metabolic flow (Paul 2013), (Bouwman *et al.*, 2011). At this stage, the regulation type within the network is identified via integration of gene expression to the flux estimation. Gene expression data for yeast cells with and without HMF supplementation were taken from Gene Expression Omnibus (GEO) and the metabolic fluxes for both control and HMF model were estimated by FBA. The sampling analysis is first done. In order to have an estimated probability distribution of flux values for every reaction in the model, uniform sampling method is employed. For irregularly shaped solution spaces Artificial Centering Hit-and-Run (ACHR) is handled and uniform random sampling method known as gpSampler (Megchelenbrink *et al.*, 2014) is used. Transcriptional regulation, significantly correlated change both in flux and in expression, post-transcriptional regulation, significant change in expression but not in flux, and metabolic regulation, significant change in flux but not in expression, are the classification types of genes (Bordel *et al.*, 2010). According to the simulation results, 145 (16.2%) of total genes are transcriptionally regulated, 174 (19.5%)

of them are metabolically regulated and 575 (64.3%) of genes are post-transcriptionally regulated (Figure 4.17). Considering the results of previous sections, the regulation type is also analyzed based on the subsystems, and the post transcriptional regulation is more common among them. While transcriptional regulation is leading in the sterol metabolism (Figure 4.17d) and glycine and serine metabolism (Figure 4.17k), metabolic regulation is dominant in the pentose phosphate pathway (Figure 4.17g) and valine leucine and isoleucine metabolism (Figure 4.17m) subsystems. Following post-transcriptional regulation, metabolic regulation is mostly observed in subsystems, while transcriptional regulation is prominent in subsystems of oxidative phosphorylation (13.9%) (Figure 4.17c) and phospholipid biosynthesis (20.5%) (Figure 4.17j).

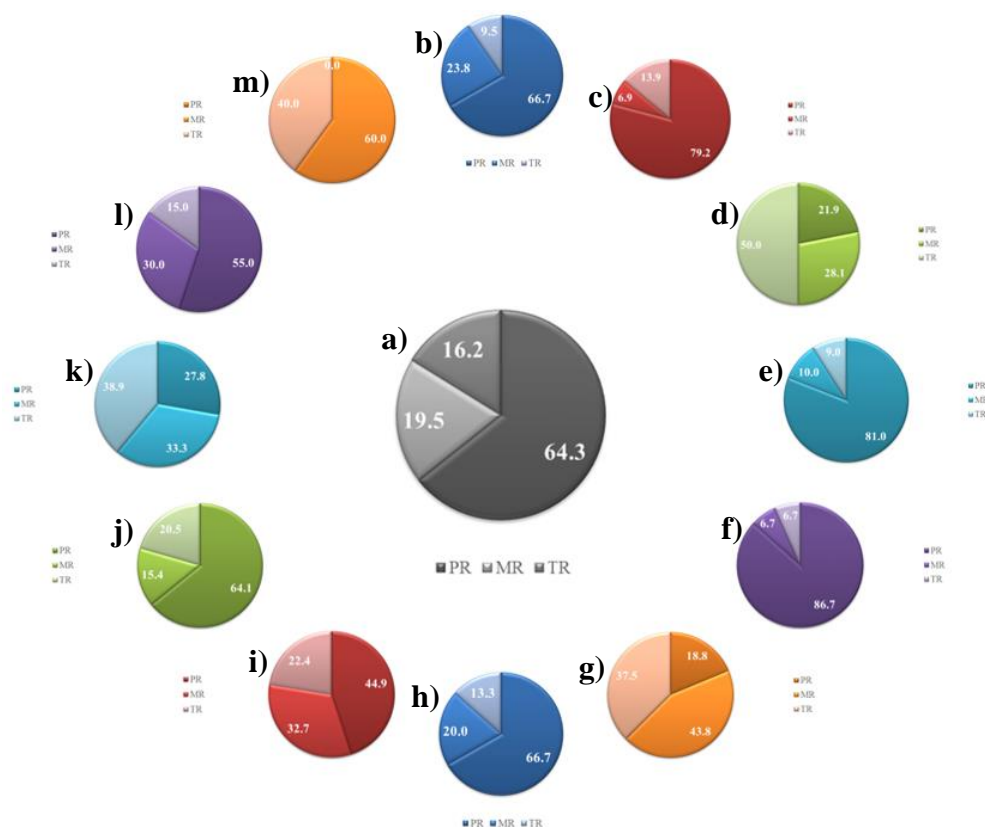


Figure 4.17. Regulation types of the model and subsystems (a) Total results under the treatment of HMF (b) Mitochondrial transport (c) Oxidative phosphorylation (d) Sterol metabolism (e) Extracellular transport (f) Glycerolipid metabolism (g) Pentose phosphate pathway (h) Nucleotide salvage pathway (i) Purine and pyrimidine biosynthesis (j) Phospholipid biosynthesis (k) Glycine and serine metabolism (l) Folate metabolism (m) Valine leucine and isoleucine metabolism.

#### 4.2.6. FSEOF and Reaction/Gene Deletions

In order to increase ethanol production while the cell continues its vital activities, various sanctions are applied to the models and reaction /gene manipulation is one of them. Flux scanning based on enforced objective flux (FSEOF) is used to determine the gene amplification/deletion targets to enhance the ethanol production. As biomass formation and ethanol production has inverse relationship, ethanol production can be maximized in a network by letting the biomass generation go to zero. Since this is not applicable, FSEOF algorithm is employed to identify the genes towards the increase of ethanol production (Choi *et al.*, 2010). The upregulated and downregulated reactions during the ethanol production were revealed based on the difference between the flux balance analysis (FBA) and FSEOF (Figure 4.18) for both models. Among the 20 reactions identified via the FSEOF algorithm, alcohol dehydrogenase reverse reaction acetaldehyde ethanol (ALCD2ir) and alcohol dehydrogenase (ethanol) (ALCD2x) reactions need to be upregulated for more ethanol production in both models (Figure 4.18a and Figure 4.18b). They are found in the alcohol dehydrogenase reaction classification and in order to generate the ethanol, NAD is converted to NADH (Smidt *et al.*, 2012).

In the HMF model, fructose-bisphosphate aldolase (FBA) and phosphofructokinase (PFK) are the upregulated reactions for ethanol production in the modified model. These reactions are present in the ethanol metabolism pathway. The cleavage of D-fructose-1,6-phosphate (FBP) to D-glyceraldehyde-3-phosphate (G3P) and dihydroxyacetone phosphate (DHAP) is managed by FBA enzyme, which plays critical role in glycolysis and gluconeogenesis (Asokumar *et al.*, 2018), (Roslan *et al.*, 2017). PFK catalyzes the phosphorylation of fructose6-phosphate to fructose-1,6-bisphosphate, and is a compulsory reaction for glycolysis. Allosteric inhibition and activation coordinate the actions of PFK enzyme (Breitenbach-Schmitt *et al.*, 1984), (Lelevich *et al.*, 2013). When the reactions catalyzed by the downregulated enzymes are considered in HMF model, there is a serious change in the flux of acetate transporter (ACtr), sedoheptulose 1,7-bisphosphate D-glyceraldehyde-3-phosphate-lyase (FBA3) and phosphofructokinase\_s7p (PFK\_3) reactions. ACtr has an impact on the transportation of acetate within the ethanol metabolism pathway. If this reaction suffers any damage within the cell, the uptake of acetate stops and ethanol production would be interrupted (Casal *et al.*, 2008). Moreover, FBA3 and PFK\_3

need to be downregulated in the ethanol process unlike the FBA and PFK. They can be found in the pentose phosphate pathway and they work one after the other. FBA and FBA3 are connected to each other by dihydroxyacetone phosphate (dhap\_c) and they are working in vice versa. PFK and PFK\_3 enzymes are also working in contrary and they promote the functioning of FBA and FBA3.

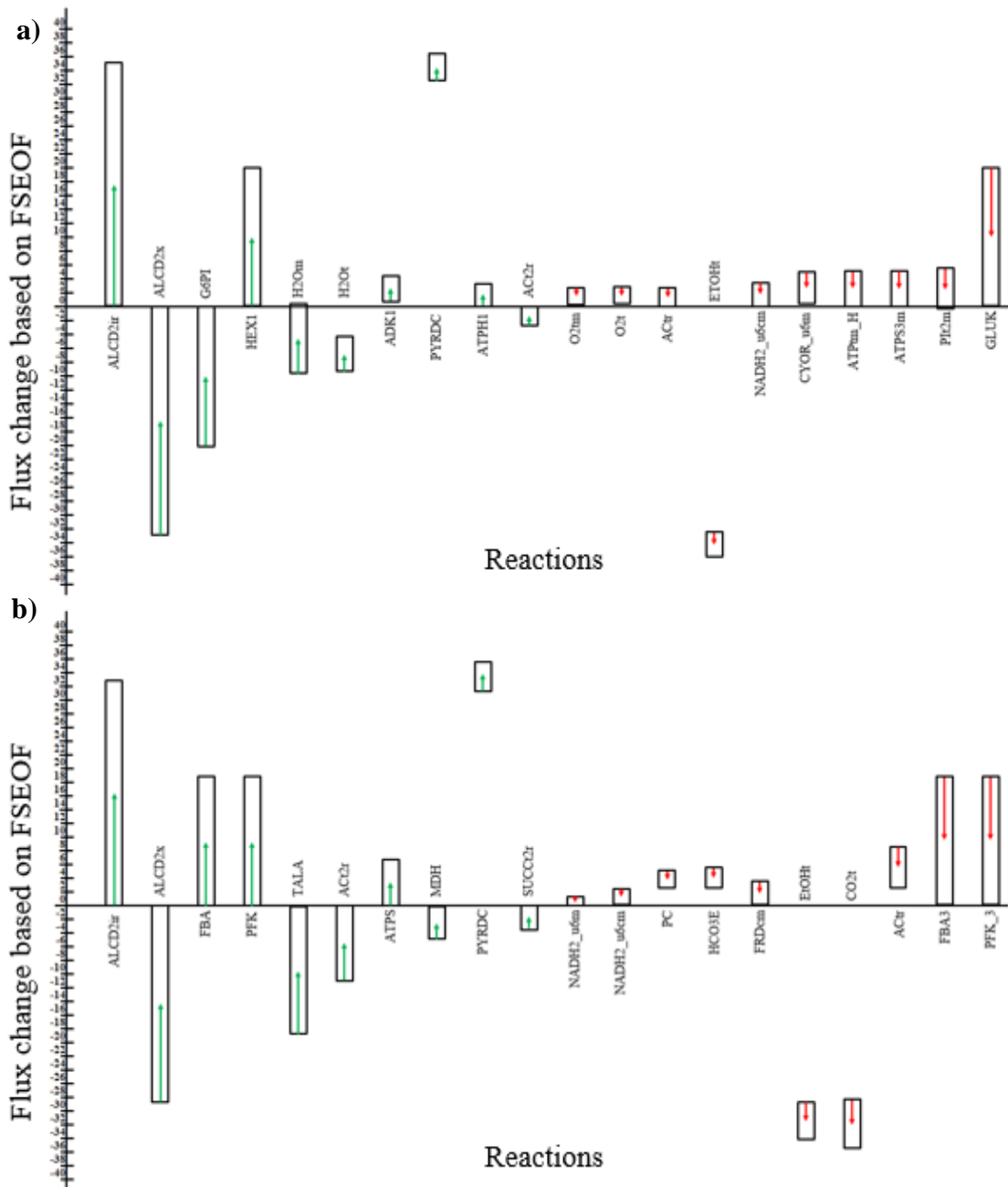


Figure 4.18. FSEOF algorithm result: The identified reactions and their flux changes (a) control model (b) modified model.

In addition to the difference between FSEOF and FBA, various other reactions were determined according to the slope calculation based on FSEOF and the effect of ethanol production was examined by deleting them from the network. In addition, OptKnock reaction deletion cases are also included for comparison.

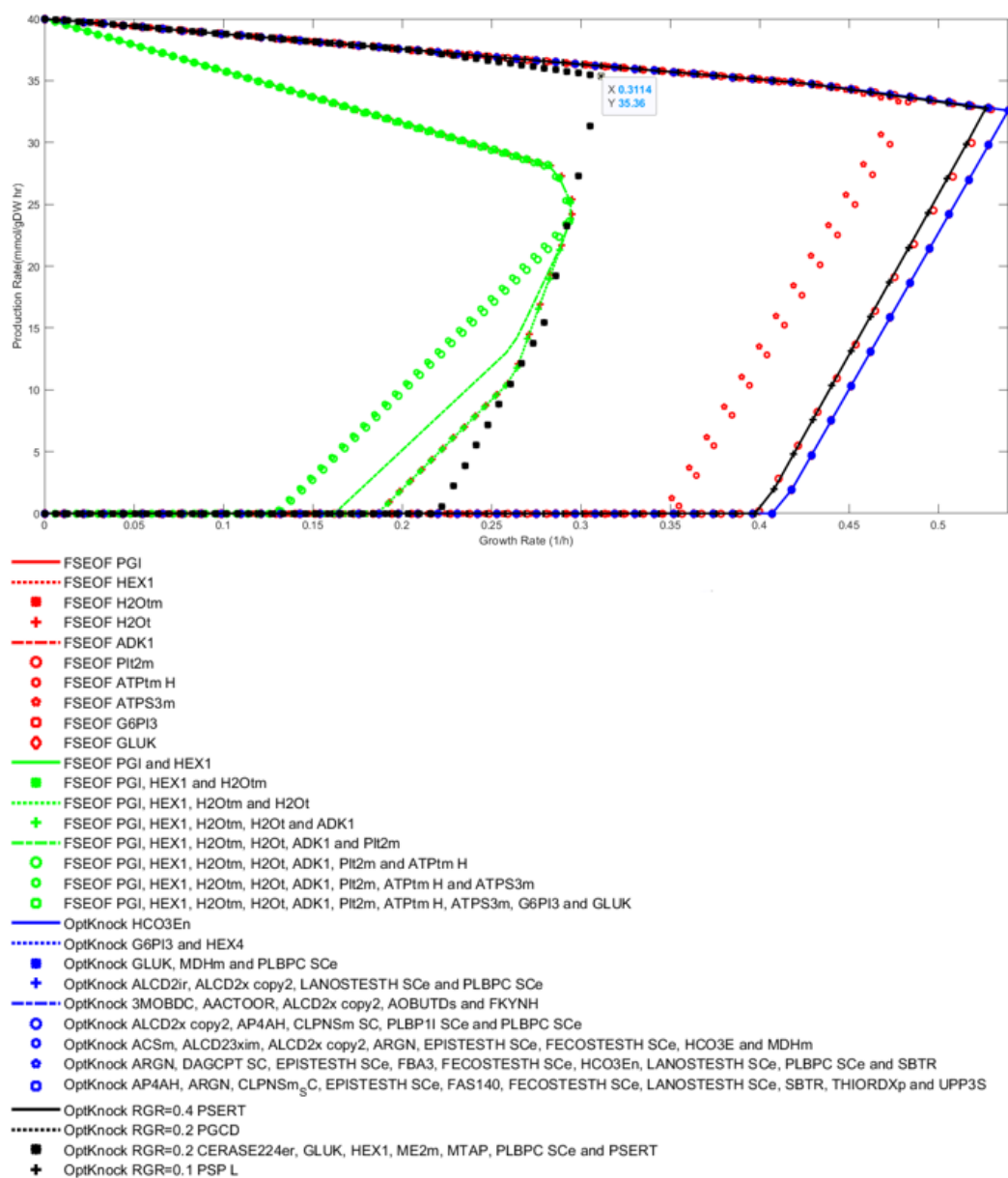


Figure 4.19. Reaction deletion cases based on FSEOF and OptKnock for control model. Red lines depict the FSEOF single deletions, green lines show FSEOF multiple deletions, blue lines are for OptKnock deletions and black lines are used to describe the reduced growth rate cases with OptKnock.

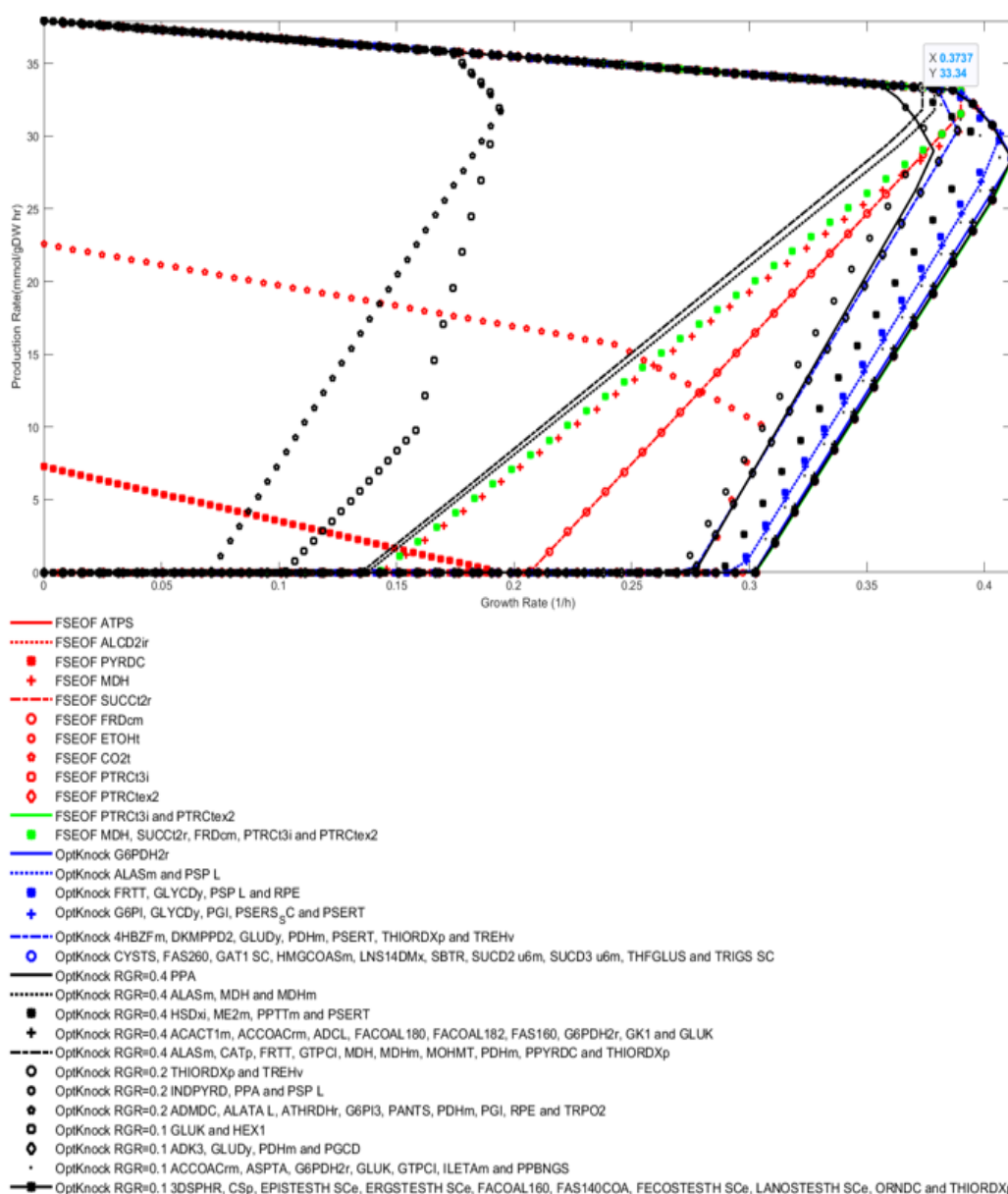


Figure 4.20. Reaction deletion cases based on FSEOF and OptKnock for HMF model. Red lines depict the FSEOF single deletions, green lines show FSEOF multiple deletions, blue lines are for OptKnock deletions and black lines are used to describe the reduced growth rate cases with OptKnock.

Figure 4.19 & 4.20 shows the production envelopes of growth rate vs ethanol production rate for the two models. The best option for the maximized ethanol production is obtained by the reduced growth rate simulations via OptKnock. In the control model, without any deletion, biomass generation is  $0.539 \text{ h}^{-1}$  and ethanol production is  $32.58 \text{ mmol gDW}^{-1}\text{h}^{-1}$ . The HMF model predicts the biomass generation as  $0.412 \text{ h}^{-1}$  and ethanol production as

28.43 mmol gDW<sup>-1</sup>h<sup>-1</sup>. In fact, HMF has a negative effect on both cell growth and ethanol production. In order to increase the ethanol production, the OptKnock algorithm by HMF model predicts the deletion of ALASm, CATp, FRTT, GTPCI, MDH, MDHm, MOHMT, PDHm, PPYRDC and THIORDXp catalyzed reactions when the growth rate is set to 0.4 h<sup>-1</sup>. Although this result is not as high as the result of control model, it shows the way ethanol production increase (Control model: 35.36 mmol gDW<sup>-1</sup>h<sup>-1</sup> and modified model: 33.34 mmol gDW<sup>-1</sup>h<sup>-1</sup>).

#### 4.2.7. Gene Deletions

Figure 4.21 and Figure 4.22 shows the single and double gene deletions of the control and modified IMM904 model. The optimal growth rate is determined via FBA and growth rate based on the single deletion is normalized to the optimal growth rate of the model (top). The redundant (black bars) and critical genes (red, yellow, green, purple, dark blue and brown bars) are identified for with and without HMF supplementation (control and modified models). When the modified model is considered (Figure 4.22), it is found that deletion of 12.4% of the genes are essential for the growth of the yeast cells (11.9% for control model- Figure 4.21), 4% of the genes are critical (8.7% for control model- Figure 4.21) and the rest is redundant. If one of the genes in the essential part is deleted, it will be fatal for this cell. Deletion of critical genes is not destructive but it affects the ability of growth and production of ethanol.

Redundant genes can be deleted because they do not have any impact on model. The percentage of genes with lethal deletion in the control model is slightly less than in the modified model. The reason for that might be that: since HMF has a harmful effect on the cell, more genes may have been involved in the model to counteract this effect and maintain cell viability. Moreover, the double gene deletions are also tested for both models (see the upper part of the figures). In both models, it can be seen that the brown color, that is, genes that are critical for deletion, predominate. YCR034W gene double deletion with most of the other genes is lethal for both of the models. This gene is fatty acid elongase and it is involved in sphingolipid biosynthesis. Additionally, modified model has more lethal double gene deletion cases than control model.

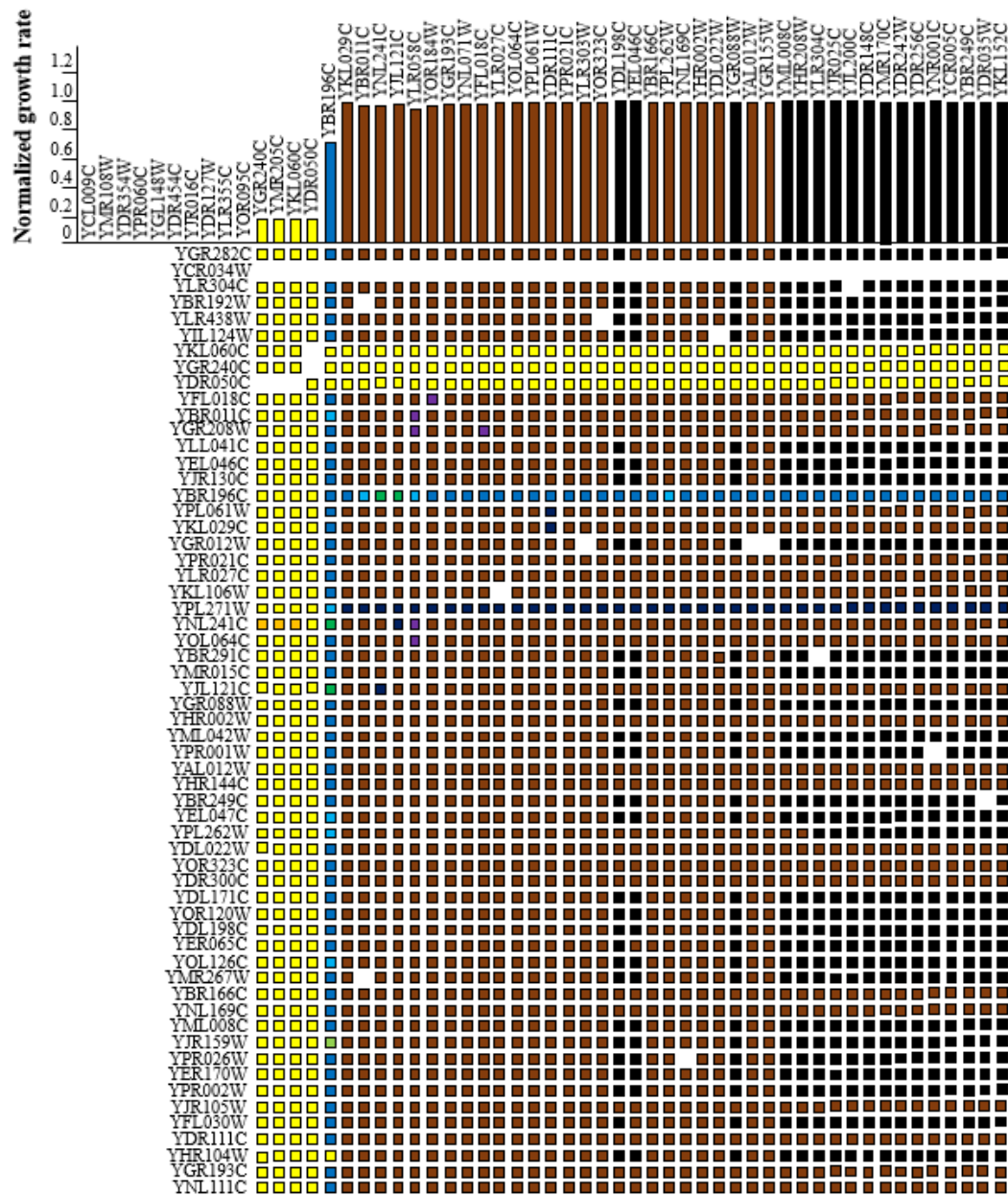


Figure 4.21. Single (top) and double (bottom) deletion of genes for control model.

### 4.3. Achievements

There are lots of metabolic networks in the literature reconstructed to study the target organism and biological science progresses by means of these reconstructions. Here, the genome scale metabolic model IMM904 is reconstructed specific to *S.cerevisiae* and control and modified models are created. Production of ethanol with biomass generation is the ultimate aim of this study under the supplementation of HMF. FBA, FVA, flexibility,

reaction classifications, flux coupling, regulation type, FSEOF and reaction/gene deletions are revealed and the results are compared for control and modified models.

When all the results are reviewed, it is seen that the ethanol production is less in the HMF model than in the control model.

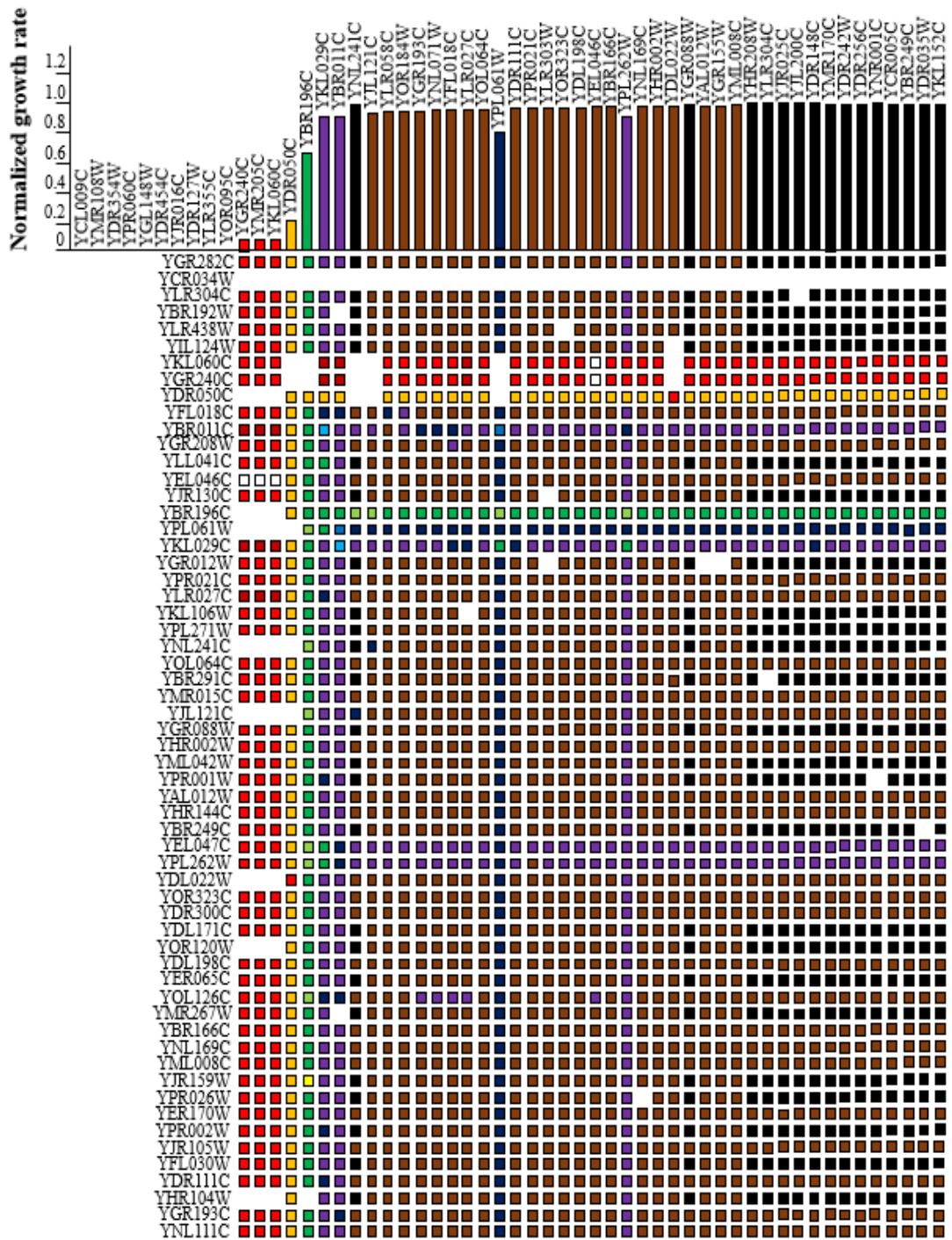


Figure 4.22. Single (top) and double (bottom) deletion of genes for modified model.

Accordingly, the destructive effect of HMF on the cell has been detailed by this study and the key points are deciphered through the estimation of internal flux distribution in the yeast metabolism. In order to develop a genetically defined ethanol overproduction, the strategies used by systems metabolic engineering of yeast can be as follows:

- The number of hard-coupled reactions should be increased to provide an overproduction of ethanol.
- The flux value of the reactions in the extracellular transport subsystem which has the highest flexibility in both of the models, should be increased.
- The flux value of the reactions in the subsystems that stand out according to the objective value of each model should be adjusted to increase ethanol production.
- The reactions/genes that emerged in FSEOF and OptKnock analyses should be deleted or enhanced to increase ethanol production and the results should be observed *in vivo*.

## 5. THERMOPLASTIC MICROFLUIDIC BIOREACTORS WITH INTEGRATED ELECTRODES TO STUDY TUMOR TREATING FIELDS ON YEAST CELLS

Tumor-treating fields (TTFields) are alternating electrical fields of intermediate frequency ( $\sim 100\text{-}500$  kHz) and low intensity ( $1\text{-}3$  V/cm) that are proposed as a cancer treatment modality (Wenger *et al.*, 2018). The mechanism of TTFields is to slow or inhibit tumor growth by disrupting mitosis division of the cancerous cells through the cell cycle proteins (Mun *et al.*, 2017, Zakhem *et al.*, 2006). Their effects may be on the misalignment of proteins with large dipole moments such as tubulin dimers and septin under the influence of electrical fields (Gera *et al.*, 2015), (Kirson *et al.*, 2004), (Kirson *et al.*, 2007). The hourglass shape of the dividing cell during telophase can cause highly non-uniform electrical fields inside the cell with higher field intensities close to the narrow furrow region (Wenger *et al.*, 2018). Such field inhomogeneity results in dielectrophoretic (DEP) forces (Pohl 1978) possibly leading to irregular aggregation of polarizable particles, thereby disrupting cell division (Kirson *et al.*, 2004), (Davies *et al.*, 2013). Studies point to the disruption of microtubule polymerization and preventing proper chromosome segregation during mitosis (Giladi *et al.*, 2015). Septin, which serves as scaffold for the actin myosin ring closing the cytokinetic furrow may fail to localize to the cell mid-zone under these electrical fields. This, in turn, may lead to ectopic blebbing during telophase and abnormal mitosis (Gera *et al.*, 2015). TTFields can also inhibit cell migration (Kim *et al.*, 2016) and DNA damage repair (Karanam *et al.*, 2017).

The promising results of TTFields have been demonstrated on glioblastoma multiforme (GBM), one of the most common and aggressive human brain cancer. They are applied on GBM patients and was found to prolong patient life (Mrugala *et al.*, 2014). TTField study is also conducted on lung cancer cells of mice and rabbit, and showed significant decrease in metastases (Kirson *et al.*, 2009a). Some researchers have combined chemotherapy (paclitaxel, doxorubicin, cyclophosphamide, dacarbazine, temozolomide) with the TTField treatment on GBM and have recorded positive results on patients. Chemotherapy at doses below the therapeutic threshold combined with TTField increased the regression of cancer as a result of cell cycle arrest (Kirson *et al.*, 2009b), (Mehta *et al.*, 2017), (Clark *et al.*, 2017), (Bender *et al.*, 2017).

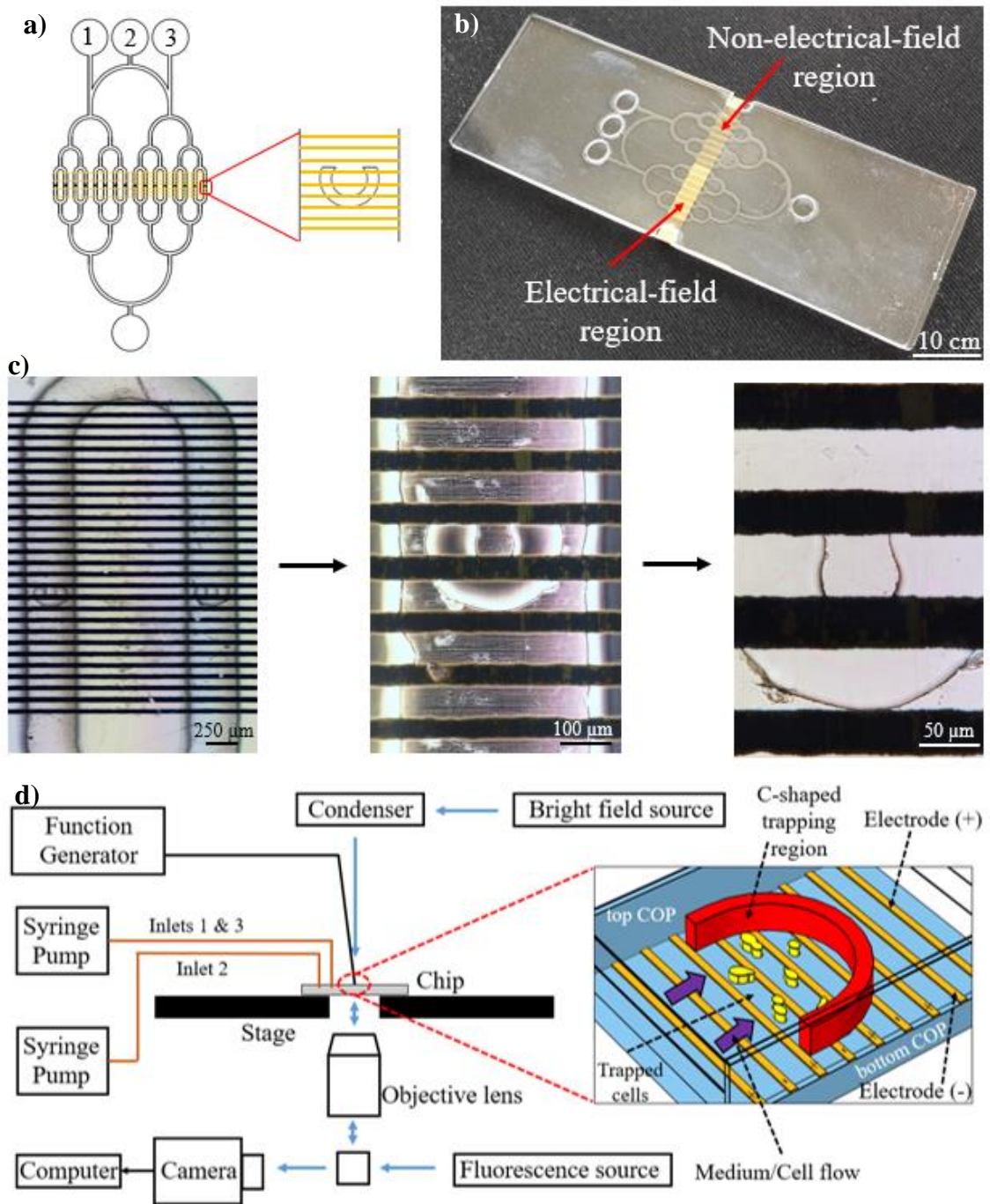


Figure 5.1. (a) Design of the microfluidic device with cell and nutrient inlets of 1, 2 and 3 (b) Fabricated device of COP (c) Electrode images within a chamber at 4X, 20X and 40X magnification (d) Experimental setup schematic.

Pemetrexed, cisplatin and paclitaxel drugs intended for lung cancer were administered along with TTFs and showed improvements in the prognosis of this disease (Pless *et al.*, 2013), (Giladi *et al.*, 2014a). Similarly, combined treatment was tested on pancreatic cancer

using gemcitabine, irinotecan, 5FU, paclitaxel and nab-paclitaxel, and the results suggested antimetabolic effect on cancer cells (Giladi *et al.*, 2014b), (Rivera *et al.*, 2019). Its application on ovarian cancer malignant pleural mesothelioma have been also classified as safe and effective (Vergote *et al.*, 2018), (Ceresoli *et al.*, 2019). The general conclusion of the application of TTFields with chemotherapy is that systemic toxicity does not increase and survival is prolonged.

TTField therapy is approved by the U.S. Food and Drug Administration for the treatment of GBM.<sup>1</sup> While TTFields are applied clinically on patients, they have been also studied in vitro using several preclinical laboratory research systems. These systems include application of sinusoidal voltages through wires with insulation of ethylene tetrafluoroethylene<sup>5</sup> and polyvinyl chloride (Kim *et al.*, 2016) with thicknesses of 0.125 mm and 0.17 mm, respectively. They are used with cell dishes, requiring high voltages (range 300-800 V). Electrodes are also insulated with very high dielectric constant ceramic ( $\epsilon_r > 5000$ ) to remedy the problem of high voltage usage. However, these materials ask for special design and manufacturing capabilities and cause heat generation, which require a refrigerated incubator (Porat *et al.*, 2017).

A PDMS microfluidic cell culture platform with embedded insulated electrodes is also reported for TTFields (Pavesi *et al.*, 2016). Electric field to the cells is applied through 100  $\mu\text{m}$  wide PDMS and 500  $\mu\text{m}$  wide cell culture medium. This PDMS device eliminates the disadvantages of classical culture dishes. It offers reduced usage of reagents, lower costs and the capability of observing cells in real time under electrical field, and thus better mimics the in vivo situation.

This microfluidic device shows that TTFields led to reduced proliferation of breast cancer cells, while leaving normal human endothelial cells largely unaffected (Pavesi *et al.*, 2016). However, because PDMS can absorb small drug molecules and may cause cross-contamination, precautions must be taken if these devices are used to test TTFields with chemotherapy treatment using different drugs. Their usage of insulated electrodes in the form of cured silver flake-PDMS mixture inside microfluidic channels also complicates the fabrication process. Furthermore, the results of microfluidic devices would be more decisive if they are capable of running multiple experiments (i.e. control group) at the same time on

the same chip. For these reasons, for the first time in this work, we engineered a thermoplastic microfluidic device with integrated electrodes to investigate the effects of TTFields on cells in a highly controlled microenvironment. Thermoplastic devices offer better surface properties and stability and could be commercialized more easily compared to their PDMS based counterparts (Gencturk *et al.*, 2017). Our fully saturated, highly stable and rigid cyclo olefin polymer (COP) microfluidic device (bioreactor) with Cr/Au electrodes allows two experiments at the same time under continuous flow. Thermal evaporation, lithography, hot embossing and thermo-compression bonding methods are used to produce these devices. These bioreactors allow single cell tracking under the fluorescence microscope with the help of C-shaped trapping regions.

We can monitor real time single cell behavior and see whether electroporation, morphological or mutational changes occur unlike the traditional studies with petri-dishes using flow cytometry to count the number of cells. This is a good example of a platform for in-depth cell cycle analysis under TTFields to identify parameters such as frequency and field strength that can be optimized to limit different types of cancer cell proliferation while minimizing detrimental effects to neighboring normal cells of various types present in tissues. Compared to previously reported insulated alternatives, the usage of uninsulated electrodes with small electrode gap of 50  $\mu\text{m}$  allows the generation of TTFields by applying very small voltages in the range of 30 mV.

## 5.1. Materials and Methods

### 5.1.1. Materials

*Saccharomyces cerevisiae* cells (EY0987 genetic background  $\text{Mat}\alpha$   $\text{his3}\Delta 1$   $\text{leu2}\Delta 0$   $\text{lys2}\Delta 0$   $\text{ura3}\Delta 0$  (S288C)) with RFP tagged Nop56 gene is kindly delivered by Peter Arvidson from Harvard University, HHMI. The COP substrates with Zeonor 10-0672-0349-1.0-05 product code and polyethylene tubing with BB31695-PE/p product code are purchased from Microfluidic ChipShop Company (Jena, Germany) and Scientific Commodities Inc. SCI (Lake Havasu City, AZ 86406, The USA), respectively. All the chemicals and reagents for medium preparation are purchased from Sigma-Aldrich (Taufkirchen, Germany).

### 5.1.2. Overview of the Microfluidic Device and Platform

Figure 5.1 shows the design, fabricated device and the experimental setup schematic of the system. In-house fabricated microfluidic device includes two individual sections, each having 8 chambers with C-shaped regions. These regions are placed along the channels to trap and hold the yeast cells sent to the device (Figure 5.1a). The design enables the cultivation of two different strains in one type of nutrient medium by sending corresponding strains through inlets 1 and 3 and the nutrient medium through inlet 2. The cultivation of one strain in two different nutrient media is also possible by sending the strain using inlet 2 and the two different nutrient media through inlet 1 and 3. Hence, there is no need to change the connections of the syringes to the inlet channels to introduce both cell cultures and nutrient flows, which can cause undesired contamination between channels and gas bubbles.

In this work, same strain type and same medium are used in the two different sections of the chip. Inlet 2 is used as dedicated line to introduce yeast cells to the two different sections of the chip. Same nutrient medium is supplied to both of these sections through inlets 1 and 3. However, the electrode design enables to perform two different experiments on the same chip at the same time. Electrodes are designed so that only one section of the device includes interdigitated electrodes with 50  $\mu\text{m}$  gap covering the whole 8 chambers in the C-trap regions of this section. The other section does not have any interdigitated electrodes. It only contains lines of the same electrode for routing purposes so that this electrode can reach the other section to form the interdigitated electrodes there (Figure 5.2). Because these lines are part of the same electrode and have the same electrical potential value, there cannot be any electrical field between these electrode lines. Therefore, the cells in the 8 chambers on this side do not experience any electrical field and are used as the control group. The electric field can be applied only to the cells in the 8 chambers on the other side of the chip. In this design, yeast cells can be kept in the C-shapes of the chambers, where electric field can be applied to each cell. Electrodes within the device on the C-shaped region is displayed in Figure 5.1c and every chamber within the device is considered as an independent microbioreactor, thus, each experiment is repeated for 8 times. Figure 5.1d shows the general schematic of the microfluidic platform. The fabricated device is placed on the stage of Nikon Ti-E inverted fluorescence microscope and tubings for nutrients and cell loading are connected to syringe pumps (New Era Pump Systems). Electric field within the

device is created by function generator (Agilent 33220A 20MHz Function/Arbitrary Waveform Generator) and data acquisition is handled with Nikon DS-Ri2 camera detector.

### 5.1.3. Device Fabrication

The microfluidic device is made using two COP (75.5 mm x 25.5 mm x 1 mm) substrates and is integrated with Cr/Au electrodes. The device design which meets the requirements of the experiments is drawn with AutoCAD. COMSOL Multiphysics 5.3a software is used to optimize the fluid dynamics within the device (Gencturk *et al.*, 2020). The design is transferred to a film photomask. Then, stainless steel mold is created by photolithography (with the mask) and electrochemical wet etching methods, respectively (Figure 5.2). The details can be found in previous sections.

A blank COP substrate is taken and inlet, outlet and electrode holes are drilled on it using a computer numerical control (CNC) machine. Burrs around holes are cleaned via ultrasonic bath. This is followed by a planarization step to obtain a smooth surface for proper bonding, which is needed because of the bumps formed around mechanically drilled regions. Hydraulic press machine with hot plates (Carver 3851 CE-0, USA) is set to 130 °C and 35 bar pressure is applied to the COP substrate with drilled holes between two glasses for 10 min. All the pieces are left for cooling to 60 °C under pressure (Figure 5.2).

After the planarization step, the mold (Figure 5.2) is used for hot-embossing of this COP substrate (Figure 5.2). The mold and the substrate are placed in the hydraulic press machine and 35 bar pressure is applied at 130 °C for 10 min. After 10 min, the system is left for cooling to 60 °C under pressure and hot-embossed piece is obtained. With this step, bottom substrate is ready for bonding. Another blank COP substrate is taken to form the top substrate for bonding. Chromium (10 nm thick) and gold (50 nm thick) layers are deposited on this substrate using a high vacuum thermal evaporator (Nanovak, Ankara/Turkey). Electrodes are patterned on metal layers using a photolithography step (Photoresist PR 1828 and developer solution MF-319) with the electrode mask of the design. Wet gold and chromium etchants are used to etch unmasked regions of the metals. Acetone, isopropyl alcohol and DIW are used to clean the photoresist, respectively and COP piece is dried via N<sub>2</sub> gun. This step forms interdigitated Cr/Au electrodes with 50 μm gap (Figure 5.2). This

is the only fabrication step applied on the top substrate before bonding. Fabrication of the microfluidic device is finished by thermo-compression bonding of the hot embossed bottom COP and electrode formed top COP substrates. The top substrate is flipped before bonding so that the electrodes are placed in-between the substrates, touching the microfluidic channels. These two substrates are put into the hydraulic press machine at 125 °C. A pressure of 25 bar is applied for 45 min (Figure 5.2). Cooling to room temperature finalizes the fabrication of the microfluidic device, shown in Figure 5.1b. The final height of the microfluidic channels are approximately 9  $\mu\text{m}$ , which is ideal to form monolayers of yeasts cells, which have sizes of around 5  $\mu\text{m}$ .

#### **5.1.4. Medium Preparation and System Operation**

For the impedance analysis part of this work, impedances of three different media that are commonly used in yeast cell research and DIW are characterized. YPD medium includes 20 g/L glucose, 10 g/L peptone and 20 g/L yeast extract. The medium for growth of Nop56:RFP tagged yeast cells includes 20 g/L glucose, 1.7 g/L yeast nitrogen base, 5 g/L ammonium sulfate, 0.1 g/L leucine, 0.02 g/L histidine, 0.03 g/L lysine and 0.02 g/L uracil. The medium for growth of Rpl5:GFP tagged yeast cells includes 20 g/L glucose, 1.7 g/L yeast nitrogen base, 5 g/L ammonium sulfate, 0.02 g/L histidine, 0.1 g/L leucine, 0.02 g/L methionine and 0.03 g/L lysine. Every medium (including DIW) is applied at a flow rate of 0.1  $\mu\text{L}/\text{min}$  via syringe pumps connected to all the inlets of the device. The electrodes are connected to the impedance analyzer (Keysight E4990A, USA). Each syringe with medium is connected to the same device one after the other, and fresh medium is flown for at least an hour before impedance measurements are made to eliminate any contamination from the previous medium. For the cell experiments, the devices are used without any treatment or internal coating of the channels after their fabrication. The tested yeast cells are non-adhesive, therefore, no cell stiction problem is experienced. Syringe pumps and function generator are connected to the microfluidic device on the microscope (Figure 5.1d). Syringe pump containing cells is connected to inlet 2 and the syringe pump of the medium is connected to the inlets 1 and 3. The nutrient medium is sent to the device at first. When the entire device is full of medium, the cells are introduced until they are seen between the electrodes in the C-shaped regions.

At this stage, the syringe pump carrying the cells is stopped without disconnecting it from its tubing. However, the medium continues to flow through the inlets 1 and 3. This way untrapped cells can be swept away and no new cell can come from the inlet side. After the cells are trapped and the medium flow is steady, the electric field is applied for 6 h (yeast cell proliferation time is 90 min), and the brightfield and fluorescence images are acquired at 15-20 min intervals up to the end of the experiments. One of the most important feature of the present microfluidic device is that it can endure long durations of experiments (more than 40 hours) without losing its mechanical integrity.

### 5.1.5. Impedance and Electrical Field Analysis

The impedance analysis is very crucial to find the magnitude of the applied electric field. Because there is no room for a reference electrode in between the interdigitated electrode gap, the magnitude of the applied electric field has to be calculated from the electrode-solution circuit model and the applied voltage signals. That is why a separate impedance analysis is done for the fabricated chips with the cell medium between the electrodes using the same conditions as the cell experiments. The circuit model used in this work can be seen on the right side of Figure 5.3, with two electrical double layer capacitances ( $C_{EDL}$ ) and the resistance of the bulk of the medium solution ( $R_{sol}$ ) all in series. This model is valid for non-faradaic electrochemical cell conditions, which is the case in the cell experiments. The voltage values applied to the gold electrodes are kept below 150 mV in the non-faradaic region, a safe level that would not cause any electrochemical reaction. Depending on the type of ions in the electrolyte, electrochemical reactions can start at different electrochemical cell potentials. The electrochemical window for DIW is 1.2 V (Shadmani *et al.*, 2019), (Sonmez *et al.*, 2018). The onset of faradaic conduction is reported to be around 0.9 V on platinum electrodes inside phosphate buffered saline solution (Jones *et al.*, 2015). Stimulation of neural cells with microelectrodes are done using voltage amplitudes of few hundred mV, i.e. 450 mV but not exceeding 1 V (Shadmani *et al.*, 2019). Impedance comprises of both real and imaginary values with the SI units of  $\Omega$  (Callegaro 2006). In the experiments for the impedance analysis, the frequency,  $f$ , of the excitation signal with a magnitude value of 10 mV and no DC value is swept from 20 Hz to 10 MHz. The measured impedance magnitude,  $|Z|$  ( $\Omega$ ) and phase,  $\theta$  ( $^\circ$ ) information of the electrodes in the microfluidic channel contacting the medium solution are recorded.

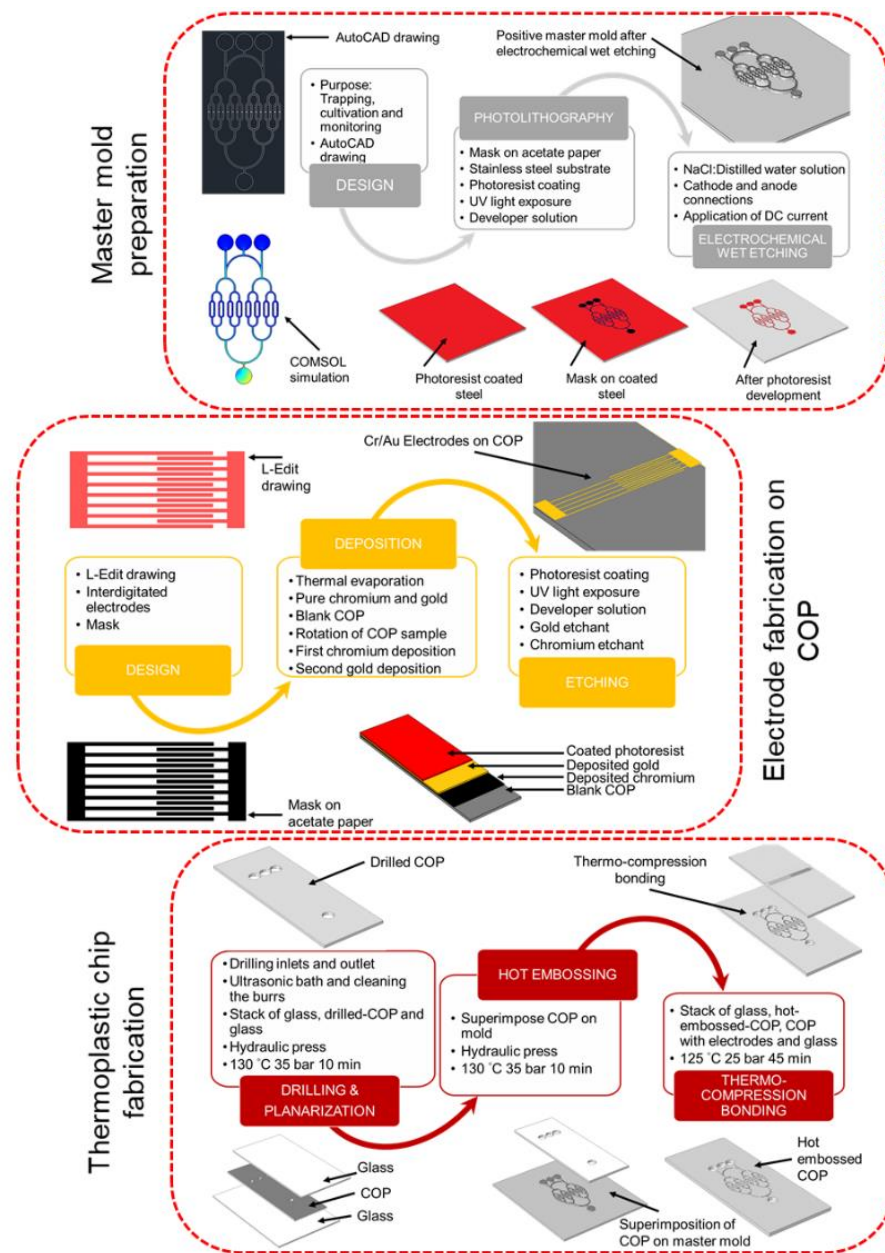


Figure 5.2. Chip fabrication steps.

The solution resistance ( $R_{sol}$ ) values for each nutrient medium are calculated from these data and the mentioned electrical equivalent circuit. During the cell experiments, the electrical field applied on the cells using a function generator are calculated knowing this  $R_{sol}$  value, circuit model and the applied voltage and frequency of the voltage signal. In the different experiments done with the same cell type and medium, sinewave voltage signals with peak to peak value,  $V_{peak\_to\_peak}$  of 150 mV and frequency of 150 kHz and  $V_{peak\_to\_peak}$  of 30 mV and frequency of 200 kHz are applied.

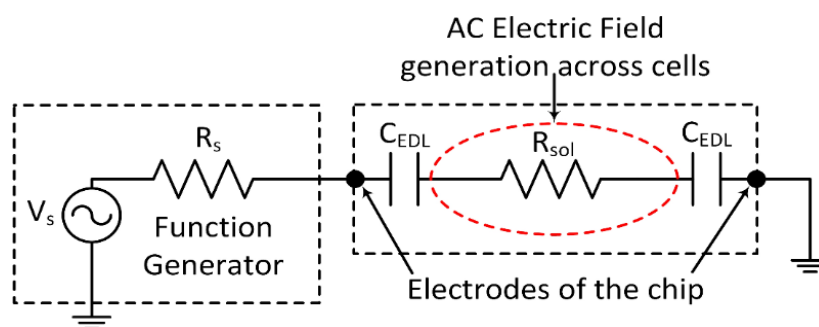


Figure 5.3. Electrical circuit model of the test setup used during cell experiments. CEDL is the electrical double layer capacitor formed between gold electrode and electrolyte.  $R_{sol}$  is the resistance of the bulk of the electrolyte solution. The voltage difference across this resistance forms the electric field the cells experience.  $R_s$  is the series resistance of the voltage source. It can also account for the series resistances of the ammeters used to measure the AC current flowing through the circuit.  $C_{sol}$  which models the capacitance of the bulk solution between electrodes is not shown for clarity purposes.

Every medium (including DIW) is sent through the microfluidic device at a flow rate of  $0.1 \mu\text{L}/\text{min}$ , because this is the flow rate used in the cell experiments during the nutrient feeding of the cells while electrical field is applied. Figure 5.4 shows the Nyquist plot of all media between 100 Hz and 300 kHz frequency at this flowrate. Every point in the Nyquist plot shows the real and imaginary part of the measured impedance for that specific frequency. The real and the imaginary values of the impedance is found from the magnitude and phase measurements of the impedance analyzer.  $\theta$  is converted to radian from degree (Equation (5.1)). The real and imaginary parts of the impedance are calculated according to Equation (5.2). Angular frequency ( $\omega$ ) is also obtained by Equation (5.3). Nyquist plots are shown here to get an insight on the real and imaginary values of the medium. However, bode plots of the impedance, which show the impedance magnitude and phase change with frequency, are more appropriate to extract the capacitance and resistance values of the electrical model shown in Figure 5.3. According to this electrical model of the electrochemical cell, the CEDL value dominates at low frequencies (depending on the conductivity of the solution, typically below 10 kHz). These capacitances get smaller and become almost short-circuit at higher frequencies. Hence, at frequencies of around 1 MHz, the impedance of the cell is formed by  $R_{sol}$  and capacitor due to the bulk of the solution

(C<sub>sol</sub>), which is parallel to this resistance (This capacitance is not shown in Figure 5.3 for clarity purposes).

$$\theta_{measured\_rad} = (\pi/180) * \theta_{measured\_deg} \quad (5.1)$$

$$Z_{measured\_real} = |Z|_{measured} \cos(\theta_{measured\_rad}) \quad \text{and} \quad Z_{measured\_ima} = |Z|_{measured} \sin(\theta_{measured\_rad}) \quad (5.2)$$

$$\omega = 2\pi f \quad (5.3)$$

$$R_{sol} = m_2 / m_1 \quad (5.4)$$

$$C_{sol} = m_1 / R_{sol} \quad (5.5)$$

Therefore, for intermediate frequency values from around 10 kHz to around MHz, but not larger than these, so that the solution capacitance does not get short-circuited, the real and imaginary plots of impedance vs. frequency can be used to extract R<sub>sol</sub> values. For these intermediate frequency values,  $\omega$  vs  $Z_{measured\_img} / Z_{measured\_real}$  data can be plotted. A trend line can be fit to this graph with a slope of m<sub>1</sub>. Similarly,  $\omega$  vs  $Z_{measured\_img}(1+\omega^2 m_1^2)$  can be plotted and new slope, m<sup>2</sup> can be found. Lastly, R<sub>sol</sub> and C<sub>sol</sub> can be calculated (Equation (5.4) and Equation (5.5)). After calculating the solution resistance, the electrical field applied on the cells during cell experiments can be determined. This can be done using the equivalent circuit model shown in Figure 5.3, which points to a simple voltage division due to complex impedances.

Here, the impedance of the bulk solution capacitor, C<sub>sol</sub>, is ignored because for the working frequencies of the cell experiments, in the range of a couple hundred kHz, its impedance contribution can be ignored. The measured impedance values tell us the overall impedance of the electrochemical cell and the solution resistance value is calculated using these parameters. Furthermore, the magnitude and frequency of the applied voltage signal are known. The cells experience electrical field only due to the voltage drop across the solution resistance. Therefore, we need to find the voltage drop across the solution resistance, but not concerned with the voltage drops across the internal resistance of the signal generator and the C<sub>EDLS</sub>. This can be done using the following voltage division equations for complex impedances. Where Z<sub>measured</sub> is the complex impedance for the

frequency used in the experiment, measured using the impedance analyzer as explained in the methods section, and marked in Figure 5.4.

$$|\Delta V_{app}| = \frac{V_{peak} R_{sol}}{|Z_{measured} + R_s|} = \frac{V_{peak} R_{sol}}{\sqrt{(Z_{measured\_real} + 150)^2 + Z_{measured\_ima}^2}} \quad (5.6)$$

## 5.2. Results and Discussion

This study is the first attempt towards the usage of uninsulated electrodes with small electrode gap of 50  $\mu\text{m}$  for the generation of TTFields by applying very small voltages in the range of 30 mV. The voltage values applied between gold electrodes of the chips are kept below 150 mV in the non-faradaic region so that no electrochemical reaction i.e. electron exchange at the electrode surface and the release of electrochemical reaction byproducts into the medium, can occur between the gold electrodes and the solution.

The validity of the non-faradaic electrical circuit model and the calculated magnitude of the electrical field the cells experience are also confirmed here as explained below. Cell experiments are conducted after impedance measurements and their analyses are accomplished for deionized water (DIW) and three different cell nutrient media in the microfluidic device. 150 mV and 150 kHz voltage signal is applied across the electrodes to generate 6.58 V/cm electrical field magnitude across the cells with the intention of causing electroporation. Furthermore, 30 mV and 200 kHz signal is applied to generate 1.33 V/cm electrical field magnitude to find the effects of TTFields on the cells. Electroporation does not solely depend on electric field strength but also on the number and duration of applied voltage pulses. Similar electroporation results can be obtained by using equivalent pulse parameters.

Typically, a single or dozen pulses of  $\mu\text{s}$  durations are used in the orders of thousand V/cm electric field magnitudes for electroporation. Similar results can be achieved using ms or s pulse durations with electric field magnitudes of hundreds and tens of V/cm, respectively. Derived models can be used to find equivalent pulse parameters for the intended electric field magnitude to cause electroporation (Pucihar *et al.*, 2011).

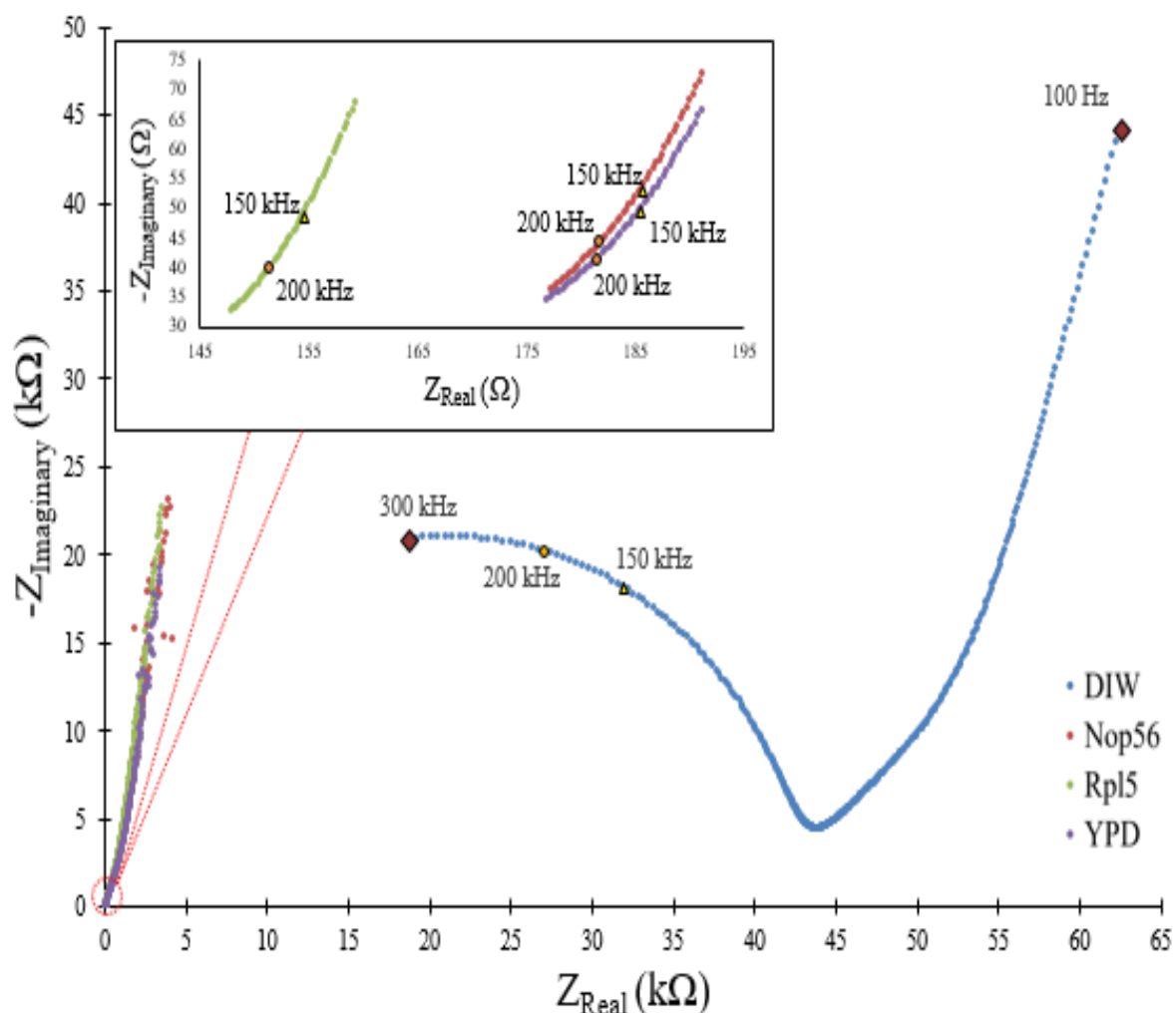


Figure 5.4. Nyquist plots of DIW, Nop56, Rpl5 and YPD media for 0.1  $\mu\text{L}/\text{min}$  flow rate. Real and imaginary impedance values is marked for the used frequencies of 150 and 200 kHz in the cell experiments.

### 5.2.1. Impedance Analysis and Electrical Field Calculations

Nyquist graphs are compact forms to show the complex impedance values of the electrochemical cells. This format is chosen to show the differences between different media and to be able to pick the real and imaginary values of the impedances to be used in the electrical field calculations. As expected, the impedance of the nutrient media is much lower than DIW (Figure 5.4). As the ions of the salt and amino acid in the medium are introduced into the water, the conductivity of the solution increases. Smaller differences among feeding media are also noticeable in the inset of Figure 5.4. Although the YPD medium and the

nutrient medium for Nop56:RFP tagged cells have very similar conductivity values, the medium for Rpl5:GFP tagged cells is more conductive than these. The only difference between these growth media for Rpl5 and Nop56 tagged cells is the existence of methionine in one and uracil in the other. Addition of methionine increases the conductivity of the solution. In Figure 5.4, the imaginary and real values of the measured impedances for different media are marked for 150 and 200 kHz frequencies because these frequencies are used in the cell experiments and their values are needed in the calculation of the applied electrical field magnitude.

$$|E_{app}| = \frac{|\Delta V_{app}|}{d} \quad (5.7)$$

$R_s$  is the internal resistance of the function generator, which is equal to 50  $\Omega$ . Since during the experiments we also monitored the flowing AC current using a precise multimeter (U1252B, Keysight Technologies, USA) in series, it also adds 100  $\Omega$  value to this series resistance. That is why 150  $\Omega$  is inserted in (Equation (5.6)). The real and imaginary values of  $Z_{measured}$  are found according to the corresponding frequency. For the first experiment ( $V = 150$  mV,  $f = 150$  kHz),  $Z_{measured\_real}$  is 185.73  $\Omega$  and  $Z_{measured\_ima}$  is 53.08  $\Omega$ , whereas for the other experiment ( $V = 30$  mV,  $f = 200$  kHz)  $Z_{measured\_real}$  is 181.90  $\Omega$  and  $Z_{measured\_ima}$  is 43.86  $\Omega$ .  $\Delta V_{applied}$  across the solution resistance is found from (Equation (5.6)). Once this value is divided by the gap,  $d$ , between the electrodes, the magnitude of the applied electrical field,  $E_{applied}$  is calculated by Equation (5.7). Since there is a lack in the literature on the electrochemical characterization of cell growth media, we tested 3 different nutrient media.

The impedance differences between the growth media are calculated and found to be close to each other. Since RFP:Nop56 tagged yeasts are used in the cell experiments, the calculations for only that medium are considered below. After cell loading, the nutrient feeding rate is set to 0.1  $\mu\text{L}/\text{min}$  and the solution resistance of the medium for Nop56 :RFP cells at this rate is found as 149.26  $\Omega$ . These results reveal that, for the high voltage experiment at 150 mV and 150 kHz, the magnitude of the applied electrical field is 6.58 V/cm and for the low voltage experiment (30 mV and 200KHz), it is 1.33 V/cm. In the above analysis, it is assumed that the electrical field is uniform in the cell trapping region between planar electrodes. This is confirmed by making 3D electrical field simulations in COMSOL that includes the effect of c-shape, even though simulation results point to high non-uniform

electrical fields in the 10  $\mu\text{m}$  vicinity of interdigitated planar electrodes. Our simple approximation predicts an average electrical field magnitude of 1.33 V/cm (6.7 mV / 50  $\mu\text{m}$ ) for the applied 30 mV peak to peak voltage. 3D COMSOL simulations reveal 1.1 to 0.9 V/cm magnitude change in one axial direction of 30  $\mu\text{m}$  length and 1.06 to 1.12 V/cm change in the orthogonal direction of 70  $\mu\text{m}$  length in the central cell trapping region of the microfluidic channel. Even though, at the edge of the electrode the electrical field can reach maximum peak value of 5.2 V/cm, this drops to 1.12 V/cm by moving 10  $\mu\text{m}$  away from the electrode edge. That results in a cell trapping region with only 21% change in the field uniformity. The results also reveal that (Equation (5.7)) overestimates the electrical field magnitude in the trapping region by 19%.

### 5.2.2. Electrical Field Effect on Yeast Cells

This section summarizes the results of the cell experiments. The control experiments (cells not-electrical-field treated) show regular proliferation of the cells as expected. In the experiment, where high electrical field of 6.58 V/cm is used, the electroporation of the cell membranes occurs, destroying the cells. Proper application of the TTFields with the electrical field magnitude of 1.33 V/cm causes a prolongation of the mitosis phase. The results are explained in three different categories which are control, high voltage treated cell and low voltage treated cell experiments. The details are as follows.

5.2.2.1. Cells Not Treated by Electrical-field Figure 5.5a and Figure 5.6a show the control cell (not-electrical-field treated) results of the experiments. A continuous increase in cell number and size is observed throughout the experiment as evident from cell count and perimeter of the cells plotted in Figure 5.5a. Morphological changes of the cells are also examined on single cell basis, and their increase in the dimension are noticeable on the right side of Figure 5.6a. These results are in accordance with the proliferation of healthy yeast cells. If a single cell is followed (Figure 5.6a-right), its perimeter increases at the beginning and then suddenly drops to almost its half due to cell division and then both mother's and daughter's perimeters again monotonically increase. The daughter can also generate another daughter (second generation), so and so forth. The left side of Figure 5.6a shows the whole fluorescence intensity generated by the cells. As usual with these type of yeast cells, there is a decline in their fluorescence intensity at the beginning because, when cells enter the new

confined microaerated environment, they are affected and their fluorescence intensity are slightly reduced. However, after a while, as the cells adopt to their environment, an increase in the fluorescence intensity is observed with cell proliferation. The time-lapse microphotographs for the control cells in Figure 5.7 also show typical cell proliferation of the yeast cells.

5.2.2.2. High Voltage Treated Cells: Electroporation. The cell experiments are conducted using fabricated microfluidic devices under the application of 150 mV and 150 kHz voltage signal. Figure 5.5b shows the results of the yeast cell experiment under the generated electrical field magnitude of 6.58 V/cm. The results point to no cell proliferation and the occurrence of electroporation of their membranes as observed by real time monitoring of the individual cells (Figure 5.7b). Although the cell perimeter increases in the first 150 min, their dimensions do not change from that point onwards (Figure 5.5b-right). The cell count is also constant throughout the experiment, which means no division occurred (Figure 5.5b-left). This is also obvious from the perimeter results of the single cells (Figure 5.6b-right). The perimeters of single cells increases in the first 150 min., then they stay in that size without dividing. There is a continuous decline in the fluorescence intensity of these cells (Figure 5.6b-left). Compared to the control cells, the fluorescence intensity never recovers. The main reason is that the cells undergo electroporation. Electroporation leads to cell death with concomitant decrease in the luminescence of the cells. The morphological changes of the single cells due to electroporation are obvious in the time-lapse microphotographs in Figure 5.7.

Electrical field has effects on cell physiology directly by intracellular disorganization, DNA and RNA impairment and inactivation of enzymes. Due to the polarization of cells, electromechanical compression on cell membrane occurs and permeabilization increases. Moreover, increasing membrane potential causes a decrease in membrane thickness. When the critical breakdown voltage is exceeded, the disruption of the cell wall occurs. Consequently, an exchange between intracellular and extracellular macromolecules become possible (Suga *et al.*, 2006), (Guyot *et al.*, 2007), (Longsine-Parker *et al.*, 2013), (Geng and Lu, 2013), (Ou *et al.*, 2017). This phenomena is known as electroporation and seen in the middle row of Figure 5.7. While the control cells continue their normal life cycle, the electroporation detected in the cells under the high electrical field leads to cell death. Smooth

envelop and round border is noticeable on the untreated cells but, blurring is observed in the cells undergoing electroporation. The blurring of images and flattened yeast border with destruction of cell membrane structure was reported in literature (Huang *et al.*, 2013c).

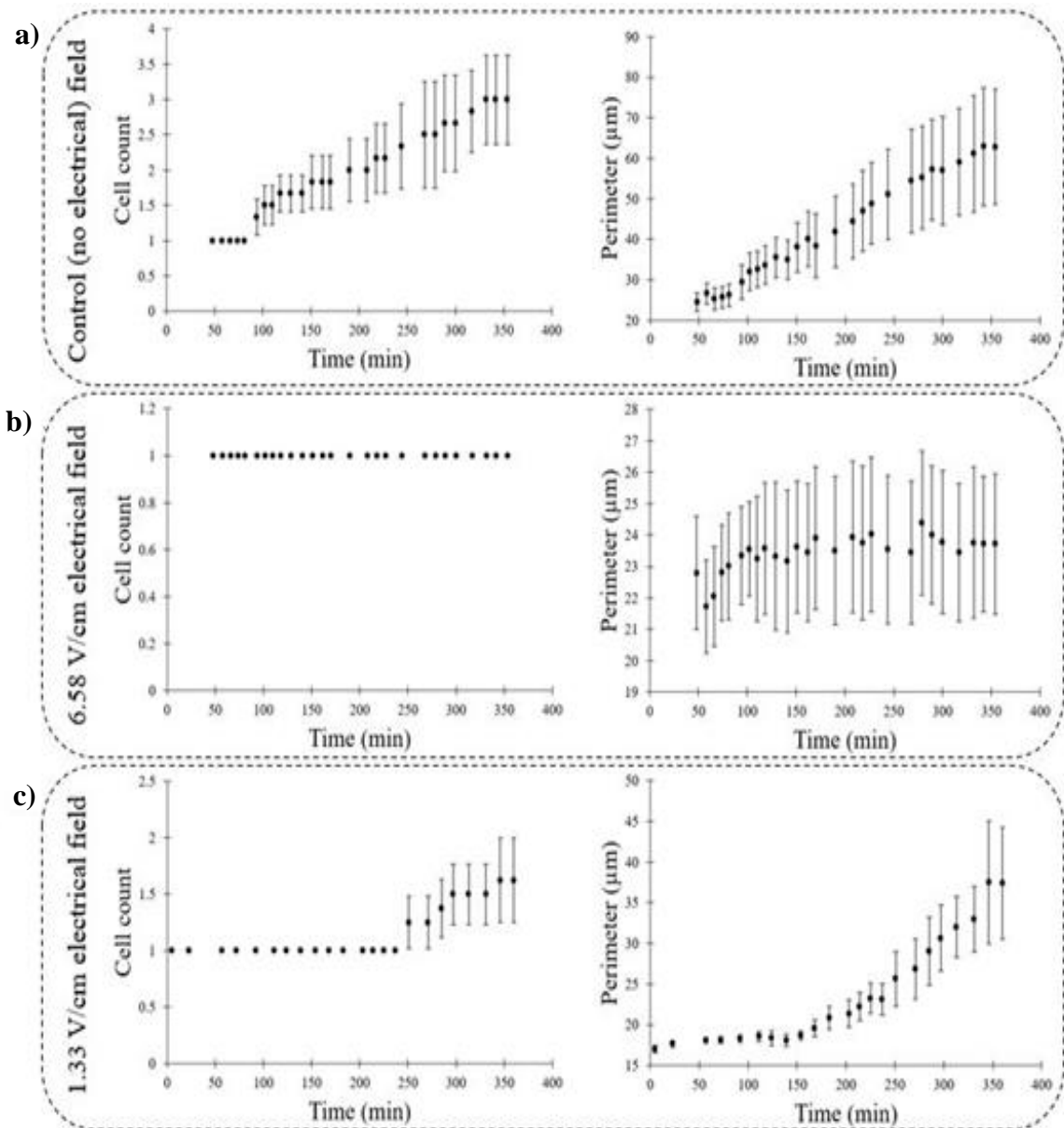


Figure 5.5. Cell count and cell perimeter-time profiles of (a) not-electrical-field treated cells as control group showing regular proliferation with increasing number and perimeter (b) 6.58 V/cm electrical-field treated cells showing absence of proliferation with no cell count increase, electroporation happens and cell perimeter increases only in the first 150 min, and (c) 1.33 V/cm electrical-field treated cells showing delayed proliferation with constant cell size and cell count in the first 150 min and 250 min, respectively.

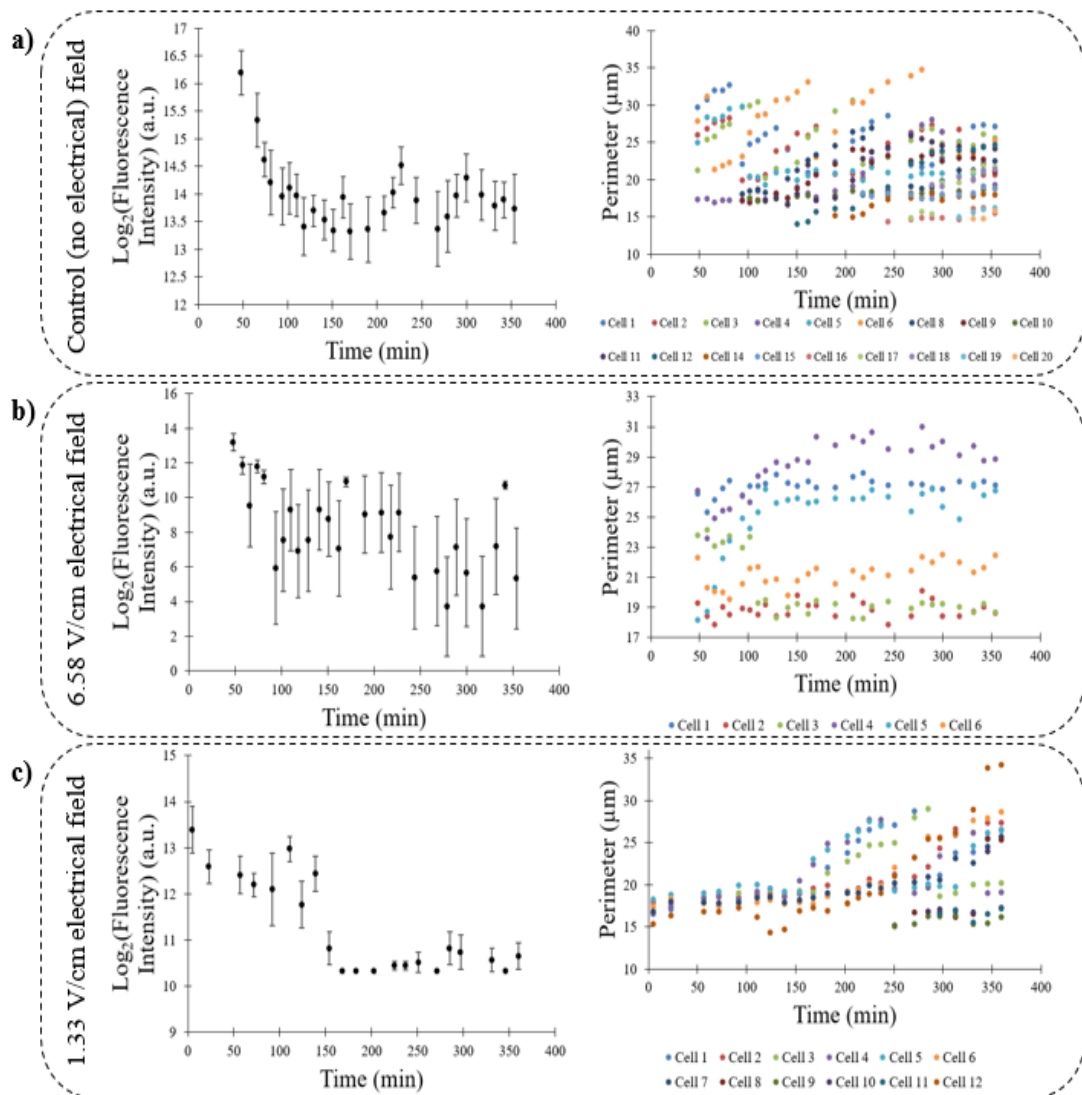


Figure 5.6. Fluorescence intensity and single cell perimeter-time profiles of (a) not-electrical-field treated cells showing regular proliferation. Decline in the fluorescence intensity at the beginning is due to shock of a new confined microaerated environment. With adaptation to the environment, increase in the fluorescence intensity starts. Perimeter profiles show the increase in the perimeter of single cell with time, then suddenly drops to almost its half due to cell division and then both mother's and daughter's perimeters again monotonically increase (b) 6.58 V/cm electrical-field treated cells showing the absence of proliferation. The perimeters of single cells increase in the first 150 min, then stay constant without dividing. Continuous decline in the fluorescence intensity points to the cell death, and (c) 1.33 V/cm electrical-field treated cells showing dimensional changes of the individual cells with delayed budding time and delayed increase in the fluorescence intensity as evidence of maintained Nop56 protein functionality.

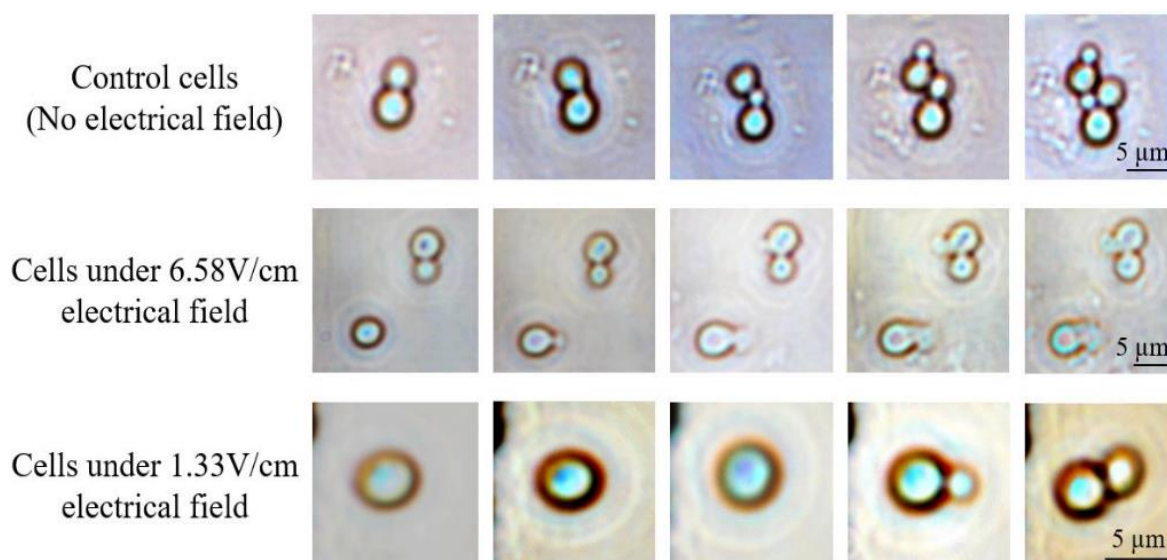


Figure 5.7. Time-lapse microphotographs of yeast cells experiments. Cells in the control group show regular increase in number and perimeter. Cells treated with 6.58 V/cm electrical-field show blurring borders with time as evidence of undergoing electroporation. Cells treated with 1.33 V/cm electrical-field stays almost the same at the beginning of the experiments then show delayed mitosis division.

5.2.2.3. Low Voltage Treated Cells: Prolongation of Mitosis. Low electric field (1.33 V/cm), which is at the right range of TTFields, is applied to the yeast cells in microfluidic device. In contrast to the high voltage experiment, a delayed cell proliferation is observed. The cell size and cell count stay constant in the first 150 min and 250 min, respectively, and then they start to increase (Figure 5.5c). The single cell monitoring also confirm this delayed cell division and cell size increase (Figure 5.6c-right). The dimensional changes of the individual cells can be clearly seen by continuous real time imaging and the budding time of the daughter cells can be noticed. The differences in the cell proliferation between the electrical field treated and control cells are obvious, when Figure 5.5a and Figure 5.6a are compared to Figure 5.5c and Figure 5.6c, respectively. There is an initial decline in the fluorescence intensity of the cells, but it remains almost constant in the first 150 min (Figure 5.6c- left). A slight increase in the fluorescence intensity is noticed after this point onwards, as the cells start to proliferate, and Nop56 protein maintains its function. The most important feature of this experiment is the prolongation of mitosis division time with the effect of the electrical field. While the average proliferation time of yeast cells is 80-90 min, the proliferation time of yeast cells under the electrical field of 1.33 V/cm increases up to 200-300 min. Figure 5.7

also proves this delayed proliferation. A misalignment of the internal molecules, such as microtubules, during mitosis is likely to occur due to the application of the electrical field. Thus, the mitotic process is disrupted and this results in an anti-proliferative effect on cells as reported in literature (Castellví *et al.*, 2015). In our experiment, the mitosis initiated normally but it took a longer time to complete. This is the outcome of the deceleration in mitosis under the electrical field stimulation (Kirson *et al.*, 2004), (Giladi *et al.*, 2015), (Pavesi *et al.*, 2016), (Liang *et al.*, 2013).

### **5.2.3. Highlights (Pros and Cons) of Thermoplastic Materials for Batch Fabrication of Microdevices**

Thermoplastic materials can be mass-produced. Most of them are optically transparent and biocompatible such as polystyrene and poly(methyl methacrylate). Since fluorescence tagged yeast cells are used in our experiments, a thermoplastic material with low auto-fluorescence is needed in our experiments and COP served this purpose. COP material has high moisture barrier and this is favorable when working with cell cultures. As a result, cells consume more oxygen from water, instead of its absorption through the surface of COP (McCann *et al.*, 2015). It is also chemically inert. The most commonly used material for developing microfluidic devices in research laboratories is PDMS, despite its several disadvantages. PDMS has high gas permeability and porous body that can absorb molecules, which may cause contamination within the microfluidic devices. Furthermore, attention must be paid to cure PDMS structures properly, otherwise uncured polymer chains can leach into solutions. Thermoplastics may also have disadvantages such as limited operation temperature. While low melting temperature points of thermoplastics can be disadvantageous for certain applications, it is an advantage for bonding. The process step of bonding is the most difficult part in our fabrication due to non-uniformity formed by the deposited Cr/Au electrodes on the COP substrate. The thermo-compression bonding parameters were precisely optimized and leak-free microfluidic bioreactors were achieved. Another limitation of thermoplastic substrates is the problem of openings access holes for reservoirs and electrode contacts. These holes are formed only at the edges of the substrates not to disrupt the uniformity of the substrates, which is very critical for bonding. This puts limitations to electrode routing. Furthermore, pure thermoplastics are expensive and hard to find in microscopy slide format. Despite the above mentioned limitations, thermoplastics

can enable batch fabrication of reproducible and reliable microfluidic devices. They offer a versatile platform for combined chemotherapy and TTField treatments on tumor cells.

### 5.3. Conclusion

In the present study, the integration of microfluidic device (bioreactor) and electrical field was aimed and the effect of the electrical field magnitude on yeast cells was observed. The microfluidic device was fabricated with 16 bioreactors in parallel. Half of these bioreactors did not have electrical field application and were used in control experiments. Hot embossing, photolithography and thermo-compression bonding methods were used to produce COP made thermoplastic microfluidic device including Cr/Au electrodes in interdigitated form. The impedance measurements of four different cell nutrient media was accomplished at 0.1  $\mu\text{L}/\text{min}$  flowrate. Electrochemical impedances of the bioreactors were evaluated by taking electrical double layer capacitances and solution resistance into consideration. 150 mV and 150 kHz corresponding to 6.58 V/cm, and 30 mV and 200 kHz corresponding to 1.33 V/cm electrical fields were applied on yeast cells. In the experiment with intentional high electrical field application, the cells underwent electroporation, while in the other experiment with the right intensity range of TTFields, the cells had prolonged mitosis. Further usage of this microfluidic platform can reveal optimal frequency and field strengths of different cell types under TTFields to selectively target the intended hazardous cells while minimizing their effect on healthy cells present in tissues. TTFields are expected to offer benefits for localized cancer types, having potential in extending patients' life and survival rate. Thus, as a promising anticancer treatment approach, they continue to be of scientific interest. Our microfluidic bioreactors integrated with uninsulated electrodes having very small gaps allow the application of very small voltages in the range of 30 mV. They provide a new, versatile and durable platform for in vitro cell studies towards the improvement of anti-cancer therapies including personalized treatment.

## 6. MAMMALIAN CELL EXPERIMENTS USING TWO PHASE MICROFLUIDIC DEVICES

Due to high potential of applications, microfluidic technology has taken its place in many fields including chemical synthesis and biological analysis to optics and information technology. Fabrication of microfluidic device and its usage has an increasing trend since its beginning and there are many forms of these devices on the literature such as drug delivery (deMello 2006), point of care diagnostic chips, organic synthesis and micro reactors (El-ali *et al.*, 2006), (Weibel and Whitesides, 2006) and (Dittrich *et al.*, 2006). Microfluidic devices are used to manipulate the liquids at small length scales. Low cost, short times for analysis, small volume of samples or reagents, ease of separation and detection with high resolution and sensitivity are the significant features of microfluidic devices. The most fundamental difference of microfluidic chips is based on its flow dynamics. Microfluidic systems that contain miscible liquids and operate in a single phase are called continuous flow, while two-phase systems that include immiscible fluids are defined as droplet-based (Sohrabi and Moraveji, 2020). In this part, droplet-based microfluidic devices will be analyzed and discussed.

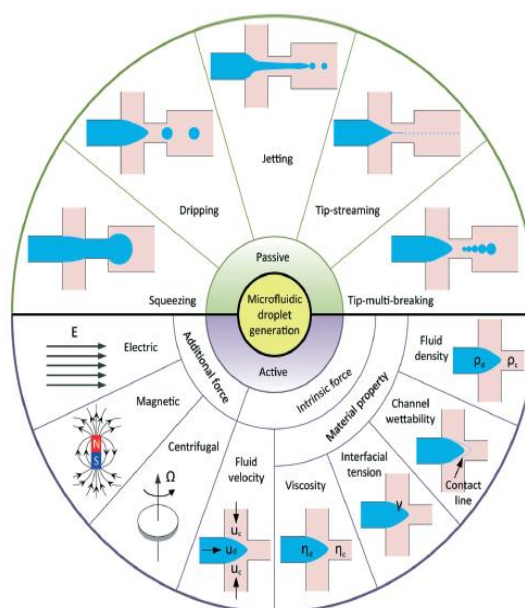


Figure 6.1. Schematic of droplet generation in passive and active techniques (Zhu, and Wang, 2017).

At macroscopic length scales, droplet formation is a well-known phenomenon for years. The relative effect of viscous forces versus surface tension manages the breakup and droplet formation. However, at microscopic length scales, significant factor is confinement (Garstecki *et al.*, 2006), (Abate *et al.*, 2012) and capillary number must be recognized (Mulligan and Rothstein, 2011). Generation and stabilization of droplets within the microfluidic devices are governed mainly by interfacial and surface tension forces (Mashagi *et al.*, 2016). Active and passive techniques are the two methods of droplet formation. In the active method, it is necessary to interfere with the device from the outside, while in the passive method, the internal dynamics of the system are used. Application of external energy input can be performed via electrical, magnetic or centrifugal controls in active method. Squeezing, dripping or jetting are the modes of passive techniques (Figure 6.1). In this study, passive method is used to generate the droplets including THP-1 mammalian cells (Zhu and Wang, 2017).

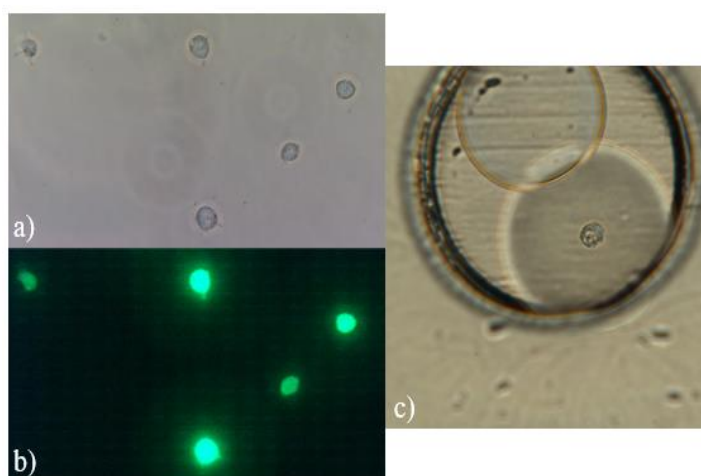


Figure 6.2. THP-1 cells (a) Brightfield microscopy images of THP-1 cells (b) Fluorescence microscopy images of THP-1 cells (c) THP-1 cells confined in a droplet.

Tsuchiya and her/his coworkers discovered the THP-1 cells (Figure 6.2a) from a boy suffering of acute monocytic leukemia. These cells are similar to human monocyte cells containing the features of morphology, secretory products, oncogene expression, expression of membrane antigens and expression of genes involved in lipid metabolism. Since THP-1 cell has the ability to have a homogeneous population, biochemical studies can be done more easily.

Thus this cell line is more advantageous than native monocytes (Auwerx 1991). With the help of the lipopolysaccharides stimulation, inflammation process is activated by the specialized regulatory proteins within the THP-1 cells. Research on the inflammation signaling pathways accelerated the exploration of targets for drugs discovery (Al-nasser *et al.*, 2021). Moreover, in vitro cancer, monocyte macrophage differentiation and macrophage related physiological process studies can be conducted by using THP-1 cells (Auwerx 1991), (Chao *et al.*, 2018), (Wang *et al.*, 2018). The average doubling time is 19 to 50 hours. In this study, THP-1 cells with the ASC gene labeled with green fluorescence were used (Figure 6.2b).

Here, THP-1 cells were confined within the droplets (Figure 6.2c) with several drugs/inhibitors such as temsirolimus, rifabutin and BAY 11-7082. Droplet generation and storage chips (made of thermoplastics) were purchased from ChipShop company. Aqueous phase contains cell or drug in nutrient medium and organic phase includes oil solutions, and both phases were sent through the device. The ultimate aim is to examine the response of cells to drugs/inhibitors deciphering the link between apoptosis and lifespan.

## 6.1. Materials and Methods

### 6.1.1. Materials

THP-1 cells with GFP tagged ASC gene is kindly provided by Prof. Nesrin Özören from the Molecular Biology and Genetics Department of Boğaziçi University. The COP made microfluidic devices with the type of droplet generation and storage (115  $\mu\text{m}$  x 115  $\mu\text{m}$ :d x w) (Product code: Fluidic 719), fluidic interfaces with the type of mini luer and tubings are purchased from Microfluidic ChipShop Company (Jena, Germany).

Temsirolimus and rifabutin are kindly delivered by Pfizer. BAY 11-7082 is bought from Sigma-Aldrich (Taufkirchen, Germany). Novec 7500 and Krytox 157 FSH were purchased from 3M and DuPont, respectively. Necessary chemicals (RPMI 1640, fetal bovine serum (FBS), MEM Non-Essential Aminoacid solution 100X (MEM-Nea), penicillin-streptomycin 100X (Pen/Strep) for medium preparation were acquired from ThermoFisher Scientific.

## **6.1.2. THP-1 Cell Culture Preparation**

6.1.2.1. Sterilization. Before THP-1 cell culturing, clean environment is needed to prevent the contamination. Laminar flow hood is first cleaned with technical grade ethanol (70%) and then UV for 15 min. Shelves inside the CO<sub>2</sub> incubator are washed with distilled water and wiped with technical grade ethanol. The incubator with shelves is cleaned with UV for 15 min. All the equipment required for culturing including schott bottle, beaker and tips are autoclaved at 121 °C for 15 min. Water inside the water bath is changed with cleaned water and centrifuge is wiped with technical grade ethanol.

6.1.2.2. Preparation of RPMI Complete Medium. Before preparation of RPMI complete medium, FBS, MEM-Nea and Pen/Strep are aliquoted. Aliquoting plays significant role in the temperature sensitivity of chemicals. FBS, MEM-Nea and Pen/Strep are sensitive to temperature changes and they can easily deteriorate. This might affect the potency or strength of the complete medium and reduce its effectiveness. Thus, FBS of 50ml, Mem-Nea of 5.5ml and Pen/Strep of 5.5ml are prepared. FBS and Pen/Strep should be stored at -20 °C and Mem-Nea should be stored at +4 °C. Complete RPMI medium contains 10% of FBS (50 ml), 1% of Mem-Nea (5.5 ml) and 1% Pen/Strep (5.5 ml). This complete medium can be used for THP-1 cell culturing and the excess amount of medium can be stored at +4 °C.

6.1.2.3. Preparation of Inoculum. CO<sub>2</sub> incubator is operated at 37 °C and 5% CO<sub>2</sub> settings. In order to arrange the humidity within the device, distilled water should be placed. The temperature of water bath is set to 37 °C and centrifuge is powered on. Frozen THP-1 stock is thawed at 37 °C in the water bath and cells were precipitated by rapid centrifugation at 2000 rpm for 2 min. Waste liquid remaining above the cells is removed with a pipette and RPMI complete medium with 20% FBS is added to wash the cells. In order for the cells to be thoroughly washed, the cell-medium mixture is pipetted and delivered. The medium-cell mixture is again centrifuged at 2000 rpm for 2 min and the waste liquid is removed via pipette. If 1 ml of cells has been melted, 2 times the volume of medium should be used to passage cells. In order to grow the cell taken from the frozen stock, RPMI complete medium must contain 20% FBS.

2 ml of RPMI complete medium with 20% FBS is put on the centrifuged cells and mixed thoroughly. 13-14 ml of RPMI complete medium with 20% FBS is placed in the 15 cm petri dishes and cells are cultured. Petri dishes in which cells are seeded are placed in the humidified CO<sub>2</sub> incubator after shaking gently in the form of a plus. THP-1 cells within the incubator left for culturing for 2 days. On the third day, after the proliferation of the cells, they are transferred to the falcon tube and precipitated by centrifugation at 2000 rpm for 2 min. Waste medium above the cells within the falcon tube are discarded and then fresh RPMI complete medium with 15% FBS is put into the tube. Cells are washed with fresh medium and again centrifuged. 15% FBS containing RPMI complete medium is put into the falcon tube for the second time and 13-14 ml of complete medium (with 15% FBS) is placed into the petri dishes. The cells are seeded and petri dishes are placed into the humidified incubator. On the third day, the procedure previously mentioned is repeated, this time with RPMI complete medium containing 10% FBS, and the cells in the petri dishes are placed in the incubator again for proliferation. Growing cells are ready for use in microfluidic experiments on the third day. In case of any contamination in the THP-1 population, it is expected from cells to stick to petri dishes.

6.1.2.4. Preparation of Frozen Stock Cultures. Frozen stock culture medium is prepared with dimethyl sulfoxide (DMSO). It contains 20% FBS, 10% DMSO, 1% Mem-Nea and 1% Pen/Strep with RPMI. Cells in the liquid culture are centrifuged at 2000 rpm for 2 min and waste medium is pipetted and discarded. Complete frozen stock culture medium is added on the cells and mixed expeditiously. Conical screw cap tubes are filled with 1 ml THP-1 culture (frozen stock culture medium and cells). Filled tubes are mixed gently and stored at -80 °C. The steps from adding frozen stock culture medium to the cells should be done quickly because DMSO in the medium can cause THP-1 cells to die.

6.1.2.5. Preparation of Oil and Drug Phase. Two phase microfluidic devices are operated with two immiscible liquids to generate droplets. Oil phase (organic phase) is prepared with Novec 7500 and Krytox 157 FSH surfactant of 3%. The reason for adding Krytox 157 FSH to the oil phase is to reduce the surface tension between the two liquids. For the drug treatment experiments, temsirolimus, rifabutin and BAY 11-7082 are used, respectively. 0.2 mg temsirolimus is added in the powder form (not sterilized) to the DMSO of 10mL.

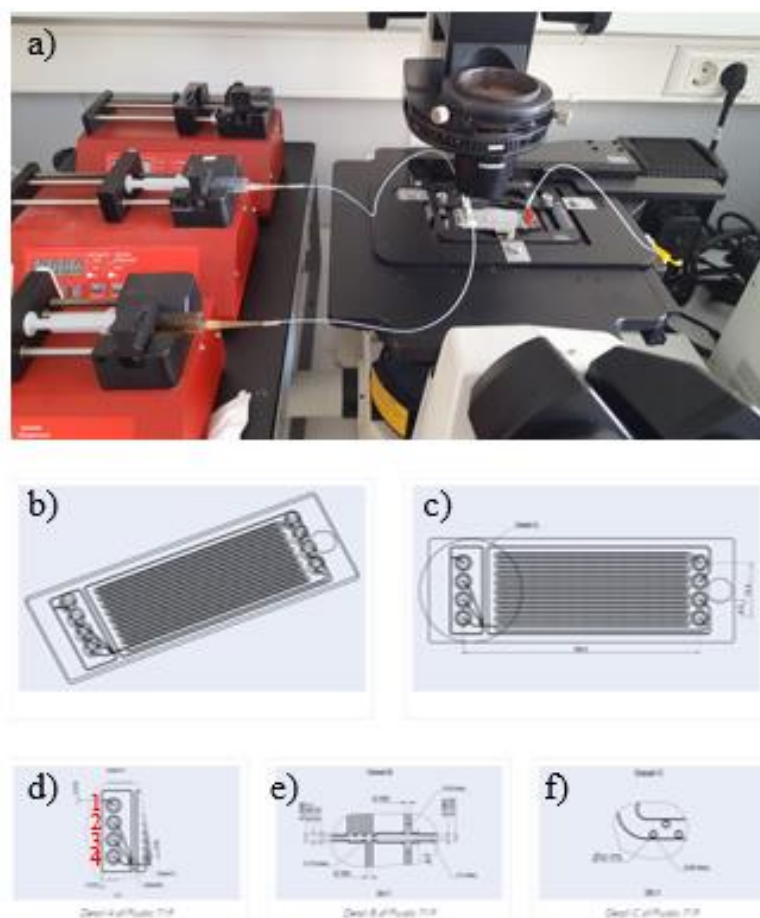


Figure 6.3. (a) Experimental setup of the microfluidic device platform (b), (c) General view of the chip (d) Inlets of the device (e) Channels for droplet generation (f) Channels for droplet storage.

200  $\mu\text{L}$  of temsirolimus-DMSO solution is taken and pipetted into 10 mL RPMI complete medium with 10% FBS. Final concentration of temsirolimus within the medium is 0.4  $\mu\text{g}/\text{mL}$ . 1.6 mg rifabutin in the powder form (not sterilized) is dissolved in 0.5 mL of methanol. 50  $\mu\text{L}$  of this solution is mixed with 10 mL RPMI complete medium (20% FBS). The final concentration of rifabutin in the medium is 1.6  $\mu\text{g}/\text{mL}$ . 1 mg of BAY 11-7082 is added in the powder form (not sterilized) to 4.8251 mL DMSO. 0.1 mL of this solution is mixed with 10 mL of RPMI complete medium. The final molarity of the solution is 10  $\mu\text{M}$ . In the droplet experiments, the concentrations of the drug solutions are adjusted to be twice the desired value, since the drug medium and cell medium coming from different channels are mixed.

Thus the concentration of temsirolimus, rifabutin and BAY 11-7082 are 0.2  $\mu\text{g/mL}$ , 0.8  $\mu\text{g/mL}$  and 5  $\mu\text{M}$  during the experiments within the droplets, respectively. Moreover, during the droplet generation in experiments, sometimes the drug containing medium may not mix with the cell containing medium. Red food dye (non-fluorescent and non-toxic) up to 20 drop is added to the drug containing medium to see whether the drug is mixed with the cell containing medium.

### 6.1.3. Experimental Setup of the Microfluidic Device Platform and Operation

The droplet generation and storage chip is placed on the Nikon Ti-E inverted fluorescence microscope (Figure 6.3a) and experimental setup is located around it. The chip has 4 inlets and 4 outlets. Inlet 1, 4 and 3 are used for continuous oil phase, THP-1 cells and drug, respectively (Figure 6.3d). Oil, THP-1 cells and drug containing phases are filled into the syringes and syringes are located on the syringe pumps. The syringe pumps are connected to the chip via PTFE tubings (left-hand side) and waste liquid is collected from the outlet of the chip (right-hand side) (Figure 6.3a).

Continuous oil phase comes from the upper and lower channels, and cells + drug come from the left channel (Figure 6.3e). Drug and cell containing droplets are created at the junction of the channels and stored in the lines (Figure 6.3b, c and f). In the experiments, due to the channel configuration of the device (Figure 5.3e), droplets are generated by flow focusing method. Before cell loading, the chip is filled with oil phase. When the chip is completely filled with oil, the cell and drug media began to be fed into the system at the same time. The THP-1 cell and drug containing medium had 100 mL/h flowrate while the oil had a flowrate of 600 mL/h.

Cells are encapsulated in the droplets with drug and the channels of the chip is filled with droplets. When all of the channels are filled, the system has stopped and cell containing droplets are marked. Brightfield and fluorescence microscopy images of the cells are recorded with the time interval of 1 h and experiments lasted for 24 h. The expression of ASC gene is followed by measuring its fluorescence intensity and by further processing using ImageJ program. In the following section, the results of the control and drug

(temsirolimus, rifabutin and BAY 11-7082) experiments of GFP:ASC labeled THP-1 cells will be presented and discussed.

## 6.2. Results and Discussion

### 6.2.1. Interaction of NLRP3 and ASC within the Cell and Their Roles

Inflammation can be identified as complex biological response of body tissues to harmful situations such as pathogens, damaged cells or irritants, and inflammation is the protective answer including immune cells, blood vessels and molecular mediators. Arteriosclerosis, obesity, liver diseases, autoimmune diseases, Alzheimer's disease and cancer are the results of excessive or chronic inflammatory responses. In the dangerous stimuli, macrophages take the major roles for starting the inflammatory responses (Yang, *et al.*, 2017), (Lin *et al.*, 2017).

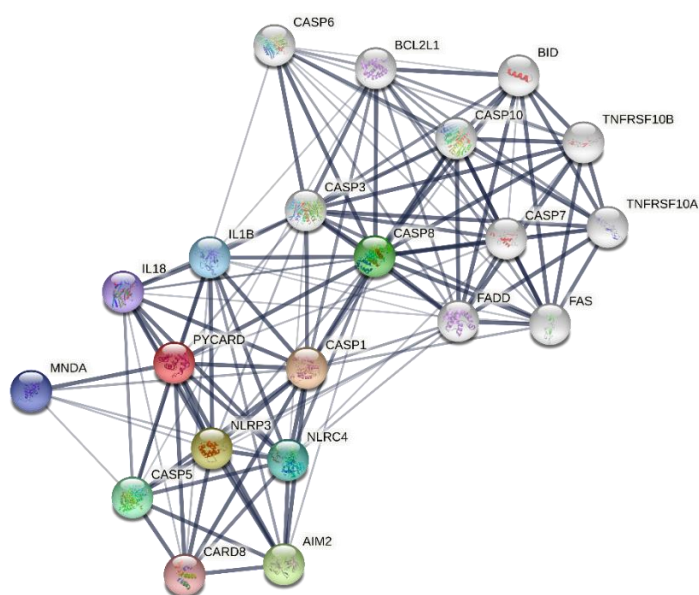


Figure 6.4. ASC (PYCARD) interaction map.

Innate and adaptive systems are two different immune systems of mammals and the innate immune system comes first during the protection against danger (Chen *et al.*, 2018). The identification of detrimental cases within the cell is done by pattern recognition receptors (PRRs). Toll-like receptors (TLRs), C-type lectin receptors (CLRs), RIG-I-like

receptors (RLRs) and nucleotide binding and oligomerization domain (NOD)-like receptors (NLRs) are the classes of PRRs. The role of TLRs and CLRs is to recognize microbes on the cell surface and in endosomes, whereas RLRs and NLRs detect microbial components in intracellular areas. The NLRs reveal the danger or pathogen associated molecular patterns (DAMPs and PAMPs) producing in inflammasome assembly and activation of caspase-1, results in cleavage of proIL-1 $\beta$  and proIL-18 (Ghiasi et al., 2018). Among the NLRs family, NLRP3 is discovered as the gene mutated in patients who have the autosomal-dominant periodic fever syndromes familial cold auto-inflammatory syndrome (FCAS), Muckle-Wells syndrome (MWS) and chronic infantile neurological cutaneous and articular syndrome (CINCA) (Lamkanfi and Dixit, 2009).

The protein NLRP3 is a protein and has a centrally located NOD motif. This motif is surrounded at the N-terminus by a pyrin domain for providing homotypic interactions with the bipartite adaptor protein apoptosis-associated speck-like protein containing CARD (ASC) (PYCARD). At the C-terminus, modulation of NLRP3 activity and sensing microbial ligands and endogenous alarmins are controlled by the 12 leucine-rich-repeat (LRR) motifs. The activity of NLRP3 is mainly encountered in the cytosol of granulocytes, monocytes, dendritic cells, T and B cells, epithelial cells and osteoblasts. This proves the theory that, NLRP3 expression is necessary for the primary defense mechanism. Priming and activation are the two check-points of the NLRP3 inflammasome. In the priming step, NLRP3 and pro-IL-1 $\beta$  are transcriptionally induced and in the activation step, ASC-NLRP3 interaction is built (Chang et al., 2018). Under certain conditions, NLRP3 triggers the startup of cysteine protease caspase-1 and caspase-1 creates the pro-inflammatory cytokines interleukin (IL)-1 $\beta$  and IL-18 to form biologically active IL-1 $\beta$  and IL-18. The interaction between the NLRP3 and caspase-1 is ensured by ASC (Lamkanfi and Kanneganti, 2010) (Figure 6.4).

ASC, a bipartite protein, includes two death domains which are N-terminal pyrin (PYD) and C-terminal caspase recruitment (CARD). Due to its death-fold domains it has a significant role in apoptotic cell death and inflammation. The conversion of procaspase-1 to active caspase-1 and maturation of interleukin-1 beta (IL-1 $\beta$ ) and IL-18 (key proinflammatory cytokines) are conducted by ASC. This conversion and maturation events lead to pyroptotic cell death (Lu *et al.*, 2014). Moreover, ASC also known as downstream target of methylation-induced gene silencing by DNA methyltransferase.

Hong and her colleagues suggested that, ASC can be perceived as a probable tumor suppressor gene, and silencing of it might result in carcinogenesis in some tumors. The relation of ASC in cell death is driven by the conversion of caspase-1 and this ends with the pyroptosis through inflammasome formation. In addition, ASC overexpression induced mitochondria or caspase 9 related apoptosis in 293T cells. In the literature, it is also shown that, ASC affects caspase 8 dependent apoptotic cell death. DNA damage or loss of extracellular matrix contact concluded with the induced ASC expression leading to apoptosis in human mammary epithelial cells (Hong *et al.*, 2013).

### **6.2.2. Confinement of THP-1 Cells within the Droplets without Drug (Control Experiment)**

In the control experiment, THP-1 cells are confined in the droplets without any drugs. When the chip is completely filled with droplets, flow of cell and oil phases to the chip are stopped and cell positions within the droplet are determined. The response of cells is recorded and images taken during the experiment with 1 h time interval are analyzed. Figure 6.5 shows the results of the experiment over time. Cell count vs time graph is given in Figure 6.5a and there is neither increase nor decrease in the cell count. The doubling time of THP-1 cells ranged from 19 to 50 h, but no proliferation is observed in the droplets and this might be the result of limited nutrient environment. Since THP-1 cells have GFP:ASC gene, fluorescence intensity of the cells are analyzed and Figure 6.5b displays the result of normalized fluorescence intensity vs time graph.

It is seen that there is negative slope in the chart trend throughout the experiment and decrease in the amount of fluorescence is observed from the beginning. In order for the ASC gene to be expressed, there must be a factor inducing the cell in the environment. However, since there is no drug/inhibitor treatment within the droplets, there is no stimulus for the cell to start inflammasome and the decrease in fluorescence intensity might be due to this. Moreover, Khorshidi and his colleagues performed droplet-based experiment with HEK293T cells, which survived up to 11 h in the droplets (Khorshidi *et al.*, 2014). On the other hand, in our experiment with THP-1 cells, it can be obtained that the cells sustained to live for 24 hours, since the expression of ASC continues, albeit with a decrease, in the cells.

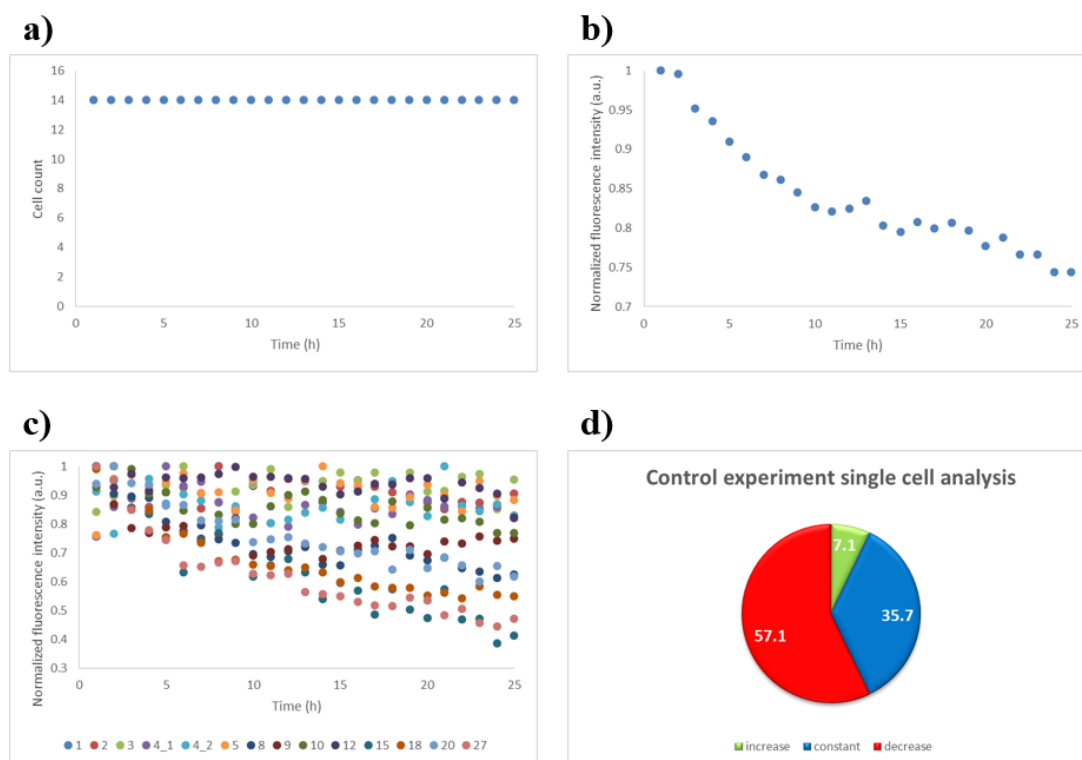


Figure 6.5. Control experiments results (a) Time profile of cell count (b) Time profile of normalized fluorescence intensity (a.u.) (c) Time profiles of single cells' normalized fluorescence intensity (a.u.) (d) Percentages of increase, constant and decrease states of single cells' fluorescence intensity.

In addition to the response of the cells as population, single cell responses are also given in the Figure 6.5 c and d. Like in Figure 6.5b, there is a reduction in the fluorescence intensity when the single cells are considered. A change between 0.3 and 1.0 is observed in the amount of fluorescence intensity of the cells and the decrease is noticeable through the end of the 24h. Figure 6.5d shows the percentages of cells with increasing, decreasing and constant fluorescence and 7.1% of the cells have increasing, 35.7% of the cells have constant and 57.1% of the cells have slight decreasing intensity trends. Although the number of cells with a reduction in fluorescence intensity is high, the number of cells with no change in intensity throughout the experiment is also quite high. Moreover, fluorescence intensity has not ceased in any cell and this indicates the vitality of the cells. In resting cells, ASC can be found both in cytoplasm and nucleus in the dissolved form (Hoss et al., 2017). During the inflammation, one large micrometer-sized ASC speck per cell is detected and this creates the concentrating CASP1 activation sites (Hoss et al., 2017), (Stutz *et al.*, 2013). Generation

of ASC specks is dependent on the inflammasome inducers (Zha *et al.*, 2016). Since there is no inducer in the control experiment ASC fluorescence intensity decrease is reasonable during the experiment.

### 6.2.3. Temsirolimus Experiment

mTOR is considered as a probable target for cancer treatment. mTOR belongs to phosphatidylinositol 3-kinase-related kinase protein (PIKK) family and it has role in cell growth, cell proliferation, cell motility, cell survival, protein synthesis and transcription. When the working mechanism of mTOR is disrupted, the probability of carcinogenesis increases and abnormal function of mTOR results in several cancer types including breast, lung and pancreas (Trendowski *et al.*, 2015). Temsirolimus is a drug and used for the treatment of several malignancies and solid tumors under the approval of Food and Drug Administration (FDA). It is an ester derivative of rapamycin and inhibitor of the kinase mammalian/mechanistic target of rapamycin (mTOR). Temsirolimus triggers the apoptosis in tumor cells via activation of caspases (Bhuyan *et al.*, 2017). This drug causes the suspension of protein synthesis that manages the proliferation, growth and survival of tumor cells. Cells exposed to temsirolimus encounters with cell cycle arrest in G1 phase and it also decreases the production of vascular endothelial growth factor (VEGF) resulting in the inhibition of tumor angiogenesis (Hastings 2007), (Wan *et al.*, 2006). Due to the antiproliferative effect of temsirolimus, inhibition of necessary survival pathways, complex cell cycle effects, induction of apoptosis and autophagy might occur (Tourneau *et al.*, 2008). In the droplet-based experiment conducted with temsirolimus, THP-1 cells are monitored for 24 h and data are recorded. In order to be sure that temsirolimus is mixed with THP-1 cells, red food dye is added to the drug medium and Figure 6.6 shows the results. In the experiment, as like control one, cell count did not change. Since THP-1 cells have proliferation times of close to 50 hours, doubling have not been observed during the experiment of 24 h (Figure 6.6a). Normalized fluorescence intensity is shown in Figure 6.6b. There is an increasing trend in this figure it has a range of in between 0.4 and 1.0. As stated previously, temsirolimus has inhibitory effect on cells due to the interference of mTOR pathway. Inflammasome should be triggered in cells under the treatment of drug and ASC-NLRP3 interaction is constituted. ASC oligomerizes into pyroptosomes, defined as perinuclear specs, then autoproteolysis of procaspase-1 into caspase-1 occurs. The induction

of the IL-1 $\beta$  is realized by caspase-1 and pyroptosis starts (Chang *et al.*, 2018). Since temsirolimus stimulates the apoptosis of cells (Cao *et al.*, 2017) and ASC plays active role in cell death (Kitazawa *et al.*, 2017) it has increasing expression in the experiment.

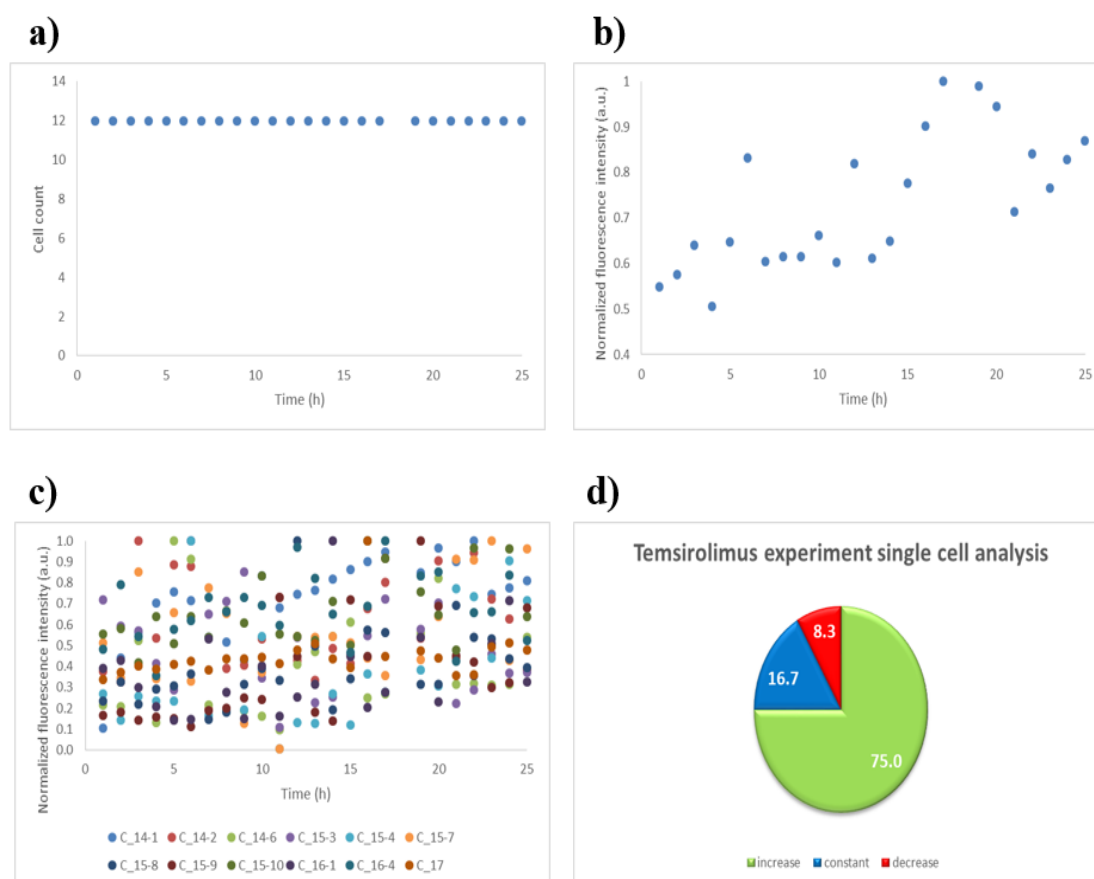


Figure 6.6. THP-1 cells are under the treatment of temsirolimus (a) Time profile of cell count (b) Time profile of normalized fluorescence intensity (a.u.) (c) Time profiles of single cells' normalized fluorescence intensity (a.u.) (d) Percentages of increase, constant and decrease states of single cells' fluorescence intensity.

Figure 6.6c depicts the single cell fluorescence intensity. Clusters are seen at high values of fluorescent intensity towards the end of the experiment (Figure 6.6c). When the cells are examined individually, most of them show increased expression of the ASC gene and Figure 6.6d confirms this. 75% of the cells showed increasing, 16.7% of the cells showed constant and 8.3% of the cells showed decreasing trend. Accordingly, while the intensity increase is in the majority among the cells, the intensity decrease is also observed. Presence of cells with decreased intensity may indicate that apoptosis has occurred. In the control

experiment, when there is no inducer in the medium, there is a decrease in ASC fluorescence intensity, while the increase in intensity in cells under the effect of temsirolimus shows that the experiments are acceptable and the drug is effective in apoptosis.

#### **6.2.4. Rifabutin Experiment**

Innate immune responses are important for the pathology of infectious and inflammatory disorders such as acute abdominal inflammation, cancers and respiratory tract disorders. During the infection of tuberculosis, neutrophils and macrophages play important roles. In collaboration with inflammatory elements such as cytokines and proteases, process finishes with the elimination of the pathogen and end of inflammation (Sasindran and Torrelles 2011), (Muefong and Sutherland, 2020). Pyroptosis which is a caspase-1 dependent cell death mechanism is correlated with the control of intracellular pathogens and activation of NLRP3 inflammasome is observed due to MTB. With the help of the IL-1 $\beta$  in protection against TB, NLRP3 interferes in the early control of intracellular MTB replication (Zumla *et al.*, 2014).

Mycobacterial infectious diseases can be treated with rifabutin, semisynthetic derivative of rifamycin and a wide spectrum antibiotic. Due to rifabutin's high activity against Mycobacterium tuberculosis (MTB) which is an etiological agent of tuberculosis (TB), it is employed as a second-line anti-tuberculosis drug. Unlike the rifampicin (first-line drug), rifabutin has limited interactions with the antiretroviral drugs and this makes it a favorable drug for the treatment of human immunodeficiency virus (HIV) and TB infected patients (Pinheiro *et al.*, 2013). The working mechanism of rifabutin is; inhibition of bacterial DNA-dependent RNA polymerase. Thus initiation of RNA formation is suppressed and inhibition of RNA synthesis and transcription occurs (Kunin 1996).

In this section, rifabutin is used to treat THP-1 cells. Figure 6.7 shows the time profile of cell count, normalized fluorescence intensity, single cell fluorescence intensity and percentages related with the experiment. As in the control and temsirolimus experiments, the cell number did not change in this experiment. Normalized fluorescence intensity of the cells have increasing trend at first but there is a decrease in the intensity through the end of the experiment Figure 6.7b.

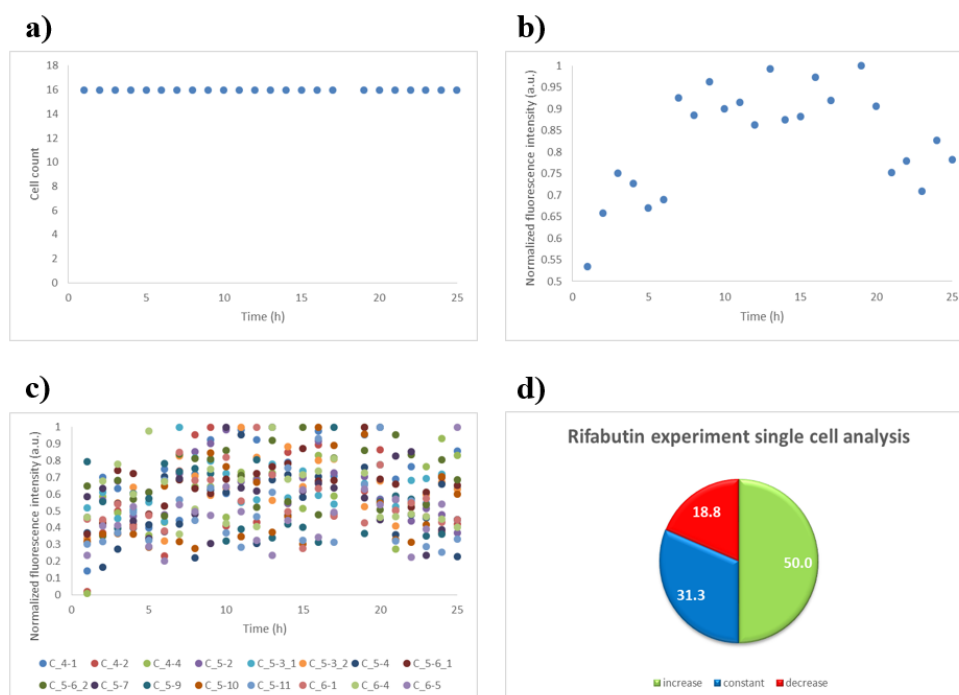


Figure 6.7. THP-1 cells are under the treatment of rifabutin (a) Time profile of cell count (b) Time profile of normalized fluorescence intensity (a.u.) (c) Time profiles of single cells' normalized fluorescence intensity (a.u.) (d) Percentages of increase, constant and decrease states of single cells' fluorescence intensity.

In literature, it is proved that; during the MTB infection, lymphocytes, plasmacytes, neutrophils, monocytes and macrophages are significantly increased. This outcome suggest that, inflammatory cells are upregulated in patients with MTB. Moreover, IL-1, IL-6, IL-10 and IL-12 are also upregulated (Liu et al., 2018). Since rifabutin is used in the treatment of MTB, it triggers the expression of ASC through NLRP3 inflammation and TB relationship. Figure 6.7c describes the single cell responses under the treatment of drug. There is no big difference in between the cells and most of them had almost same reaction. Li and her/his colleagues investigated the rifabutin effect on the proliferation and apoptosis in lots of cancer cell lines. They stated that, rifabutin caused ceased proliferation and provoked the apoptosis. Proliferating marker protein Ki67 and anti-apoptotic protein Mcl-1 had a decreasing concentration whereas pro-apoptotic protein active caspase-3 had increasing level within the cancer cells demonstrating the intervened proliferation and apoptosis effects of rifabutin (Li *et al.*, 2016). In our experiment, the expression of ASC gene, triggered by rifabutin, is first stopped the proliferation and started the apoptosis. Moreover, ASC is directly linked with

the CASP-3 (Figure 6.4) and CASP-3 has role in apoptosis. As stated previously, CASP-3 has increasing level within the cells under inflammation conditions. The decrease in cell fluorescence intensity towards the end of the experiment may be due to CASP-3 resulting in cell death. Finally, when looking at Figure 6.7d, increased ASC gene expression is seen in half of the cells, while the number of fluorescence decreasing cells, that is, cells with initiation of apoptosis, takes up to 20%. The number of cells with no change in ASC gene expression is around 30%. In these cells, the apoptosis-related ASC gene may have expired.

### **6.2.5. BAY 11-7082 Experiment**

Nuclear factor kappa light polypeptide gene enhancer in B cells (NF $\kappa$ B) is a protein coding gene. Transcription factors of NF $\kappa$ B family are activated and expressed by a several stimuli such as proinflammatory cytokines and environmental stressors. Controlling the transcription of hundreds of genes such as encoding for proteins comprising in immune regulation but which are also significant for cell survival, differentiation and proliferation on non-immune cells are governed by NF $\kappa$ B. Abnormal activity of NF $\kappa$ B results in many diseases such as tumor development and metastasis. Thus, inhibition of NF $\kappa$ B can be considered as an alternative option for tumor treatment and anti-cancer drugs works for the inhibition of NF $\kappa$ B (Rauert-wunderlich *et al.*, 2013). Under basal conditions, NF $\kappa$ B is located in the cytoplasm and it is inactivated by inhibitory I $\kappa$ B subunits. Proteasomal degradation of I $\kappa$ B is done via phosphorylation of itself and this contributes to permitting nuclear translocation of NF $\kappa$ B and transcriptional activation of target genes (Dai *et al.*, 2004).

BAY 11-7082 (BAY) is an anti-inflammatory drug and can be used as an inhibitor of the expression of transcription factor NF $\kappa$ B. In case on inflammation, in response to cytokines and cellular stresses, I $\kappa$ B kinase (IKK) adds phosphate to I $\kappa$ B and ubiquitination and proteolytic degradation occurs. Then, NF $\kappa$ B activation and nuclear translocation materializes (Krishnan *et al.*, 2013). However, working mechanism of BAY starts with the inhibition of IKK and this leads to downregulation of NF $\kappa$ B. Inflammatory cytokine inhibition, heme oxygenase-1 induction, ICAM-1 activation suppression, ATPase activity of NLRP3 inflammasome reduction and neutrophil apoptosis increase are also the functions of BAY (Lee *et al.*, 2012), (Zhong *et al.*, 2016).

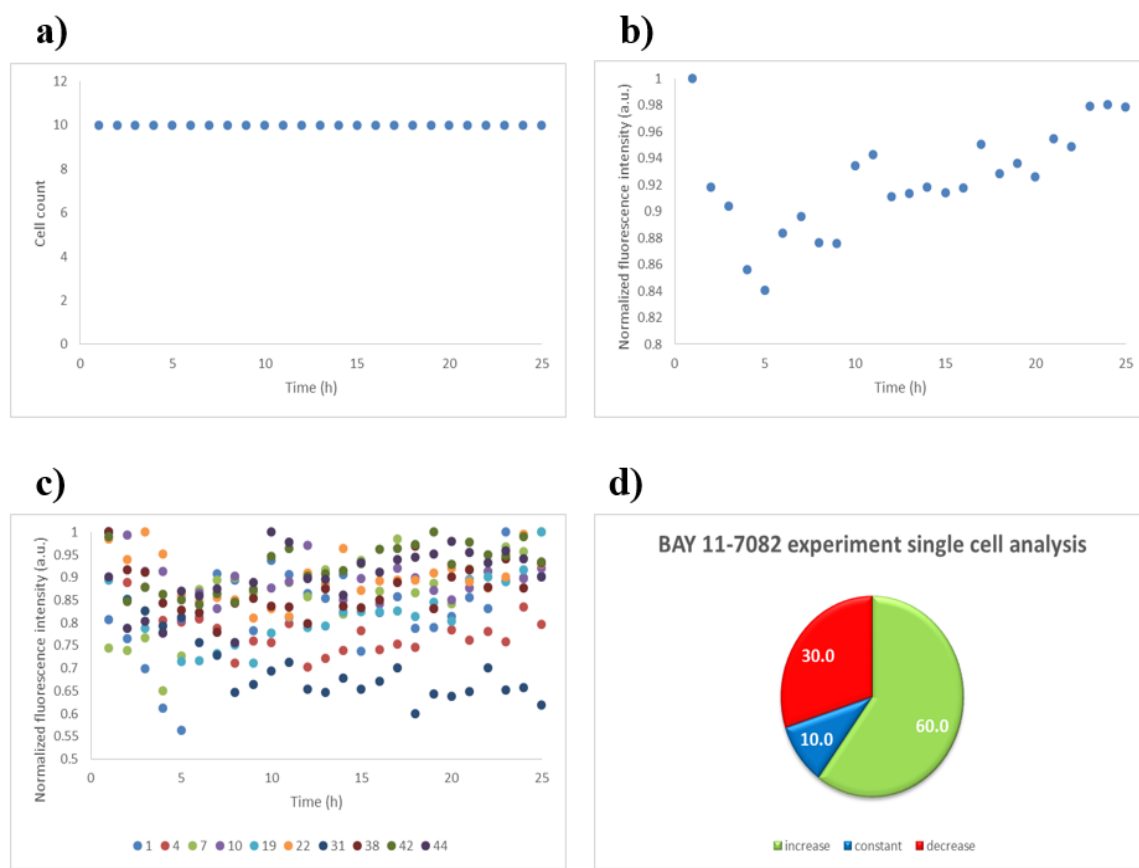


Figure 6.8. THP-1 cells are under the treatment of BAY 11-7082 (a) Time profile of cell count (b) Time profile of normalized fluorescence intensity (a.u.) (c) Time profiles of single cells' normalized fluorescence intensity (a.u.) (d) Percentages of increase, constant and decrease states of single cells' fluorescence intensity.

As stated previously, ASC has role in the activity of NLRP3. In addition, ASC is in collaboration with PYD family (ASC also contains PYD) such as PYPAF1 and PYPAF7 and they are connected with NF $\kappa$ B activity or procaspase-1 activation (Manji *et al.*, 2002), (Wang *et al.*, 2002). However, in the literature ASC is described as a suppressor of NF $\kappa$ B activity (Stehlik *et al.*, 2003), proposing that the ASC might have a dual role. In 2006, Sarkar and her colleagues worked on the dual role of ASC and found that; ASC effect on NF $\kappa$ B is dependent on the dosage of molecules. In detail, the duty of receptor interacting serine/threonine kinase 2 (RIP2) in cell is to induce NF $\kappa$ B signal. RIP2-deficient cells have reduced NF $\kappa$ B activation and cytokine generation. On the contrary, overexpressed RIP2 and caspase-1 in HEK293 cells showed increased activity of NF $\kappa$ B proving that RIP2 is necessary for NF $\kappa$ B activation. Besides, when the ASC level is low, induction of NF $\kappa$ B

continued. However, despite the existence of RIP2 and caspase-1, overexpression of ASC caused an inhibition of NF $\kappa$ B. Therefore, ASC activity have biphasic dose response within the cells. Figure 6.8 shows the response of THP-1 cells under the BAY treatment.

Cell count did not change in this experiment too (Figure 5.8a). THP-1 proliferation is not observed in droplet experiments, whether the cell is under the influence of drugs or not. An increase in the ASC expression is detected similar to the temsirolimus experiment (Figure 5.8b vs Figure 5.6b). The BAY treatment of THP-1 cells causes the inhibition of TNF-like weak inducer apoptosis (TWEAK) triggered p100 processing (necessary for NF $\kappa$ B regulation) and TNF-induced phosphorylation and degradation of I $\kappa$ B $\alpha$ . The inhibition of these pathways results in downregulation of NF $\kappa$ B (Wunderlich, Siegmund, & Maier, 2013). Due to the suppressed cell management capacity of NF $\kappa$ B, apoptosis within the cell might be triggered. It can be said that the increase in the expression of ASC, which is responsible for apoptosis, is normal in the cells whose cellular functions are inhibited by BAY. When the single cell response is considered, it is noteworthy that there is no great difference in the ASC gene fluorescence intensity of the cells (Figure 5.8c). Most of the cells showed similar response to BAY treatment (Figure 5.8c). It can be understood from the decrease in fluorescence intensity that apoptosis has started in the cells (in the 30 percent part), that is, the cells are about to die. 60% of the cells showed an increasing fluorescence intensity and constant fluorescence is observed in a small part of the cells.

Considering all the experiments together, it is observed that there is a decrease in the expression of the ASC gene in the absence of any inducer in the medium (control experiment). The percentage of cells with the highest increase in fluorescence is in the temsirolimus experiment, while the percentage of cells with no change (constant) in fluorescence is highest in the control experiment.

### **6.3. Conclusion**

Fluid manipulation is necessary in every field of world's technology. By using the fluid manipulation, micro and nanotechnologies are used to reduce the required dimensions of equipment and machinery. One or two phase microfluidic devices (continuous and dispersed) are operated as needed and while the small molecule screening can be done via

droplet-based devices, single cell analysis can be done via continuous microfluidic devices. In this study, we are able to generate small droplets with THP-1 cells inside. Several drug administrations are performed in each experiment, and the cell response is monitored via the ASC gene. In the experiments, cells are first followed without drugs (control experiment). Since there is no stimulus inducing the ASC gene in the environment, a continuously decreasing fluorescence intensity is observed in this experiment. Then; temsirolimus, mTOR inhibitor, rifabutin, anti-tuberculosis, and BAY 11-7082, NF $\kappa$ B inhibitor are applied and data are recorded. While ASC gene expression increased continuously in the temsirolimus and BAY 11-7082 experiments, first an increase and then a decrease is observed in the rifabutin experiment. It is evident from our study that ASC plays a critical role in communications between the inflammasome and the signalosome.

## 7. CONCLUSIONS AND RECOMMENDATIONS

### 7.1. Conclusions

In conclusion, the following achievements are obtained on the basis of the thesis work:

- A detailed literature review on microfluidic devices has been made, and cultivation, separation/isolation, detection and analysis, and reaction studies have been classified and presented separately.
- Several microbioreactors (microfluidic devices) are designed and drawn with CAD tools. The velocity profile within the optimized device is estimated via COMSOL Multiphysics software. Appropriate flowrates are determined for the experiments with yeast and mammalian cells.
- The designed microbioreactor is successfully fabricated via hot embossing and thermo-compression bonding.
- Yeast cells are trapped and cultured within the pre-determined zones and several experiments are conducted, confirming that the chip served the intended purpose.
- The brightfield and fluorescence microscopy images are taken at regular time intervals and they are analyzed via Fiji image processing program. Several parameters including cell count, cell perimeter/area and fluorescence intensity are calculated.
- In the HU experiment, while the cell count and perimeter did not change during the application of HU, they increased towards the end. The fluorescence intensity initially decreased but it has rising trend with the HU treatment. Since HU is a DNA synthesis/replication inhibitor, it affects the progression of S-phase and HU treatment causes S phase to continue in slow motion but does not cause to stop the cell cycle. The protein synthesis, which should follow Nop56 protein expression, did not take place within the cell during the HU treatment

- In the metformin experiment, the cell count continued to increase even under the treatment of metformin. Cell perimeter is first increased, and then decreased through the end of the experiment. The fluorescence intensity decreased at the beginning, then remained stable. Since metformin acts as the cell growth inhibitor, a decrease in cell size is a reasonable outcome. Metformin is used to regulate the insulin level, thus the glucose uptake mechanism of cells might be disturbed. Cells continued to their cell division, so cell count increased, but their dimensional growth (cell size) decreased due to the drug effect on cells. Moreover, there is an extension in the time of S/G2/M phase.
- Temsirolimus experiment suppressed the cell proliferation because cell count did not change after the treatment. Cell perimeter initially increased, but decreased with the application of temsirolimus. When the drug treatment stopped, fluorescence intensity started to increase through the end. Similarly, in literature, temsirolimus is reported to cause G0/G1 cell-cycle arrest and decrease in the amount of cells that progress in S and G2/M phases for carcinoma cells. In this study, temsirolimus affected both Nop56 expression and cell growth and proliferation, in agreement with literature reports. Hence perturbations in Nop56 levels lead to altered ribosome biogenesis, localization, and cellular fitness.
- In case of HMF supplementation, cell count did not increase after the HMF addition. While the cell perimeter increased before the HMF application, it decreased slowly through the end of experiment with the supply of HMF free fresh nutrient medium. HMF treatment suppresses normal functioning of cell cycle but it does not cause cells to die. The individual cell proliferation continued during the HMF supplement and new cells joined the culture. Since HMF inhibits protein and RNA synthesis, there is a sharp decrease in the intensity of Nop56 fluorescence during the HMF treatment, and generally localizes in highly conserved regions of functional RNAs.
- The effect of HMF on yeast cells is also investigated in a computational study conducted with COBRA toolbox. It has been proven that HMF has a negative effect on yeast cells in models with and without HMF and ethanol production is limited due to HMF. The reasons are deeply investigated by calculating the internal flux distribution within yeast metabolic network.

- Interdigitated Cr/Au electrodes are integrated to the designed and in-house fabricated single phase microfluidic device and TFields experiments are done. While electroporation is observed in cells in high electric field environment, mitosis time is prolonged in low electric field environment.
- The experiments with mammalian THP-1 cells are performed in the two-phase microfluidic devices and the cells are confined in the droplets with various drugs. THP-1 cells have GFP:ASC gene and this gene has role in apoptosis. Temsirolimus, rifabutin and BAY 11-7082 drugs are employed during the experiments and the effects of these drugs on THP-1 cells are deeply investigated on single cell basis. While the fluorescence intensity increased in the temsirolimus and BAY 11-7082 experiments, it first increased and then decreased in the rifabutin experiment. It is deduced that the cells are affected by all these drug and apoptosis began.
- In brief, Lab-on-a-Chip platform (both single and two-phase) is operating successfully and can be used for cell culturing experiments and for studying the drug effects on tumors and may shed light on the putative treatment strategies towards cancer.

## **7.2. Recommendations**

- In the experiments COP based impermeable thermoplastic substrate is used. Experiments can be repeated with PDMS material to account for the oxygenated environment.
- The chip design allows two different experiments at the same time. The number of chambers can be increased and the design should be improved in order to carry out high-throughput experiments at once.
- Since mammalian cells grow in an environment at 5% CO<sub>2</sub> and 37°C, an environmental chamber should be placed around the microscope and the image acquisition process should be automated.

- Cell proliferation could not be monitored in all of the experiments including control experiment because THP-1 cells have doubling time of 24 h to 50h. The experiment time need to be extended.
- Experiments conducted with electrodes can be repeated with brain or other mammalian cells and the number of applied electric fields should be increased.

## REFERENCES

Abaci, H. E., Devendra, R., Smith, Q., Gerecht, S. and Drazer, G., 2012, “Design and development of microbioreactors for long-term cell culture in controlled oxygen microenvironments” *Biomedical Microdevices*, 14, 1, 145–152.

Abate, A. R., Mary, P., Steijn, V. and Weitz, D. A., 2012, “Experimental validation of plugging during drop formation in a T-junction”, *Lab on a Chip*, 12, 1516–1521.

Abdel-Wahab, A. A., Ataya, S. and Silberschmidt, V. V., 2017, “Temperature-dependent mechanical behaviour of PMMA: Experimental analysis and modelling”, *Polymer Testing*, 58, 86–95.

Adams, A., Okagbare, P. I., Feng, J., Hupert, M. L., Patterson, D., Go, J. and Nikitopoulos, D., 2008, “Highly efficient circulating tumor cell isolation from whole blood and label-free enumeration using polymer-based microfluidics with an integrated conductivity sensor, *Journal of the American Chemical Society*, 5, 8633–8641.

Aeinehvand, M. M., Ibrahim, F., Harun, S. W., Djordjevic, I., Hosseini, S., Rothan, H. A., Yusof, R. and Madou, M. J., 2015, “Biosensing enhancement of dengue virus using microballoon mixers on centrifugal microfluidic platforms”, *Biosensors and Bioelectronics*, 67, 424–430.

Agostini, S., Houlbrèque, F., Biscéré, T., Harvey, B. P., Heitzman, J. M., Takimoto, R. and Rodolfo-metalpa, R., 2021, “Greater mitochondrial energy production provides resistance to ocean acidification in “winning” hermatypic corals”, *Frontiers in Marine Science*, 7, 1–11.

Akagi, J., Takeda, K., Fujimura, Y., Matuszek, A., Khoshmanesh, K. and Wlodkowic, D., 2012, “Microflow cytometry in studies of programmed tumour cell death”, *Procedia Engineering*, 47, 88–91.

Akagi, J., Khoshmanesh, K., Hall, C. J., Cooper, J. M., Crosier, K. E., Crosier, P. S. and Wlodkowic, D., 2013a, “Fish on chips: microfluidic living embryo array for accelerated in vivo angiogenesis assays”, *Sensors and Actuators, B: Chemical*, 189, 11–20.

Akagi, J., Hall, C. J., Crosier, K. E., Crosier, P. S. and Wlodkowic, D., 2013b, “Immobilization of zebrafish larvae on a chip-based device for environmental scanning electron microscopy (ESEM) imaging”, *Proceedings of Society of Photo-Optical Instrumentation Engineers*, 8923(v), 892346.

Akagi, J., Khoshmanesh, K., Hall, C. J., Crosier, K. E., Crosier, P. S., Cooper, J. M. and Wlodkowic, D., 2012, “Fish on chips: automated microfluidic living embryo arrays”, *Procedia Engineering*, 47, 84–87.

Akagi, J., Zhu, F., Hall, C. J., Crosier, K. E., Crosier, P. S. and Wlodkowic, D., 2014, “Integrated chip-based physiometer for automated fish embryo toxicity biotests in pharmaceutical screening and ecotoxicology”, *Cytometry Part A*, 85, 6, 537–547.

Akagi, J., Zhu, F., Skommer, J., Hall, C. J., Crosier, P. S., Cialkowski, M. and Wlodkowic, D., 2015, “Microfluidic device for a rapid immobilization of zebrafish larvae in environmental scanning electron microscopy”, *Cytometry Part A*, 87, 3, 190–194.

Aki, K., Ogawa, K. and Ichihara, A., 1968, “Transaminases of branched chain amino acids. IV. purification and properties of two enzymes from rat liver”, *Biochimica et Biophysica Acta*, 4, 1592, 276-284.

Alapan, Y., Kim, C., Adhikari, A., Gray, K. E., Gurkan-Cavusoglu, E., Little, J. A. and Gurkan, U. A., 2016, “Sickle cell disease biochip: a functional red blood cell adhesion assay for monitoring sickle cell disease”, *Translational Research*, 173, 74-91.e8.

Almeida, J. R. M., Röder, A. and Modig, T., 2008, “NADH- vs NADPH-coupled reduction of 5-hydroxymethyl furfural (HMF) and its implications on product distribution in *Saccharomyces cerevisiae*”, *Applied Microbiology and Biotechnology*, 78, 939–945.

Al-nasser, M. M., Al-dosari, M. S., Parvez, M. K., Al-anazi, M. R., Alkahtane, A. A., Alotheid, H. and Al-qahtani, A. A., 2021, "The potential effects of *Indigofera coerulea* extract on THP-1 human cell line", *Journal of King Saud University - Science*, 33, 4, 101446.

Altmann, B., Löchner, A., Swain, M., Kohal, R., Giselbrecht, S., Gottwald, E. and Tomakidi, P., 2014, "Biomaterials differences in morphogenesis of 3D cultured primary human osteoblasts under static and microfluidic growth conditions", *Biomaterials*, 35, 10, 3208–3219.

Asghar, W., Velasco, V., Kingsley, J. L., Shoukat, M. S., Shafiee, H., Anchan, R. M. and Demirci, U., 2014, "Selection of functional human sperm with higher dna integrity and fewer reactive oxygen species", *Advanced Healthcare Materials*, 3, 10, 1671–1679.

Asokumar, N., Kim, S. D. and Ma, K., 2018, "Innovative energy & research alcohol dehydrogenases catalyzing the production of ethanol at high temperatures", *Innovative Energy and Research*, 7, 4.

Auerswald, J. and Knapp, H. F., 2003, "Quantitative assessment of dielectrophoresis as a microfluidic retention and separation technique for beads and human blood erythrocytes", *Microelectronic Engineering*, 68, 879–886.

Auwerx, J., 1991, "The human leukemia cell line, THP-1: A multifaceted model for the study of monocyte-macrophage differentiation", *Experientia*, 47, 22-31.

Baday, M., Calamak, S., Durmus, N. G., Davis, R. W., Steinmetz, L. M. and Demirci, U., 2016, "Integrating cell phone imaging with magnetic levitation (i-lev) for label-free blood analysis at the point-of-living", *Small*, 12(9), 1222–1229.

Bayouhdh, S., Othmane, A., Ponsonnet, L. and Ben Ouada, H., 2008, "Electrical detection and characterization of bacterial adhesion using electrochemical impedance spectroscopy-based flow chamber", *Colloids and Surfaces A: Physicochemical and Engineering Aspects*, 318, 1–3, 291–300.

Becker, H. and Gärtner, C., 2000, “Polymer microfabrication methods for microfluidic analytical applications”, *Electrophoresis*, 21, 1, 12–26.

Becker, H. and Heim, U., 2000, “Hot embossing as a method for the fabrication of polymer high aspect ratio structures”, *Sensors and Actuators*, 130–135.

Becker, S. A., Feist, A. M., Mo, M. L., Hannum, G., Palsson, B. Ø. and Herrgard, M. J., 2007, “Quantitative prediction of cellular metabolism with constraint-based models : the COBRA Toolbox”, *Nature Protocols*, 2, 3, 727–738.

Bedian, L., Villalba-rodríguez, A. M., Hernández-vargas, G., Parra-saldivar, R. and Iqbal, H. M. N., 2017, “International journal of biological macromolecules bio-based materials with novel characteristics for tissue engineering applications – a review”, *International Journal of Biological Macromolecules*, 98, 837–846.

Belanger, M. C. and Marois, Y., 2001, “Hemocompatibility, biocompatibility, inflammatory and in vivo studies of primary reference materials low-density polyethylene and polydimethylsiloxane: a review”, *Journal of Biomedical Materials Research*, 467–477.

Bender, E., Kozak, K., Howard, S., Hayes, L., Bayouth, J. and Robins, H. I., 2017, “The effect of optunetm tumor treating fields transducer arrays on skin radiation dose during radiotherapy”, *Journal of Clinical Neuroscience*, 42, 172–175.

Berg, G. M. and Jørgensen, N. O. G., 2006, “Purine and pyrimidine metabolism by estuarine bacteria”, *Aquatic Microbial Ecology*, 42, 215–226.

Bernstein, K. A., Bleichert, F., Bean, J. M., Cross, F. R. and Baserga, S. J., 2007, “Ribosome biogenesis is sensed at the start cell cycle checkpoint”, *Molecular Biology of the Cell*, 18, 953–964.

Bersini, S., Gilardi, M., Arrigoni, C., Talo, G., Zamai, M., Zagra, L., Caiolfa, V. and Moretti, M., 2016, “Human in vitro 3D co-culture model to engineer vascularized bone-

mimicking tissues combining computational tools and statistical experimental approach”, *Biomaterials*, 76, 157–172.

Bhuyan, A. A., Cao, H. and Lang, F., 2017, “Triggering of eryptosis, the suicidal erythrocyte death by mammalian target of rapamycin (mTOR) inhibitor temsirolimus”, *Cellular Physiology and Biochemistry*, 42, 1575-1591.

Blank, H. M., Perez, R., He, C., Maitra, N., Metz, R., Hill, J. and Polymenis, M., 2017, “Translational control of lipogenic enzymes in the cell cycle of synchronous, growing yeast cells”, *The European Molecular Biology Organization Journal*, 36, 4, 487–502.

Bogomolnaya, L. M., Pathak, R., Cham, R., Guo, J., Surovtseva, Y. V., Jaeckel, L. and Polymenis, M., 2004, “A new enrichment approach identifies genes that alter cell cycle progression in *Saccharomyces cerevisiae*”, *Current Genetics*, 45, 6, 350–359.

Boitard, L., Cottinet, D., Kleinschmitt, C., Bremond, N., Baudry, J., Yvert, G. and Bibette, J., 2012, “Monitoring single-cell bioenergetics via the coarsening of emulsion droplets”, *Proceedings of the National Academy of Sciences of the United States of America*, 109, 19, 7181–7186.

Bolic, A., Larsson, H., Hugelier, S., Eliasson Lantz, A., Krühne, U. and Gernaey, K. V., 2016, “A flexible well-mixed milliliter-scale reactor with high oxygen transfer rate for microbial cultivations”, *Chemical Engineering Journal*, 303, 655–666.

Bordel, S., Agren, R. and Nielsen, J., 2010, “Sampling the solution space in genome-scale metabolic networks reveals transcriptional regulation in key enzymes”, *PLoS Computational Biology*, 6, 7, e1000859.

Bork, N. P., 2005, “Is there biological research beyond Systems Biology ? A comparative analysis of terms”, *Molecular Systems Biology*, 1.

Bosshart, H. and Heinzemann, M., 2016, “THP-1 cells as a model for human monocytes”, *Annals of Translational Medicine*, 4, 21, 4–7.

Bouwman, J., Lindenbergh, A., Eunen, K. Van, Siderius, M., Pj, W., Natl, P. and Sci, A., 2011, “Metabolic regulation rather than de novo enzyme synthesis dominates the osmo-adaptation of yeast”, *Yeast*, 28, 43–53.

Brazda, N., Voss, C., Estrada, V., Lodin, H., Weinrich, N., Seide, K. and Müller, H. W., 2013, “A mechanical microconnector system for restoration of tissue continuity and long-term drug application into the injured spinal cord”, *Biomaterials*, 34, 38, 10056–10064.

Breitenbach-Schmitt, J., Heinisch, J., Schmitt, H. D. and Zimmermann, F. K., 1984, “Yeast mutants without phosphofructokinase activity can still perform glycolysis and alcoholic fermentation”, *Molecular Genetics and Genomics*, 195, 530-535.

Brien, P. J. O., Luo, W., Rogozhnikov, D., Chen, J. and Yousaf, M. N., 2015, “Spheroid and tissue assembly via click chemistry in microfluidic flow”, *Bioconjugate Chemistry*, 26, 1939–1949.

Brynildsen, M. P., Wong, W. W. and Liao, J. C., 2005, “Transcriptional regulation and metabolism”, *Biochemical Society Transactions*, 33, 6, 1423–1426.

Burke, D. J. and Church, D., 1991, “Protein synthesis requirements for nuclear division, cytokinesis, and cell separation in *Saccharomyces cerevisiae*”, *Molecular and Cellular Biology*, 11, 7, 3691–3698.

Callegaro, L., 2006, *Electrical Impedance: Principles, Measurement, and Applications*, CRC Press, Boca Raton.

Cao, H., Bissinger, R., Umbach, A. T., Gawaz, M. and Lang, F., 2017, “Temsirolimus sensitive stimulation of platelet activity, apoptosis and aggregation by collagen related peptide”, *Cellular Physiology and Biochemistry*, 42, 1252-1263.

Carman, G. M. and Henry, S. A., 1999, "Phospholipid biosynthesis in the yeast *Saccharomyces cerevisiae* and interrelationship with other metabolic processes", *Progress in Lipid Research*, 38 361-399.

Carman, G. M. and Han, G. S., 2011, "Regulation of phospholipid synthesis in the yeast *Saccharomyces cerevisiae*", *Annual Review of Biochemistry*, 7, 80, 859–883.

Cartlidge, R., Nugegoda, D. and Wlodkovic, D., 2017, "Millifluidic Lab-on-a-Chip technology for automated toxicity tests using the marine amphipod *Allorchestes compressa*", *Sensors and Actuators B : Chemical*, 239, 660–670.

Carugo, D., Capretto, L., Carugo, D., Capretto, L., Nehru, E., Mansour, M. and Bressloff, N., 2013, "A microfluidic-based arteriolar network model for biophysical and bioanalytical investigations" *Current Analytical Chemistry*, 9, 47–59.

Casal, M., Paiva, S., Queiros, O. and Soares-Silva, I., 2008, "Transport of carboxylic acids in yeasts", *Federation of European Microbiological Societies Microbiology Reviews*, 32, 974–994.

Castellví, Q., Ginestà, M. M., Capellà, G. and Ivorra, A., 2015, "Tumor growth delay by adjuvant alternating electric fields which appears non-thermally mediated", *Bioelectrochemistry*, 105, 16–24.

Cemazar, J., Miklavcic, D. and Kotnik, T., 2013, "Microfluidic devices for manipulation, modification and characterization of biological cells in electric fields--a review", *Informacije MIDEM: Journal of Microelectronics, Electronic Components and Materials*, 43, 3, 143–161.

Ceresoli, G. L., Aerts, J. G., Dziadziuszko, R., Ramlau, R., Cedres, S., van Meerbeeck, J. P. and Grosso, F., 2019, "Tumour treating fields in combination with pemetrexed and cisplatin or carboplatin as first-line treatment for unresectable malignant pleural mesothelioma (STELLAR): a multicentre, single-arm phase 2 trial", *The Lancet Oncology*, 20, 12, 1702–1709.

Cha, K. J., Hong, J. M. and Cho, D., 2013, “Enhanced osteogenic fate and function of MC3T3-E1 cells on nanoengineered polystyrene surfaces with nanopillar and nanopore arrays”, *Biofabrication*, 5, 025007.

Cha, K. J., Limb, J., Na, M. H. and Kimb, D. S., 2016, “Physically microstriped-nanoengineered polystyrene surface (PMS-NPS) for regulating cell attachment and alignment fabricated by nano-injection molding”, *Microelectronic Engineering*, 158, 11–15.

Cha, K. J., Na, M., Kim, H. W. and Kim, D. S., 2014. “Nano Petri dishes: a new polystyrene platform for Nano Petri dishes : a new polystyrene platform for studying cell-nanoengineered surface interactions”, *Journal of Micromechanics and Microengineering*, 24, 055002.

Chandrasekaran, A., Kalashnikov, N., Rayes, R., Wang, C., Spicer, J. and Moraes, C., 2017, “Thermal scribing to prototype plastic microfluidic devices, applied to study the formation of neutrophil extracellular traps”, *Lab on a Chip*, 17, 2003–2012.

Chang, T. Y., Pardo-Martin, C., Allalou, A., Wählby, C. and Yanik, M. F., 2012, “Fully automated cellular-resolution vertebrate screening platform with parallel animal processing”, *Lab on a Chip*, 12, 4, 711–716.

Chang, K. T., Chang, Y. J., Chen, C. L. and Wang, Y. N., 2015, “Multichannel lens-free CMOS sensors for real-time monitoring of cell growth”, *Electrophoresis*, 36, 3, 413–419.

Chang, Y. Y., Kao, M. C., Lin, J. A., Chen, T. Y., Cheng, C. F. and Huang, C. J., 2018, “Effects of MgSO<sub>4</sub> on inhibiting Nod-like receptor protein 3 inflammasome involve decreasing intracellular calcium”, *Journal of Surgical Research*, 221, 257-265.

Chao, T., Wang, T., Lee, C., Yiin, S., Ho, C., Wu, S. and Chern, C., 2018, “Anti-cancerous effect of inonotus taiwanensis polysaccharide extract on human acute monocytic

leukemia cells through ros-independent intrinsic mitochondrial pathway”, *International Journal of Molecular Sciences*, 19, 393.

Chaturvedi, V. and Verma, P., 2016, “Microbial fuel cell: a green approach for the utilization of waste for the generation of bioelectricity”, *Bioresources and Bioprocessing*, 3, 1, 38.

Chaudry, A., *Cell Culture*, <https://www.scq.ubc.ca/cell-culture/>, Accessed July 2021.

Chen, X., Cui, D., Liu, C., Li, H. and Chen, J., 2007, “Continuous flow microfluidic device for cell separation, cell lysis and DNA purification”, *Analytica Chimica Acta*, 584, 2, 237–243.

Chen, Y., Zhao, Y., Qiu, K., Chu, J., Lu, R., Sun, M. and Xiong, Y., 2011, “An innovative miniature microbial fuel cell fabricated using photolithography”, *Biosensors and Bioelectronics*, 26, 2841–2846.

Chen, K. C., Pan, Y. C., Chen, C. L., Lin, C. H., Huang, C. S. and Wo, A. M., 2012, “Enumeration and viability of rare cells in a microfluidic disk via positive selection approach”, *Analytical Biochemistry*, 429, 2, 116–123.

Chen, J. Y., Huang, Y. T., Chou, H. H., Wang, C. P. and Chen, C. P., 2015, “Rapid and inexpensive blood typing on thermoplastic chips”, *Lab on a Chip*, 15, 4533–4541.

Chen, F., Wei, G., Xu, J., Ma, X. and Wang, Q., 2018, “Naringin ameliorates the high glucose- induced rat mesangial cell inflammatory reaction by modulating the NLRP3 Inflammasome”, *BMC Complementary and Alternative Medicine*, 18, 192.

Chen, H., Li, J., Wan, C., Fang, Q., Bai, F. and Zhao, X., 2019, “Improvement of inhibitor tolerance in *Saccharomyces cerevisiae* by overexpression of the quinone oxidoreductase family gene YCR102C”, *Federation of European Microbiological Societies Yeast Research*, 19, foz055.

Cheung, M. C., McKenna, B., Wang, S. S., Wolf, D. and Ehrlich, D. J., 2015, “Image-based cell-resolved screening assays in flow”, *Cytometry Part A*, 87, 6, 541–548.

Chin, C. D., Linder, V. and Sia, S. K., 2012, “Commercialization of microfluidic point-of-care diagnostic devices”, *Lab on a Chip*, 12, 2118–2134.

Choi, H. S., Lee, S. Y., Kim, T. Y. and Woo, H. M., 2010, “In silico identification of gene amplification targets for improvement of lycopene production”, *Applied and Environmental Microbiology*, 76, 10, 3097–3105.

Chow, K. and Du, H., 2011, “Dielectrophoretic characterization and trapping of different waterborne pathogen in continuous flow manner”, *Sensors and Actuators A : Physical*, 170, 24–31.

Christensen, T. B., Pedersen, C. M., Bang, D. D. and Wolff, A., 2007, “Sample preparation by cell guiding using negative dielectrophoresis” *Microelectronic Engineering*, 84, 5–8, 1690–1693.

Chung, Y.-C., Jan, M.-S., Lin, Y.-C., Lin, J.-H., Cheng, W.-C. and Fan, C.-Y., 2004, “Microfluidic chip for high efficiency DNA extraction”, *Lab on a Chip*, 4, 2, 141–147.

Chung, Y. C., Wen, B. J. and Lin, Y. C. 2007, “Optimal fuzzy sliding-mode control for bio-microfluidic manipulation”, *Control Engineering Practice*, 15, 9, 1093–1105.

Chung, S. H., Baek, C., Cong, V. T. and Min, J., 2015, “The microfluidic chip module for the detection of murine norovirus in oysters using charge switchable micro-bead beating”, *Biosensors and Bioelectronics*, 67, 625–633.

Clark, P. A., Gaal, J. T., Strebe, J. K., Pasch, C. A., Deming, D. A., Kuo, J. S. and Robins, H. I., 2017, “The effects of tumor treating fields and temozolomide in MGMT expressing and non-expressing patient-derived glioblastoma cells”, *Journal of Clinical Neuroscience*, 36, 120–124.

Climent, M. Á., Torregrosa, M. D., Vázquez, S., Gironés, R. and Arranz, J. A., 2017, “Aged patients with metastatic castration resistant prostate cancer: Should we treat with chemotherapy?” *Cancer Treatment Reviews*, 55, 173–180.

Coriell Institute for Medical Research, *What is cell culture*, <https://www.coriell.org/research-services/cell-culture/what-is-cell-culture>, Accessed February 2017.

Covert, M. W., Knight, E. M., Reed, J. L., Herrgard, M. J. and Palsson, B. O., 2004, “Integrating high-throughput and computational data elucidates bacterial networks”, *Nature*, 429, 6987, 92-96.

Crawford, L., Higgins, J. and Putnam, D., 2015, “A simple and sensitive method to quantify biodegradable nanoparticle biodistribution using europium chelates”, *Scientific Reports*, 5, 1–9.

Dai, Y., Pei, X., Rahmani, M., Conrad, D. H., Dent, P. and Grant, S., 2004, “Interruption of the NF- $\kappa$ B pathway by Bay 11-7082 promotes UCN-01 – mediated mitochondrial dysfunction and apoptosis in human multiple myeloma cells”, *Neoplasia*, 103, 7, 2761–2770.

Dalby, M. J., McCloy, D., Robertson, M., Agheli, H., Sutherland, D., Affrossman, S. and Oreffo, R. O. C., 2006, “Osteoprogenitor response to semi-ordered and random nanotopographies”, *Biomaterials*, 27(15), 2980–2987.

Date, A., Pasini, P. and Daunert, S., 2010, “Integration of spore-based genetically engineered whole-cell sensing systems into portable centrifugal microfluidic platforms”, *Analytical and Bioanalytical Chemistry*, 398, 1, 349–356.

Davies, A. M., Weinberg, U. and Palti, Y., 2013, “Tumor treating fields: A new frontier in cancer therapy”, *Annals of the New York Academy of Sciences*, 1291, 1, 86–95.

de Tayrac, R., Chentouf, S., Garreau, H., Braud, C., Guiraud, I., Boudeville, P. and Vert, M., 2008, “In vitro degradation and in vivo biocompatibility of poly(lactic acid) mesh for soft tissue reinforcement in vaginal surgery”, *Journal of Biomedical Materials Research Part B*, 85, 2, 529–536.

Dean, L., 2005, *Blood and the cells it contains*, <http://www.ncbi.nlm.nih.gov/books/NBK2263/>, Accessed December 2016.

deMello, A. J., 2006, “Control and detection of chemical reactions in microfluidic systems”, *Nature*, 442, 394–402.

Dez, C., and Tollervey, D., 2004, “Ribosome synthesis meets the cell cycle”, *Current Opinion in Microbiology*, 7, 6, 631–637.

Dharmasiri, U., Balamurugan, S., Adams, A. A., Okagbare, P. I., Obubuafo, A. and Soper, S. A., 2009, “Highly efficient capture and enumeration of low abundance prostate cancer cells using prostate-specific membrane antigen aptamers immobilized to a polymeric microfluidic device”, *Electrophoresis*, 30, 18, 3289–3300.

Dharmasiri, U., Njoroge, S. K., Witek, M. A., Adebisi, M. G., Kamande, J. W., Hupert, M. L., Barany, F. and Soper, S. A., 2011, “High-throughput selection, enumeration, electrokinetic manipulation, and molecular profiling of low-abundance circulating tumor cells using a microfluidic system”, *Analytical Chemistry*, 83, 2301–2309.

Dittrich, P. S., Tachikawa, K. and Manz, A., 2006, “Micro total analysis systems. latest advancements and trends”, *Analytical Chemistry*, 78, 12, 3887–3908.

Dong, T. and Zhao, X., 2015, “Rapid identification and susceptibility testing of uropathogenic microbes via immunosorbent atp-bioluminescence assay on a microfluidic simulator for antibiotic therapy”. *Analytical Chemistry*, 87, 2410–2418.

Dupont, S., Beney, L., Ferreira, T. and Gervais, P., 2011, “Nature of sterols affects plasma membrane behavior and yeast survival during dehydration”, *Biochimica et Biophysica Acta*, 1808, 6, 1520–1528.

Dusny, C. and Gru, A., 2020, “Microfluidic single-cell analysis in biotechnology: from monitoring towards understanding”, *Science Direct*, 26–33.

Dutt, S., Kirti, S., Vaidya, T., Parkash, J. and Kashyap, S., 2018, “External application of NADPH enhances biomass accumulation, seed germination and modulates expression of oxidative pentose phosphate pathway genes in Arabidopsis”, *Indian Journal of Plant Physiology*, 23, 4, 748–759.

Ebersberger, I., Simm, S., Leisegang, M. S., Schmitzberger, P., Mirus, O., Von Haeseler, A. and Schleiff, E., 2014, “The evolution of the ribosome biogenesis pathway from a yeast perspective”, *Nucleic Acids Research*, 42, 3, 1509–1523.

Ebewele, R. O., 2000, *Polymer Science and Technology*, CRC Press, New York.

Ebrahim, A., Lerman, J. A., Palsson, B. O. and Hyduke, D. R., 2013, “COBRAPy: COntstraints-Based Reconstruction and Analysis for Python”, *BMC Systems Biology*, 7, 74.

El-ali, J., Sorger, P. K. and Jensen, K. F., 2006, “Cells on chips”, *Nature*, 442, 403–411.

Elavarasan, T., Chhina, S. K., Parameswaran, M. and Sankaran, K., 2013, “Resazurin reduction based colorimetric antibiogram in microfluidic plastic chip”, *Sensors and Actuators, B: Chemical*, 176, 174–180.

Fagone, P., Donia, M., Mangano, K., Quattrocchi, C., Mammana, S., Coco, M. and Nicoletti, F., 2013, “Comparative study of rapamycin and temsirolimus demonstrates superimposable anti-tumour potency on prostate cancer cells”, *Basic and Clinical Pharmacology and Toxicology*, 112, 1, 63–69.

Falconnet, D., Niemistö, A., Taylor, R. J., Ricicova, M., Galitski, T., Shmulevich, I. and Hansen, C. L., 2011, “High-throughput tracking of single yeast cells in a microfluidic imaging matrix”, *Lab on a Chip*, 11, 3, 466–473.

Fasullo, M. and Endres, L., 2015, “Nucleotide salvage deficiencies, dna damage and neurodegeneration”, *International Journal of Molecular Sciences*, 16, 9431–9449.

Fey, S. J. and Wrzesinski, K., 2013, “Determination of acute lethal and chronic lethal dose thresholds of valproic acid using 3d spheroids constructed from the immortal human”, *Valproic Acid*, 141–165.

Floriano, P. N., Christodoulides, N., Romanovicz, D., Bernard, B., Simmons, G. W., Cavell, M. and McDevitt, J. T., 2005, “Membrane-based on-line optical analysis system for rapid detection of bacteria and spores”. *Biosensors and Bioelectronics*, 20, 10, 2079–2088.

Fok, S., Domachuk, P., Rosengarten, G., Krause, N., Braet, F., Eggleton, B. J. and Soon, L. L., 2008, “Planar microfluidic chamber for generation of stable and steep chemoattractant gradients”, *Biophysical Journal*, 95, 3, 1523–1530.

Fuad, N. M. and Wlodkowic, D., 2013, “Microfluidic embryosort technology - towards in flow analysis, sorting and dispensing of individual vertebrate embryos”, “Proceedings of SPIE - The International Society for Optical Engineering”, 8923, 1–6.

Fukuda, J., Sakai, Y. and Nakazawa, K., 2006, “Novel hepatocyte culture system developed using microfabrication and collagen/polyethylene glycol microcontact printing”, *Biomaterials*, 27, 7, 1061–1070.

Garstecki, P., Fuerstman, M. J., Stone, A. and Whitesides, G. M., 2006, “Formation of droplets and bubbles in a microfluidic T-junction — scaling and mechanism of break-up”, *Lab on a Chip*, 6, 437–446.

Geissler, M., Beauregard, J. A., Charlebois, I., Isabel, S., Normandin, F., Voisin, B. and Veres, T., 2011, “Extraction of nucleic acids from bacterial spores using bead-based mechanical lysis on a plastic chip”, *Engineering in Life Sciences*, 11, 2, 174–181.

Gencturk, E., Mutlu, S. and Ulgen, K. O., 2017, “Advances in microfluidic devices made from thermoplastics used in cell biology and analyses”, *Biomicrofluidics*, 11, 051502.

Gencturk, E., Yurdakul, E., Celik, A. Y., Mutlu, S. and Ulgen, K. O., 2020, “Cell trapping microfluidic chip made of Cyclo olefin polymer enabling two concurrent cell biology experiments with long term durability”, *Biomedical Microdevices*, 22, 1.

Geng, T. and Lu, C., 2013, “Microfluidic electroporation for cellular analysis and delivery”, *Lab on a Chip*, 13, 3803–3821.

Genin, M., Clement, F., Fattaccioli, A., Raes, M. and Michiels, C., 2015, “M1 and M2 macrophages derived from THP-1 cells differentially modulate the response of cancer cells to etoposide”, *BMC Cancer*, 15, 1, 1–14.

Gera, N., Yang, A., Holtzman, T. S., Lee, S. X., Wong, E. T. and Swanson, K. D., 2015, “Tumor treating fields perturb the localization of septins and cause aberrant mitotic exit”, *PLoS ONE*, 10, 5, 1–20.

Gershlak, J. R., Hernandez, S., Fontana, G., Perreault, L. R., Hansen, K. J., Larson, S. A. and Gaudette, G. R., 2017, “Biomaterials crossing kingdoms : using decellularized plants as perfusable tissue engineering scaffolds”, *Biomaterials*, 125, 13–22.

Ghiasi S., M., Dahllöf, M. S., Osmail, Y. Osmail, M. and Mandrup-Poulsen, T., 2018, “Regulation of the  $\beta$ -cell inflammasome and contribution to stress-induced cellular dysfunction and apoptosis”, *Molecular and Cellular Endocrinology*, 478, 106-114.

Giladi, M., Weinberg, U., Schneiderman, R. S., Porat, Y., Munster, M., Voloshin, T., Blatt, R., Cahal, S., Itzhaki, A., Onn, A., Kirson, E. D. and Palti, Y., 2014a, “Alternating electric fields (tumor-treating fields therapy) can improve chemotherapy treatment efficacy in non-small cell lung cancer both in vitro and in vivo”, *Seminars in Oncology*, 41, 5, 6, 35-41.

Giladi, M., Schneiderman, R. S., Porat, Y., Munster, M., Itzhaki, A., Mordechovich, D. and Palti, Y., 2014b, “Mitotic disruption and reduced clonogenicity of pancreatic cancer cells in vitro and in vivo by tumor treating fields”, *Pancreatology*, 14, 54–63.

Giladi, M., Schneiderman, R. S., Voloshin, T., Porat, Y., Munster, M., Blat, R. and Palti, Y., 2015, “Mitotic spindle disruption by alternating electric fields leads to improper chromosome segregation and mitotic catastrophe in cancer cells”, *Scientific Reports*, 5, 1–16.

Girard, M. P., Osmanov, S., Assossou, O. M. and Kieny, M.-P., 2011, “Human immunodeficiency virus (HIV) immunopathogenesis and vaccine development: A review”, *Vaccine*, 29, 37, 6191–6218.

Gokdel, Y. D., Mutlu, S. and Yalcinkaya, A. D., 2010, “Self-terminating electrochemical etching of stainless steel for the fabrication of micro-mirrors”, *Journal of Micromechanics and Microengineering*, 20, 9.

Golden, J. P., Verbarq, J., Jr, P. B. H. and Ligler, F. S., 2013, “Automated processing integrated with a microflow cytometer for pathogen detection in clinical matrices”, *Biosensors and Bioelectronics*, 40, 10–16.

Gómez-herrerros, F., Rodríguez-galán, O., Morillo-huesca, M., Maya, D., Arista-romero, M., Cruz, J. De, and Muñoz-centeno, M. C., 2013, “Balanced production of ribosome components is required for proper G 1 / S transition in *Saccharomyces cerevisiae*”, *Journal of Biological Chemistry*, 288, 44, 31689–31700.

Gong, X., Yi, X., Xiao, K., Li, S., Kodzius, R., Qin, J. and Wen, W., 2010, “Wax-bonding 3D microfluidic chips”, *Lab on a Chip*, 10, 19, 2622–2627.

Goodman, G., 1994, “Global markets for chlorine and PVC: Potential impacts of greenpeace attacks”, *Journal of Vinyl and Additive Technology*, 16, 3, 156–161.

Gorsich, S. W., Dien, B. S., Nichols, N. N., Slininger, P. J., Liu, Z. L. and Skory, C. D., 2006, “Tolerance to furfural-induced stress is associated with pentose phosphate pathway

genes ZWF1, GND1, RPE1, and TKL1 in *Saccharomyces cerevisiae*”, *Applied Microbiology and Biotechnology*, 71, 339–349

Gourikutty, B. S. N., Chia-pin, C. and Puiu, D., 2016, “An integrated on-chip platform for negative enrichment of tumour cells”, *Journal of Chromatography B*, 1028, 153–164.

Gourikutty, B. S. N., Chang, C. and Daniel, P., 2016, “Microfluidic immunomagnetic cell separation from whole blood”, *Journal of Chromatography B*, 1011, 77–88.

Gross, A., Schoendube, J., Zimmermann, S., Steeb, M., Zengerle, R. and Koltay, P., 2015, “Technologies for single-cell isolation”, *International Journal of Molecular Sciences*, 16, 8, 16897–16919.

Guillamo, M. and Verrips, C. T., 2001, “The glutamate synthase (GOGAT) of *Saccharomyces cerevisiae* plays an important role in central nitrogen metabolism”, *Federation of European Microbiological Societies Yeast Research*, 1, 169–175.

Guyot, S., Ferret, E., Boehm, J. B. and Gervais, P., 2007, “Yeast cell inactivation related to local heating induced by low-intensity electric fields with long-duration pulses”, *International Journal of Food Microbiology*, 113, 2, 180–188.

Hall, M. N., 2008, “mTOR-What Does It Do?”, *Transplantation Proceedings*, 40, 10, 5–8.

Han, X., Van Berkel, C., Gwyer, J., Capretto, L. and Morgan, H., 2012, “Microfluidic lysis of human blood for leukocyte analysis using single cell impedance cytometry”, *Analytical Chemistry*, 84, 2, 1070–1075.

Han-shu, F., Ming-fei, L. and Jing, S. U. N., 2019, “New methods for cell cycle analysis”, *Chinese Journal of Analytical Chemistry*, 47, 9, 1293–1301.

Haandbæk, N., Bürgel, S. C., Rudolf, F., Heer, F. and Hierlemann, A., 2016, “Characterization of single yeast cell phenotypes using microfluidic impedance cytometry and optical imaging”, *American Chemical Society Sensors*, 1(8), 1020–1027.

Hansen, A. S., Hao, N. and OShea, E. K., 2015, “High-throughput microfluidics to control and measure signaling dynamics in single yeast cells”, *Nature Protocols*, 10, 8, 1181–1197.

Hasunuma, T., Syahidah, K., Ismail, K., Nambu, Y. and Kondo, A., 2014, “Co-expression of TAL1 and ADH1 in recombinant xylose-fermenting *Saccharomyces cerevisiae* improves ethanol production from lignocellulosic hydrolysates in the presence of furfural”, *Journal of Bioscience and Bioengineering*, 117, 2, 165–169.

Heirendt, L., Arreckx, S., Pfau, T., Mendoza, S. N., Richelle, A., Heinken, A. and Fleming, R. M. T., 2019, “Creation and analysis of biochemical constraint-based models using the COBRA Toolbox v.3.0”, *Nature Protocols*, 14, 3, 639–702.

Henry, S. A., Kohlwein, S. D. and Carman, G. M., 2012, “Metabolism and regulation of glycerolipids in the yeast *Saccharomyces cerevisiae*”, *Genetics*, 190, 317–349.

Hjortmo, S., Patring, J. and Andlid, T., 2008, “Growth rate and medium composition strongly affect folate content in *Saccharomyces cerevisiae*”, *International Journal of Food Microbiology*, 123, 93–100.

Hoek, J. A. N. B., Cahill, A. and Pastorino, J. G., 2007, “Alcohol and mitochondria: a dysfunctional relationship”, *Gastroenterology*, 122, 7, 2049–2063.

Hong, S., Hwang, I., Leed, Y. S., Parka, S., Lee, W. K. and Yua, J. W., 2013, “Restoration of ASC expression sensitizes colorectal cancer cells to genotoxic stress-induced caspase-independent cell death”, *Cancer Letters*, 331, 2, 183–191.

Hoss, F., Rodriguez-Alcazar, J. F. and Latz, E., 2017, “Assembly and regulation of ASC specks”, *Cellular and Molecular Life Sciences*, 74, 7, 1211–1229.

Huang, C. W., Cheng, J. Y., Yen, M. H. and Young, T. H., 2009, “Electrotaxis of lung cancer cells in a multiple-electric-field chip”, *Biosensors and Bioelectronics*, 24, 12, 3510–3516.

Huang, S.-B., Wang, S.-S., Hsieh, C.-H., Lin, Y. C., Lai, C.-S. and Wu, M.-H., 2013a, “An integrated microfluidic cell culture system for high-throughput perfusion three-dimensional cell culture-based assays: effect of cell culture model on the results of chemosensitivity assays”, *Lab on a Chip*, 13, 6, 1133–1143.

Huang, G., Wang, S., He, X., Zhang, X., Lu, T. J. and Xu, F., 2013b, “Helical spring template fabrication of cell-laden microfluidic hydrogels for tissue engineering”, *Biotechnology and Bioengineering*, 110, 3, 980–989.

Huang, K., Yu, L., Liu, D., Gai, L. and Wang, J., 2013c, “Modeling of yeast inactivation of PEF-treated Chinese rice wine: Effects of electric field intensity, treatment time and initial temperature”, *Food Research International*, 54, 1, 456–467.

Huang, Y., Persoone, G., Nugegoda, D. and Wlodkowic, D., 2016, “Enabling sub-lethal behavioral ecotoxicity biotests using microfluidic Lab-on-a-Chip technology”, *Sensors and Actuators B : Chemical*, 226, 289–298.

Huang, M., Bao J., Hallström, B. M., Petranovic, D. and Nielsen, J., 2017, “Efficient protein production by yeast requires global tuning of metabolism”, *Nature Communications*, 8, 1131.

Hülshager, H., Potel, J. and Niemann, E. G., 1983, “Electric field effects on bacteria and yeast cells”, *Radiation and Environmental Biophysics*, 22, 2, 149–162.

Hümmer, D., Kurth, F., Naredi-Rainer, N. and Dittrich, P. S., 2016, “Single cells in confined volumes: microchambers and microdroplets”, *Lab on a Chip*, 16, 3, 447–458.

Hyun, K., Yoon, T., Hyun, S. and Jung, H., 2015, “Two-stage micro fluidic chip for selective isolation of circulating tumor cells ( CTCs )”, *Biosensors and Bioelectronic*, 67, 86–92.

Ikeda, T., Konishi, Y. and Ichihara, A., 1976, “Transaminase of branched chain amino acids. XI. Leucine (methionine) transaminase of rat liver mitochondria”, *Biochimica et Biophysica Acta*, 445, 3, 622-631.

Ivanova, E. P., Khanh, V., Gervinskas, G., Mitik-dineva, N., Day, D., Jones, R. T. and Juodkazis, S., 2012, “Highly selective trapping of enteropathogenic *E. coli* on Fabry – Pérot sensor mirrors”, *Biosensors and Bioelectronics*, 35, 369–375.

Jackson, J. M., Witek, M. A., Hupert, M. L., Brady, C., Pullagurla, S., Kamande, J. and Soper, S. A., 2014, “UV activation of polymeric high aspect ratio microstructures: ramifications in antibody surface loading for circulating tumor cell selection”, *Lab on a Chip*, 14, 1, 106–117.

Jeon, J. S., Chung, S., Kamm, R. D. and Charest, J. L., 2011, “Hot embossing for fabrication of a microfluidic 3D cell culture platform”, *Biomedical Microdevices*, 13, 325–333.

Jeong, K. J., Wang, L., Stefanescu, C. F., Lawlor, M. W., Polat, J., Dohlman, C. H. and Kohane, D. S., 2011, “Polydopamine coatings enhance biointegration of a model polymeric implant”, *Soft Matter*, 7, 18, 8305–8312.

Jeziarski, S., Klein, A. S., Benz, C., Schaefer, M., Nagl, S. and Belder, D., 2013, “Towards an integrated device that utilizes adherent cells in a micro-free-flow electrophoresis chip to achieve separation and biosensing”, *Analytical and Bioanalytical Chemistry*, 405, 16, 5381–5386.

Jimenez, M., Miller, B. and Bridle, H. L., 2017, “Efficient separation of small microparticles at high flowrates using spiral channels: Application to waterborne pathogens”, *Chemical Engineering Science*, 157, 247–254.

Jo, M. C. and Qin, L., 2018, “Microfluidic platforms for yeast-based aging studies”, *Small*, 12, 42, 5787–5801.

Jones, M. H., Scott, J. and Member, S., 2015, “Scaling of electrode-electrolyte interface model parameters in phosphate buffered saline”, *IEEE Transactions on Biomedical Circuits and Systems*, 9, 3, 441–448.

Kakihara, Y., Makhnevych, T., Zhao, L., Tang W. and Houry, W. A., 2014, “Nutritional status modulates box C/D snoRNP biogenesis by regulated subcellular relocalization of the R2TP complex”, *Genome Biology*, 15.

Kamande, J. W., Hupert, M. L., Witek, M. A., Wang, H., Torphy, R. J., Dharmasiri, U., Njoroge, S. K., Jackson, J. M., Aufforth, R. D., Snavely, A., Yeh, J. J. and Soper, S. A., 2013, “Modular microsystem for the isolation, enumeration, and phenotyping of circulating tumor cells in patients with pancreatic cancer”, *Analytical Chemistry*, 85, 9092–9100.

Kaminski, T. S., Scheler, O. and Garstecki, P., 2016, “Droplet microfluidics for microbiology: Techniques, applications and challenges”, *Lab on a Chip*, 16, 12, 2168–2187.

Karanam, N. K., Srinivasan, K., Ding, L., Sishc, B., Saha, D. and Story, M. D., 2017, “Tumor-Treating fields elicit a conditional vulnerability to ionizing radiation via the downregulation of BRCA1 signaling and reduced DNA double-strand break repair capacity in non-small cell lung cancer cell lines”, *Cell Death and Disease*, 8, 3, e2711-10.

Kasznicki, J., Sliwinska, A. and Drzewoski, J., 2014, “Metformin in cancer prevention and therapy”, *Annals of Translational Medicine*, 6, 57.

Khorshidi, M. A., Rajeswari, P. K. P., Wählby, C., Joensson, H. N. and Svahn, H. A., 2014, “Automated analysis of dynamic behavior of single cells in picoliter droplets”, *Lab on a Chip*, 5.

Khoshmanesh, K., Akagi, J., Nahavandi, S., Kalantar-Zadeh, K., Baratchi, S., Williams, D. E. and Wlodkowic, D., 2011, “Interfacing cell-based assays in environmental scanning electron microscopy using dielectrophoresis”, *Analytical Chemistry*, 83, 8, 3217–3221.

Kim, Y., Moon, S., Kuritzkes, D. R. and Demirci, U., 2009, “Quantum dot-based HIV capture and imaging in a microfluidic channel”, *Biosensors and Bioelectronics*, 25, 253–258.

Kim, E. H., Song, H. S., Yoo, S. H. and Yoon, M., 2016, “Tumor treating fields inhibit glioblastoma cell migration, invasion and angiogenesis”, *Oncotarget*, 7, 40, 65125–65136.

Kim, J. and Guan, K. L., 2019, “mTOR as a central hub of nutrient signalling and cell growth”, *Nature Cell Biology*, 21, 1, 63–71.

Kirson, E. D., Gurvich, Z., Schneiderman, R., Dekel, E., Itzhaki, A., Wasserman, Y. and Palti, Y., 2004, “Disruption of cancer cell replication by alternating electric fields”, *Cancer Research*, 64, 9, 3288–3295.

Kirson, E. D., Dbalý, V., Tovaryš, F., Vymazal, J., Soustiel, J. F., Itzhaki, A. and Palti, Y., 2007, “Alternating electric fields arrest cell proliferation in animal tumor models and human brain tumors”, *Proceedings of the National Academy of Sciences of the United States of America*, 104, 24, 10152–10157.

Kirson, E. D., Giladi, M., Gurvich, Z., Itzhaki, A., Mordechovich, D., Schneiderman, R. S. and Palti, Y. 2009a, “Alternating electric fields (TFields) inhibit metastatic spread of solid tumors to the lungs” *Clinical and Experimental Metastasis*, 26, 7, 633–640.

Kirson, E. D., Schneiderman, R. S., Dbalý, V., Tovaryš, F., Vymazal, J., Itzhaki, A. and Palti, Y., 2009b, “By adjuvant alternating electric fields ( TFields )”, *BMC Medical Physics*, 13, 1–13.

Kitazawa, M., Hida, S., Fujii, C., Taniguchi, S., Ito, K., Matsumura, T. and Miyagawa, S., 2017, “ASC induces apoptosis via activation of caspase-9 by enhancing gap junction-mediated intercellular communication”, *Plos ONE*, 1–14.

Klug, L. and Daum, G., 2014 “Yeast lipid metabolism at a glance”, *Federation of European Microbiological Societies Yeast Research*, 14, 369–388.

Klümper, H. J., Beijnen, J. H., Gurney, H. and Schellens, J. H. M., 2010, “Inhibitors of mTOR”, *The Oncologist*, 15, 1262–1269.

Koh, C. G., Zhang, X., Liu, S., Golan, S., Yu, B., Yang, X. and Lee, L. J., 2010, “Delivery of antisense oligodeoxyribonucleotide lipopolyplex nanoparticles assembled by microfluidic hydrodynamic focusing”, *Journal of Controlled Release*, 141, 1, 62–69.

Koonin, E. V., Senkevich, T. G. and Dolja, V. V., 2006, “The ancient virus world and evolution of cells”, *Biology Direct*, 27, 1–27.

Kricka, L. J., Fortina, P., Panaro, N. J., Wilding, P., Alonso-Amigoc G. and Becker, H., 2002, “Fabrication of plastic microchips by hot embossing”, *Lab on a Chip*, 1.

Krishnan, N., Bencze, G., Cohen, P. and Tonks, N. K., 2013, “The anti-inflammatory compound BAY 11-7082 is a potent inhibitor of Protein Tyrosine Phosphatases”, *Federation of European Biochemical Societies Journal*, 280, 12, 2830–2841.

Kumeria, T., Kurkuri, M. D., Diener, K. R., Parkinson, L. and Losic, D., 2012, “Label-free reflectometric interference microchip biosensor based on nanoporous alumina for detection of circulating tumour cells”, *Biosensors and Bioelectronics*, 35, 1, 167–173.

Kummrow, A., Theisen, J., Frankowski, M., Tuchscheerer, a, Yildirim, H., Brattke, K. and Neukammer, J., 2009, “Microfluidic structures for flow cytometric analysis of hydrodynamically focussed blood cells fabricated by ultraprecision micromachining”, *Lab on a Chip*, 9, 7, 972–981.

Kunin, C. M., 1996, “Antimicrobial Activity of Rifabutin”, *Clinical Infectious Diseases*, 22, 3-14.

Laczka, O., Maesa, J., Godino, N., Fougthansen, M., Kutter, J. P., Snakenborg, D. and Baldrich, E., 2011, “Improved bacteria detection by coupling magneto-immunocapture

and amperometry at flow-channel microband electrodes”, *Biosensors and Bioelectronics*, 26, 3633–3640.

La Ferla, M., Mercatanti, A., Rocchi, G., Lodovichi, S., Cervelli, T., Pignata, L. and Galli, A., 2015, “Expression of human poly ( ADP-ribose ) polymerase 1 in *Saccharomyces cerevisiae* : Effect on survival , homologous recombination and identification of genes involved in intracellular localization”, *Mutation Research - Fundamental and Molecular Mechanisms of Mutagenesis*, 774, 14–24.

Lafontaine, D. L. J. and Tollervey, D., 2000, “Synthesis and assembly of the box C+D small nucleolar RNPs”, *Molecular and Cellular Biology*, 20, 8, 2650–2659.

Lamkanfi, M. and Dixit, V. M., 2009, “Inflammasomes: guardians of cytosolic sanctity”, *Immunological Reviews*, 95–105.

Lamkanfi, M. and Kanneganti, T. D., 2010, “Nlrp3: an immune sensor of cellular stress and infection”, *International Journal of Biochemistry & Cell Biology*, 42, 6, 792–795.

Larhlimi, A., David, L., Selbig, J. and Bockmayr, A., 2012, “F2C2 : a fast tool for the computation of flux coupling in genome-scale metabolic networks”, *BMC Bioinformatics*, 13, 57.

Leahy, S. and Lai, Y., 2017, “A cantilever biosensor exploiting electrokinetic capture to detect *Escherichia coli* in real time”, *Sensors and Actuators B : Chemical*, 238, 292–297.

Leary, D. J. and Huang, S., 2001, “Regulation of ribosome biogenesis within the nucleolus”, *Federation of European Biochemical Societies Letters*, 509, 2, 145–150.

Lee, S. H., Ou, M. C., Chen, T. Y. and G.B. Lee, G. B., 2007, “Integrated microfluidic chip for fast diagnosis of piscine nodavirus”, *IEEE*, Lyon, 10-14 June 2007, 1, 943–946.

Lee, J., Soper, S. A. and Murray, K. K., 2009, “Development of an efficient on-chip digestion system for protein analysis using MALDI-TOF MS”. *The Analyst*, 134, 12, 2426–2433.

Lee, J., Rhee, M. H., Kim, E. and Cho, J. Y., 2012, “BAY 11-7082 is a broad-spectrum inhibitor with anti-inflammatory activity against multiple targets”, *Mediators in Inflammation*, 2012.

Lee, A., Park, J., Lim, M., Sunkara, V., Kim, S. Y., Kim, G. H. and Cho, Y., 2014, “All-in-one centrifugal microfluidic device for size-selective circulating tumor cell isolation with high purity”, *Analytical Chemistry*, 86, 11349–11356.

Legras, J. L., Merdinoglu, D., Cornuet, J. M. and Karst, F., 2007, “Bread, beer and wine: *Saccharomyces cerevisiae* diversity reflects human history”, *Molecular Ecology*, 16, 10, 2091–2102.

Lelevich, S. V., Khrustalev, V. V. and Barkovsky, E. V., 2013, “Inhibition of rat muscle and liver phosphofructokinases by high doses of ethanol”, *Biochemistry Research International*, 2013.

Lempiainen, H. and Shore, D., 2009, “Growth control and ribosome biogenesis”, *Current Opinion in Cell Biology*, 21, 855–863.

Lewis, N. E., Hixson, K. K., Conrad, T. M., Lerman, J. A., Charusanti, P., Polpitiya, A. D. and Palsson, B. Ø., 2010, “Omic data from evolved *E. coli* are consistent with computed optimal growth from genome-scale models”, *Molecular Systems Biology*, 6, 390.

Li, X., Zhang, X., Zhao, S., Wang, J., Liu, G. and Du, Y., 2014, “Micro-scaffold array chip for upgrading cell-based high-throughput drug testing to 3D using benchtop equipment”, *Lab on a Chip*, 14, 3, 471–481.

Li, J., Huang, Y., Gao, Y., Wu, H., Dong, W. and Liu, L., 2016, “Antibiotic drug rifabutin is effective against lung cancer cells by targeting the eIF4E- b -catenin axis”, *Biochemical and Biophysical Research Communications*, 472, 299–305.

Liang, J., Mok, A. W., Zhu, Y. and Shi, J., 2013, “Resonance versus linear responses to alternating electric fields induce mechanistically distinct mammalian cell death”, *Bioelectrochemistry*, 94, 61–68.

Liberale, C., Cojoc, G., Bragheri, F., Minzioni, P., Perozziello, G., La Rocca, R. and Cristiani, I., 2013, “Integrated microfluidic device for single-cell trapping and spectroscopy”, *Scientific Reports*, 3, 1258.

Limongi, T., Lizzul, L., Giugni, A., Tirinato, L., Pagliari, F., Tan, H. and Torre, B., 2017, “Injection molder for the fabrication of polymeric porous poly-epsilon-caprolactone scaffolds for preliminary mesenchymal stem cells tissue engineering applications”, *Microelectronic Engineering*, 175, 12–16.

Lin, Y., Jen, C., Huang, M., Wu, C. and Lin, X., 2001, “Electroporation microchips for continuous gene transfection”, *Sensors and Actuators B*, 79, 137–143.

Lin, Y. S., Yang, C. H., Lu, K., Huang, K. S. and Zheng, Y. Z., 2011, “Synthesis of agar microparticles using temperature-controlled microfluidic devices for *Cordyceps militaris* cultivation”, *Electrophoresis*, 32, 22, 3157–3163.

Lin, H., Huang, C., Lu, S., Kuo, I. and Chau, L., 2014, “Direct detection of orchid viruses using nanorod-based fiber optic particle plasmon resonance immunosensor”, *Biosensors and Bioelectronics*, 51, 371–378.

Lin, H. Y., Chang, Y. Y., Kao, M. C. and Huang, C. J., 2017, “Naloxone inhibits nod-like receptor protein 3 inflammasome”, *Trauma and Critical Care*, 219, 72-77.

Liu, Z. L., Moon, J., Andersh, B. J., Slininger, P. J. and Weber, S., 2008, “Multiple gene-mediated NAD ( P ) H-dependent aldehyde reduction is a mechanism of in situ detoxification of furfural and 5-hydroxymethylfurfural by *Saccharomyces cerevisiae*”, *Applied Microbiology and Biotechnology*, 81, 743–753.

Liu, Z. L., Ma, Æ. M. and Song, Æ. M., 2009, “Evolutionarily engineered ethanologenic yeast detoxifies lignocellulosic biomass conversion inhibitors by reprogrammed pathways”, *Molecular Genetics and Genomics*, 282, 233–244.

Liu, Q. I. U. Y. U. E., Han, F. E. N., Pan, L. I. P., Jia, H. Y. A. N., Li, Q. I. and Zhang, Z. D. E., 2018, “Inflammation responses in patients with pulmonary tuberculosis in an intensive care unit”, *Experimental and Therapeutic Medicine*, 15, 2719–2726.

Logan, B. E., Hamelers, B., Rozendal, R., Schröder, U. and Rabaey, K., 2006, “Microbial fuel cells: methodology and technology”, *Environmental Science & Technology*, 40, 5181– 5192.

Lok, K. S., Kwok, Y. C., Lee, P. P. F. and Nguyen N. T., 2012, “Ferrofluid plug as valve and actuator for whole-cell PCR on chip”, *Sensors and Actuators B*, 166– 167, 893–897.

Longsine-Parker, W., Wang, H., Koo, C., Kim, J., Kim, B., Jayaramane, A. and Han, A., 2013, “Microfluidic electro-sonoporation: a multi-modal cell poration methodology through simultaneous application of electric field and ultrasonic wave”, *Lab on a Chip*, 13, 2144–2152.

Lu, A., Magupalli, V. G., Ruan, J., Yin, Q. and Egelman, E. H., 2014, “Unified polymerization mechanism for the assembly of ASC dependent inflammasomes”, *Cell Press*, 13, 156, 6, 1193–1206.

Lucchetta, G., Sorgato, M. and Zanchetta, E., 2015, “Effect of injection molded micro-structured polystyrene surfaces on proliferation of MC3T3-E1 cells”, *Express Polymer Letters*, 9, 4, 354–361.

Ma, M. and Liu, Z. L., 2010, “Comparative transcriptome profiling analyses during the lag phase uncover YAP1 , PDR1 , PDR3 , RPN4 , and HSF1 as key regulatory genes in genomic adaptation to the lignocellulose derived inhibitor HMF for *Saccharomyces cerevisiae*”, *BMC Genomics*, 11, 1, 660.

Ma, Z., Zheng, Y., Cheng, Y., Xie, S. and Ye, X., 2016, “Development of an integrated micro fluidic electrostatic sampler for bioaerosol”, *Journal of Aerosol Science*, 95, 84–94.

Madhusudana, S. N., Sundaramoorthy, S. and Ullas, P. T., 2010, “Utility of human embryonic kidney cell line HEK-293 for rapid isolation of fixed and street rabies viruses: comparison with Neuro-2a and BHK-21 cell lines”. *International Journal of Infectious Diseases*, 14, 12, e1067–e1071.

Madigan, M., Bender, K., Buckley, D., Sattley, W. and Stahl, D., 2018, *Brock Biology of Microorganisms*, 15<sup>th</sup> edition, Pearson Education Limited.

Maier, A., Vo, B., Boles, E. and Fuhrmann, F., 2002, “Characterisation of glucose transport in *Saccharomyces cerevisiae* with plasma membrane vesicles (countertransport) and intact cells Gal2 transporters”, *Federation of European Microbiological Societies Yeast Research*, 2, 539–550.

Manji, G. A., Wang, L. and Geddes, B. J., 2002, “PYPAF1, a PYRIN-containing Apaf1-like protein that assembles with ASC and regulates activation of NF- $\kappa$ B, *Journal of Biological Chemistry*, 11570-11575.

Mardanpour, M. M. and Yaghmaei, S., 2016, “Characterization of a microfluidic microbial fuel cell as a power generator based on a nickel electrode”, *Biosensors and Bioelectronics*, 79, 327–333.

Mardanpour, M. M. and Yaghmaei, S., 2017, “Dynamical analysis of microfluidic microbial electrolysis cell via integrated experimental investigation and mathematical modeling”, *Electrochimica Acta*, 227, 317–329.

Marinkovic, Z. S., Vulin, C., Acman, M., Song, X., Di Meglio, J. M., Lindner, A. B. and Hersen, P., 2019, “A microfluidic device for inferring metabolic landscapes in yeast monolayer colonies”, *eLIFEsciences*, 8, e47951.

Mark, D., Haeberle, S., Roth, G., von Stetten, F. and Zengerle, R., 2010, "Microfluidic lab-on-a-chip platforms: requirements, characteristics and applications", *Chemical Society Reviews*, 39, 3, 1153.

Mashaghi, S., Abbaspourrad, A., Weitz, D. A. and Oijen, A. M. Van., 2016, "Droplet microfluidics: A tool for biology, chemistry and nanotechnology", *Trends in Analytical Chemistry*, 82, 118–125.

Matlock-colangelo, L., Coon, B., Pitner, C. L., Frey, M. W. and Baeumner, A. J., 2016, "Functionalized electrospun poly (vinyl alcohol) nanofibers for on-chip concentration of E . coli cells", *Analytical and Bioanalytical Chemistry*, 408, 1327–1334.

Matsuura, K., Takenami, M. and Kuroda, Y., 2012, "Screening of sperm velocity by fluid mechanical characteristics of a cyclo-olefin polymer microfluidic sperm-sorting device", *Reproductive BioMedicine Online*, 24, 1, 109–115.

Matteucci, M., Lakshmikanth, T., Shibu, K., De Angelis, F., Schadendorf, D., Venuta, S. and Di Fabrizio, E., 2007, "Preliminary study of micromechanical stress delivery for cell biology studies", *Microelectronic Engineering*, 84, 5–8, 1729–1732.

Mauk, M. G., Chiou, R., Genis, V. and Carr, E., 2013, "Image analysis of microfluidics: visualization of flow at the microscale", *120<sup>th</sup> ASEE Annual Conference and Exposition*, Atlanta, June 23-26.

Mayer, C. and Grummt, I., 2006, "Ribosome biogenesis and cell growth: mTOR coordinates transcription by all three classes of nuclear RNA polymerases", *Oncogene*, 25, 48, 6384–6391.

McCann, R., Bagga, K., Stalcup, A., Vázquez, M. and Brabazon, D., 2015, "Laser micro-engineering of functionalised cyclic olefin polymers for microfluidic applications", *Laser-based Micro- and Nanoprocessing*, 9351.

Megchelenbrink, W., Huynen, M. and Marchiori, E., 2014, “optGpSampler: An improved tool for uniformly sampling the solution-space of genome-scale metabolic networks”, *Plos One*, 9, 2, e86587.

Mehta, G., Lee, J., Cha, W., Tung, Y. C., Linderman, J. J. and Takayama, S., 2009, “Hard top soft bottom microfluidic devices for cell culture and chemical analysis”, *Analytical Chemistry*, 81, 10, 3714–3722.

Mehta, M., Wen, P., Nishikawa, R., Reardon, D. and Peters, K., 2017, “Critical review of the addition of tumor treating fields (TTFields) to the existing standard of care for newly diagnosed glioblastoma patients”, *Critical Reviews in Oncology / Hematology*, 111, 60–65.

Memmolò, P., Miccio, L., Merola, F., Gennari, O., Netti, P. A. and Ferraro, P., 2014, “3D morphometry of red blood cells by digital holography”, *Cytometry Part A*, 85, 12, 1030–1036.

Miller, P. G. and Shuler, M. L., 2016, “Design and demonstration of a pumpless 14 compartment microphysiological system”, *Biotechnology and Bioengineering*, 113, 10, 2213–2227.

Mills, E. W. and Green, R., 2017, “Ribosomopathies: There’s strength in numbers”, *Science* 358, 608.

Minn, A. J. and Wherry, E. J., 2016, “Minireview combination cancer therapies with immune checkpoint blockade: convergence on interferon signaling”, *Cell*, 165, 2, 272–275.

Mitchell, P., Petfalski, E., Houalla, R., Podtelejnikov, A., Mann, M. and Tollervey, D., 2003, “Rrp47p is an exosome-associated protein required for the 3’ processing of stable RNAs”, *Molecular and Cellular Biology*, 23, 19, 6982–6992.

Montagud, A., Zelezniak, A., Navarro, E., Fernández de Córdoba, P., Urchueguía, J. F. and Patil, K. R., 2011, “Flux coupling and transcriptional regulation within the metabolic

network of the photosynthetic bacterium *Synechocystis* sp. PCC6803”, *Biotechnology Journal*, 6, 330–342.

Moon, S., Onur, H., Ozcan, A., Khademhosseini, A., Hæggstrom, E., Kuritzkes, D. and Demirci, U., 2009, “Integrating microfluidics and lensless imaging for point-of-care testing”, *Biosensors and Bioelectronics*, 24, 3208–3214.

Morant-miñana, M. C. and Elizalde, J., 2015, “Microscale electrodes integrated on COP for real sample *Campylobacter* spp. Detection”, *Biosensors and Bioelectronic*, 70, 491–497.

Mottet, G., Perez-toralla, K., Tulukcuoglu, E., Bidard, F., Pierga, J., Bidard, F. and Viovy, J. L., 2014, “A three dimensional thermoplastic microfluidic chip for robust cell capture and high resolution imaging”, *Biomicrofluidics*, 8, 024109.

Mrugala, M. M., Engelhard, H. H., Tran, D. D., Kew, Y., Cavaliere, R., Villano, J. L., Bota, D. A., Rudnick, J., Sumrall, A. L., Zhu, J. J. and Butowskik, N., 2014, “Clinical practice experience with novottf-100a system for glioblastoma: the patient registry dataset (PRiDe)”, *Seminars in Oncology*, 41, 5, 6, 4-13.

Muefong, C. N. and Sutherland, J. S., 2020, “Neutrophils in tuberculosis- associated inflammation and lung pathology”, *Frontiers in Immunology*, 1–9.

Mukherjee, S., Su, S., Panmanee, W., Irvin, R. T., Hassett, D. J. and Choi, S., 2013, “A microliter-scale microbial fuel cell array for bacterial electrogenic screening”, *Sensors and Actuators A : Physical*, 201, 532–537.

Mulligan, M. K. and Rothstein, J. P., 2011, “The effect of confinement-induced shear on drop deformation and breakup in microfluidic extensional flows”, *Physics of Fluids*, 23, 022004.

Mun, E. J., Babiker, H. M., Weinberg, U., Kirson, E. D. and Hoff, D. D. Von., 2017, “Tumor-treating fields: a fourth modality in cancer treatment”, *Clinical Cancer Research*, 1–11.

Nagai, H. and Fuchiwaki, Y., 2015, “Portable microfluidic system for rapid genetic testing”, *Electronics and Communications in Japan*, 98, 12, 510–514.

Navawongse, R., Choudhury, D., Raczowska, M., Stewart, J. C., Lim, T., Rahman, M. and Claridge-Chang, A., 2016, “Drosophila learn efficient paths to a food source”, *Neurobiology of Learning and Memory*, 131, 176–181.

Nery, E. W., Kamil, Ź., Wróblewski, W., Chudy, M. and Ciosek, P., 2014, “Biosensors and Bioelectronics Flow-through sensor array applied to cytotoxicity assessment in cell cultures for drug-testing purposes”, *Biosensors and Bioelectronics*, 51, 55–61.

Ngamsom, B., Esfahani, M. M. N., Phurimsak, C., Lopez-martinez, M. J., Raymond, J., Broyer, P. and Pamme, N., 2016, “Multiplex sorting of foodborne pathogens by on-chip free-flow magnetophoresis”, *Analytical Chimica Acta*, 918, 69–76.

Nissan, T. A., Baûler, J., Petfalski, E., Tollervey, D. and Hurt, E., 2002, “60S pre-ribosome formation viewed from assembly in the nucleolus until export to the cytoplasm”, *The European Molecular Biology Organization Journal*, 21, 20, 5539–5547.

Nomura, T., Miyazaki, J., Miyamoto, A., Kuriyama, Y., Tokumoto, H. and Konishi, Y., 2013, “Exposure of the yeast *Saccharomyces cerevisiae* to functionalized polystyrene latex nanoparticles: influence of surface charge on toxicity”, *Environmental Science & Technology*, 47, 3417–3423.

Notebaart, R. A., Teusink, B. and Siezen, R. J., 2008, “Co-regulation of metabolic genes is better explained by flux coupling than by network distance”, *PLoS Computational Biology*, 4, 1, e26.

Nourizad, N., Ehn, M., Gharizadeh, B., Hober, S. and Nyrén, P., 2003, "Methylotrophic yeast *Pichia pastoris* as a host for production of ATP-diphosphohydrolase (apyrase) from potato tubers (*Solanum tuberosum*)", *Protein Expression and Purification*, 27, 2, 229-237.

Nunes, P. S., Ohlsson, P. D., Ordeig, O. and Kutter, J. P., 2010, "Cyclic olefin polymers: Emerging materials for lab-on-a-chip applications", *Microfluidics and Nanofluidics*, 9, 2-3, 145-161.

Nwankire, C. E., Venkatanarayanan, A., Glennon, T., Keyes, T. E., Forster, R. J. and Ducreé, J., 2015, "Label-free impedance detection of cancer cells from whole blood on an integrated centrifugal microfluidic platform", *Biosensors and Bioelectronics*, 68, 382-389.

Odabasi, I. E., Gencturk, E., Puza, S., Mutlu, S. and Ulgen, K. O., 2018, "A low cost PS based microfluidic platform to investigate cell cycle towards developing a therapeutic strategy for cancer", *Biomedical Microdevices*, 1-13.

Oliveira, L., Nakayasu, E. S., Joffe, L. S., Guimara, A. J., Nimrichter, L. and Rodrigues, M. L., 2010a, "Characterization of yeast extracellular vesicles: evidence for the participation of different pathways of cellular traffic in vesicle biogenesis", *PloS One*, 5, 6, e11113.

Oliveira, D. L., Nakayasu, E. S., Joffe, L. S., Guimarães, A. J., Sobreira, T. J. P., Nosanchuk, J. D. and Rodrigues, M. L., 2010b, "Biogenesis of extracellular vesicles in yeast", *Communicative & Integrative Biology*, 533-535.

Orth, J. D., Thiele, I. and Palsson, B. Ø., 2011, "What is flux balance analysis?", *Nature Biotechnology*, 28, 3, 245-248.

Ou, Q., Nikolic-jaric, M. and Gänzle, M., 2017, "Mechanisms of inactivation of *Candida humilis* and *Saccharomyces cerevisiae* by pulsed electric fields", *Bioelectrochemistry*, 115, 47-55.

Palsson, B. O., 2015, *Systems Biology Constraint-based Reconstruction and Analysis*, Cambridge University Press, Cambridge.

Pandya, H. J., Kanakasabapathy, M. K., Verma, S., Chug, M. K., Memic, A., Gadjeva, M. and Shafiee, H., 2017, “Label-free electrical sensing of bacteria in eye wash samples: A step towards point-of-care detection of pathogens in patients with infectious keratitis”, *Biosensors and Bioelectronics*, 91, 32–39.

Pantel, K. and Alix-Panabières, C., 2012, “Detection methods of circulating tumor cells”, *Journal of Thoracic Disease*, 4, 5, 446–447.

Papin, J. A., Hunter, T., Palsson, B. O., Subramaniam, S. and Pines, N. T., 2005, Reconstruction of cellular signalling networks and analysis of their properties, *Molecular Cell Biology*, 6, 99–111.

Park, T., Park, D. S. and Murphy, M. C., 2011, “High flow rate capture of circulating tumor cells using a small footprint polymer device”, *15<sup>th</sup> International Conference on Miniaturized Systems for Chemistry and Life Sciences*, Seattle/Washington, October 2-6, 1185–1187.

Park, S., Min, H., Kyoung, Y., Min, S., Chan, J., Lee, O. and Seo, J., 2011, “Bioresource Technology Expression of aldehyde dehydrogenase 6 reduces inhibitory effect of furan derivatives on cell growth and ethanol production in *Saccharomyces cerevisiae*”, *Bioresource Technology*, 102, 10, 6033–6038.

Park, J. M., Park, H. M., Kim, W. J., Kim, H. U., Kim, T. Y. and Lee, S. Y., 2012, “Flux variability scanning based on enforced objective flux for identifying gene amplification targets”, *BMC Systems Biology*, 6, 106.

Paul, M. J., 2013, “Photosynthetic carbon dioxide fixation”, *Encyclopedia of Biological Chemistry*, 497-502.

Pavesi, A., Adriani, G., Tay, A., Warkiani, M. E., Yeap, W. H., Wong, S. C. and Kamm, R. D., 2016, “Engineering a 3D microfluidic culture platform for tumor-treating field application”, *Scientific Reports*, 6, 1–10.

Penaherrera, A., Payes, C., Sierra-Rodero, M., Vega, M., Rosero, G., Lerner, B. and Perez, M. S., 2016, “Evaluation of cell culture in microfluidic chips for application in monoclonal antibody production”, *Microelectronic Engineering*, 158, 126–129.

Pinheiro, M., Caio, M., Moiteiro, C., Lu, M., Brezesinski, G. and Reis, S., 2013, “The influence of rifabutin on human and bacterial membrane models: implications for its mechanism of action”, *The Journal of Physical Chemistry B*, 117, 6187–6193.

Piruska, A., Nikcevic, I., Lee, S. H., Ahn, C., Heineman, W. R., Limbach, P. A. and Seliskar, C. J., 2005, “The autofluorescence of plastic materials and chips measured under laser irradiation”, *Lab on a Chip*, 5, 12, 1348–1354.

Pless, M., Droege, C., von Moos, R., Salzberg, M. and Betticher, D., 2013, “A phase I/II trial of tumor treating fields (TTFields) therapy in combination with pemetrexed for advanced non-small cell lung cancer” *Lung Cancer*, 81, 3, 445–450.

Pohl, H. A., 1978, *Dielectrophoresis: The Behavior of Neutral Matter in Nonuniform Electric Fields*, Cambridge University Press, Cambridge.

Polouliakh, N., 2019, *In Silico Transcription Factor Discovery via Bioinformatics Approach: Application on iPSC Reprogramming Resistant Genes*, Academic Press.

Polymenis, M. and Aramayo, R., 2015, “Translate to divide: control of the cell cycle by protein synthesis”, *Microbial Cell*, 2, 4, 94–104.

Porat, Y., Giladi, M., Schneiderman, R. S., Blat, R., Shteingauz, A., Zeevi, E. and Palti, Y., 2017, “Determining the optimal inhibitory frequency for cancerous cells using tumor treating fields (TTFields)”, *Journal of Visualized Experiments*, 123, 1–8.

Powers, T. and Walter, P., 1999, "Regulation of ribosome biogenesis by the rapamycin-sensitive TOR-signaling pathway in *Saccharomyces cerevisiae*", *Molecular Biology of the Cell*, 10, 4, 987–1000.

Pucihar, G., Krmelj, J., Reberč, M., Napotnik, T. B. and Miklavč, D., 2011, "Equivalent pulse parameters for electroporation", *IEEE Transactions on Biomedical Engineering*, 58, 11, 3279–3288.

Pujol-Vila, F., Giménez-Gómez, P., Santamaria, N., Antúnez, B., Vigués, N., Díaz-González, M. and Muñoz-Berbel, X., 2016, "Portable and miniaturized optofluidic analysis system with ambient light correction for fast in situ determination of environmental pollution", *Sensors and Actuators B: Chemical*, 222, 55–62.

Puza, S., Gencturk, E., Odabasi, I. E., Iseri, E., Mutlu, S. and Ulgen, K. O., 2017, "Fabrication of cyclo olefin polymer microfluidic devices for trapping and culturing of yeast cells", *Biomedical Microdevices*, 19, 2, 40.

Qiu, X., De Jesus, J., Pennell, M., Troiani, M. and Haun, J. B., 2015, "Microfluidic device for mechanical dissociation of cancer cell aggregates into single cells", *Lab on a Chip*, 15, 1, 339–350.

Queiroz, J. H. De, Uribelarrea, J., Pareilleux, A., Biotechnologie-microbiologie, C. D. T. and Alimentaire, D. D. G. B., 1993, Estimation of the energetic biomass yield and efficiency of oxidative phosphorylation in cell-recycle cultures of *Schizosaccharomyces pombe*, *Applied Microbiology and Biotechnology*, 39, 609-614.

Raasch, M., Rennert, K., Jahn, T., Peters, S., Henkel, T., Huber, O. and Mosig, A., 2015, "Microfluidically supported biochip design for culture of endothelial cell layers with improved perfusion conditions", *Biofabrication*, 7, 1.

Rahimnejad, M., Adhami, A., Darvari, S., Zirepour, A. and Oh, S.-E., 2015, "Microbial fuel cell as new technology for bioelectricity generation: a review", *Alexandria Engineering Journal*, 54, 3, 745–756.

Rauert-wunderlich, H., Siegmund, D., Maier, E., Giner, T., Bargou, R. C., Wajant, H. and Stü, T., 2013, “The IKK inhibitor Bay 11-7082 induces cell death independent from inhibition of activation of NFκB transcription factors”, *Plos One*, 8, 3, 1–10.

Ravi, M., Paramesh, V., Kaviya, S. R., Anuradha, E. and Paul Solomon, F. D., 2015, “3D cell culture systems: Advantages and applications”, *Journal of Cellular Physiology*, 230, 1, 16–26.

Rawls, K. D., Dougherty, B. V., Blais, E. M., Stancli, E., Kolling, G. L., Vinnakota, K. and Papin, J. A., 2019, “A simplified metabolic network reconstruction to promote understanding and development of flux balance analysis tools”, *Computers in Biology and Medicine*, 105, 64–71.

Reed, J. L., Famili, I., Thiele, I. and Palsson, B. O., 2006, “Towards multidimensional genome annotation”, *Nature*, 7, 130–141.

Reinholt, S. J., Behrent, A., Greene, C., Kalfe, A. and Bäumner, A. J., 2014, “Isolation and amplification of mrna within a simple microfluidic lab on a chip”, *Analytical Chemistry*, 86, 849–856.

Renne, M. F. and Kroon, A. I. P. M. De., 2018, “The role of phospholipid molecular species in determining the physical properties of yeast membranes”, *Federation of European Biochemical Societies Letters*, 592, 1330–1345.

Revuelta, J. L., Serrano-amatriain, C., Ledesma-amaro, R. and Jiménez, A., 2018, “Formation of folates by microorganisms: towards the biotechnological production of this vitamin”, *Applied Microbiology and Biotechnology*, 102, 8613–8620.

Reznik, E., Mehta, P. and Segre, D., 2013, “Flux imbalance analysis and the sensitivity of cellular growth to changes in metabolite pools”, *PLOS Computational Biology*, 9, 8.

Rini, B. I., 2008, “Temsirrolimus, an inhibitor of mammalian target of rapamycin”, *Clinical Cancer Research*, 14, 5, 1286–1291.

Rivera, F., Benavides, M., Gallego, J. and Guillen-ponce, C., 2019, “Tumor treating fields in combination with gemcitabine or gemcitabine plus nab-paclitaxel in pancreatic cancer : Results of the PANOVA phase 2 study”, *Pancreatology*, 19, 64–72.

Rosenzweig, D. H., Carelli, E., Steffen, T. and Jarzem, P., 2015, “3D-Printed ABS and PLA scaffolds for cartilage and nucleus pulposus tissue regeneration”, *International Journal of Molecular Sciences*, 16, 15118–15135.

Roslan, H. A., Hossain, A. and Gerunsin, J., 2017, “Molecular and 3D-Structural characterization of fructose- 1 , 6-bisphosphate aldolase derived from metroxylon sagu”, *Brazilian Archives of Biology and Technology*, 60, e17160108.

Rothert, A., Deo, S. K., Millner, L., Puckett, L. G., Madou, M. J. and Daunert, S., 2005, Whole-cell-reporter-gene-based biosensing systems on a compact disk microfluidics platform, *Analytical Biochemistry*, 342, 11–19.

Runge, T., Sackmann, J., Karl, W., Lars, S. and Blank, M., 2017, “Ultrasonically manufactured microfluidic device for yeast analysis”, *Microsystem Technologies*, 23, 6, 2139–2144.

Russo, A. and Russo, G., 2017, “Ribosomal proteins control or bypass p53 during nucleolar stress”, *International Journal of Molecular Sciences*, 18, 1, 1–16.

Sadr, N., Zhu, M., Osaki, T., Kakegawa, T., Yang, Y., Moretti, M. and Khademhosseini, A., 2011, “SAM-based cell transfer to photopatterned hydrogels for microengineering vascular-like structures”, *Biomaterials*, 32(30), 7479–7490.

Sakai, Y., Yoshiura, Y. and Nakazawa, K., 2011a, “Embryoid body culture of mouse embryonic stem cells using microwell and micropatterned chips Gelatin spot Medium Medium Medium Medium”, *Journal of Bioscience and Bioengineering*, 111, 1, 85–91.

Sakai, Y. and Nakazawa, K., 2011b, “Biochips & tissue chips novel microchip technique for the transfer of spheroids as floating cultures to micropatterned-adherent cultures”, *Biochips & Tissue chips*, 3–7.

Sano, M. B., Salmanzadeh, A. and Davalos, R. V., 2012, “Multilayer contactless dielectrophoresis: Theoretical considerations”, *Electrophoresis*, 33, 13, 1938–1946.

Sasindran, S. J. and Torrelles, J. B., 2011, “Mycobacterium tuberculosis infection and inflammation: what is beneficial for the host and for the bacterium?”, *Frontiers in Microbiology*, 1–16.

Schmidt, G. W., Frey, O. and Rudolf, F., 2018, “The cellclammer: a convenient microfluidic device for time-lapse imaging of yeast”, *Genome Instability Methods and Protocols*, 537–555.

Schellenberger, J., Que, R., Fleming, R. M. T., Thiele, I., Orth, J. D., Feist, A. M. and Palsson, B. Ø., 2011, “Quantitative prediction of cellular metabolism with constraint-based models : the COBRA Toolbox v2.0”, *Nature Protocols*, 6, 9, 1290–1307.

Sehnem, N. T., Machado, A. S., Leite, F. C. B., Pita W. B., de Moraes Jr. M. A. and Ayub, M. A. Z., 2013 “5-Hydroxymethylfurfural induces ADH7 and ARI1 expression in tolerant industrial *Saccharomyces cerevisiae* strain P6H9 during bioethanol production”, *Bioresource Technology*, 133, 190–196.

Seo, J. H., Park, B. H., Oh, S. J., Choi, G., Kim, D. H., Lee, E. Y. and Seo, T. S., 2017, “Development of a high-throughput centrifugal loop-mediated isothermal amplification microdevice for multiplex foodborne pathogenic bacteria detection”, *Sensors and Actuators B*, 246, 146–153.

Shadmani, A., Viswam, V., Chen, Y. and Bounik, R., 2019, “Stimulation and artifact-suppression techniques for in-vitro high-density microelectrode array systems”, *IEEE Transactions on Biomedical Engineering*, 66, 9, 2481–2490.

Shadpour, H., Musyimi, H., Chen, J. and Soper, S. A., 2006, “Physiochemical properties of various polymer substrates and their effects on microchip electrophoresis performance”, *Journal of Chromatography A*, 1111, 2, 238–251.

Shembekar, N., Chaipan, C., Utharala, R. and Merten, C. A., 2016, “Droplet-based microfluidics in drug discovery, transcriptomics and high-throughput molecular genetics”, *Lab on a Chip*, 16, 8, 1314–1331.

Shemesh, J., Bransky, A., Khoury, M. and Levenberg, S., 2010, “Advanced microfluidic droplet manipulation based on piezoelectric actuation”, *Biomedical Microdevices*, 12, 5, 907–914.

Sherman, F., 1997, “An introduction to the genetics and molecular biology of the yeast *Saccharomyces cerevisiae*”, *The Encyclopedia of Molecular Biology and Molecular Medicine*, 6, 302–325.

Sinclair, D. A., 2005, “Toward a unified theory of caloric restriction and longevity regulation”, *Mechanisms of Ageing and Development*, 126, 987–1002.

Sivashankar, S., Puttaswamy, S. V., Lin, L. H., Dai, T. S., Yeh, C. T. and Liu, C. H., 2013, “Culturing of transgenic mice liver tissue slices in three-dimensional microfluidic structures of PEG-DA (poly(ethylene glycol) diacrylate)”, *Sensors and Actuators, B: Chemical*, 176, 1081–1089.

Skolimowski, M., Nielsen, M. W., Emnéus, J., Molin, S., Taboryski, R., Sternberg, C. and Geschke, O., 2010, “Microfluidic dissolved oxygen gradient generator biochip as a useful tool in bacterial biofilm studies” *Lab on a Chip*, 10, 16, 2162–2169.

Smidt, O. De, Preez, J. C. and Albertyn, J., 2011, “Molecular and physiological aspects of alcohol dehydrogenases in the ethanol metabolism of *Saccharomyces cerevisiae*”, *Federation of European Microbiological Societies Yeast Research*, 12, 33–47.

Sohrabi, S. and Moraveji, M. K., 2020, “Droplet microfluidics: fundamentals and its applications”, *The Royal Society of Chemistry Advances*, 10, 27560–27574.

Sonmez, B. G., Ertop, O. and Mutlu, S., 2018, “Realization and AC modeling of electronic circuits with water-gated field effect transistors (WG-FETs) based on gate probe distance”, *Journal of Micromechanics and Microengineering*, 28, 115017.

Spinelli, J. B. and Haigis, M. C., 2019, “The multifaceted contributions of mitochondria to cellular metabolism”, *Nature Cell Biology*, 20, 7, 745–754.

Steel, C. C., Grbin, P. R. and Nichol, A. W., 2001, “The pentose phosphate pathway in the yeasts”, *Biochemistry and Molecular Biology Education*, 29, 245–249.

Stehlik, C., Krajewska, M. and Welsh, K., 2003, “The PAAD/PYRIN-only protein POP1/ASC2 is a modulator of ASC-mediated nuclear-factor-kappa B and pro-caspase-1 regulation”, *The Biochemical Journal*, 101-113.

Stincone, A., Prigione, A., Cramer, T., Wamelink, M. M. C., Campbell, K., Cheung, E. and Ralser, M., 2015, “The return of metabolism: biochemistry and physiology of the pentose phosphate pathway”, *Biological Reviews*, 90, 927–963.

Stutz, A., Horvath, G. L., Monks, B. G. and Latz, E., 2013, “ASC speck formation as a readout for inflammasome activation”, *The Inflammasome*, 91-101.

Suga, M., Goto, A. and Hatakeyama, T., 2006, “Control by osmolarity and electric field strength of electro-induced gene transfer and protein release in fission yeast cells”, *Journal of Electrostatics*, 64, 796–801.

Szappanos, B., Kovács, K., Szamecz, B., Honti, F., Costanzo, M., Baryshnikova, A. and Papp, B., 2011, “An integrated approach to characterize genetic interaction networks in yeast metabolism”, *Nature Genetics*, 43, 656–662.

Szita, N., Boccazzi, P., Zhang, Z., Boyle, P., Sinskey, A. J. and Jensen, K. F., 2005, “Development of a multiplexed microbioreactor system for high-throughput bioprocessing”, *Lab on a Chip*, 5, 8, 819–826.

Tachibana, H., Saito, M., Shibuya, S., Tsuji, K. and Miyagawa, N., 2015, “On-chip quantitative detection of pathogen genes by autonomous microfluidic PCR platform”, *Biosensors and Bioelectronics*, 74, 725–730.

Tamura, T., 2019, “Growth-coupled overproduction is theoretically possible for most metabolites in *Saccharomyces cerevisiae* under anaerobic conditions”, *bioRxiv*, 1–15.

Tao, S. L., Lubeley, M. W. and Desai, T. A., 2003, “Bioadhesive poly (methyl methacrylate) microdevices for controlled drug delivery”, *Science*, 88, 215–228.

Thapa, M., Bommakanti, A., Shamsuzzaman, M., Gregory, B., Samsel, L., Zengel, J. M. and Lindahl, L., 2013, “Repressed synthesis of ribosomal proteins generates protein-specific cell cycle and morphological phenotypes”, *Molecular Biology of the Cell*, 24, 23, 3620–3633.

Thomson, E., Ferreira-Cerca, S. and Hurt, E., 2013, “Eukaryotic ribosome biogenesis at a glance”, *Cell Science at a Glance*, 4815–4821.

Todisco, S., Agrimi, G., Castegna, A. and Palmieri, F., 2006, “Identification of the mitochondrial NAD transporter in *Saccharomyces cerevisiae*”, *Journal of Biological Chemistry*, 281, 3, 1524–1531.

Toepke, M. W. and Beebe, D. J., 2006, “PDMS absorption of small molecules and consequences in microfluidic applications”, *Lab on a Chip*, 6, 12, 1484–1486.

Tomlinson, M. J., Tomlinson, S., Yang, X. B. and Kirkham, J., 2013, “Cell separation: Terminology and practical considerations”, *Journal of Tissue Engineering*, 4, 1–14.

Tourneau, C. Le, Faivre, S., Serova, M. and Raymond, E., 2008, “mTORC1 inhibitors: is temsirolimus in renal cancer telling us how they really work?”, *British Journal of Cancer*, 1197–1203.

Trantidou, T., Elani, Y., Parsons, E. and Ces, O., 2017, “Hydrophilic surface modification of PDMS for droplet microfluidics using a simple, quick, and robust method via PVA deposition”, *Microsystems & Nanoengineering*, 3, 16091.

Trendowski, M., Christen, T. D., Andonova, A. A., Narampanawe, B., Thibaud, A., Kusang, T. and Fondy, T. P., 2015, “Effects of mTOR inhibitors and cytoskeletal-directed agents alone and in combination against normal and neoplastic hematopoietic cells in vitro”, *Investigational New Drugs*, 1162–1174.

Tsai, N. C. and Sue, C. Y., 2006, “SU-8 based continuous-flow RT-PCR bio-chips under high-precision temperature control”, *Biosensors and Bioelectronics*, 22, 2, 313–317.

Tsao, C. W. and DeVoe, D. L., 2009, “Bonding of thermoplastic polymer microfluidics”, *Microfluidics and Nanofluidics*, 6, 1, 1–16.

Tsuchiya, S., Yamabe, M., Yamaguchi, Y., Kobayashi, Y., Konno, T. and Tada, K., 1980, “Establishment and characterization of a human acute monocytic leukemia cell line (THP-1)”, *International Journal of Cancer*, 26, 2, 171–176.

Uhlig, K., Wegener, T., He, J., Zeiser, M., Bookhold, J., Dewald, I. and Duschl, C., 2016, “Patterned thermoresponsive microgel coatings for noninvasive processing of adherent cells”, *Biomacromolecules*, 17, 3, 1110–1116.

Uno, H., Wang, Z. H., Nagaoka, Y., Takada, N., Obuliraj, S., Kobayashi, K. and Urisu, T., 2014, “Improvements in the performance of an incubation-type planar patch clamp biosensor using a salt bridge electrode and a plastic (PMMA) substrate”, *Sensors and Actuators, B: Chemical*, 193, 660–668.

Urrego, L. F., Lopez, D. I., Ramirez, K. A., Ramirez, C. and Osma, J. F., 2015, Biomicrosystem design and fabrication for the human papilloma virus 16 detection, *Sensors and Actuators B : Chemical*, 207, 97–104.

van Midwoud, P. M., Janse, A., Merema, M. T., Groothuis, G. M. and Verpoorte, E., 2012, “Comparison of biocompatibility and adsorption properties of different plastics for advanced microfluidic cell and tissue culture models”, *Analytical Chemistry*, 84, 9, 3938–3944.

Vanegas, J. M., Contreras, M. F., Faller, R. and Longo, M. L., 2012, “Role of unsaturated lipid and ergosterol in ethanol tolerance of model yeast biomembranes”, *Biophysical Journal*, 102, 3, 507–516.

Verbarg, J., Kamgar-Parsi, K., Shields, A. R., Howell, Jr. P. B. and Frances S. Ligler., 2012, “Spinning magnetic trap for automated microfluidic assay systems”, *Lab on a Chip*, 12, 1793–1799.

Verbarg, J., Plath, W. D., Shriver-Lake, L. C., Howell, P. B., Erickson, J. S., Golden, J. P. and Ligler, F. S., 2013, “Catch and release: integrated system for multiplexed detection of bacteria”, *Analytical Chemistry*, 85, 10, 4944–4950.

Vergote, I., von Moos, R., Manso, L., Van Nieuwenhuysen, E., Concin, N. and Sessa, C., 2018, “Tumor treating fields in combination with paclitaxel in recurrent ovarian carcinoma: results of the INNOVATE pilot study”, *Gynecologic Oncology*, 150, 3, 471–477.

Vinayavekhin, N., Kongchai, W., Piapukiew, J. and Chavasiri, W., 2020, “*Aspergillus niger* upregulated glycerolipid metabolism and ethanol utilization pathway under ethanol stress”, *Microbiology Open*, 1–21.

Volpatti, L. R. and Yetisen, A. K., 2014, “Commercialization of microfluidic devices”, *Trends in Biotechnology*, 32, 7, 347–350.

Wan, X., Shen, N., Mendoza, A., Khanna, C. and Helman, L. J., 2006, “CCI-779 inhibits rhabdomyosarcoma xenograft growth by an antiangiogenic mechanism linked to the targeting of mTOR / Hif-1 a / VEGF signaling”, *Neoplasia*, 8, 5, 394 – 401.

Wang, L., Manji, G. A. and Grenier, J. M., 2002, “PYPAF7, a novel PYRIN-containing Apaf1-like protein that regulates activation of NF-kappa B and caspase-1-dependent cytokine processing”, *Journal of Biological Chemistry*, 29874-29880.

Wang, S., Zhang, X., Yu, B., Lee, R. J. and Lee, L. J., 2010, “Targeted nanoparticles enhanced flow electroporation of antisense oligonucleotides in leukemia cells”, *Biosensors and Bioelectronics*, 26, 2, 778–783.

Wang, Z., Uno, H., Takada, N. and Kumar, O., 2012, “Multichannel incubation type planar patch clamp biosensor using plastic (PMMA) substrates and characterization by laser-gated ion-channel protein”, *Royal Society of Chemistry*, 4903, 1033–1035.

Wang, K. I. K., Salcic, Z., Yeh, J., Akagi, J., Zhu, F., Hall, C. J. and Wlodkowic, D., 2013, “Toward embedded laboratory automation for smart lab-on-a-chip embryo arrays”, *Biosensors and Bioelectronics*, 48, 188–196.

Wang, D., Hiebl, V., Ladurner, A., Latkolik, S. L., Bucar, F., Heiß, E. H. and Atanasov, A. G., 2018, “6-Dihydroparadol , a ginger constituent , enhances cholesterol efflux from THP-1-derived macrophages”, *Molecular Nutrition & Food Research*, 62, 1800011.

Wei, C. W., Cheng, J. Y. and Young, T. H., 2006, “Elucidating in vitro cell-cell interaction using a microfluidic coculture system”, *Biomedical Microdevices*, 8, 1, 65–71.

Wei, X., Lee, H. and Choi, S., 2016, Biopower generation in a microfluidic bio-solar panel, *Sensors and Actuators: B. Chemical*, 228, 151–155.

Weibel, D. B. and Whitesides, G. M., 2006, “Applications of microfluidics in chemical biology”, *Current Opinion in Chemical Biology*, 10, 584–591.

Weigum, S. E., Floriano, P. N. and Mcdevitt, J. T., 2007, “Miniaturisation for chemistry, biology & bioengineering Cell-based sensor for analysis of EGFR biomarker expression in oral cancer”, *Lab on a Chip*, 7, 8, 995–1003.

Wenger, C., Miranda, P. C., Salvador, R., Thielscher, A., Bomzon, Z., Giladi, M. and Korshoej, A. R., 2018, “A review on tumor-treating fields (TTFields): clinical implications inferred from computational modeling”, *IEEE Reviews in Biomedical Engineering*, 11, 195–207.

Witek, M. A., Wei, S., Vaidya, B., Adams, A. A., Zhu, L., Stryjewski, W. and Soper, S. A., 2004, “Cell transport via electromigration in polymer-based microfluidic devices”, *Lab on a Chip*, 4, 5, 464–472.

Woolford Jr., J. and L., Baserga, S. J., 2013, “Ribosome biogenesis in the yeast *Saccharomyces cerevisiae*”, *Yeastbook Gene Expression & Metabolism*, 643–681.

Workman, V. L., Dunnett, S. B., Kille, P. and Palmer, D. D., 2008, “On-chip alginate microencapsulation of functional cells”. *Macromolecular Rapid Communications*, 29, 2, 165–170.

Wu, M. H., Chang, Y. H., Liu, Y. T., Chen, Y. M., Wang, S. S., Wang, H. Y. and Pan, T. M., 2011, “Development of high throughput microfluidic cell culture chip for perfusion 3-dimensional cell culture-based chemosensitivity assay”, *Sensors and Actuators, B: Chemical*, 155, 1, 397–407.

Xie, Z., Zhang, Y., Zou, K., Brandman, O., Luo, C., Ouyang, Q. and Li, H., 2012, “Molecular phenotyping of aging in single yeast cells using a novel microfluidic device”, *Aging Cell*, 11, 4, 599–606.

Xu, Z., Lu, C., Riordon, J., Sinton, D. and Moffitt, M. G., 2016, “Microfluidic manufacturing of polymeric nanoparticles: comparing flow control of multiscale structure in single-phase staggered herringbone and two-phase reactors”, *Langmuir*, 32, 48, 12781–12789.

Yang, J. M., Bell, J., Huang, Y., Tirado, M., Thomas, D., Forster, A. H. and Krihak, M., 2002, “An integrated, stacked microlaboratory for biological agent detection with DNA and immunoassays”, *Biosensors and Bioelectronics*, 17, 6–7, 605–618.

Yang, W., Kug, K. and Choi, S., 2017, “A laminar-flow based microbial fuel cell array”, *Sensors and Actuators B : Chemical*, 243, 292–297.

Yazbeck, V. Y., Buglio, D., Georgakis, G. V., Li, Y., Iwado, E., Romaguera, J. E. and Younes, A., 2008, “Temsirolimus downregulates p21 without altering cyclin D1 expression and induces autophagy and synergizes with vorinostat in mantle cell lymphoma”, *Experimental Hematology*, 36, 4, 443–450.

Yeh, C. H., Lin, P. W. and Lin, Y. C., 2010, “Chitosan microfiber fabrication using a microfluidic chip and its application to cell cultures”, *Microfluidics and Nanofluidics*, 8, 115–121.

Yeo, L. Y., Chang, H. C., Chan, P. P. Y. and Friend, J. R., 2011, “Microfluidic devices for bioapplications”, *Small*, 7, 1, 12–48.

Yi, L., Xiaodong, W. and Fan, Y., 2008, “Microfluidic chip made of COP (cyclo-olefin polymer) and comparison to PMMA (polymethylmethacrylate) microfluidic chip”, *Journal of Materials Processing Technology*, 208, 1–3, 63–69.

Young, E. W. K., Berthier, E., Guckenberger, D. J., Sackmann, E., Lamers, C., Meyvantsson, I. and Beebe, D. J., 2011, “Rapid prototyping of arrayed microfluidic systems in polystyrene for cell-based assays”, *Analytical Chemistry*, 83, 1408–1417.

Yu, B. Y., Elb, C., Shen, C., Paul, J. and Ren, C. L., 2018, “An integrated microfluidic device for the sorting of yeast cells using image processing”, *Scientific Reports*, 1–12.

Zakhem, H. El, Lanoisellé, J., Lebovka, N. I., Nonus, M. and Vorobiev, E., 2006, “Behavior of yeast cells in aqueous suspension affected by pulsed electric field”, *Journal of Colloid and Interface Science*, 300, 553–563.

Zeng, A., Ross, A. and Deckwer, W., 1990, “A method to estimate the efficiency of oxidative phosphorylation and biomass yield from ATP of a facultative anaerobe in continuous culture”, *Biotechnology and Bioengineering*, 36, 965-969.

Zha, Q., Wei, H., Li, C., Liang, Y., Xu, L., Marrow-derived, B. and Bmdms, M., 2016, “ATP-induced inflammasome activation and pyroptosis is regulated by amp-activated protein kinase in macrophages”, *Frontiers in Immunology*, 1–16.

Zhang, Z., Boccazzi, P., Choi, H.-G., Perozziello, G., Sinskey, A. J. and Jensen, K. F., 2006, “Microchemostat-microbial continuous culture in a polymer-based, instrumented microbioreactor”, *Lab on a Chip*, 6, 7, 906–913.

Zhang, X., Khimji, I., Gurkan, U. A., Safae, H., Catalano, P. N., Keles, H. O., Kayaalp, E. and Demirci, U., 2011, “Lensless imaging for simultaneous microfluidic sperm monitoring and sorting”, *Lab on a Chip*, 11, 2535–2540.

Zhang, X., Wasserberg, D., Breukers, C., Terstappen, L. W. M. M. and Beck, M., 2016, “Temperature-switch cytometry—releasing antibody on demand from inkjet-printed gelatin for on-chip immunostaining”, *American Chemical Society Applied Materials & Interfaces*, 8, 41, 27539–27545.

Zhang, S., Zeng, X., Ren, M., Mao, X. and Qiao, S., 2017a, “Novel metabolic and physiological functions of branched chain amino acids: a review”, *Journal of Animal Science and Biotechnology*, 4–15.

Zhang, M. M., Xiong, L., Tang, Y. J., Mehmood, M. A. and Zhao, Z. K., 2019, “Enhanced acetic acid stress tolerance and ethanol production in *Saccharomyces cerevisiae* by modulating expression of the de novo purine biosynthesis genes”, *Biotechnology for Biofuels*, 12, 116, 1–13.

Zhao, X., Luo, C. and Wang, H., 2019, “Protein dynamic analysis of the budding yeast sporulation process at the single-cell level in an air-enriched microfluidic device”, *Integrative Biology*, 11, 3, 79–86.

Zheng, Y. and Jiang, Y., 2016, “mTOR inhibitors at a glance”, *Molecular and Cellular Pharmacology*, 7, 2, 15–20.

Zhong, Z., Umemura, A., Diaz-meco, M. T., Moscat, J., Karin, M., Zhong, Z. and Shalpour, S., 2016, NF- $\kappa$ B restricts inflammasome activation via elimination of damaged mitochondria, *Cell*, 164, 5, 896–910.

Zhu, F., Akagi, J., Hall, C. J., Crosier, K. E., Crosier, P. S., Delaage, P. and Wlodkowic, D., 2013, “A high-throughput lab-on-a-chip interface for zebrafish embryo tests in drug discovery and ecotoxicology”, *Proceedings of SPIE - The International Society for Optical Engineering*, 8923, 892345.

Zhu, F., Baker, D., Skommer, J., Sewell, M. and Wlodkowic, D., 2015, “Real-time 2D visualization of metabolic activities in zebrafish embryos using a microfluidic technology”, *Cytometry Part A*, 87, 5, 446–450.

Zhu, P. and Wang, L., 2017, “Passive and active droplet generation with microfluidics: a review”, *Lab on a Chip*, 17, 34–75

Zinser, E., Paltauf, F. and Daum, G., 1993, “Sterol composition of yeast organelle membranes and subcellular distribution of enzymes involved in sterol metabolism”, *Journal of Bacteriology*, 175, 10, 2853–2858.

Zumla, A., Rao, M., Parida, S. K., Keshavjee, S., Cassell, G., Wallis, R. and Maeurer, M., 2014, “Inflammation and tuberculosis: host-directed therapies”, *The Journal of Internal Medicine*, 373–387.

## APPENDIX A: PERMISSIONS FOR REUSED FIGURES

### A.1. Permission for Figure 1.1



Home
Help ▾
Live Chat
Sign in
Create Account

**Microfluidic Manufacturing of Polymeric Nanoparticles: Comparing Flow Control of Multiscale Structure in Single-Phase Staggered Herringbone and Two-Phase Reactors**



Author: Zheqi Xu, Changhai Lu, Jason Riordon, et al

Publication: Langmuir

Publisher: American Chemical Society

Date: Dec 1, 2016

Copyright © 2016, American Chemical Society

**PERMISSION/LICENSE IS GRANTED FOR YOUR ORDER AT NO CHARGE**

This type of permission/license, instead of the standard Terms and Conditions, is sent to you because no fee is being charged for your order. Please note the following:

- Permission is granted for your request in both print and electronic formats, and translations.
- If figures and/or tables were requested, they may be adapted or used in part.
- Please print this page for your records and send a copy of it to your publisher/graduate school.
- Appropriate credit for the requested material should be given as follows: "Reprinted (adapted) with permission from {COMPLETE REFERENCE CITATION}. Copyright {YEAR} American Chemical Society." Insert appropriate information in place of the capitalized words.
- One-time permission is granted only for the use specified in your RightsLink request. No additional uses are granted (such as derivative works or other editions). For any uses, please submit a new request.

If credit is given to another source for the material you requested from RightsLink, permission must be obtained from that source.

BACK
CLOSE WINDOW

## A.2. Permission for Figure 2.1



This is a License Agreement between Elif Gencturk ("User") and Copyright Clearance Center, Inc. ("CCC") on behalf of the Rightsholder identified in the order details below. The license consists of the order details, the CCC Terms and Conditions below, and any Rightsholder Terms and Conditions which are included below.  
All payments must be made in full to CCC in accordance with the CCC Terms and Conditions below.

Order Date	04-Aug-2021	Type of Use	Republish in a thesis/dissertation
Order License ID	1138339-1	Publisher	ROYAL SOCIETY OF CHEMISTRY
ISSN	1473-0197	Portion	Image/photo/illustration

### LICENSED CONTENT

Publication Title	Lab on a chip	Rightsholder	Royal Society of Chemistry
Article Title	Microchemostat-microbial continuous culture in a polymer-based, instrumented microbioreactor.	Publication Type	Journal
Author/Editor	Royal Society of Chemistry (Great Britain)	Start Page	906
Date	01/01/2001	End Page	913
Language	English	Issue	7
Country	United Kingdom of Great Britain and Northern Ireland	Volume	6

### REQUEST DETAILS

Portion Type	Image/photo/illustration	Distribution	Worldwide
Number of images / photos / illustrations	1	Translation	Original language of publication
Format (select all that apply)	Electronic	Copies for the disabled?	No
Who will republish the content?	Academic institution	Minor editing privileges?	No
Duration of Use	Life of current edition	Incidental promotional use?	No
Lifetime Unit Quantity	Up to 499	Currency	USD
Rights Requested	Main product		

### NEW WORK DETAILS

Title	Dr.	Institution name	Bogazici University
Instructor name	Elif Gencturk	Expected presentation date	2021-08-11

### ADDITIONAL DETAILS

Order reference number	N/A	The requesting person / organization to appear on the license	Elif Gencturk
------------------------	-----	---	---------------

### REUSE CONTENT DETAILS

Title, description or numeric reference of the portion(s)	DEVELOPMENT OF MICROFLUIDIC PLATFORMS FOR THERAPEUTIC PURPOSES	Title of the article/chapter the portion is from	Microchemostat-microbial continuous culture in a polymer-based, instrumented microbioreactor.
Editor of portion(s)	Zhang, Zhiyu; Boccazzi, Paolo; Choi, Hyun-Goo; Perozziello, Gerardo; Sinskey, Anthony J.; Jensen, Klavs F.	Author of portion(s)	Zhang, Zhiyu; Boccazzi, Paolo; Choi, Hyun-Goo; Perozziello, Gerardo; Sinskey, Anthony J.; Jensen, Klavs F.
Volume of serial or monograph	6	Issue, if republishing an article from a serial	7
Page or page range of portion	906-913	Publication date of portion	2006-06-27

### A.3. Permission for Figure 2.2



This is a License Agreement between Elif Gencturk ("User") and Copyright Clearance Center, Inc. ("CCC") on behalf of the Rightsholder identified in the order details below. The license consists of the order details, the CCC Terms and Conditions below, and any Rightsholder Terms and Conditions which are included below.  
All payments must be made in full to CCC in accordance with the CCC Terms and Conditions below.

Order Date	04-Aug-2021	Type of Use	Republish in a thesis/dissertation
Order License ID	1138341-1	Publisher	WILEY - V C H VERLAG GMBH & CO. KGAA
ISSN	0173-0835	Portion	Image/photo/illustration

#### LICENSED CONTENT

Publication Title	Electrophoresis	Rightsholder	John Wiley & Sons - Books
Article Title	Synthesis of agar microparticles using temperature-controlled microfluidic devices for Cordyceps militaris cultivation.	Publication Type	Journal
Author/Editor	ELECTROPHORESIS SOCIETY, INTERNATIONAL ELECTROPHORESIS SOCIETY.	Start Page	3157
Date	01/01/1980	End Page	3163
Language	English, English	Issue	22
Country	Germany	Volume	32

#### REQUEST DETAILS

Portion Type	Image/photo/illustration	Distribution	Worldwide
Number of images / photos / illustrations	1	Translation	Original language of publication
Format (select all that apply)	Electronic	Copies for the disabled?	No
Who will republish the content?	Author of requested content	Minor editing privileges?	No
Duration of Use	Life of current edition	Incidental promotional use?	No
Lifetime Unit Quantity	Up to 499	Currency	USD
Rights Requested	Main product		

#### NEW WORK DETAILS

Title	Dr.	Institution name	Bogazici University
Instructor name	Elif Gencturk	Expected presentation date	2021-08-11

#### ADDITIONAL DETAILS

The requesting person / organization to appear on the license	Elif Gencturk
---	---------------

#### REUSE CONTENT DETAILS

Title, description or numeric reference of the portion(s)	DEVELOPMENT OF MICROFLUIDIC PLATFORMS FOR THERAPEUTIC PURPOSES	Title of the article/chapter the portion is from	Synthesis of agar microparticles using temperature-controlled microfluidic devices for Cordyceps militaris cultivation.
Editor of portion(s)	Lin, Yung-Sheng; Yang, Chih-Hui; Lu, Kang; Huang, Keng-Shiang; Zheng, Ying-Zhen	Author of portion(s)	Lin, Yung-Sheng; Yang, Chih-Hui; Lu, Kang; Huang, Keng-Shiang; Zheng, Ying-Zhen
Volume of serial or monograph	32	Publication date of portion	2011-11-01
Page or page range of portion	3157-3163		

#### A.4. Permission for Figure 2.3

##### ELSEVIER LICENSE TERMS AND CONDITIONS

Aug 04, 2021

---

---

This Agreement between Elif Gencturk ("You") and Elsevier ("Elsevier") consists of your license details and the terms and conditions provided by Elsevier and Copyright Clearance Center.

License Number	5122010461018
License date	Aug 04, 2021
Licensed Content Publisher	Elsevier
Licensed Content Publication	Journal of Bioscience and Bioengineering
Licensed Content Title	Embryoid body culture of mouse embryonic stem cells using microwell and micropatterned chips
Licensed Content Author	Yusuke Sakai, Yukiko Yoshiura, Kohji Nakazawa
Licensed Content Date	Jan 1, 2011

Licensed Content Volume 111

Licensed Content Issue 1

Licensed Content Pages 7

Start Page 85

End Page 91

Type of Use reuse in a thesis/dissertation

Portion figures/tables/illustrations

Number of  
figures/tables/illustrations 1

Format both print and electronic

Are you the author of this  
Elsevier article? No

Will you be translating? No

Institution name	Bogazici University
Expected presentation date	Aug 2021
Portions	Figure 1
Requestor Location	Elif Gencturk Bogazici University Chemical Engineering Department İstanbul, 34342 Turkey Attn: Elif Gencturk
Publisher Tax ID	GB 494 6272 12
Total	0.00 USD
Terms and Conditions	

## A.5. Permission for Figure 2.4



This is a License Agreement between Elif Gencturk ("User") and Copyright Clearance Center, Inc. ("CCC") on behalf of the Rightsholder identified in the order details below. The license consists of the order details, the CCC Terms and Conditions below, and any Rightsholder Terms and Conditions which are included below.  
All payments must be made in full to CCC in accordance with the CCC Terms and Conditions below.

Order Date	04-Aug-2021	Type of Use	Republish in a thesis/dissertation
Order License ID	1138347-1	Publisher	ROYAL SOCIETY OF CHEMISTRY
ISSN	1473-0197	Portion	Image/photo/illustration

### LICENSED CONTENT

Publication Title	Lab on a chip	Rightsholder	Royal Society of Chemistry
Article Title	Rapid and inexpensive blood typing on thermoplastic chips.	Publication Type	Journal
Author/Editor	Royal Society of Chemistry (Great Britain)	Start Page	4533
Date	01/01/2001	End Page	4541
Language	English	Issue	24
Country	United Kingdom of Great Britain and Northern Ireland	Volume	15

### REQUEST DETAILS

Portion Type	Image/photo/illustration	Distribution	Worldwide
Number of images / photos / illustrations	1	Translation	Original language of publication
Format (select all that apply)	Electronic	Copies for the disabled?	No
Who will republish the content?	Academic institution	Minor editing privileges?	No
Duration of Use	Life of current edition	Incidental promotional use?	No
Lifetime Unit Quantity	Up to 499	Currency	USD
Rights Requested	Main product		

### NEW WORK DETAILS

Title	Dr.	Institution name	Bogazici University
Instructor name	Elif Gencturk	Expected presentation date	2021-08-11

### ADDITIONAL DETAILS

Order reference number	N/A	The requesting person / organization to appear on the license	Elif Gencturk
------------------------	-----	---	---------------

### REUSE CONTENT DETAILS

Title, description or numeric reference of the portion(s)	DEVELOPMENT OF MICROFLUIDIC PLATFORMS FOR THERAPEUTIC PURPOSES	Title of the article/chapter the portion is from	Rapid and inexpensive blood typing on thermoplastic chips.
Editor of portion(s)	Chen, Jun-You; Huang, Yi-Ting; Chou, Hsin-Hao; Wang, Cheng-Po; Chen, Chien-Fu	Author of portion(s)	Chen, Jun-You; Huang, Yi-Ting; Chou, Hsin-Hao; Wang, Cheng-Po; Chen, Chien-Fu
Volume of serial or monograph	15	Issue, if republishing an article from a serial	24
Page or page range of portion	4533-4541	Publication date of portion	2015-12-21

## A.6. Permission for Figure 2.5



This is a License Agreement between Elif Gencturk ("User") and Copyright Clearance Center, Inc. ("CCC") on behalf of the Rightsholder identified in the order details below. The license consists of the order details, the CCC Terms and Conditions below, and any Rightsholder Terms and Conditions which are included below.  
All payments must be made in full to CCC in accordance with the CCC Terms and Conditions below.

Order Date	04-Aug-2021	Type of Use	Republish in a thesis/dissertation
Order License ID	1138351-1	Publisher	PERGAMON
ISSN	0956-5663	Portion	Image/photo/illustration

### LICENSED CONTENT

Publication Title	Biosensors & bioelectronics	Rightsholder	Elsevier Science & Technology Journals
Article Title	Two-stage microfluidic chip for selective isolation of circulating tumor cells (CTCs)	Publication Type	Journal
Date	01/01/1989	Start Page	86
Language	English	End Page	92
Country	United Kingdom of Great Britain and Northern Ireland	Volume	67

### REQUEST DETAILS

Portion Type	Image/photo/illustration	Distribution	Worldwide
Number of images / photos / illustrations	1	Translation	Original language of publication
Format (select all that apply)	Electronic	Copies for the disabled?	No
Who will republish the content?	Academic institution	Minor editing privileges?	No
Duration of Use	Life of current edition	Incidental promotional use?	No
Lifetime Unit Quantity	Up to 499	Currency	USD
Rights Requested	Main product		

### NEW WORK DETAILS

Title	Dr.	Institution name	Bogazici University
Instructor name	Elif Gencturk	Expected presentation date	2021-08-11

### ADDITIONAL DETAILS

Order reference number	N/A	The requesting person / organization to appear on the license	Elif Gencturk
------------------------	-----	---	---------------

### REUSE CONTENT DETAILS

Title, description or numeric reference of the portion(s)	DEVELOPMENT OF MICROFLUIDIC PLATFORMS FOR THERAPEUTIC PURPOSES	Title of the article/chapter the portion is from	Two-stage microfluidic chip for selective isolation of circulating tumor cells (CTCs)
Editor of portion(s)	Hyun, Kyung-A; Lee, Tae Yoon; Lee, Su Hyun; Jung, Hyo-Il	Author of portion(s)	Hyun, Kyung-A; Lee, Tae Yoon; Lee, Su Hyun; Jung, Hyo-Il
Volume of serial or monograph	67	Issue, if republishing an article from a serial	N/A
Page or page range of portion	86-92	Publication date of portion	2015-05-15

## A.7. Permission for Figure 2.6



This is a License Agreement between Elif Gençtürk ("User") and Copyright Clearance Center, Inc. ("CCC") on behalf of the Rightsholder identified in the order details below. The license consists of the order details, the CCC Terms and Conditions below, and any Rightsholder Terms and Conditions which are included below. All payments must be made in full to CCC in accordance with the CCC Terms and Conditions below.

Order Date	04-Aug-2021	Type of Use	Republish in a thesis/dissertation
Order License ID	1138353-1	Publisher	ELSEVIER S.A.
ISSN	0925-4005	Portion	Image/photo/illustration

### LICENSED CONTENT

Publication Title	Sensors and actuators. B, Chemical	Rightsholder	Elsevier Science & Technology Journals
Article Title	Microfluidic Lab-on-a-Chip technology for automated toxicity tests using the marine amphipod <i>Allorchestes compressa</i>	Publication Type	Journal
Date	01/01/1990	Start Page	660
Language	English	End Page	670
Country	Switzerland	Volume	239

### REQUEST DETAILS

Portion Type	Image/photo/illustration	Distribution	Worldwide
Number of images / photos / illustrations	1	Translation	Original language of publication
Format (select all that apply)	Electronic	Copies for the disabled?	No
Who will republish the content?	Academic institution	Minor editing privileges?	No
Duration of Use	Life of current edition	Incidental promotional use?	No
Lifetime Unit Quantity	Up to 499	Currency	USD
Rights Requested	Main product		

### NEW WORK DETAILS

Title	Dr.	Institution name	Bogazici University
Instructor name	Elif Gençtürk	Expected presentation date	2021-08-11

### ADDITIONAL DETAILS

Order reference number	N/A	The requesting person / organization to appear on the license	Elif Gençtürk
------------------------	-----	---	---------------

### REUSE CONTENT DETAILS

Title, description or numeric reference of the portion(s)	DEVELOPMENT OF MICROFLUIDIC PLATFORMS FOR THERAPEUTIC PURPOSES	Title of the article/chapter the portion is from	Microfluidic Lab-on-a-Chip technology for automated toxicity tests using the marine amphipod <i>Allorchestes compressa</i>
Editor of portion(s)	Cartledge, Rhys; Nugegoda, Dayanthi; Wlodkovic, Donald	Author of portion(s)	Cartledge, Rhys; Nugegoda, Dayanthi; Wlodkovic, Donald
Volume of serial or monograph	239	Issue, if republishing an article from a serial	N/A
Page or page range of portion	660-670	Publication date of portion	2017-02-01

## A.8. Permission for Figure 2.7



This is a License Agreement between Elif Gencturk ("User") and Copyright Clearance Center, Inc. ("CCC") on behalf of the Rightsholder identified in the order details below. The license consists of the order details, the CCC Terms and Conditions below, and any Rightsholder Terms and Conditions which are included below. All payments must be made in full to CCC in accordance with the CCC Terms and Conditions below.

Order Date	04-Aug-2021	Type of Use	Republish in a thesis/dissertation
Order License ID	1138356-1	Publisher	ELSEVIER S.A.
ISSN	0925-4005	Portion	Image/photo/illustration

### LICENSED CONTENT

Publication Title	Sensors and actuators. B, Chemical	Rightsholder	Elsevier Science & Technology Journals
Article Title	Development of a high-throughput centrifugal loop-mediated isothermal amplification microdevice for multiplex foodborne pathogenic bacteria detection	Publication Type	Journal
Date	01/01/1990	Start Page	146
Language	English	End Page	153
Country	Switzerland	Volume	246

### REQUEST DETAILS

Portion Type	Image/photo/illustration	Distribution	Worldwide
Number of images / photos / illustrations	1	Translation	Original language of publication
Format (select all that apply)	Print, Electronic	Copies for the disabled?	No
Who will republish the content?	Academic institution	Minor editing privileges?	No
Duration of Use	Life of current edition	Incidental promotional use?	No
Lifetime Unit Quantity	Up to 499	Currency	USD
Rights Requested	Main product		

### NEW WORK DETAILS

Title	Dr.	Institution name	Bogazici University
Instructor name	Elif Gencturk	Expected presentation date	2021-08-11

### ADDITIONAL DETAILS

Order reference number	N/A	The requesting person / organization to appear on the license	Elif Gencturk
------------------------	-----	---	---------------

### REUSE CONTENT DETAILS

Title, description or numeric reference of the portion(s)	DEVELOPMENT OF MICROFLUIDIC PLATFORMS FOR THERAPEUTIC PURPOSES	Title of the article/chapter the portion is from	Development of a high-throughput centrifugal loop-mediated isothermal amplification microdevice for multiplex foodborne pathogenic bacteria detection
Editor of portion(s)	Seo, Ji Hyun; Park, Byung Hyun; Oh, Seung Jun; Choi, Goro; Kim, Do Hyun; Lee, Eun Yeol; Seo, Tae Seok	Author of portion(s)	Seo, Ji Hyun; Park, Byung Hyun; Oh, Seung Jun; Choi, Goro; Kim, Do Hyun; Lee, Eun Yeol; Seo, Tae Seok
Volume of serial or monograph	246	Issue, if republishing an article from a serial	N/A
Page or page range of portion	146-153	Publication date of portion	2017-07-01

## A.9. Permission for Figure 2.8



This is a License Agreement between Elif Gencturk ("User") and Copyright Clearance Center, Inc. ("CCC") on behalf of the Rightsholder identified in the order details below. The license consists of the order details, the CCC Terms and Conditions below, and any Rightsholder Terms and Conditions which are included below. All payments must be made in full to CCC in accordance with the CCC Terms and Conditions below.

Order Date	04-Aug-2021	Type of Use	Republish in a thesis/dissertation
Order License ID	1138358-1	Publisher	PERGAMON
ISSN	0956-5663	Portion	Image/photo/illustration

### LICENSED CONTENT

Publication Title	Biosensors & bioelectronics	Publication Type	Journal
Article Title	An innovative miniature microbial fuel cell fabricated using photolithography.	Start Page	2841
Date	01/01/1989	End Page	2846
Language	English	Issue	6
Country	United Kingdom of Great Britain and Northern Ireland	Volume	26
Rightsholder	Elsevier Science & Technology Journals		

### REQUEST DETAILS

Portion Type	Image/photo/illustration	Distribution	Worldwide
Number of images / photos / illustrations	1	Translation	Original language of publication
Format (select all that apply)	Print, Electronic	Copies for the disabled?	No
Who will republish the content?	Academic institution	Minor editing privileges?	No
Duration of Use	Life of current edition	Incidental promotional use?	No
Lifetime Unit Quantity	Up to 499	Currency	USD
Rights Requested	Main product		

### NEW WORK DETAILS

Title	Dr.	Institution name	Bogazici University
Instructor name	Elif Gencturk	Expected presentation date	2021-08-11

### ADDITIONAL DETAILS

Order reference number	N/A	The requesting person / organization to appear on the license	Elif Gencturk
------------------------	-----	---	---------------

### REUSE CONTENT DETAILS

Title, description or numeric reference of the portion(s)	DEVELOPMENT OF MICROFLUIDIC PLATFORMS FOR THERAPEUTIC PURPOSES	Title of the article/chapter the portion is from	An innovative miniature microbial fuel cell fabricated using photolithography.
Editor of portion(s)	Chen, You-Peng; Zhao, Yue; Qiu, Ke-Qiang; Chu, Jian; Lu, Rui; Sun, Min; Liu, Xian-Wei; Sheng, Guo-Ping; Yu, Han-Qing; Chen, Jie; Li, Wen-Jie; Liu, Gang; Tian, Yang-Chao; Xiong, Ying	Author of portion(s)	Chen, You-Peng; Zhao, Yue; Qiu, Ke-Qiang; Chu, Jian; Lu, Rui; Sun, Min; Liu, Xian-Wei; Sheng, Guo-Ping; Yu, Han-Qing; Chen, Jie; Li, Wen-Jie; Liu, Gang; Tian, Yang-Chao; Xiong, Ying
Volume of serial or monograph	26	Issue, if republishing an article from a serial	6
Page or page range of portion	2841-2846	Publication date of portion	2011-02-15